2009-12-02

The Effect of Flowable Fill on the Lateral Resistance of Driven-Pile Foundations

Dustin David Miner
Brigham Young University - Provo

The Effect of Flowable Fill on the Lateral Resistance of Soil Surrounding Driven-Pile Foundations

Dustin D. Miner

A thesis submitted to the faculty of
Brigham Young University
in partial fulfillment of the requirements for the degree of

Master of Science

Kyle M. Rollins, Chair
Travis M. Gerber
Fernando S. Fonseca

Department of Civil and Environmental Engineering

Brigham Young University

December 2009

ABSTRACT

The Effect of Flowable Fill on the Lateral Resistance

of Soil Surrounding Driven-Pile Foundations

Dustin D. Miner

Department of Civil and Environmental Engineering

Master of Science

Flowable fill was used to strengthen the soft soil surrounding piles and behind the pile cap. The flowable fill placed beneath the pile cap surrounding the piles showed no appreciable increase in lateral resistance, this was partially due to the fact that the flowable fill placed had an unconfined compressive strength of 30 psi. Flowable fill was also used to replace a 12 ft wide, 6 ft thick, and 6 ft deep zone consisting of an average 475 psf clay that was adjacent to a 9-pile group in 3x3 pile configuration capped with a 9 ft x 9 ft x 2.5 ft, 5000 psi concrete cap. The flowable fill placed behind the pile cap had an unconfined compressive strength of about 137 psi. Lateral load testing of the pile foundation was then undertaken. The results of this testing were compared with similar testing performed on the same foundation with native soil conditions. The lateral resistance of the native soil was 282 kips at 1.5 inches of displacement, and the total

lateral resistance of the pile foundation with flowable fill placed behind the pile cap was increased by about 53% or 150 kips. Of the 150 kips, 90% to 100% can be attributed to the increased passive force on the face of the flowable fill zone and shearing of the base and sides denoting that the flowable fill zone behaved as a rigid block.

The long term strength of the flowable fill when water is allowed to flow over it is still in question. Samples of the 137 psi flowable fill were cured in a fog room for 700 days and showed a 56% decrease in their unconfined compressive strength. Any increase in lateral strength from the flowable fill would be compromised over a period of time less than 700 days. Site specific characteristics concerning water flow would need to be evaluated to determine if flowable fill would be an acceptable material to increase the lateral resistance of a pile group.

ACKNOWLEDGMENTS

I wish to thank my Professor Dr. Kyle M. Rollins for giving me the opportunity to work on such an exciting project, and for all of his technical assistance and support. I also thank my thesis committee members of Dr. Travis M. Gerber and Dr. Fernando S. Fonseca who gave their time to help me answer the many questions I had in regards to this thesis. I also couldn't have done this without the assistance of my fellow students Matthew Adsero, Nathan Lemme and Mark Herbst. I need to thank David Anderson, Rodney Mayo and David Halgren who from a construction and testing standpoint made these tests possible. Most importantly I need to thank my wife, Mary Anne and daughter Sadie, who were patient with me and continually checked on my progress. Also I would like to thank the many organizations that donated time, materials, and finical support, including but not limited to, The National Cooperative Highway Research Program (NCHRP), Hayward Baker, Build Inc, Wadsworth Brothers, and The Utah Department of Transportation (U-DOT).

TABLE OF CONTENTS

LIST OF TABLES

LIST OF FIGURES

1 Introduction

The infrastructure of United States Interstate system is aging, with many bridge structures deemed structurally unsound. Many of the bridge structures associated with the interstate system were designed and built many years before seismicity and the associated parameters were taken into consideration for bridge design. These bridges need retrofitting to meet current seismic code specifications. In the past, structural components were added to the foundations to improve lateral resistance, which improves the foundations performance in the event of an earthquake. Recently, strengthening the soft soil surrounding the piles and pile cap in lieu of structural retrofits has been a suggested alternative to increase the lateral resistance of driven pile foundations at reduced cost.

One suggested technique in strengthening the soft soil surrounding the piles is to replace the existing soil with flowable fill. As the name suggests this material is flowable and is currently used to fill in voids, basements, mines, sewers etc. The American Concrete Institute defines flowable fill as those materials with a 28-day compressive strength of less than 1200 psi (ACI, 1994). Flowable fill is also self compacting, self leveling and can typically be pumped to where it is needed without any finish work.

The use of flowable fill to increase the lateral strength of soils surrounding driven pile foundations has not previously been verified or quantified, although it seems particularly well suited to the problem. The lateral resistance of deep foundations is

primarily developed within 5 to 10 pile diameters of the ground surface. For typical piles with diameters of 1 to 2 ft, this corresponds to a total depth of 10 to 20 ft. Although an excavation of this depth may not be possible, a shallower excavation could provide a significant increase in lateral resistance. Therefore, flowable fill offers the potential of significantly increasing lateral pile foundation resistance without the need for expensive structural retrofit. In addition, increased strength resulting from flowable fill use could increase the passive resistance acting against bridge abutments and pile caps, which would further increase the lateral resistance of a bridge foundation system.

1.1 Project Objectives

The objectives of this research were four-fold.

- Evaluate the increase in lateral pile group resistance due to placement of flowable fill,
- Evaluate the increase in lateral passive resistance due to flowable fill,
- Compare cost and effectiveness of soil improvement relative to additional structural elements, and
- Produce a well-document case history of field performance for calibration of computer models so additional parametric studies can be performed.

The research for this project was one component of a much larger research project which is funded by the National Cooperative Highway Research Program (NCHRP). NCHRP has identified specific tasks that it would like to ultimately accomplish through this investigation. The above list represents four of the specific tasks that were to be accomplished through this research.

This report will focus only on the increased lateral resistance to pile group foundations through replacing the soft soil surrounding the foundation with flowable fill; however, flowable fill was not the only soil improvement technique implemented during this phase of research. Pile foundations were also tested after the soft soil surrounding the foundations was treated with various geometries of compacted fill, jet grouting, mass mixing, and geopiers. Reports of the results associated with these particular soil treatments can be found in the related thesis work of Herbst (2008), Adsero (2008), and Lemme (In Press).

1.2 Scope of Investigation

Four identical full-scale foundations, placed thirty ft apart, were designed, constructed, and tested during this phase of research. Each foundation consisted of nine piles, in a 3 x 3 configuration, driven to a depth of approximately 40 ft below grade. Prior to driving, the piles were instrumented with strain gages at predetermined depths. Inclinometer and shape accelerometer array casings, which extended the length of the driven piles, were also placed in selected middle row piles. A 9.25-ft square reinforced concrete pile cap which extended from the ground surface to 2.5 ft below grade was constructed on top of the piles. A reinforced concrete corbel was attached to the concrete pile cap to create a load transfer surface during testing of the foundation systems. A hydraulic actuator was placed between two foundations which were being tested. Steel pipe extensions were attached to each end of the actuator to span the distance between the actuator and foundation. The extensions were then attached to the corbel to enable lateral load transfer from the actuators to the pile caps.

The foundations were first tested with native soil conditions. One test was performed with soil directly behind the pile cap; the second test was performed with the soil directly behind the pile cap excavated to the depth of the pile cap. The results of these two tests were used to determine the total and passive force acting on the foundation when it is loaded laterally under native soil conditions. The shape arrays, strain gages, and inclinometers were also used to determine the displacements and moments in the piles with respect to depth below grade. It should be mentioned that flowable fill was placed beneath and behind the cap prior to the installation of the piles. This flowable fill was very low strength, and the tests had to be repeated with a higher strength flowable fill. The weaker flowable fill was 13.5 ft long, 9 ft wide at the top and 7.5 ft at the bottom, and had a depth of about 6 ft. After the first two tests were completed, the weaker flowable fill behind the cap was excavated and replaced by a stronger flowable fill with dimensions 12 ft long, 6 ft wide and 6 ft deep. Afterward, lateral load tests were performed on the same foundation both with flowable fill directly in front of the pile cap and after excavating the flowable fill in front of the pile cap to eliminate any passive force contribution. The results of these tests were then compared with the results obtained when the foundation was loaded with native soil conditions to determine the degree of improvement to both lateral pile resistance and passive resistance on the pile cap itself.

2 Literature Review

A soil cement slurry (sands or soils with up to 25% non-plastic or slightly plastic fines mixed with 5 to 10% cement with a water to cement ratio of 4 to 7) can be pumped into an excavation without compaction. Superplastisizers can also be added to the mix. Typical slurries can have 28 day compressive strengths of 100 psi, and have been used as backfills behind structures having limited access. Flowability and strength tests are prescribed for soil-cement slurries by ASTM standards.

2.1 Basic Overview

Controlled Low-Strength Material (CLSM) is defined by the American Concrete Institute as a self-compacted, cementitious material used primarily as a backfill in lieu of compacted fill. Controlled Low-Strength Material is generally referred to as flowable fill; however, it is also described as flowable mortar, flowable fly ash, plastic soil-cement, soil-cement slurry, K-Krete and other similar names. Controlled Low-Strength Materials are also defined as materials that have an unconfined compressive strength of 1200 psi. In applications that involve future excavation, it is common for CLSM specifications to require a maximum average unconfined compressive strength of 200 psi at 28 days (ACI, 1994).

CLSM is typically utilized as a replacement for compacted fill in backfill, void fill, utility bedding, and bridge approach applications. There are several benefits of using CLSM in these applications. CLSM can be placed in confined places such as underground structures in void filling applications. CLSM is used as bedding and cover material for utilities in trenches, where worker safety is a priority. Because CLSM is largely self-leveling and self-compacting, there is no need for compaction equipment and amount of labor is reduced (Trejo et al, 2004).

Controlled Low-Strength Materials are also used in unique applications, in which the mixture is adjusted to accentuate special properties. Controlled Thermal Fill is a specialty CLSM that has very high air entrainment, which provides insulation properties. Controlled Density Fill is a collapsible CLSM used in Engineered Material Arresting Systems at airports.

2.2 History

In 1964, the U.S. Bureau of Reclamation documented the first known use of CLSM, as pipe bedding material on over 320 miles of the Canadian River Aqueduct Project, which runs from north of Amarillo to south of Lubbock, Texas. In the 1970s, Detroit Edison Company and Kuhlman Corporation experimented with a concrete mixture consisting mainly of fly ash with small amounts of cement. The mixture, known as flowable fly ash, was used as backfill material on the Belle River Project and resulted in the project finishing approximately $1 million under budget (Adaska, 1997).

In 1977, four patents were issued for mixture design, backfill technique, pipe bedding, and dike construction to K-Krete Inc. for their CLSM mixture known as K-Krete. The patents were eventually ceded to the National Ready Mix Concrete Association (NRMCA) and K-Krete quickly emerged as an accepted replacement material for compacted fill. In 1984, American Concrete Institute established Committee 229, Controlled Low Strength Materials (CLSM). In 1994, committee 229 published a comprehensive guidance document that described mixture designs, construction methods, and laboratory research occurring at that time (Adaska, 1997).

2.3 Applications

The primary application of CLSM is as backfill in place of compacted soil. The flowable characteristics of CLSM allow for it to be readily placed into a trench or into restricted or confined areas where placing and compacting fill is difficult. CLSM also makes an excellent bedding material for utilities because the mixture easily fills voids and provides uniform support. Although CLSM may be placed continuously in most applications, it is placed in lifts when backfilling around pipes to prevent the pipes from floating.

CLSM may be mixed in central-mix concrete plants and ready-mixed concrete trucks. Once CLSM is transported to the jobsite, the mixture may be placed using chutes, conveyors, buckets, or pumps depending upon the application and access. Internal vibration or compaction is not needed to consolidate CLSM mixtures. The fluidity or

flowability and self-compacting properties are sufficient for CLSM mixtures to consolidate under their own weight.

CLSM mixtures have been used as base and subbase courses for highways and roads, structural fills for embankments and bridge approaches, and can even be used as the top course for low volume roads. Advantages to using CLSM mixtures include: placement in any weather, even in freezing weather and in shallow water, 100 percent compaction with no effort, placement in confined areas that are inaccessible to conventional equipment, increased soil bearing capacity, prevention of post-fill settlement, increased speed of backfill operation, decreased variability in the density of backfill material, improved job safety, decreased labor and equipment cost, and ability to be excavated for future needs.

2.4 Mixture Design

CLSM mixtures typically contain fly ash, Portland cement and water. Filler materials such as bottom ash, sand, or other fine aggregates can also be used in the mixture. Cementitious compounds such as Class C fly ash, slag cement, or cement kiln dust may replace of Portland cement in certain applications. The fluidity or flowablity of these mixtures occurs due to the spherical particle shape of fly ash in combination with water, which lubricates the particle surfaces.

Non-concrete grade fly ash, which may be less expensive than sand, is a major ingredient in CLSM mixtures. However, when sand is more economical, the amount of fly ash in a mixture can be reduced. The water content is dependent on the types and

amounts of solids present in the mixture and can be adjusted to meet fluidity requirements for the mixture. Portland cement content is typically low to provide a weak cementitious matrix.

The two basic types of CLSM mixtures are high fly ash content and low fly ash content. The high fly ash content mixtures typically contain between 60 and 75 percent fly ash and between 3 and 5 percent Portland cement. The low fly ash content mixtures contain between 70 and 85 percent sand, between 5 and 15 percent fly ash, and again between 3 and 5 percent Portland cement. Table 2-1 and Table 2-2 summarize the proportions of high and low fly ash content mixtures that have been adopted by many state DOTs (Kosmatka et al, 2003).

Table 2-1 High fly ash content clsm mixture

Component	**Range**		**Mixture Design**	
	kg/m^3	(lb/yd^3)	kg/m^3	(lb/yd^3)
Fly Ash	950 to 1540	(1600 to 2600)	1234	(2080)
Portland Cement	45 to 75	(80 to 125)	62	(104)
Water	220 to 370	(375 to 625)	247*	(416)*
			1543	**(2600)**
* equal to 189 liters (50 gallons)				

Table 2-2 Low fly ash content clsm mixture

Component	**Range**		**Mixture Design**	
	kg/m^3	(lb/yd^3)	kg/m^3	(lb/yd^3)
Fly Ash*	120 to 300	(200 to 500)	178	(300)
Portland Cement	30 to 120	(50 to 200)	59	(100)
Sand	1480 to 1780	(2500 to 3000)	1542	(2600)
Water	200 to 490	(330 to 830)	297**	(500)**
			2076	**(3500)**
* high calcium fly ash is used in lower amounts than low calcium fly ash				
** equal to 227 liters (60 gallons)				

CLSM mixtures have maximum average compressive strengths of 1200 psi, however most CLSM mixtures are designed to achieve a maximum compressive strength of 50 to 200 psi to allow for future excavation. CLSM mixtures with a maximum compressive strength 200 psi have at least two to three times the bearing capacity of well-compacted backfill material as shown in Table 2-3.

Table 2-3 Comparison of clsm and compacted earth fill

Property	**Typical CLSM**	**Compacted Earth**
Compressive Strength	< 300 psi*	< 50 psi
Density	115 – 145 pcf	100 – 125 pcf
Placement	Self-leveling	Mechanical compaction
* By definition, must be less than 1200 psi (ACI, 1994)		

2.5 Physical Properties

The most important physical properties of CLSM mixtures to be considered when designing are: strength development, fluidity, hardening time, subsidence, and segregatory bleeding. Strength development in CLSM mixtures is directly related to the amount of cementitious material and water content. In low calcium (CaO), Class F fly ash mixtures, the Portland cement and water content are directly related to strength development. In high calcium (CaO), Class C fly ash mixtures, no Portland cement may be required and strength development is directly related to the fly ash and water content. Water is added to achieve a desired fluidity or slump; however, at a given cementitious material content, increased water usually results in a decrease in compressive strength development over time (Adaska, 1997).

Fluidity is directly related to the water and entrained air content. In order to take advantage of the self-compacting qualities of CLSM mixtures, the mixture must be as

fluid as possible. Typical air entrainment content for CLSM mixtures ranges from 20 to 30 percent (Adaska, 1997).

Hardening time is directly related to the cementitious materials content. Typical high fly ash content CLSM mixtures achieve a sufficient set to support the weight of an average person in about three to four hours, depending on the temperature and humidity. Heavy construction equipment can move across the surface without any apparent damage with in 24 hours. Also some low fly ash content CLSM mixtures that contain high calcium Class C fly ash have reportedly set sufficiently to allow for the return of traffic to a street patching applications within one to two hours of placement (Adaska, 1997).

Bleeding and subsidence are possible in high fly ash content CLSM mixtures with relatively high slumps. Evaporation of the bleed water and absorption into the surrounding soil often results in minimal subsidence. Shrinkage may occur laterally and vertically, but no additional shrinkage of CLSM mixtures occurs after initial set (Adaska, 1997).

ASTM Test Methods for CLSM.

[A] **ASTM D4832** – Standard Test Method for Preparation and Testing of Controlled Low Strength Material (CLSM) Test Cylinders

[B] **ASTM D5971** – Standard Practice for Sampling Freshly Mixed Controlled Low Strength Material

[C] **ASTM D6023** – Standard Test Method for Unit Weight, Yield, Cement Content, and Air Content (Gravimetric) of Controlled Low Strength Material

[D] **ASTM D6024** – Standard Test Method for Ball Drop on Controlled Low Strength Material to Determine Suitability for Load Application

[E] **ASTM D6103** – Standard Test Method for Flow Consistency of Controlled Low Strength Material

Currently 42 states have specifications for applying CLSM for utility bedding, void fill, bridge approach, or backfill. Accordingly, 90 percent of the 3000 ready-mix concrete producers in the United States produce some form of CLSM. CLSM is also becoming an environment-friendly utilization of industrial by-product and waste materials (Trejo et al, 2004). CLSM is a readily available, highly versatile material that can be applied with less equipment and less labor than compacted earth fill and will immediately save time and money and increase job safety. CLSM or flowable fill is a viable replacement material for weak soils surrounding bridge pile caps and represents a technology which can be readily implemented on a broad scale.

3 Geotechnical Site Characterization

The following chapter will describe the soil conditions of the site used for testing. The site was located north of Salt Lake City at the interchange of Redwood Road and I-215 on a Utah Department of Transportation (UDOT) right-of-way. An aerial view of the site is found in Figure 3-1 . The top 4 ft of the site was littered with huge pieces of asphalt, and was excavated from the entire test site. All of the geotechnical field investigations took place before the excavation, and the results from these investigations have been modified to refer to the soil conditions below the excavation.

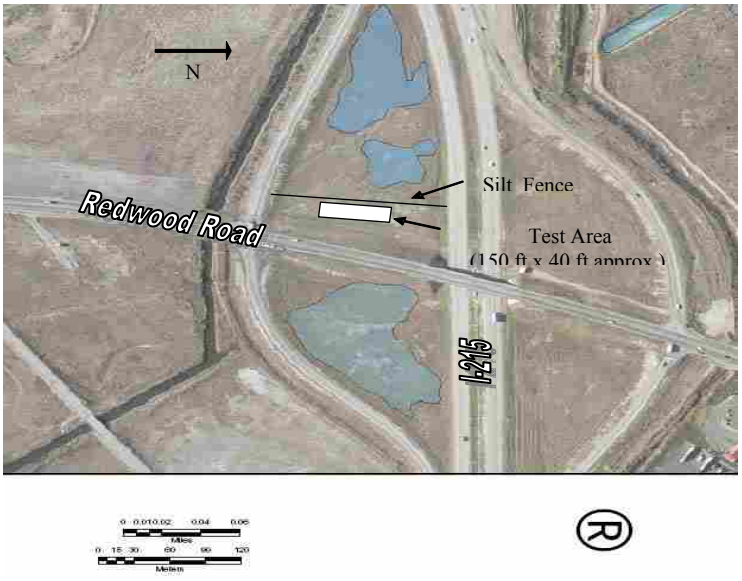

Figure 3-1 Aerial view of the test area

3.1 Field Investigations

Geotechnical site conditions were evaluated using field and laboratory testing. Field testing included one drilled hole with undisturbed sampling, four cone penetration test (CPT) soundings, and shear wave velocity testing. Laboratory testing included unit weight and moisture content determination, Atterberg limits testing, and undrained shear testing. A generalized soil boring log at the test site is provided in Figure 3-3. The depth is referenced to the top of the excavation which was 2.5 ft above the base of the pile cap as shown in that figure. A plan view of the borehole and CPT locations relative to the finished pile caps are shown in Figure 3-2.

3.2 Soil Profile, Classification and Shear Strength

A generalized soil boring log at the test site is provided in Figure 3-3 (a). The depth is referenced to the top of the excavation which was 2.5 ft above the base of the pile cap as shown in Figure 3-3. The soil profile consists predominantly of cohesive soils; however, some thin sand layers are located throughout the profile. The cohesive soils typically classify as CL or CH materials with plasticity indices of about 20 as shown in Figure 3-3 (a). In contrast, the soil layer from a depth of 15 to 25 ft consists of interbedded silt (ML) and sand (SM) layers as will be highlighted by the subsequent plots of CPT cone tip resistance.

The liquid limit, plastic limit and natural moisture content are plotted in Figure 3-3 (b) at each depth where Atterberg limit testing was performed. The water table is at a depth of 1.5 ft, which is equivalent to a depth of 5.5 ft below the pre-

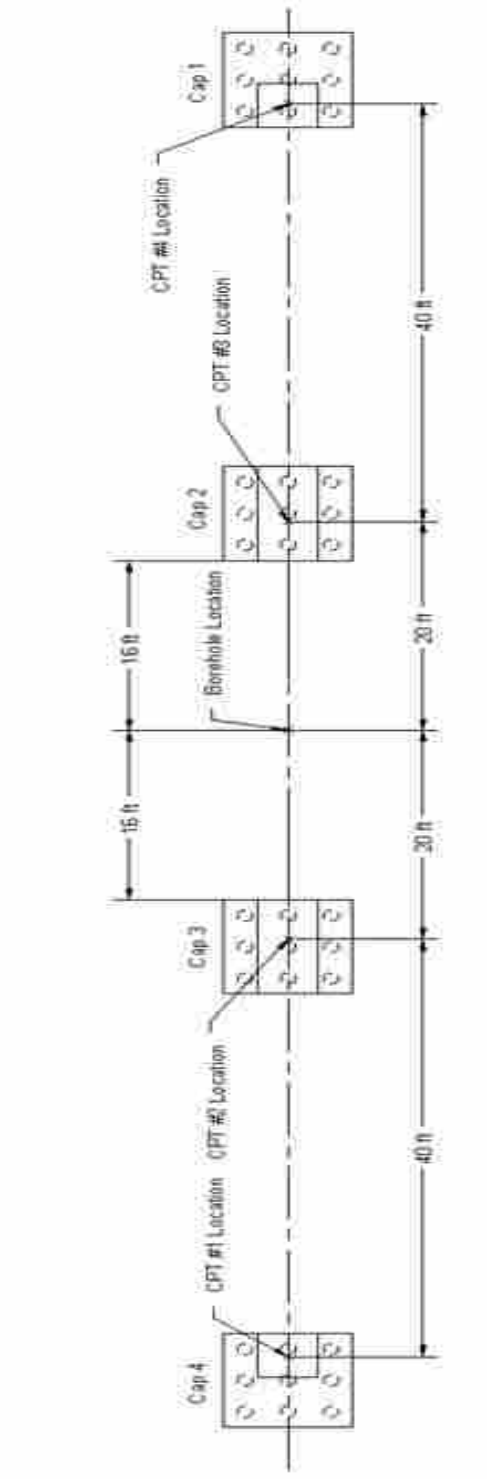

Figure 3-2 Plan view showing location of boring and cpt soundings relative to completed pile caps.

excavation ground surface. The natural water content is less than the liquid limit near the ground surface suggesting that the soil is overconsolidated. However, the water content is greater than the liquid limit for soil specimens from a depth of 5 to 27 ft. This suggests that these materials may be sensitive. Below a depth of 30 ft the water content is approximately equal to the liquid limit, suggesting that the soils are close to normally consolidated.

The undrained shear strength is plotted as a function of depth in Figure 3-3(c). Undrained shear strength was measured using a miniature vane shear test (Torvane test) on undisturbed samples immediately after they were obtained in the field. In addition, unconfined compression tests were performed on most of the undisturbed samples. Both the Torvane and unconfined compression tests indicate that the undrained shear strength decreases rapidly from the ground surface to a depth of about 6 ft. However, the undrained shear strength from the unconfined compression tests is typically about 30% lower than that from the Torvane tests. After a depth of 6 ft the trend reverses, and the shear strength begins to increase with depth. This profile is typical of a soil profile with a surface crust that has been overconsolidated by desiccation. The unconfined compression tests performed on samples taken at the depths of 27 and 48 ft yielded soil strengths substantially lower than that from the Torvane test. These unconfined compression tests appear to have been conducted on soil with sand lenses, and are not likely to be representative of the in-situ soil. The undrained shear strength was also computed from the cone tip resistance using the following correlation equation

$$s_u = \frac{(q_c - \sigma)}{N_k} \quad \textbf{(3-1)}$$

where q_c is the cone tip resistance, σ is the total vertical stress, and N_k is a variable which was taken to be 15 for this study.

The undrained shear strength obtained from the above equation is also shown in Figure 3-3(c), and the agreement with the strengths obtained from the Torvane and unconfined compression tests is reasonably good. Nevertheless, there is much greater variability and the drained strength in the interbedded sand layers is ignored. A summary of laboratory test results is provided in Table 3-1.

Table 3-1 - Laboratory test results.

	In-Place		Atterberg Limits					
Depth below Excavated Surface (ft)	Saturated Unit Weight (pcf)	Natural Water Content (%)	Liquid Limit (%)	Plastic Limit (%)	Plastic Index (%)	Unconfined Compressive Strength (psf)	Miniature Vane Shear Strength (Torvane) (psf)	Unified Soil Classification Symbol
1.25	117.6	34.2	39	18	21	1104	-	CL
2.75	117.4	34.4	38	18	20	626	620	CL
5.75	104.6	56	51	21	30	384	320	CH
8.5	112.4	41.5	38	18	20	684	534	CL
11.5	110.8	44.1	38	19	19	741	500	CL
16.5	126.6	24.2	19	18	1	1081	560	ML
26.75	116.9	35	27	14	13	237	780	CL
33.5	124.6	26.1	27	14	13	1306	780	CL
36.75	117.1	34.8	35	17	18	1381	840	CL
41.75	112.0	42.1	46	17	29	1037	520	CL
48	117.2	34.6	33	16	17	297	660	CL

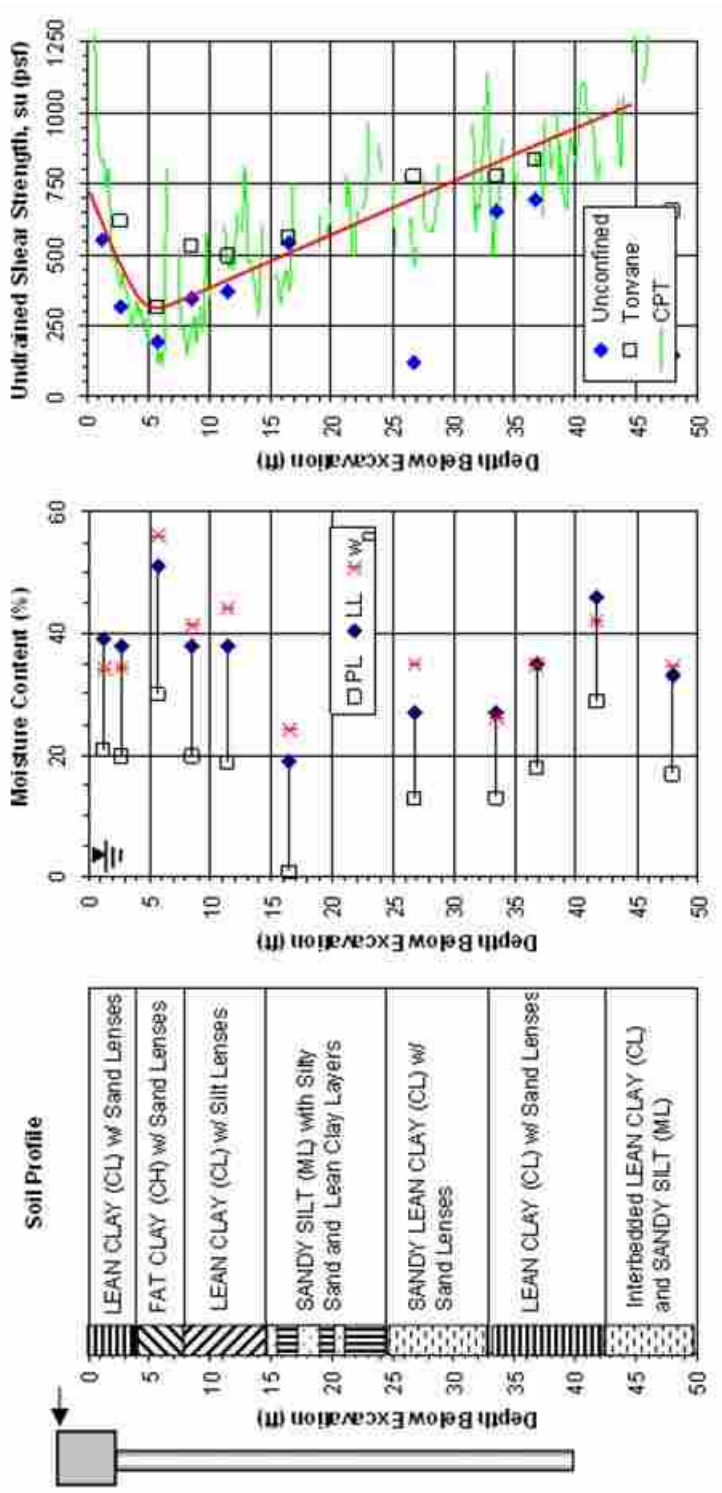

Figure 3-3 Plot of soil profile, atterberg linits and natural water content vs. depth, and undrained shear strength vs. depth Cone Penetration and Seismic Cone testing.

Four cone penetration tests (CPT) were performed across the test site. Plots of cone tip resistance, friction ratio, and pore pressure for the centermost test are provided as a function of depth in Figure 3-4. In addition, the interpreted soil profile is also shown. From the ground surface to a depth of about 15 ft the soil profile appears to be relatively consistent with a cone tip resistance of about 6 tsf and a friction ratio of about 1%. However, one thin sand layer is clearly evident between 6 and 8 ft. The cone tip resistance, friction ratio, and pore pressure plots clearly show the interbedded silt and sand layering in the soil profile between 15 and 27 ft below the ground surface.

Figure 3-5 provides plots of the cone tip resistance, friction ratio and pore pressure as a function of depth for all four of the CPT soundings. The measured parameters and layering are generally very consistent for all four sounding which indicates that the lateral pile load tests can be fairly compared from one foundation to the next.

Figure 3-6 provides a plot of the shear wave velocity as a function of depth obtained from the downhole seismic cone testing. The interpreted soil profile and cone tip resistance are also provided in Figure 3-6 for reference. The shear wave velocity in the upper 10 ft of the profile is between 300 and 400 ft/sec. This velocity is relatively low and suggests low shear strength. Between depths of 10 to 20 ft the velocity increases to about 550 ft/sec. This increase in velocity is likely associated with the interbedded sand layers in these depths. Below 20 ft, the velocity drops to a value of approximately 500 ft/sec and remains relatively constant to a depth of 45 ft.

Knowledge of the average shear wave velocity, standard penetration resistance, and undrained shear strength of the soil to a depth of 100 ft is generally necessary to

determine a specific International Building Code (IBC) seismic site classification. However, this is not the case if the site is classified as Site Class E. Any soil profile with more than 10 ft of soil having the following characteristics is classified as a Site Class E.

1. Plasticity index, $PI < 20$
2. Moisture content, $w \geq 40\%$
3. Undrained Shear strength, $S_u < 500$ psf

A close look at Table 3-1 and Figure 3-3 shows that this site meets all three of the above criteria. Therefore, the soil profile information obtained to a depth of 50 ft is sufficient to classify the site as an IBC Site Class E.

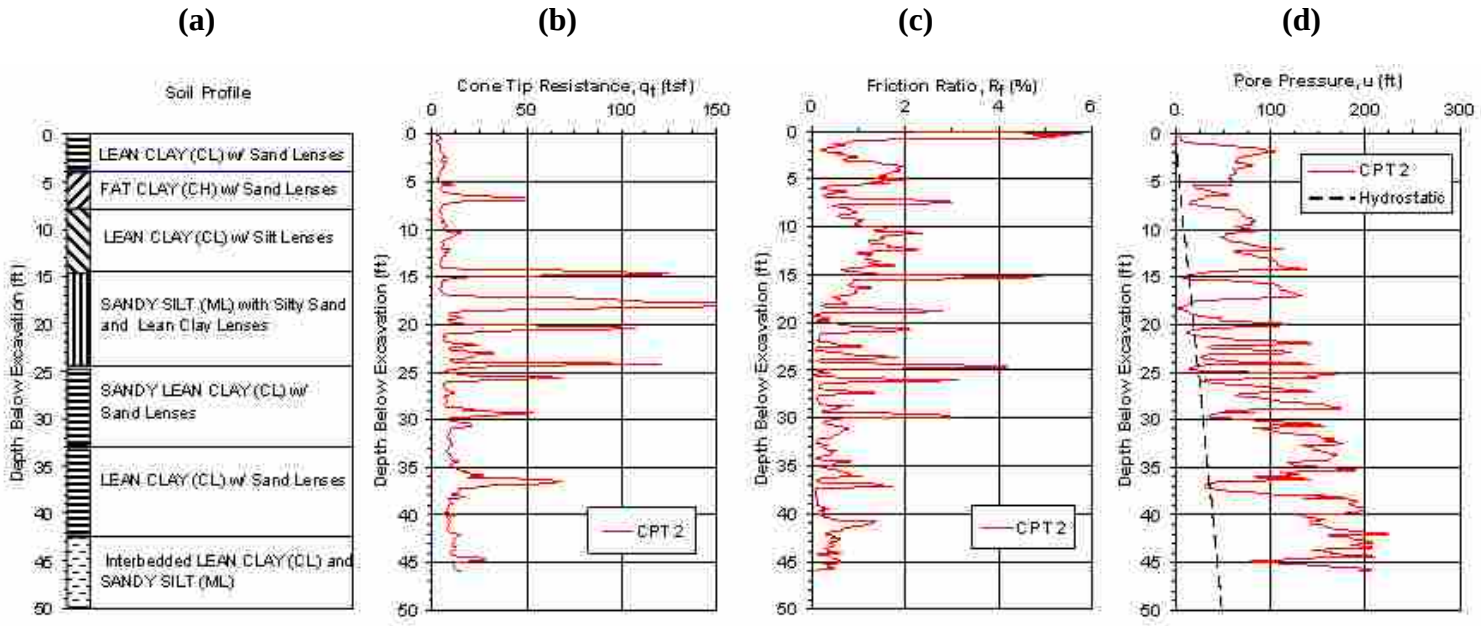

Figure 3-4 – Plot of (a) soil profile, (b) cone tip resistance vs. depth, (c) friction ratio vs. depth, and (d) pore pressure vs. depth curves from cone penetration test (cpt) sounding 2 near the center of the site.

(a) **(b)** **(c)** **(d)**

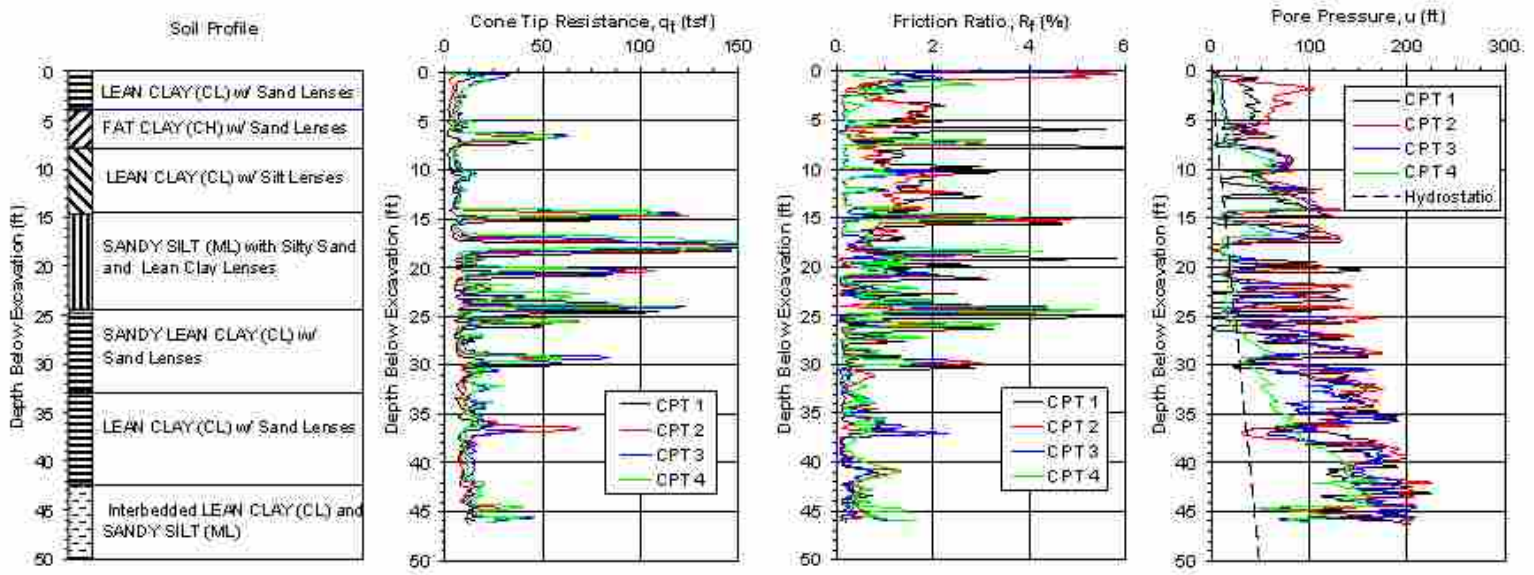

Figure 3-5 Plot (a) soil profile, (b) cone tip resistance vs. depth, (c) friction ratio vs. depth and, (d) pore pressure vs. depth from all four cone penetration test (cpt) soundings.

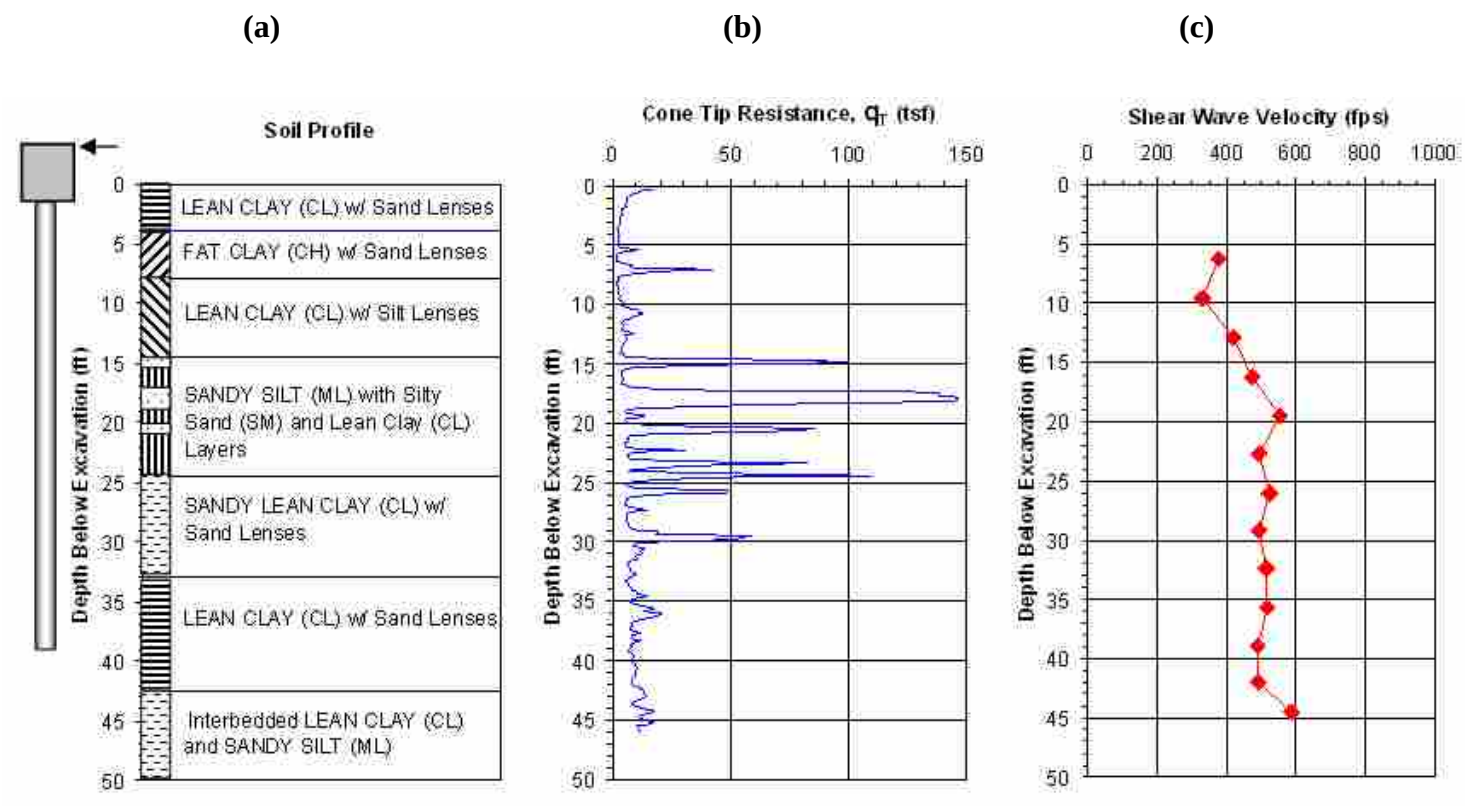

Figure 3-6 Plot of (a) soil profile, (b) cone tip resistance vs. depth, and (c) shear wave velocity vs. depth from seismic cone testing.

4 Test Layout and Procedure

The following section will detail the construction process for the foundations and define the properties of the materials used to build the foundations. This section will also explain the basic layout of the actuators and pile caps, along with the instrumentation configuration on each of the foundations.

4.1 Construction, Layout, and Materials

Once the site had been excavated to the proper depth of 4.5 ft below the original grade, the four pile groups were driven. An overall plan view of the four pile group locations is shown in Figure 3-2. As shown in Figure 4-1, each pile group consisted of nine test piles which were driven in a 3 x 3 orientation with a nominal center to center spacing of 3 ft in both directions. The tests piles were 12.75 inch OD pipe piles with a 0.375 inch wall thickness. They were driven closed-ended with a hydraulic hammer to a depth of approximately 45 ft below the excavated ground surface on June 13-15, 2007. The test piles had a beveled end which allowed a 1.5 inch thick plate to be welded flush with the edge of the pile at the bottom. The steel conformed to ASTM A252 Grade 2 specifications and had a yield strength of 58,700 psi based on the 0.2% offset criteria. The moment of inertia of the pile was 279 in^4; however, angle irons were welded on

opposite sides of two to three test piles within each group, which increased the moment of inertia to 342 in^4.

The center piles of each row were instrumented with strain gages prior to installation (see Figure 4-1). (Note: For caps 2 and 4, the middle pile of the center row was not instrumented with strain gages). The strain gages were placed at pre-determined depths of 2, 6, 11, and 13.5 ft below the tops of the piles. Strain gages were placed along the north and south sides of the piles in the direction of loading. The strain gage depths were determined through computer modeling to be the most critical depths in developing bending moment curves for the laterally loaded piles. Figure 4-2 is a photo of an installed pile group.

The piles were driven so that they would extend 2 ft into the base of the pile cap. In some cases this was not accomplished so the piles were cut off to this elevation. A steel reinforcing cage was installed at the top of each test pile to connect the test piles to the pile cap. The reinforcing cage consisted of 6 - #8 reinforcing bars which were confined within a #4 bar spiral with a diameter of 8 inches and a pitch of 6 inches. The reinforcing cage extended 2.25 ft above the base of the cap and 8.75 ft below the base. The steel pipe pile was filled with concrete with an average unconfined compressive strength of 5150 psi based on tests of four specimens. A drawing showing the cross-section of the test piles is provided in Figure 4-3. Once the piles were filled, construction of the pile cap was then commenced.

Figure 4-4 shows the plan and profile drawings of pile caps 1 and 2. Pile caps 1 and 2 (the two northern most pile caps) were constructed by excavating 2.5 ft into the virgin clay. The concrete was poured directly against vertical soil faces on the front and

back sides of each pile cap. This construction procedure made it possible to evaluate passive force against the front and back faces of the pile caps. In contrast, plywood forms were used along the sides of all of the caps and were braced laterally against the adjacent soil faces. This construction procedure created a gap between the cap sidewall and the soil so that side friction would be eliminated.

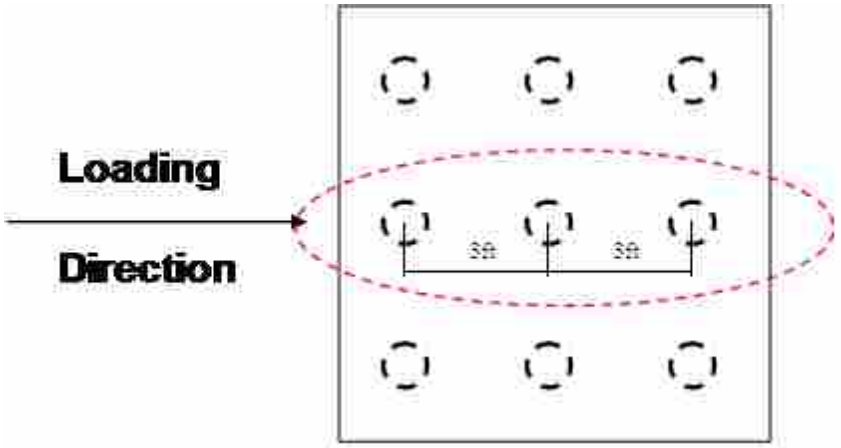

Figure 4-1 Driven 3x3 pile group all 3ft on center in both directions (piles instrumented with strain gages circled).

Pile cap 3 was constructed in a similar manner, except that flowable fill was installed under the pile cap to a depth of 6 ft below grade, 9 ft wide, and 13.5 ft in the direction of loading before piles were driven. Flowable fill was also installed on the north side of the cap to the same depth as that installed under the cap. Pile cap 4 was constructed in the same way as cap 3, except that compacted fill was installed prior to pile driving. The compacted fill was installed to a depth of 3 ft below the bottom of the pile cap with a width of 9 ft transverse to the load direction and a length of 14 ft in the direction of loading. Compacted fill was also installed along the north side of the cap to the level of the cap.

Figure 4-2 Driven pile layout prior to cap construction.

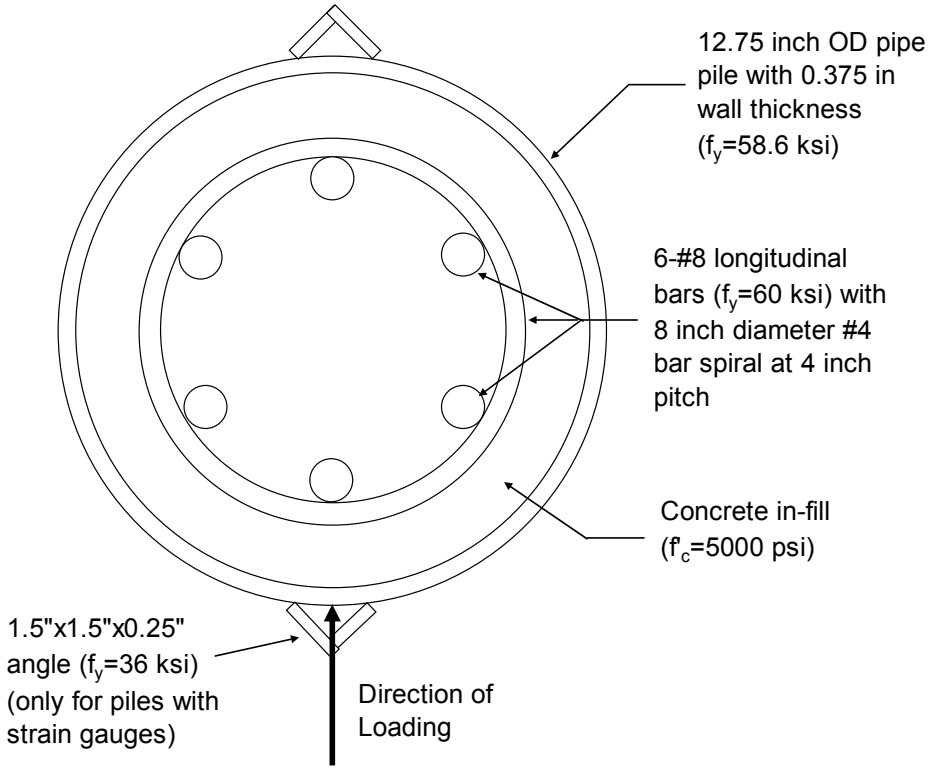

Figure 4-3 Cross-section of piles within the pile groups.

Steel reinforcing mats were placed in the top and bottom of each cap with a three inch concrete cover. The top reinforcing mat in the pile caps was designed with #7 bars at 10 inch spacing in both directions, with a decrease in spacing to 6 inches in the transverse direction under the short corbel on caps 1 and 4. The bottom mats were designed with #9 bars at 6.5 inch spacing longitudinally and #7 bars at 10 inch spacing transverse to the load direction. Plan view drawings of the top and bottom reinforcing mats for piles caps 1, 2, 3, and 4 are provided in Figure 4-5 and Figure 4-6.

A corbel was constructed on each cap to allow the actuator to apply load above the ground surface without affecting the soil around the pile cap. The corbel extended the full length of the pile cap for caps 2 and 3 to allow the actuators to be attached to both sides of the caps. Alternatively, the corbel only extended about half of the pile cap length in cap 1 and 4 as only one sided was needed for the actuator attachment. This is shown in Figure 4-4 which illustrates the corbel configuration on top of caps 1 and 2. The corbel was designed using the traditional ACI design method described in section 11.9 of the ACI code. The corbel was reinforced with #5 bar hoops and #9 bars as the main reinforcement as shown in Figure 4-7 and Figure 4-8. Also included in Figure 4-9 is a cross sectional view of the corbel steel looking at the interface where the actuator connects to the corbel. Design calculations and more detailed steel reinforcement drawings are provided in Appendix A.

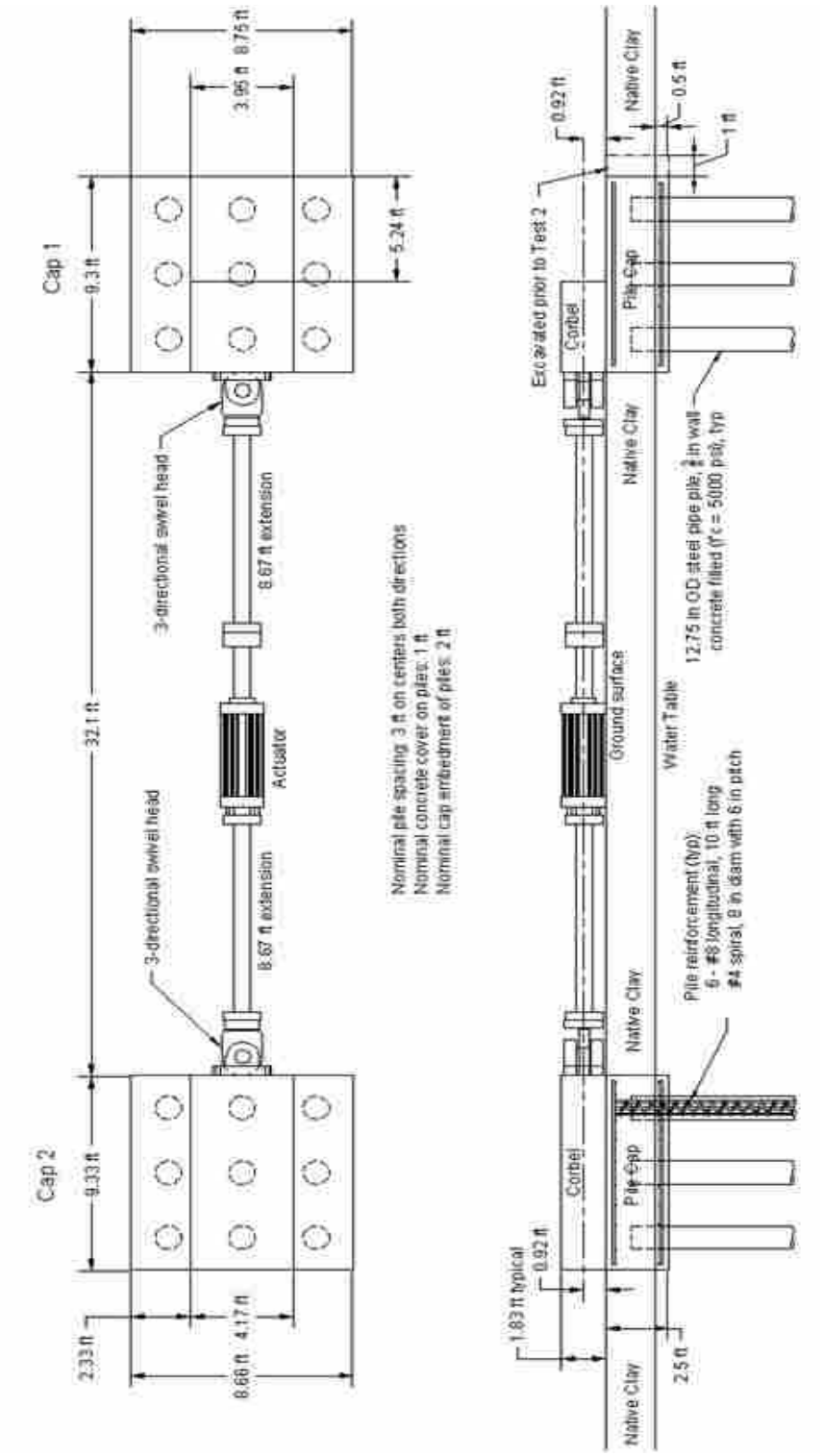

Figure 4-4 Plan and profile drawings of pile caps 1 and 2.

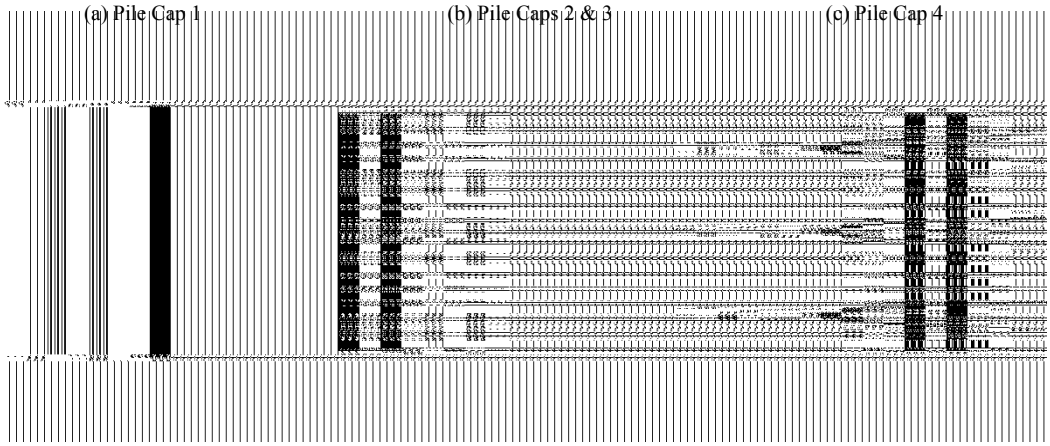

Figure 4-5 Layout of bottom reinforcing mat for the test pile groups.

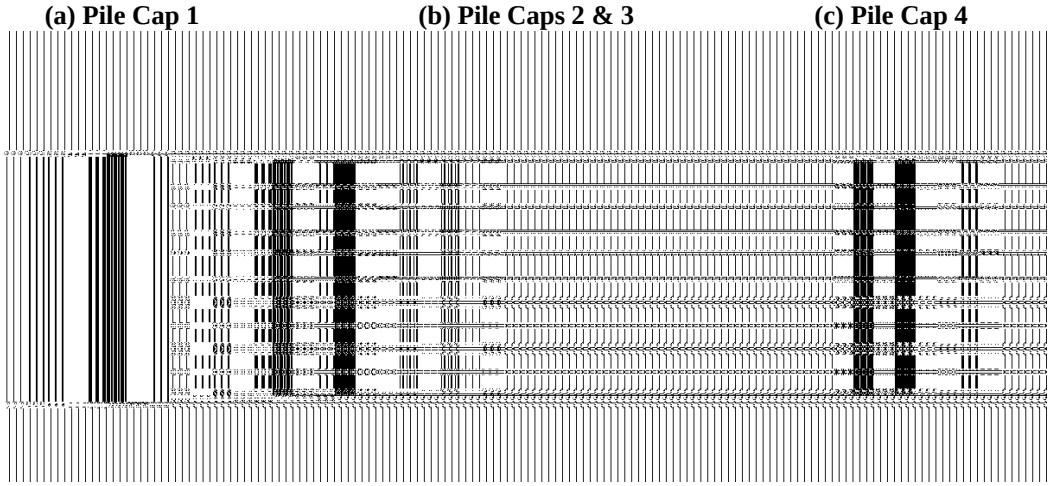

Figure 4-6 Layout of top reinforcing mat for the test pile groups.

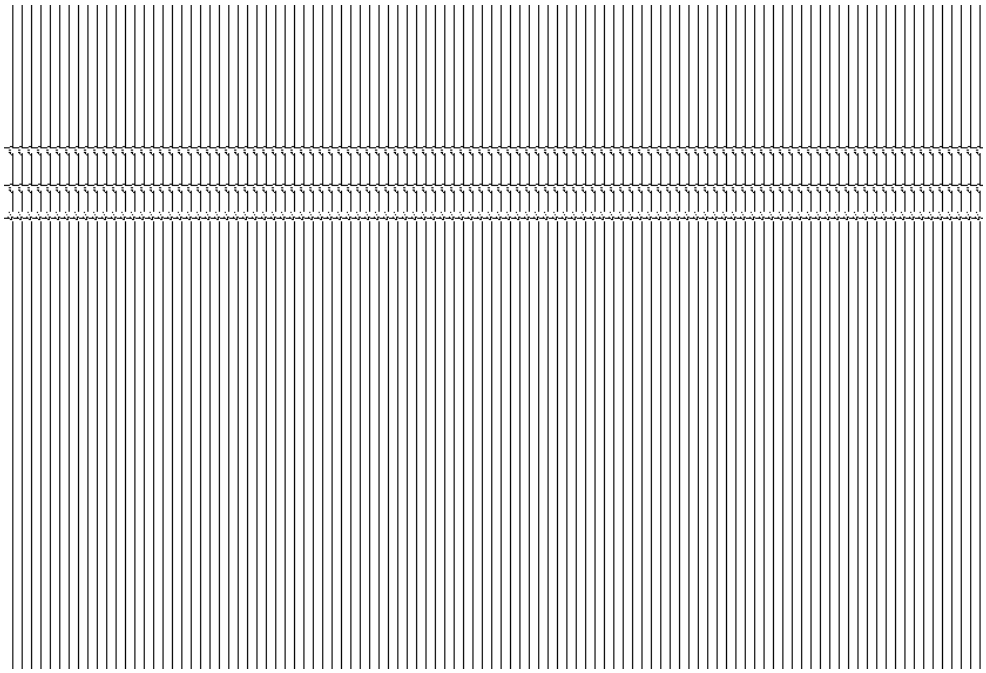

Figure 4-7 Corbel steel layout for caps 1 and 4.

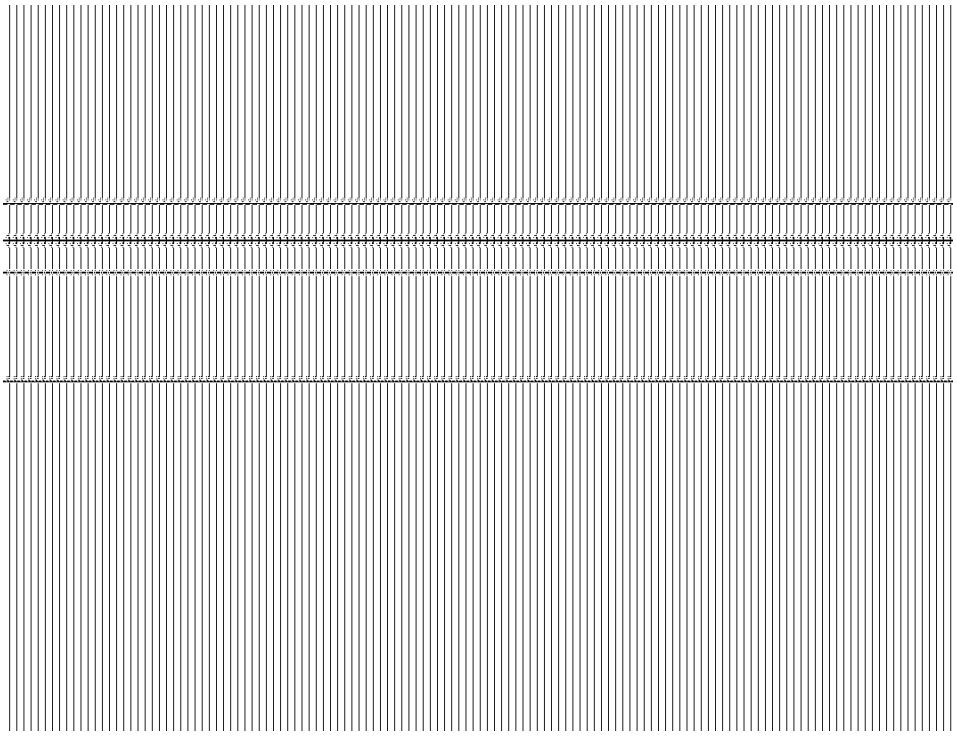

Figure 4-8 Corbel steel layout for caps 2 and 3.

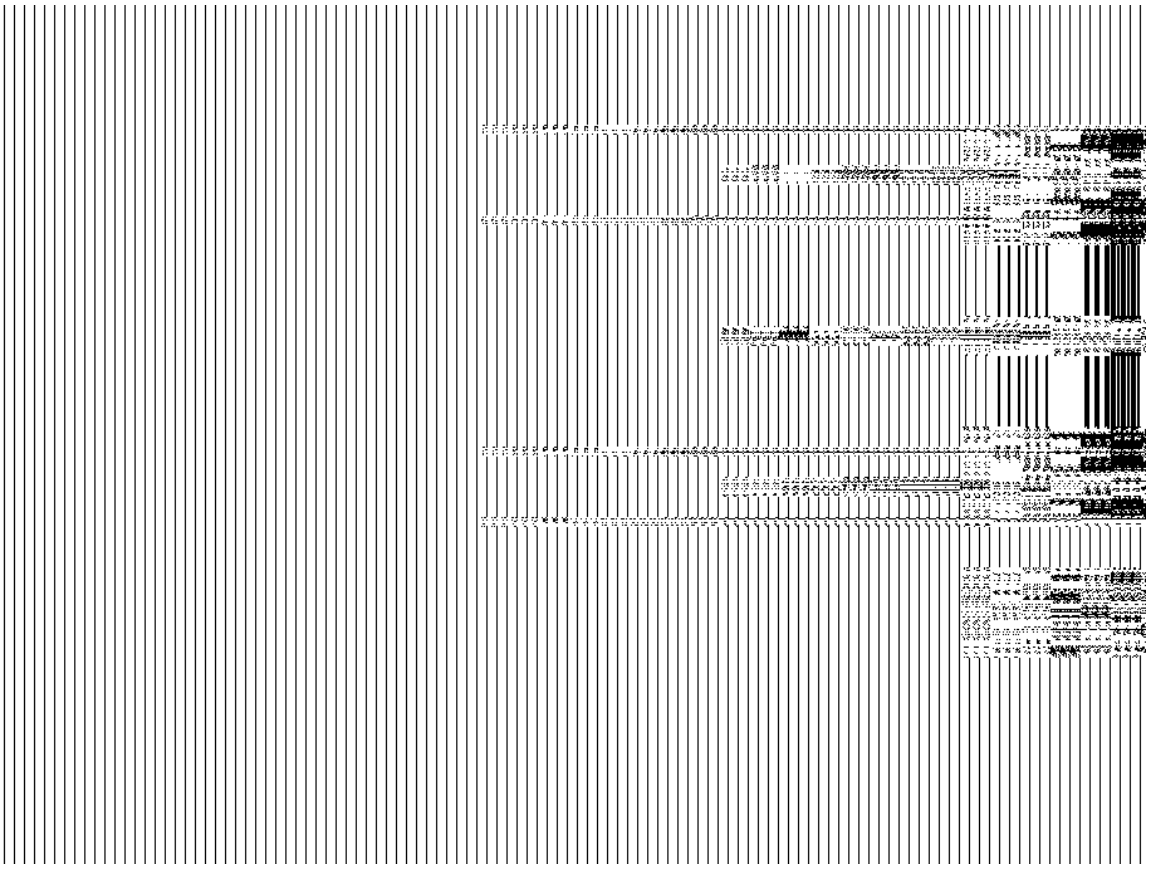

Figure 4-9 View of corbel steel looking at the actuator connection interface.

4.2 Actuator Layout

Most of the tests conducted involved reacting one pile group against another, through applying a lateral load with an MTS actuator with the load centered at a height of 0.92 (11 inches) above the top of the pile cap. Each of the actuators had a capacity of about 600 kips in compression and 450 kips in tension. The pile groups were spaced approximately 32 ft apart edge to edge. This spacing was considered to be large enough to ensure that the volumes of affected soil created by the displacement of each foundation would not significantly interfere with each other. The actuators were fitted with two 8.67-ft extension pieces each made of 8.5 inch outside diameter 69 ksi steel pipe with a wall thickness of 0.75 inches in order to span the distance between the two foundations.

Plates 18x18 inch and 5 inches thick of 36 ksi were welded to the ends of the extensions to connect the extensions to the actuators and the pile caps. The actuators were attached to each corbel using steel tie-rods which extended through PVC sleeves in the corbel and were bolted to the back face of the corbel. The tie-rods were pre-stressed to minimize displacement of the steel during the load tests. A three-dimensional swivel head was located at each end of the actuator to provide a zero moment or "pinned" connection. Each swivel could accommodate ± 5º of pile cap rotation about a horizontal line (pitch) and ± 15º of pile cap rotation about a vertical line (yaw). A photo the actuators and extensions positioned between the two piles caps in the field is provided in Figure 4-10.

Figure 4-10 Photo of actuator setup between caps 1 & 2.

4.3 Instrumentation

Six types of instrumentation were used during the tests: strain gages, inclinometers, shape accelerometer arrays, string potentiometers, actuator pressure

transducer for load measurements, and surface grids to evaluate heave/settlement or crack patterns. As noted previously, the middle piles were instrumented with waterproof electrical resistance type strain gages (Texas Measurements Group model WFLA-6-120-*LT) at depths of 2, 6, 11, and 13.5 ft below the top of the pile. Angle irons (as shown in Figure 4-3) were welded on opposite sides of the instrumented piles to a depth of 20 ft to protect the strain gauges during pile driving.

The strain gauge depths were selected to provide the maximum negative and positive moments along the pile. For a "fixed-head" or "restrained-head" pile the maximum negative moment is expected to occur at the pile-pile cap interface. Preliminary LPILE analyses suggested that the maximum positive moment would likely occur between 11 and 13 ft below the top of the piles. The depths of the strain gages will vary slightly due to the different driving depth of each individual pile. However, the individual driving depth of each pile was carefully recorded so the actual depths of the strain gages could be obtained. Also, some of the strain gages were damaged in the installation process and, therefore, some instrumented piles will not have data for all strain gage depths.

In addition to the strain gages, the north and south middle piles of each pile group were instrumented with inclinometer tubes. These tubes were placed in the center of the piles before they were filled with concrete and ran the entire depth of the pile. After the concrete was poured and cured, the inclinometer tubes served as a means of obtaining the pile and pile cap displacements during testing. Inclinometer measurements were typically performed before testing and then again once the final displacement increment had been reached. Using a standard inclinometer and corresponding data mate, the slope

in the pile was recorded at 2 ft depth intervals. This procedure made it possible to develop displacement vs. depth curves at selected intervals and determine the deflected shape of the pile at the start of each test. Inclinometer readings typically provide displacement measurements with an accuracy of 0.05 inches per 50 readings.

Next to the inclinometer tubes a 1 inch outside diameter PVC pipe was also placed before the concrete was placed. These tubes were fitted with a new measuring technology called a shape accelerometer array manufactured by Measurand, Inc. In addition to the middle north and south piles, the center piles were also equipped with the shape arrays. Each shape array consisted of a 25-ft long flexible waterproof cable which had triaxial micro-electrical-mechanical (mems) type accelerometers embedded at 1 ft intervals. By double integrating the accelerations at each level throughout time, the shape arrays provided real-time displacement vs. depth profiles at 1 ft intervals throughout the entire testing period relative to the initial deflected shape. The shape arrays were designed to provide displacements with accuracy similar to that from an inclinometer. To provide accurate measurements from the shape arrays, a tight fit between the 1 inch PVC pipe and the array must be maintained. To accomplish this, webbing of various thicknesses was inserted along the length of the shape array minimizing any gaps between the array and the PVC pipe. The shape arrays measured displacements in both the X and Y directions. For consistency the X direction was chosen as the direction of loading.

Lateral pile cap displacement was measured using two string potentiometers (string potentiometer) attached to the pile cap at the elevation of the loading point (0.92 ft above the top of the cap) on the east and west sides of the actuator attachment point.

Lateral pile cap displacement was also measured on the back side of each corbel with two string potentiometers attached 0.167 ft (2 inches) and 1.75 ft (21 inches) above the top of the pile cap directly in line with the load direction. Finally, vertical pile cap displacement was measured at two points along the length of each pile cap to evaluate pile cap rotation. Each potentiometer was attached to an independent reference beam supported at a distance of about 6 ft from the side of the pile cap. The diagram in Figure 4-11 shows the locations of the string potentiometer used in the various tests.

Applied load was measured by pressure transducers on the actuator which were calibrated in the laboratory prior to testing in the field. Load data were recorded using the actuator control computer and software.

Grids were painted on the surface area behind the cap being tested. The grid was 12 ft wide by 10 ft long and had grid lines every 2 ft. The grids were surveyed before the test and at the maximum displacement during the test. The grid was also used to map the shear planes that developed during lateral loading.

4.4 Test Procedure

This section describes the general lateral load test procedure used for this series of tests: If there are variations to an individual test it will be noted in their individual section.

Lateral pile group load testing was conducted from July 16 to August 29, 2007. The piles had been in the ground for about one month prior to the first test. Load was applied to the pile caps using the actuator which was powered by a portable pump with a 60 gallon/minute capacity. The pump unit was powered by a portable diesel generator.

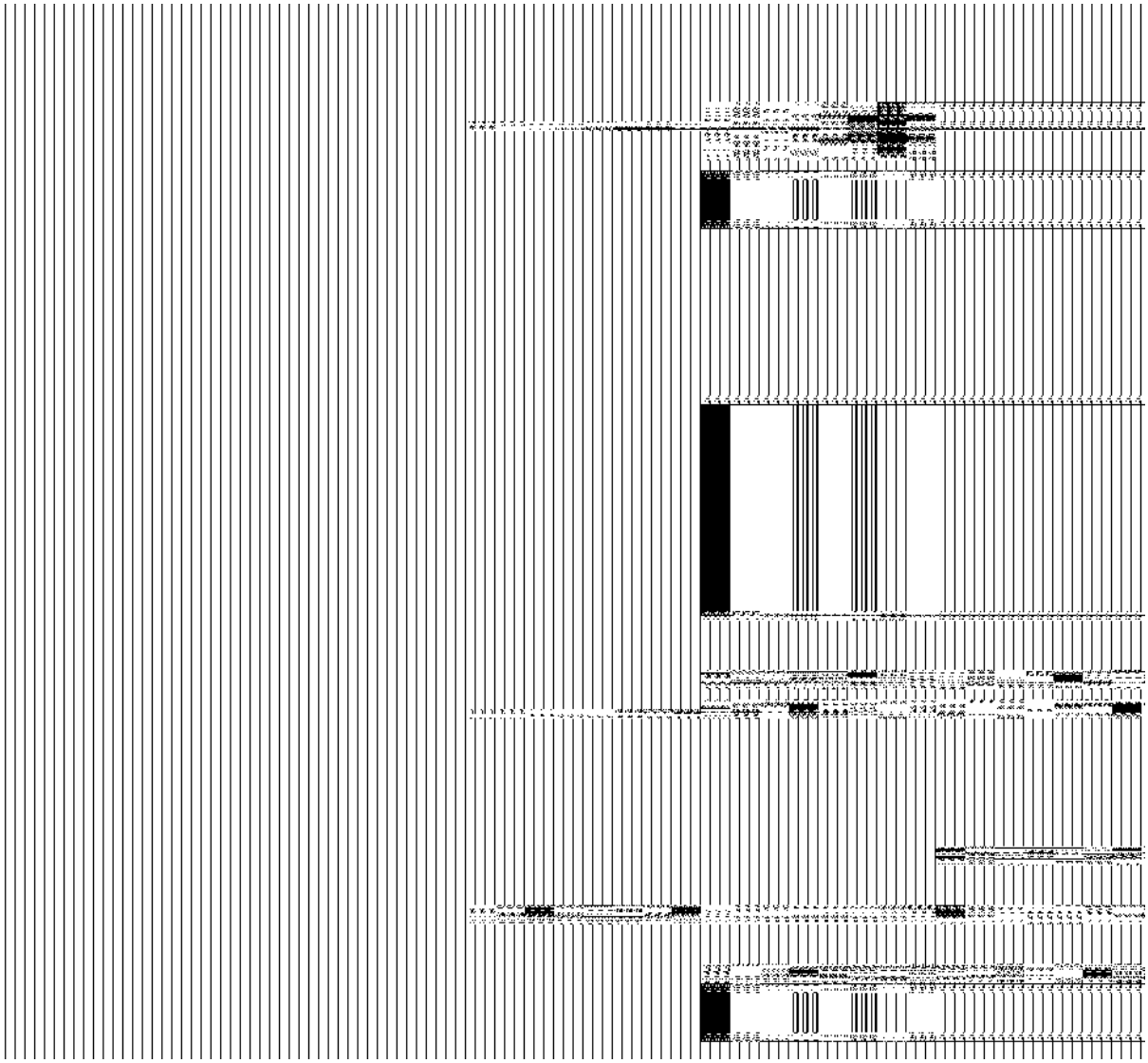

Figure 4-11 Typical instrumentation layout.

The lateral load tests were carried out with a displacement control approach with pile cap displacement increments of approximately 0.125, 0.25, 0.50, 0.75, 1.0, and 1.5 inches. During this process the actuator extended or contracted at a rate of about 1.5 inches/minute. In addition, at each increment 10 cycles with a peak displacement amplitude of about ±0.05 inches were applied with a frequency of approximately 1 Hz to evaluate dynamic response of the pile cap. After this small displacement cycling at each

increment, the pile group was pulled back to the initial starting point prior to loading to the next higher displacement increment. Typically, the testing procedure was paused at the end of the 1.5 inch (final) test increment cyclic portion and held for 20 to 30 minutes while inclinometer measurements were made before ramping back down to zero displacement.

A schematic testing layout for the tests 1, 2, 3, 5, 10 and 12 included in this report is shown in Figure 4-12, Figure 4-13, Figure 4-14, Figure 4-15, Figure 4-16, and Figure 4-17, respectively. The first test consisted of a lateral pull into the virgin clay. The second was a lateral push into the virgin clay, but with the passive force removed by a 1 ft wide excavation to the depth of the cap. Test 3 was a test where the cap was pulled into the native soil with the weaker flowable fill beneath the cap. Test 5 was a push on cap 3 into flowable fill that was beneath the cap and around the piles. Figure 4-19 shows the plan and profile layouts for these tests. In test 10 the untreated clay behind the cap was replaced with a stronger flowable fill and the pile cap was loaded laterally. Test 12 essentially was the same was test 10 only with a 1 ft excavation adjacent to the cap.

4.5 Flowable Fill Properties

For tests 3 and 5 the flowable fill that was place beneath the cap was a very low strength material and only one sample remained intact enough to test. That sample had an unconfined compressive strength of 30 psi. For tests 10 and 12 the material behind the cap was excavated and replace with a stronger flowable fill. This stronger material had an average compressive strength of 137 psi with a standard deviation of 43. The stronger material was placed on August 16, 2007 and the tests were performed on August 24, and

August 29, 2007. The flowable fill only had eight days to cure prior to test 10 and thirteen days to cure prior to test 12. To achieve a result more representative of what the actual strength of the flowable fill was, the samples were only cured seven and fourteen rather than twenty-eight days to determine the unconfined compressive strength.

Table 4-1 shows the unconfined compressive strength as well as the curing time for each specimen tested. The specimens were standard four by eight inch samples. It should be mentioned that there were two batches of flowable fill. Specimens one and two came from the first truck, and specimens three and four came from the second truck.

Table 4-1 Unconfined compressive strengths of the stiffer lowable fill samples

Specimen	Curing Time (days)	Unconfined Compressive Strength (psi)
1	7	77.19
2	14	147.22
3	7	144.83
4	14	179.85

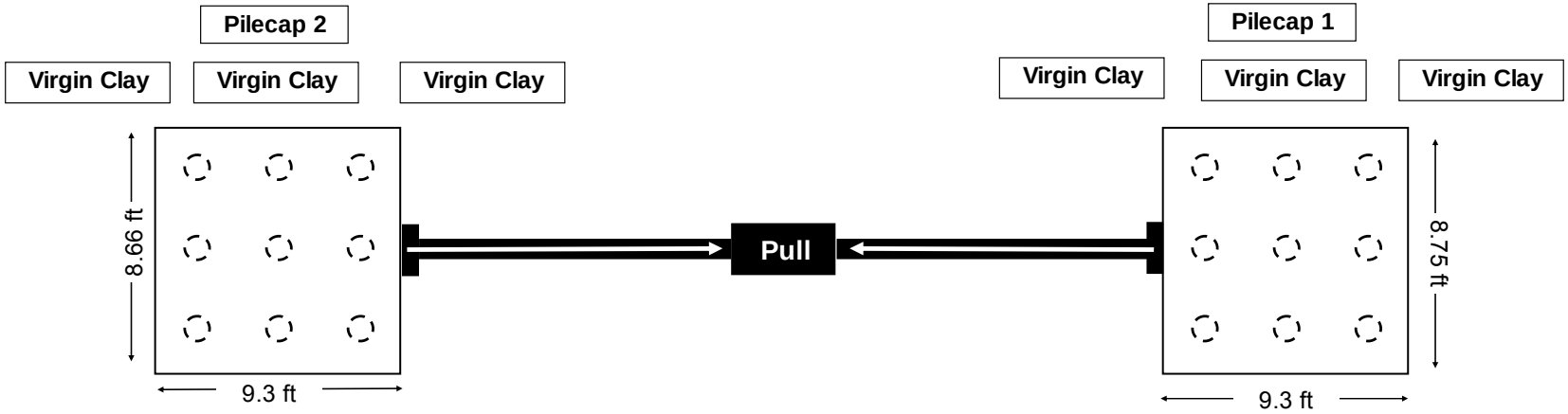

Figure 4-12 Test 1 lateral push into virgin clay.

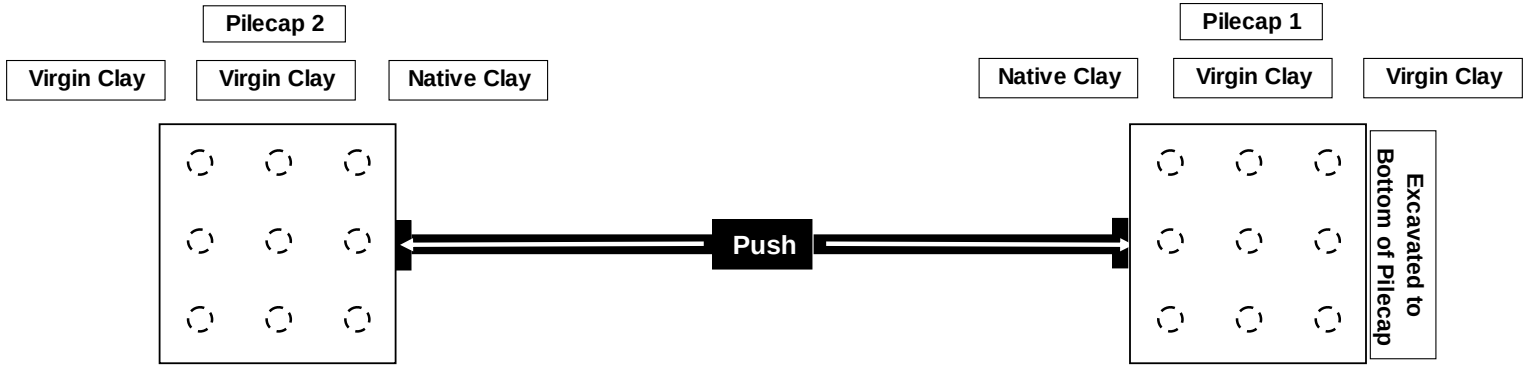

Figure 4-13 Test 2 lateral push into virgin clay with soil excavated adjacent to cap 1 to eliminate passive pressure on the cap.

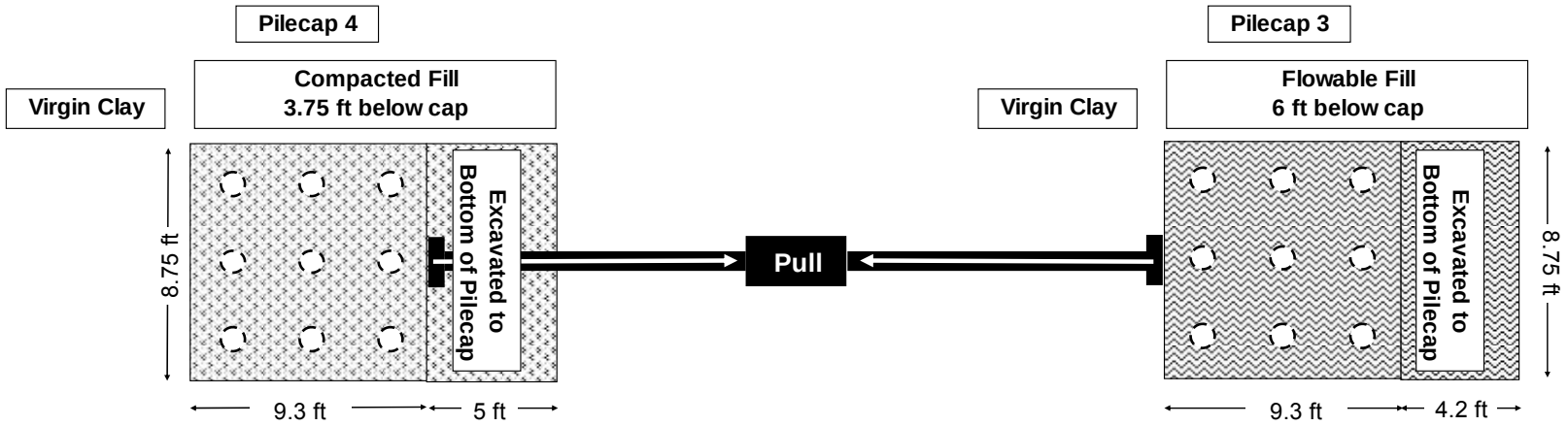

Figure 4-14 Testing schematic for test 3 with the weaker flowable fill beneath the cap.

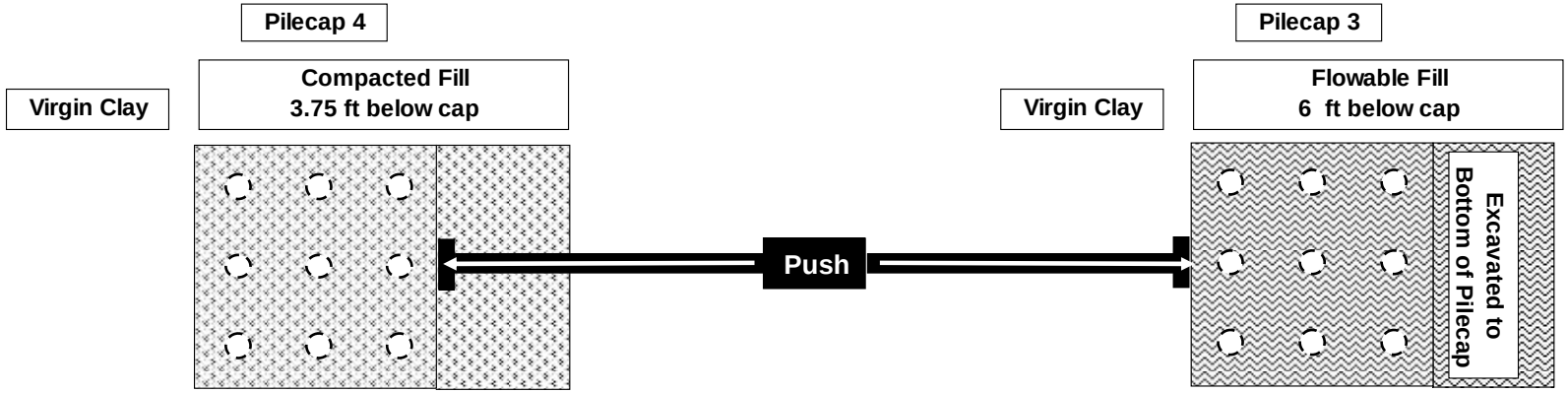

Figure 4-15 Testing schematic for test 5 with the weaker flowable fill beneath the cap.

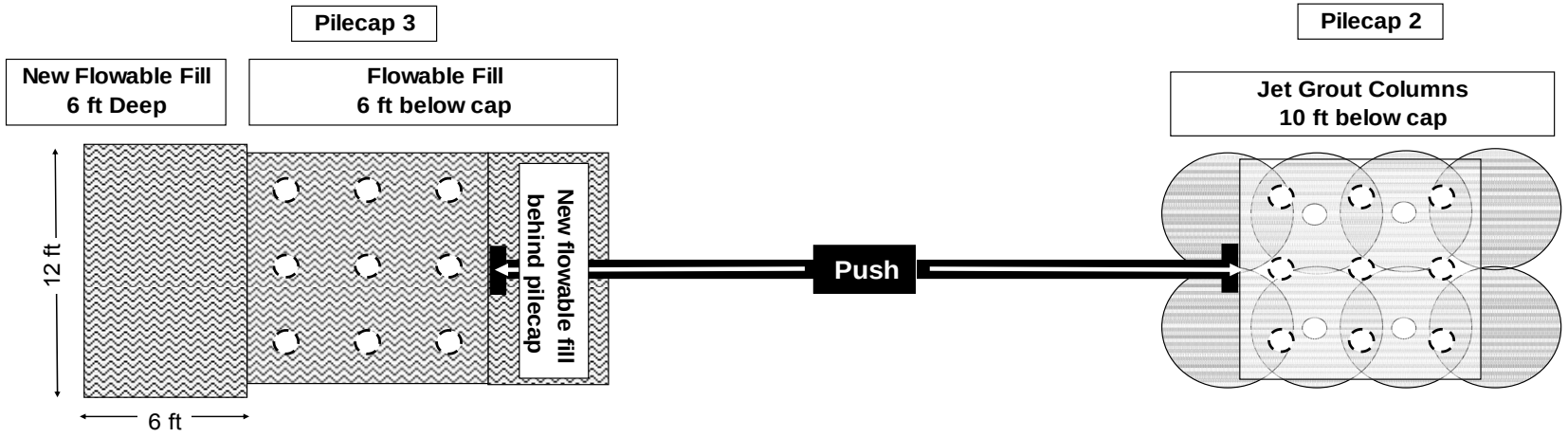

Figure 4-16 Testing schematic for test 10 with the stronger flowable fill behind the cap.

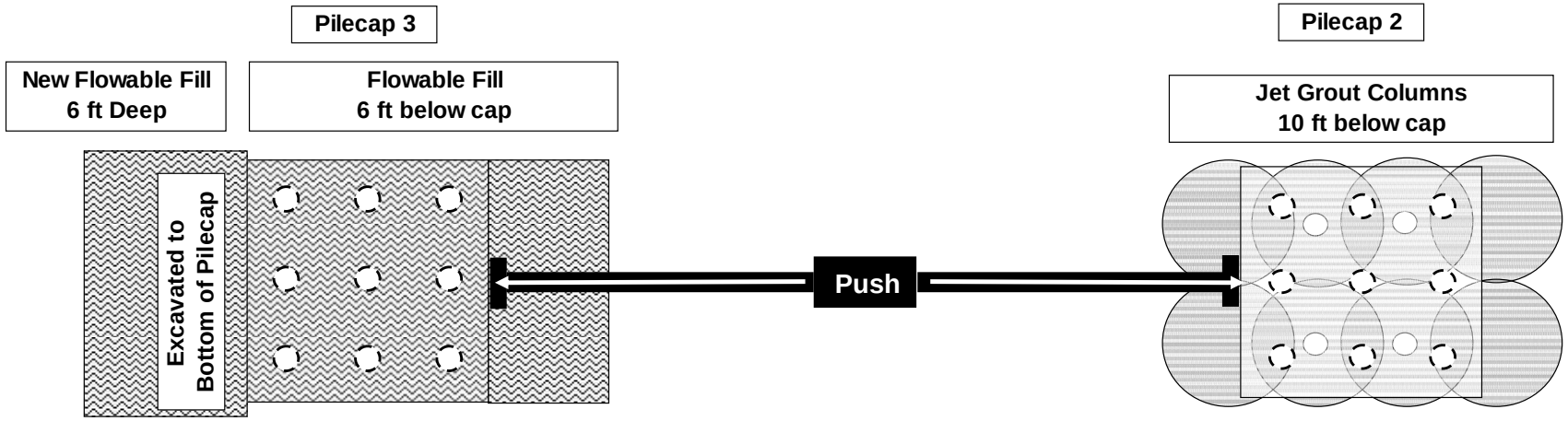

Figure 4-17 Testing schematic for test 12 with the stronger flowable fill behind the cap and a one ft. excavation behind the pile cap.

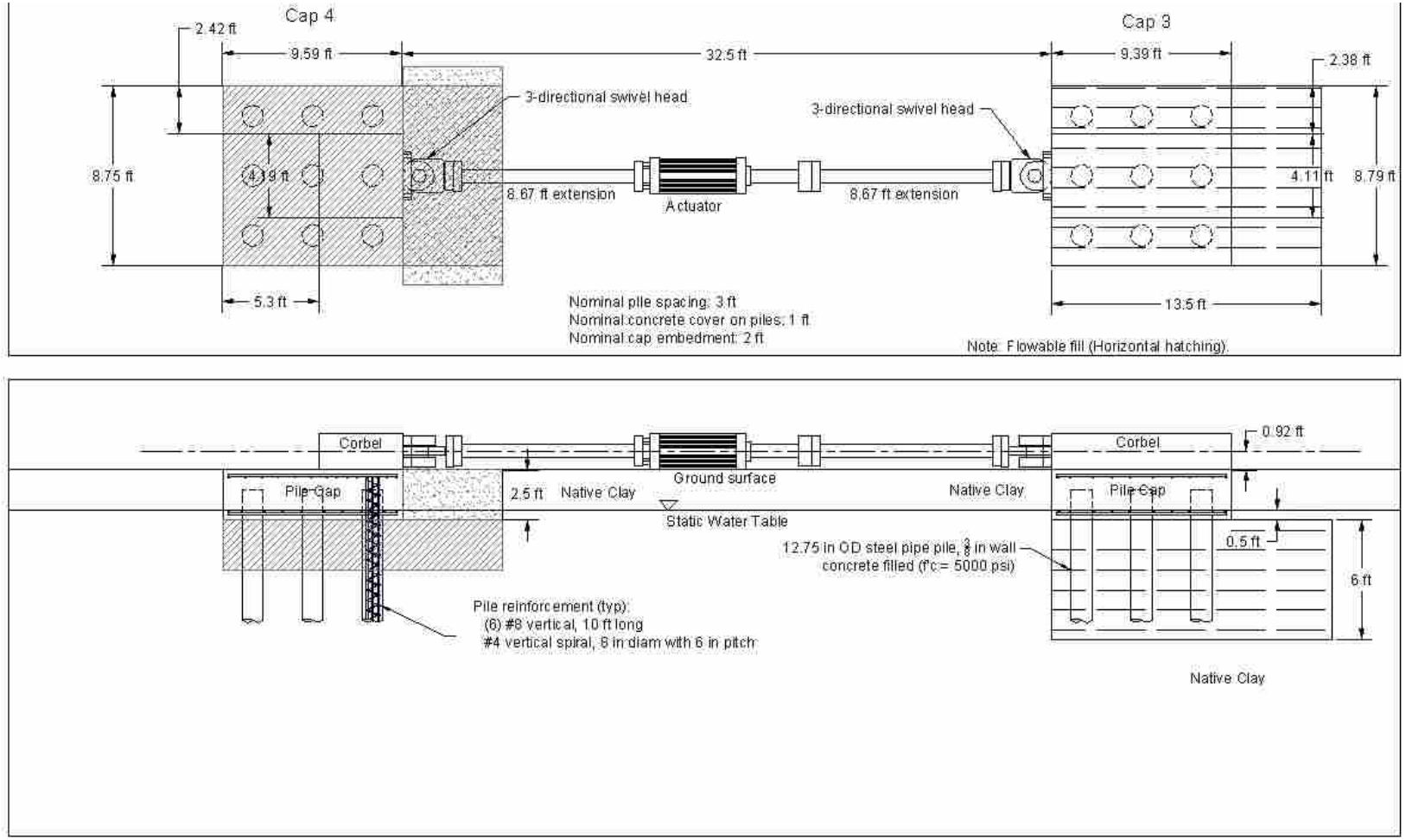

Figure 4-18 Plan and profile views of cap 3 (right) and cap 4 (left) during tests 3 and 5.

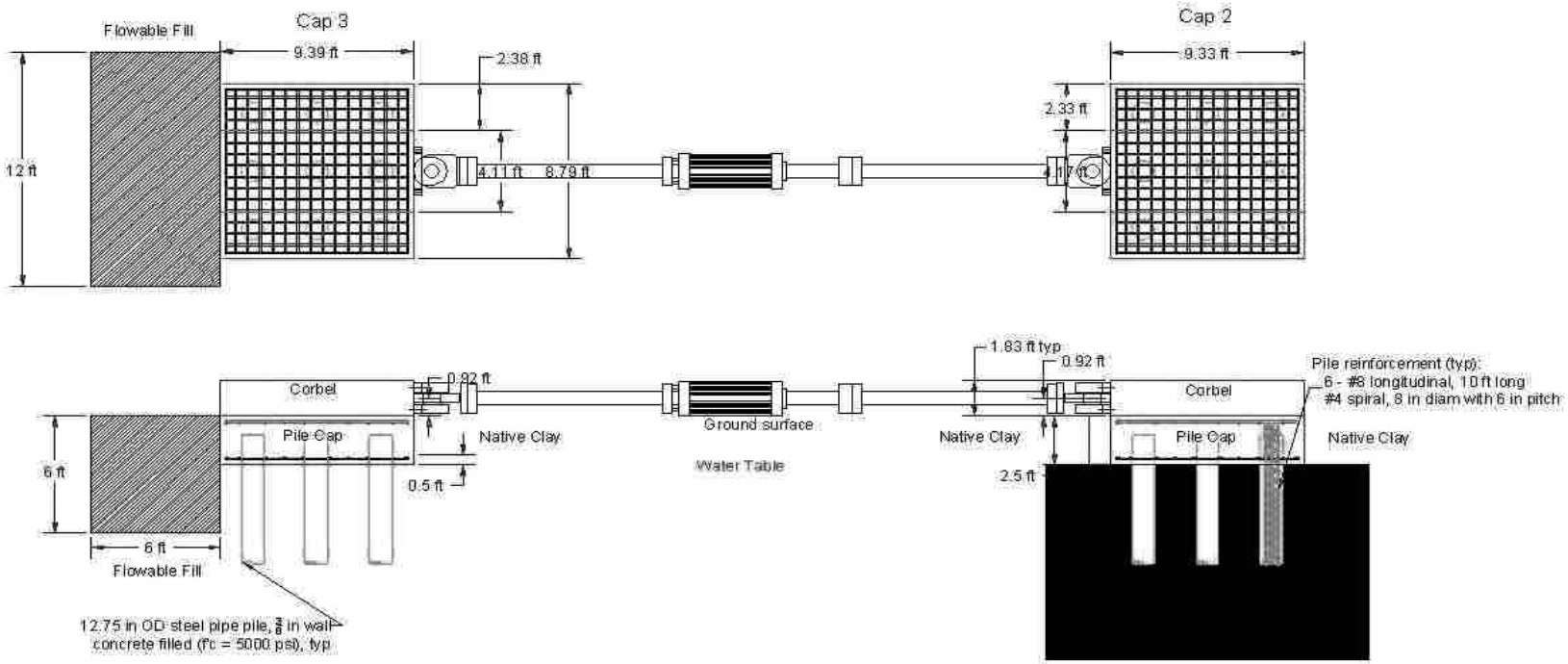

Figure 4-19 Plan and profile views of cap 3 (left) and cap 2 (right) during tests 10 and 12. For dimensions on cap 2 see Adsero (2008).

5 Test Results

The results of the six tests are discussed and compared in this section. The first test (test 1) consisted of a lateral pull into the virgin clay. The second test (test 2) was a lateral push into the virgin clay, but with the passive force removed by a 1-ft wide excavation to the depth of the cap. The third test (test 3) was a lateral pull into the native clay with flowable fill surrounding the piles. The fourth test (test 5) was a push with the flowable fill surrounding the piles however the passive pressure was not present. For the fifth test (test 10) a stiffer flowable fill was placed on the south side of the cap and was laterally loaded. The sixth test (test 12) had a 1 ft wide excavation of the flowable fill to the depth of the cap and was laterally pulled again to obtain the passive results of the flowable fill.

5.1 Virgin Clay Test

The first test was performed on the virgin clay between cap 1 and cap 2, the northern most caps. This particular test involved a lateral pull as shown in Figure 4-12. The objective of this test was to determine the lateral strength of the virgin soil for comparison to later soil improvements.

All instrumentation of string potentiometers, shape arrays, inclinometers, actuator pressure transducer, strain gages, and surface grids were in place and initial

measurements taken prior to the test. The location of all the instrumentation for caps 1 and 2 is found in chapter 4 Test Layout and Procedure. Strain gages on cap 1 were located on the three middle piles, but only on the south and north piles of cap 2. The test followed the standard procedure with one exception. On the 1.5 inch increment test, the pile caps were displaced to that target displacement. Once the displacement was reached, the actuator proceeded into the cyclic test, and then ramped back down to zero displacement and was not held for inclinometer readings. In order to obtain the inclinometer readings for the 1.5 inch test increment an additional reload ramp was necessary from which the inclinometer measurements were taken. Finally, since this was the first test the values measured were all zero set to the initial values of this test just prior to commencement.

5.1.1 Load vs. Displacement Results

Plots of the complete pile cap load vs. displacement curves for cap 1 and cap 2 for the test 1 are presented in Figure 5-1 and Figure 5-2. These curves were obtained from the actuator pressure transducers and the string potentiometers attached to their corresponding cap. These plots provide the load path during loading, unloading and reloading for each cycle. At the end of each loading cycle it was necessary to apply a tensile force to bring the actuator displacement back to zero. This does not appear to be a result of yielding in the pile based on measured bending moments. The behavior could result from a flow of weak soil into the gap behind the pile during loading or lateral resistance due to side shear on the pile as it moves in the opposite direction. During re-loading, the load is typically less than that obtained during virgin loading and

considerably linear. The peak load during reloading is typically about 90% of the peak load during the initial loading. After the displacement exceeds the maximum previous displacement for a give cycle, the load increases and the Load vs. Displacement curve transitions into what appears to be the virgin curve.

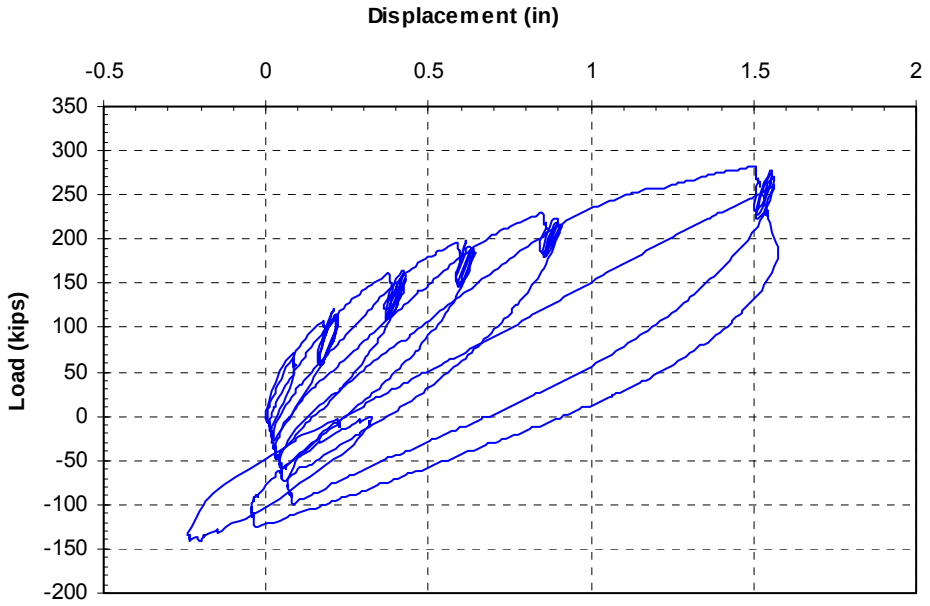

Figure 5-1 Complete load vs. displacement curve for cap 1 during test 1.

The virgin pile head load vs. displacement curves for each pile group are shown in Figure 5-3 by plotting the peak values and eliminating the unload and reload segments. Although the actuator was set to push the caps to target displacement increments of 0.125, 0.25, 0.5, 0.75, 1.0, 1.5 inches, small seating movement and distortions in the actuator during load led to slightly smaller displacements than anticipated. For example, the actual peak displacement increments for cap 1 were 0.08, 0.18, 0.38, 0.59, 0.85, and 1.51 inches respectively. Peak displacement increments for cap 2 were 0.08, 0.19, 0.39, 0.61, 0.87, and 1.48 inches respectively as measured by the corresponding string

potentiometers. Because the increments were arbitrarily selected, these small discrepancies are insignificant.

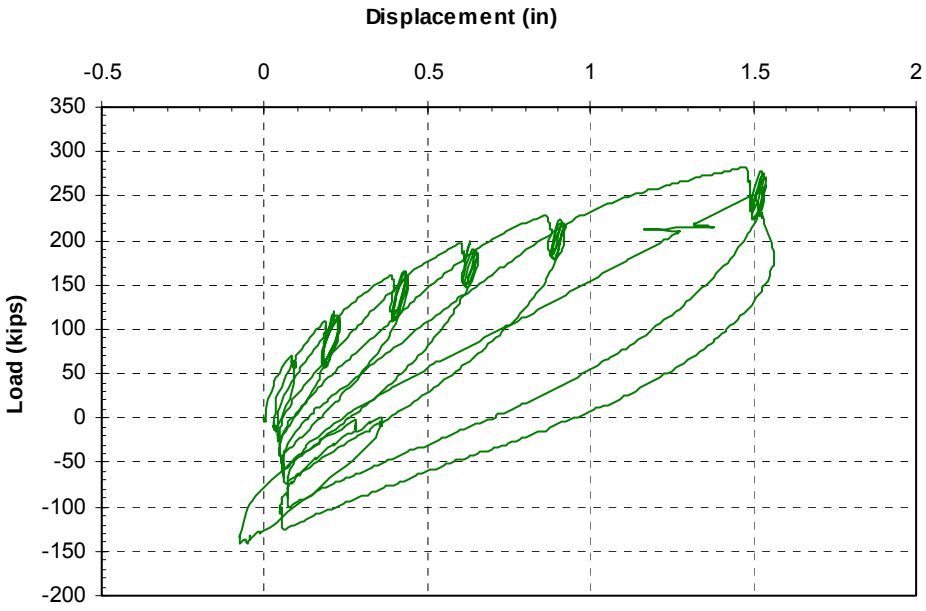

Figure 5-2 Complete load vs. displacement curve for cap 2 during test 1.

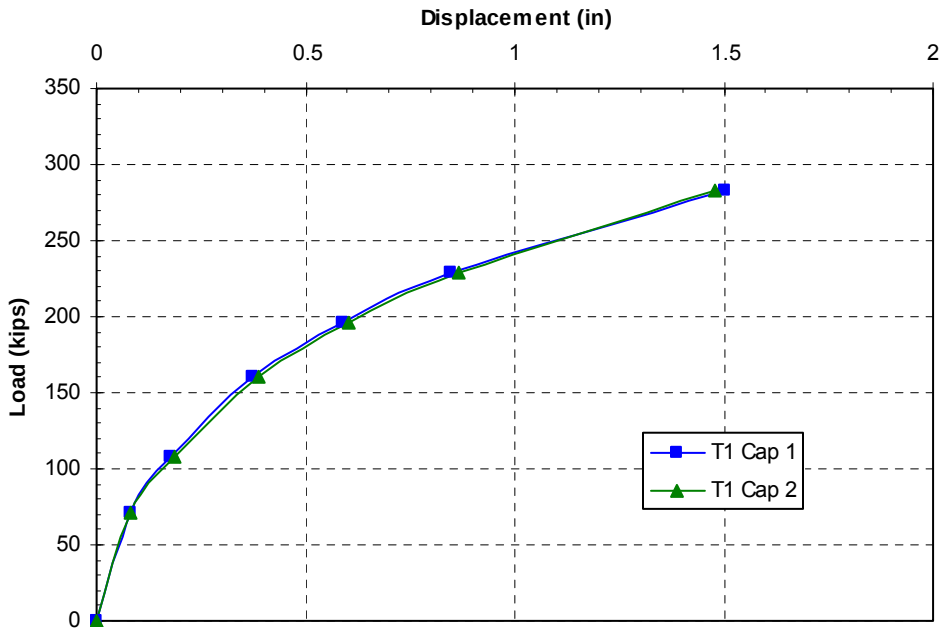

Figure 5-3 Comparison of peak load vs. displacement curves for caps 1 and 2 during test 1.

The curves in Figure 5-3 exhibit the conventional hyperbolic shape that would be expected for a pile in soft clay. However, because the peak displacement was limited to 1.5 inches to prevent excessive moments in the pile, the slope of the load vs. displacement curve never reached a horizontal asymptote. Nevertheless, the last part of the curve is relatively linear suggesting that the lateral resistance is primarily due to the flexural resistance of the pile. The maximum applied load during the last pull was 282.2 kips and resulted in a displacement of 1.50 inches for cap 1 and 1.48 inches for cap 2. For comparison purposes this load of 282 kips at 1.5 inch displacement will be used for the virgin soil.

Despite the fact that the two pile groups were 32 ft apart and had minor variations in construction details, the two Load vs. Displacement curves shown in Figure 5-3 are nearly identical. These results suggest that the soil properties across the site are sufficiently uniform that valid comparisons can be made between the pile caps with various soil improvement techniques relative to the untreated conditions.

5.1.2 Rotation vs. Load Results

Pile cap rotation vs. load curves based on the string potentiometer and shape array measurements for caps 1 and 2 during test 1 are provided in Figure 5-4 and Figure 5-5 respectively. For cap 1 the curves are fairly consistent up to a load of about 230 kips after which the rotation measured from the string potentiometers begins to increase more rapidly with load. At the final load of 282 kips the rotation measured by the different instrumentation differed by 0.1 degrees whereas they only differed by 0.04 degrees or less before the 230 kip loading.

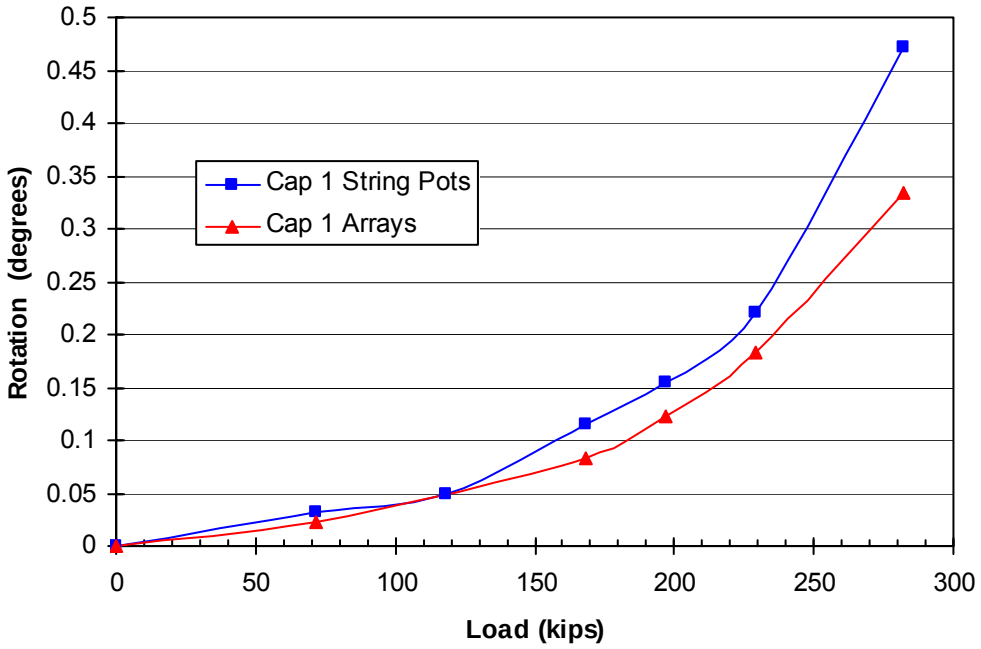

Figure 5-4 Peak pile cap load vs. pile head rotation from the string potentiometers and arrays for cap 1 during test 1.

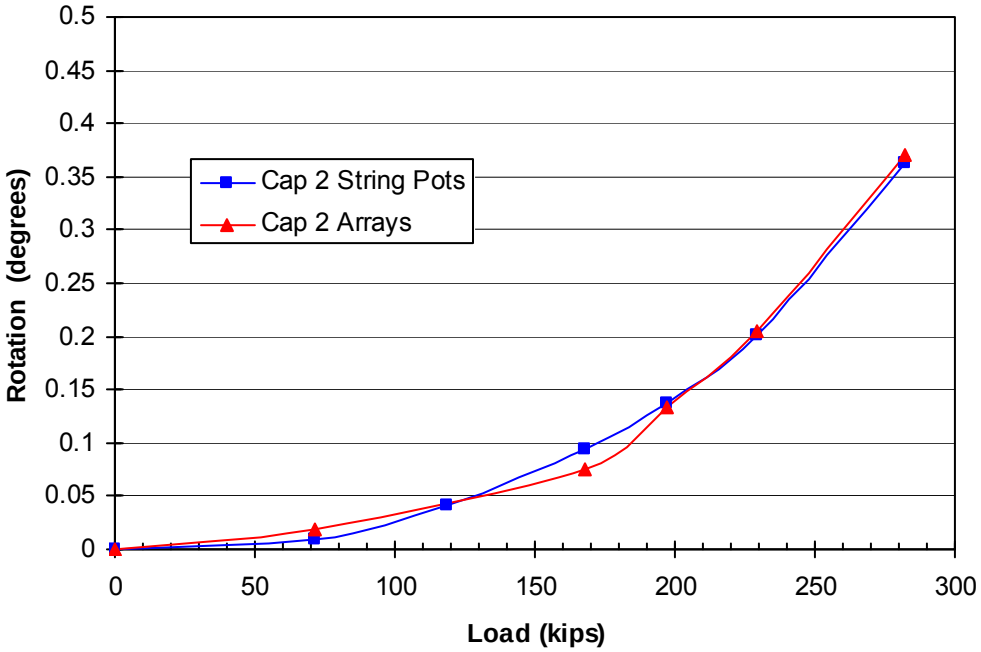

Figure 5-5 Peak pile cap load vs. pile head rotation from the string potentiometers and arrays for cap 2 during test 1.

Cap 2, on the other hand, experiences great agreement between both the string potentiometers and the arrays throughout the test. The curves are fairly linear up to a load of about 170 kips after which the rotation begins to increase more rapidly with load. Measured rotations are fairly consistent for both caps, with the exception of the 282 kip measurement from the string potentiometers on cap 1, which appears to be over estimating the rotation. While pile cap rotation is clearly observed, it is considerably lower than the rotation of the single pile under "free-head" conditions, where rotation is significantly greater.

5.1.3 Depth vs. Displacement Results

The shape arrays and inclinometers were used to record displacement vs. depth profiles in the piles during the tests. The shape arrays recorded continuously during loading and could therefore be used to provide displacement profiles at any instance during the test. In contrast, 15 to 20 minutes were required to make inclinometer measurements on the four instrumented piles at a given displacement increment, therefore, inclinometer measurements were only made initially prior to testing and after the final maximum displacement increment to prevent disruption of the testing procedure. To provide an indication of the accuracy of the downhole measurements, displacements from the string potentiometers at the elevation of the applied load are compared to those obtained from the shape arrays at the maximum load for each loading increment. In addition, displacement profiles from the inclinometers were compared to those from the shape arrays during the 1.5 inch hold portion of the test in which inclinometer data were recorded.

Displacement vs. depth curves obtained from the shape accelerometer arrays in the piles within pile cap 1 and 2 are provided in Figure 5-6 and Figure 5-7, respectively. The average displacements measured by the string potentiometers at the elevation of the load application for each load increment are also shown in these figures for comparison purposes.

Due to a defective array, the data collected from the south (A-142) array on cap 1 were erroneous. As a result, only the center array (A-104) and the north array (A-106) are used to compare to the string potentiometer and inclinometer data. Additionally, the data from A-106 was adjusted for the X direction not being aligned with the direction of loading (using the method discussed in Section 4.3). On cap 2, the south array (A-112) produced erroneous data which will not be presented. Nevertheless, the center array (A-115) and the north array (A-134) provide useful comparisons which are shown in Figure 5-7. Additionally, due to operator error no array data were recorded for the target 0.25 inch displacement increment, therefore this data is missing from the plots in Figure 5-6 and Figure 5-7.

To make a comparison between the arrays and the string potentiometers in Figure 5-6**,** the array data for cap 1 had to be extrapolated to the same depth as the string potentiometers since the arrays terminated at the base of the corbel. To do this, a linear trend line was generated using the measured displacements at depths of 1.83 and 2.83 ft below the top of the corbel and extrapolating 0.92 ft upward to the elevation of the load point At these depths it can be assumed that the array would behave linearly as that portion of the array was enclosed in the concrete pile cap. Using this approach, the pile head displacement obtained from array 106 varied less than 0.05 inch from that measured

by the string potentiometer, while the difference in pile head displacement from array 104 and the string potentiometer varied from 0.1 inches at 282 kips to 0.01 inches at 71.5 kips. Thus, array 106 tends to give more accurate results than array 104 when compared to the string potentiometers on cap 1.

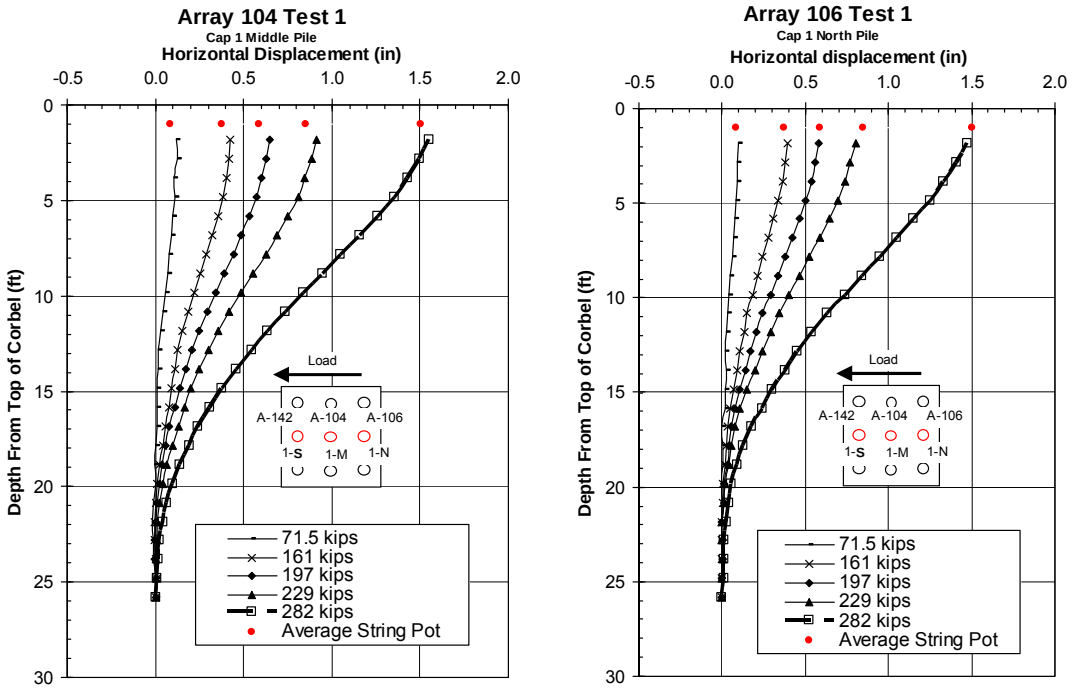

Figure 5-6 Displacement vs. depth curves obtained from shape arrays at several displacement increments for pile cap 1 during test 1. Pile head displacement from string potentiometers are shown for comparison.

The displacements from the arrays on cap 2 showed even greater agreement with those from the string potentiometers as seen in Figure 5-7. For example, in the worst case, pile head displacements from Array 115 in the center pile were less than 0.04 inch different than those from the string potentiometers. Array 134 in the north pile also provided close agreement with slightly higher displacements than the string potentiometers and a difference of only 0.04 inch or less.

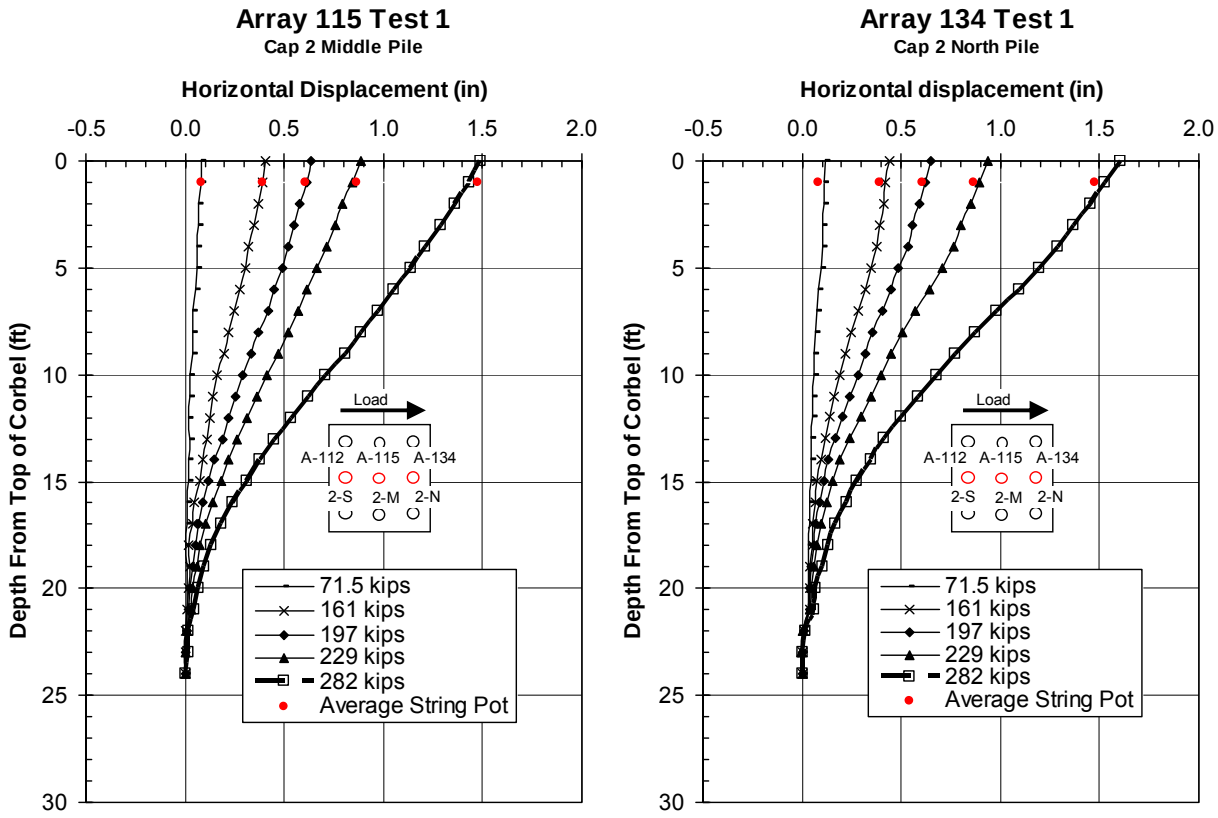

Figure 5-7 Displacement vs. depth curves obtained from shape arrays at several displacement increments for pile cap 2 during test 1. Pile head displacement from string potentiometers are shown for comparison.

Figure 5-8 provides the displacement vs. depth curves obtained from the shape arrays and the two inclinometer pipes in pile cap 1 at the maximum pile head displacement of 1.5 inches. When looking at the inclinometer and array comparison for cap 1, the slopes of the center array (A-104) and the inclinometers are nearly identical from the top of the corbel until about 17 ft below the top of corbel; however, the displacements at the same depths during that same interval vary from 0.17 to 0.14 inches. On the other hand, displacements from array 106 and the north inclinometer vary by less than 0.05 inch with the greatest discrepancy at a depth of 15 ft below the base of the pile cap.

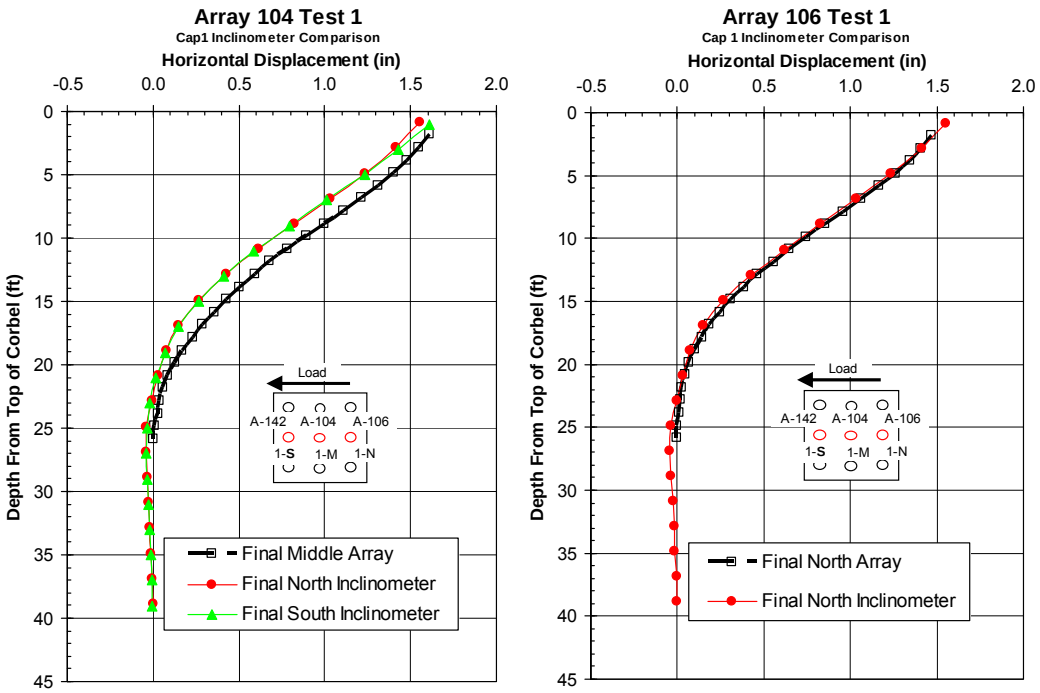

Figure 5-8 Test 1 inclinometer vs. array comparisons for cap 1 at maximum displacement.

One reason for the discrepancies could be due to the fact that the arrays were only 24 ft long whereas the inclinometers ran the entire length of the piles. If there was any displacement in the pile deeper than the arrays could measure, the arrays could not account for that since they were set up to reference displacement from the deepest node. As seen in Figure 5-8, the inclinometers often indicate a negative displacement at depths below the arrays, which could account for some of the discrepancies between the arrays and the inclinometers.

Another reason for discrepancies between the arrays and the inclinometer could be due to the difficulty of getting a tight fit between the shape array and the pipe. If the fit is not tight, the array could move within the PVC pipe housing the array and yield displacements which were different, usually less, than those in the pile. One other consideration for the discrepancies could be the fact that array 104 and the inclinometers

are measuring different piles in the cap. This could account for some small discrepancies, but not to the full degree that is shown by array 104 in this test.

Figure 5-9 show the inclinometer and array data for cap 2. Array 115 shows a slope variance with the inclinometers, which could be due to the fact that it is the middle pile being compared to the north and south piles. Array 134 in the north pile shows almost a perfect match with the north inclinometer only varying by 0.04 inches at its greatest discrepancy.

Overall, the two inclinometer profiles for each cap are remarkably similar in each case. The displacement profiles from the shape arrays are also quite consistent with the profiles from the inclinometers. These results provide increased confidence in the accuracy of the profiles. An overview of the results shows that the piles start to bend at about 23 ft below the top of the corbel. The most significant curvature tends to occur between 21 and 16 ft below the top of corbel, which is an indication to the location of the maximum bending moments.

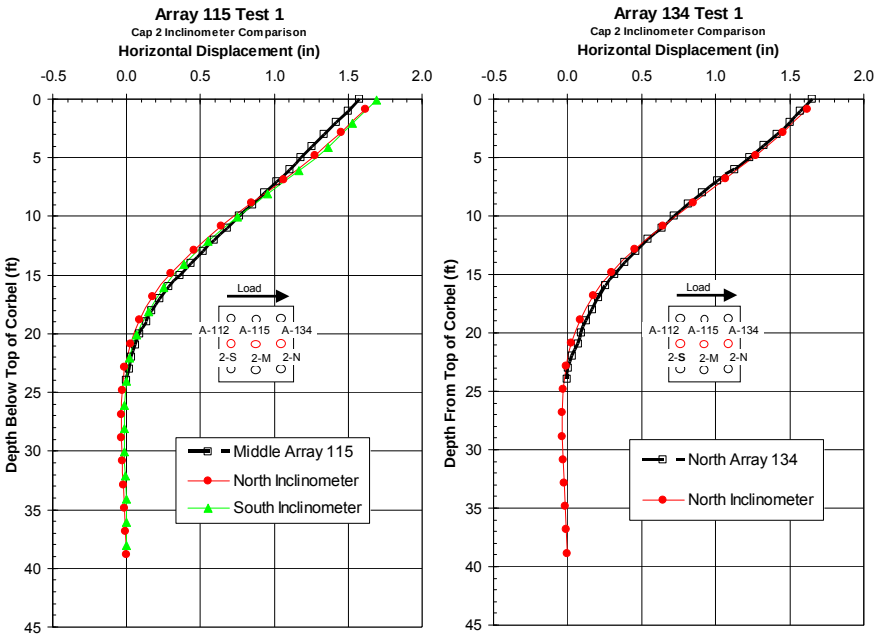

Figure 5-9 Test 1 inclinometer vs. array comparisons for cap 2 at maximum displacement.

5.1.4 Bending Moment vs. Depth

When evaluating the lateral resistance of deep foundations, it is important to know the maximum bending moment and the depth in the pile where it occurs. The bending moment, M, was calculated from the array displacement data using equation 5-1

$$M = EI\frac{\partial^2 y}{\partial x^2} \quad \textbf{(5-1)}$$

where E is the modulus of elasticity, I is the moment of inertia, and $\partial^2 y / \partial x^2$ is the curvature along the length of the pile. This equation can be approximated numerically using equation 5-2

$$M = \frac{EI(f_{-1} - 2f_0 + f_1)}{h^2} \quad \textbf{(5-2)}$$

where f_{-1} is the horizontal displacement one level above the point of consideration, f_0 is the displacement at the point of interest, f_1 is the displacement one level below the point of interest, and h is the distance between displacement measurement levels.

The moment computed using equation (5-2) is very sensitive to minor variations or errors in the measured displacement vs. depth curves. To reduce the influence of minor variances in the measured displacement data on the computed moment, a 5^{th} order polynomial equation was developed based on the measured data to smooth the displacement vs. depth curves. The displacements used in equation (5-2) were then based on smoothed values computed with the polynomial equation. While the difference in the

displacement values at any depth were generally very small, this procedure resulted in more realistic moment vs. depth curves.

As indicated previously, the spacing between the array nodes was 12 inches, which corresponds to the interval h. A composite EI of 14.15 x 10^9 lbs-in^2 for the concrete filled pile was used based on the EI of the steel pile and the uncracked EI of the concrete used to fill the pile. To calculate the EI of the steel pile, a modulus of elasticity of 29 x 10^6 psi and a moment of inertia of 344 in^4 were used. Similarly for the EI of the concrete, a modulus of elasticity of 4.1 x 10^6 psi based off of the 5100 psi unconfined compressive strength and a moment of inertia of 1018 in^4 were used. Additionally, using equation (5-2) a positive displacement will result in a maximum bending moment directly under the cap which will be a negative bending moment.

To complement the bending moments obtained from the arrays, strain gages were also used to derive bending moments. As mentioned before, strain gages were placed at depths of 2, 6, 11, and 13.5 ft below the top of the pile and the top of the piles were driven with approximately 2 ft of stickup. Since piles cannot be driven to precisely to a given elevation, these depths vary to some degree. The bending moments from the stain gages where obtained from the equation

$$M = \frac{EI\varepsilon_{Combined}}{y} \qquad \textbf{(5-3)}$$

where EI is the composite modulus of elasticity and moment of inertia for the pile which are the same values used in the array bending moments equation, $\varepsilon_{Combined}$ is the

difference in strain obtained from the strain gages located opposite each other at the depth of interest, and y is the diameter of the pile or 12.75 inches.

The notation chosen to describe the sign convention of the moments was that a positive displacement of the cap would result in a negative moment at the bottom of the cap. The datum of these graphs was changed to be measured as the depth below the bottom of the pile cap. This was done because once the piles are embedded into the pile cap the EI changes and becomes difficult to estimate with certainty. The negative bending moments calculated at the interface of the piles and pile cap will have some degree of error due to the changing EI. This error is minimized by the fact that the displacements used to derive the bending moments included those that were obtained from within the pile cap. These bending moments were then truncated to the bottom of the pile cap where the EI could be estimated.

Using equations (5-2) and (5-3) with the procedures described above, moment vs. depth graphs were obtained. The curves were obtained from the shape arrays and inclinometer readings while the individual points represent moments computed at the locations of the strain gages. The maximum total load associated with each target displacement is also given.

Figure 5-10 shows the moment vs. depth curves for the center pile of cap 1. Array 104 and the strain gages "measured" the maximum positive bending moment between the depths of 9 to 11 ft below the bottom of the pile cap. The maximum positive moment feom the 282 kip load was between 69 and 72 kip-ft. The strain gages for the middle pile correspond with the array by only varying as little at 1 kip-ft and at most only 7 kip-ft for the positive moments. The negative moments "measured" by the strain gages

in Figure 5-10 tend to be slightly greater than the trend derived by the array. However, if the array were to continue on its trend into the pile cap there would still only be a 10 kip-ft difference or less for all the loads except for the 282 kip load. At the 282 kip load the moment from the strain gage at the bottom of the cap "measured" -79 kip-ft, while the trend of the array would be around -59 kip-ft, thus leaving a wide range as to what the actual magnitude of the negative moment might be.

Bending moments for the north pile were also derived and are shown in Figure 5-11. The only strain gages on this pile that remained operational for the test were at the bottom of the pile cap and 4 ft below. The array "shows" the maximum bending moment occurring between 11 to 13 ft. At the 282 kip load the greatest moment the pile experienced was 73 kip-ft, which is almost identical to the values measured in the middle pile at the same load. The maximum negative moments derived by array 106 tend to be greater than the strain gages if their trend continued to the bottom of the cap. At the 282 kip load the moment from the strain gage at the bottom of the cap "measured" -69 kip-ft, while the trend of the array would be around -80 kip-ft.

There is a notable discrepancy with the data from the north pile for the bending moments at 4 ft below the cap. The array data tends to converge to zero moment at that depth, but the strain gages still show a significant amount of positive moment. In comparing the bending moments of the middle and north piles of cap 1, both have similar maximum positive moments, but the north piles' moments seem to be about 1.5 ft deeper. The maximum negative moments for the strain gages at the bottom of the cap varied up to 10 kip-ft at the maximum load. The arrays vary from -59 kip-ft from the middle pile to -80 kip-ft from the north pile at maximum load of 282 kips. The discrepancies between

the arrays are believed to be due to the different displacements recorded as well as numerical errors resulting from the polynomial fit and subsequent differentiation process, but due to similar slopes, the bending moments still demonstrate similar trends.

Even though arrays are a fairly new technology, moments derived from them compare well to the moments derived from the inclinometer data using the same numerical method. The displacements shown in Figure 5-8 were used to produce Figure 5-12. The maximum positive moment from the inclinometers show a great congruency with only 2 kip-ft difference whereas the arrays differ by about 10 kip-ft. The maximum negative moments are the opposite. The arrays only vary by 2 kip-ft, while the inclinometers vary by 16 kip-ft. The instruments together only varied by 10 kip-ft at 16 ft below the cap, but increasingly deviate further apart as the depth decreases and approach the cap. This provides some evidence that the method used to derive the bending moments is more accurate at greater depths.

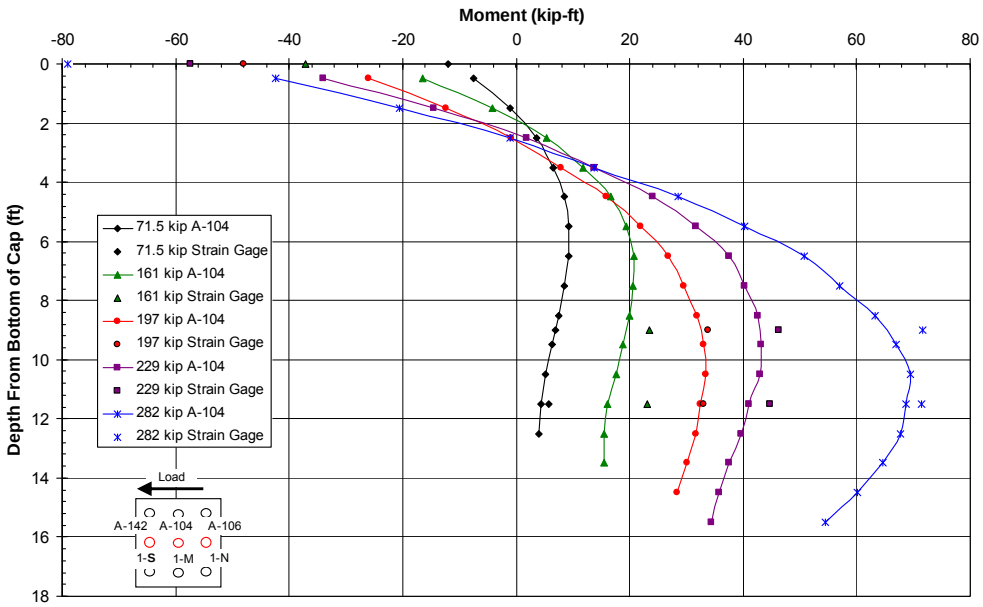

Figure 5-10 Test 1 cap 1 middle pile bending moment vs. depth as derived from the strain gage and array 104 displacement data.

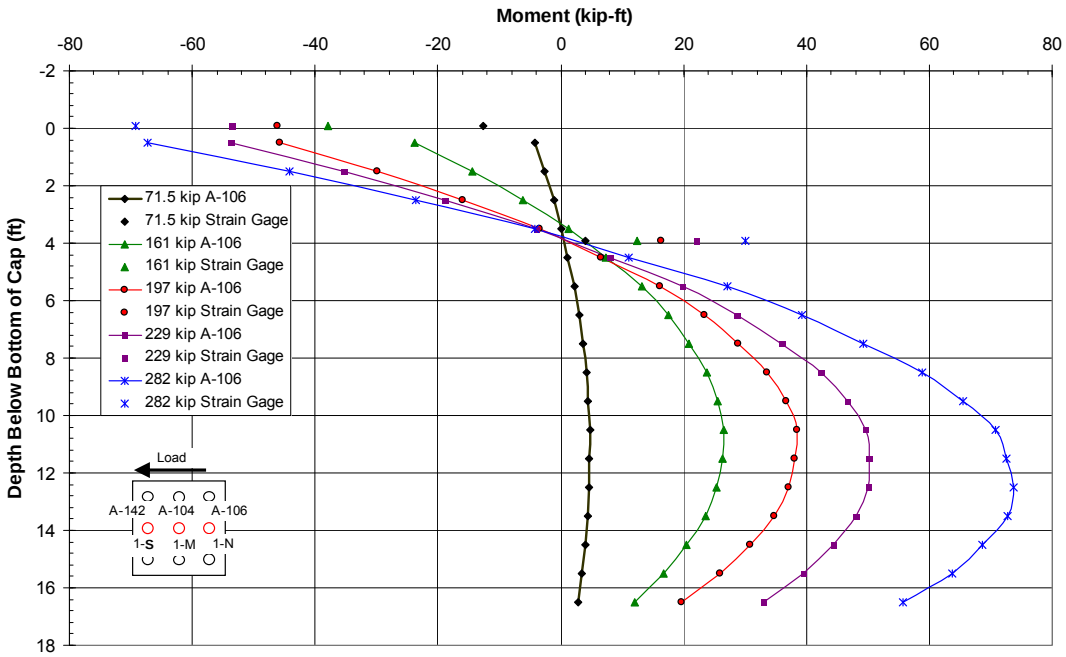

Figure 5-11 Test 1 cap 1 north pile bending moment vs. depth as derived from the strain gage and array 106 displacement data.

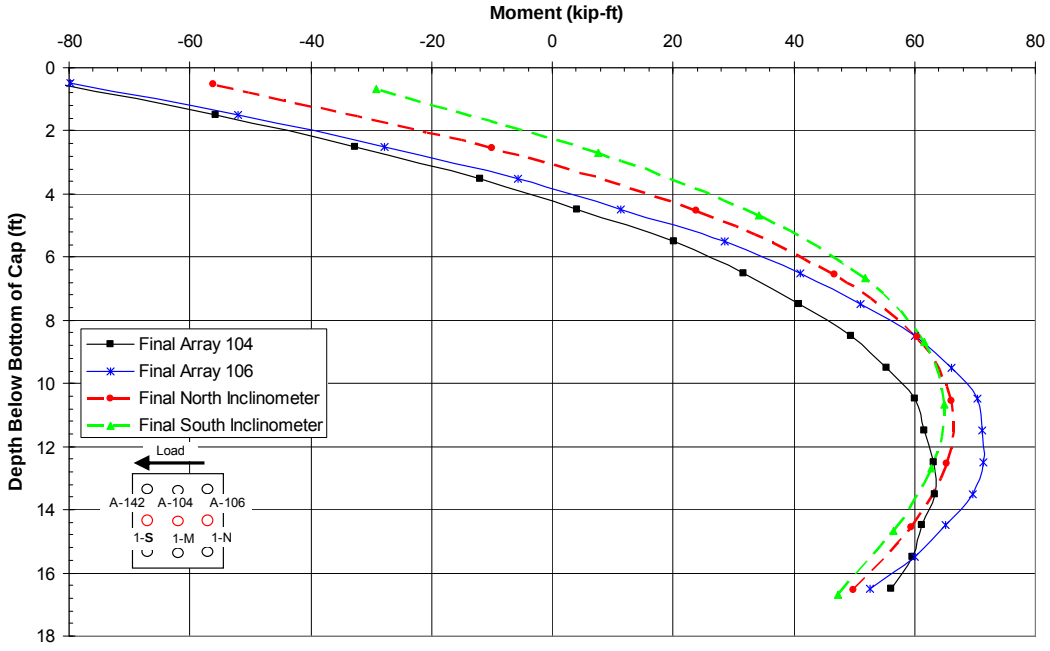

Figure 5-12 Test 1 cap 1 bending moments vs. depth of the arrays and inclinometers at maximum displacement.

Just as bending moments vs. depth graphs were obtained for cap 1, the same analysis was done for cap 2. As mentioned previously, there were no data for the south pile. The middle pile of cap 2 had no strain gages so there is no comparison in Figure 5-13. Maximum positive bending moments in the middle pile appear to occur between 13 and 14 ft below the bottom of the cap, with the greatest moment being 71 kip-ft. The maximum negative moments directly under the cap range from -1 to -33 kip-ft.

The location of maximum positive moments for the north pile of cap 2 occur a little higher than the middle pile ranging between 10.5 and 11.5 ft below the bottom of the cap. The greatest moment in the north pile at the 282 kip load was 69 kip-ft which is comparable to the middle pile. The maximum negative moments for the north pile are slightly greater than the middle pile ranging from -5 to -40 kip-ft, nevertheless, they are still considerably lower than what was measured on cap 1. The strain gage data tend to result in lower moments than that of the shape array by about 15 kip-ft, but still denote the general trend derived from the array's displacements.

The displacements from Figure 5-9 were used to produce Figure 5-15, which shows a greater agreement for the north array and the inclinometers on cap 2. However, the middle array on cap 2 shows a different trend. The maximum positive moment calculated using the inclinometers and the north array are in good agreement with about a 4 kip-ft difference whereas the middle array shows about the same magnitude of bending moment; the difference is in the depth of the moment by almost 3 ft. This gives evidence that the discrepancies in measured displacements, although small, have a great impact on the derived bending moments using the numerical method. The maximum negative moments show a degree of similarity with the north array and the inclinometer. Their

results span a range of about 20 kip-ft, but are still 10 to 12 kip-ft lower than that measured on cap 1. Not much can be discerned from the trend of the middle array's negative bending moments as it had to be truncated due to inconsistencies of the numerical method at depths just below the cap.

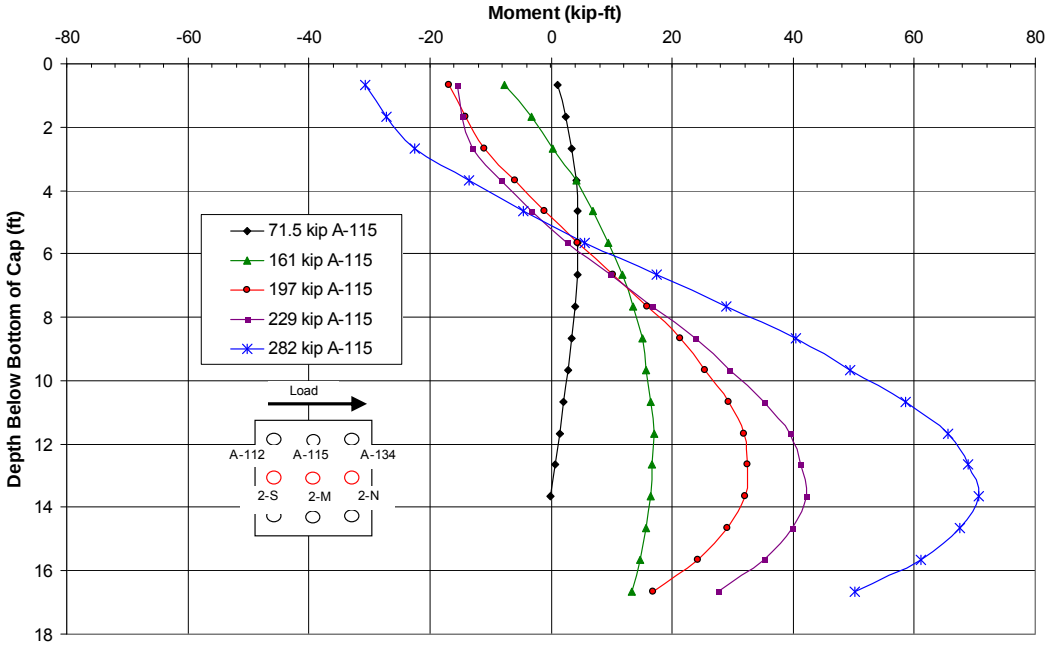

Figure 5-13 Test 1 cap 2 middle pile bending moment vs. depth as derived from array 115 displacement data.

In the final review of test 1, the behavior of both pile caps in the weak virgin clay was consistent. Both caps displaced close to 1.5 inches at a load of 282 kips. The depth vs. displacement comparisons was consistent with the arrays closely matching the string potentiometers and inclinometers with the exception of the middle array of cap 1. The bending moment results also demonstrate fairly consistent behavior with the exception of

the middle array in cap 2. Because the measured behavior on both caps was relatively similar, the following statements can be made regarding the bending moments.

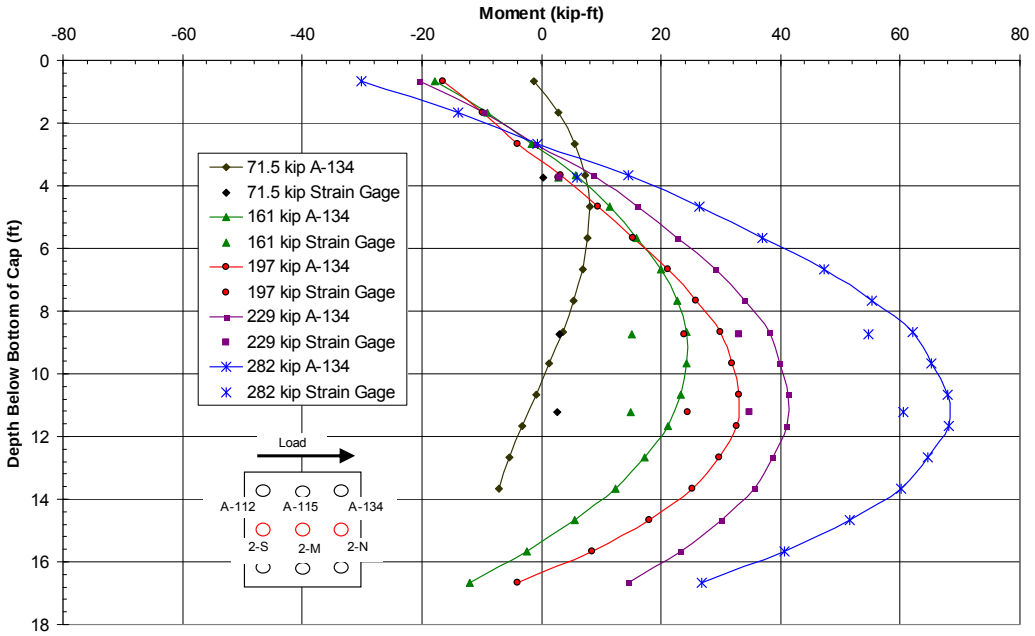

Figure 5-14 Test 1 cap 2 north pile bending moment vs. depth as derived from strain gage and array 134 displacement data.

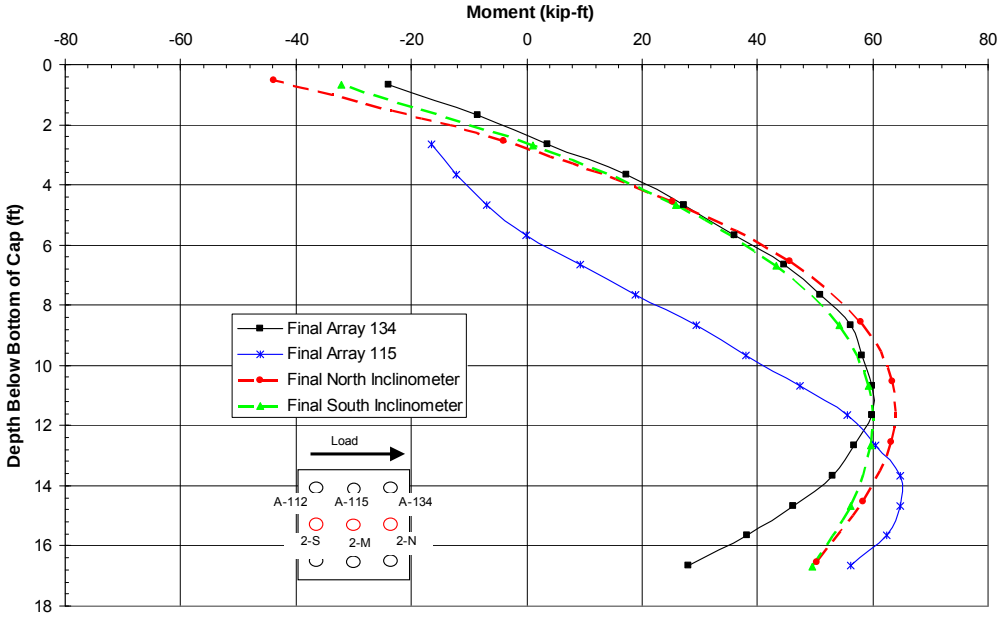

Figure 5-15 Test 1 cap 2 bending moments vs. depth of the arrays and inclinometers at maximum displacement.

The negative bending moment is always greatest at the base of the cap, while the depth to the maximum moment increases from 9 ft to 12 ft below the cap as the pile head displacement increases from 0.5 in to 1.5 inches. Both the maximum negative and positive moments increase as the pile cap displacement increases. The front piles, closest to the load source or actuator, experienced a maximum bending moment at the depths of 10.5 to 11.5 ft below the bottom of the cap, the middle piles at 9.5 to 12.5 ft, and the back piles at 11 to 13 ft. The difference between the array and strain gage measurements resulted in calculated maximum positive moment differences of less than 10 kip-ft. Significant differences were observed for the maximum negative moment calculated from the strain gages and shape arrays.

5.1.5 Moment vs. Load Results

Figure 5-16 and Figure 5-17 shows the maximum positive and negative bending moments vs. applied pile cap load, respectively for cap 1 during test 1. Similarly, Figure 5-18 and Figure 5-19 shows the maximum positive and negative bending moments vs. applied pile cap load, respectively for cap 2 during test 1. Bending moments were computed using data from both shape arrays and strain gauges when available. Initially, the curves are relatively linear; however, the bending moment tends to increase more rapidly with load at the higher load levels as the soil resistance is overcome. The curves from the strain gauges provide relatively consistent moment vs. load curves with little evidence of strong group interaction effects for the displacement levels involved. The agreement between the curves computed by the strain gauges and shape arrays varies.

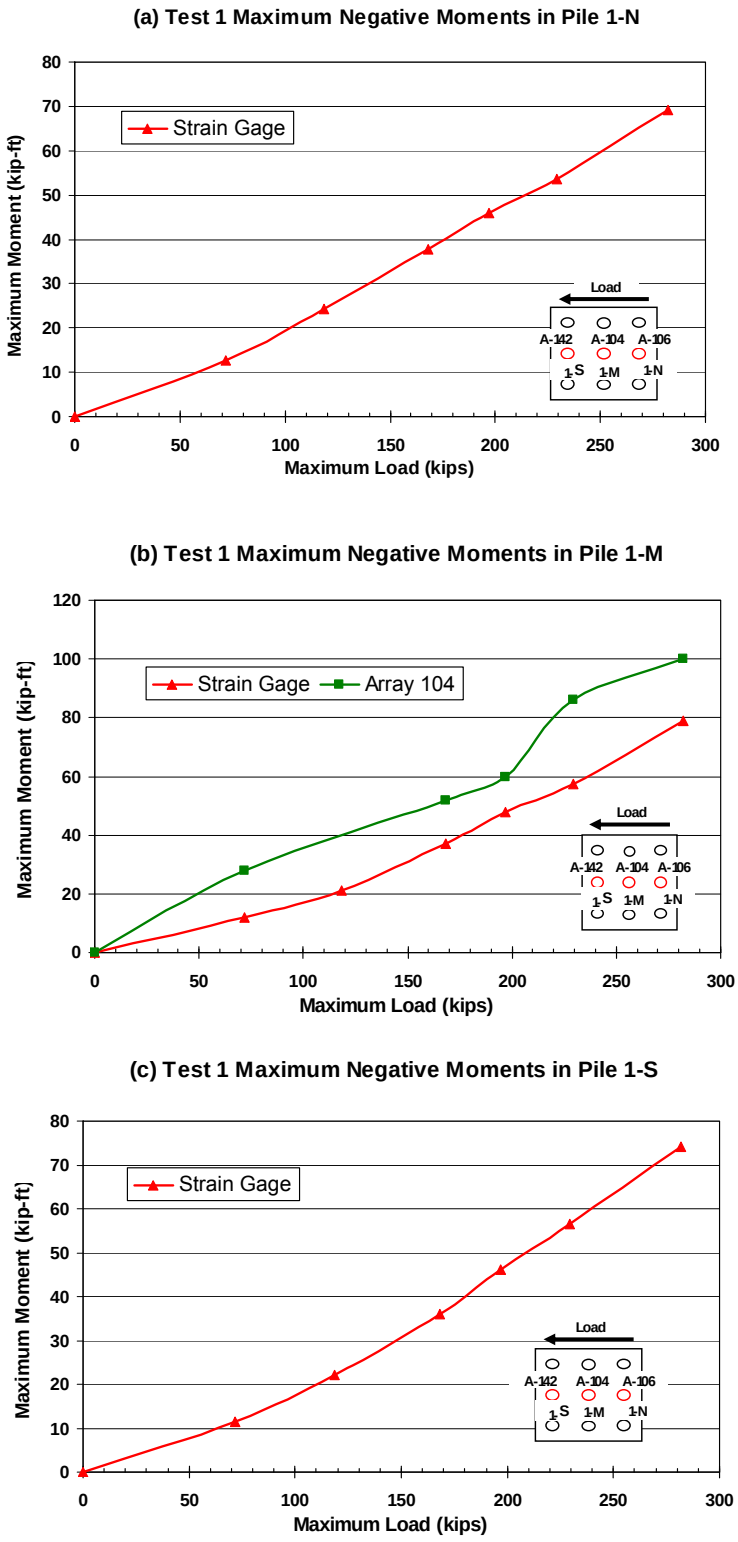

Figure 5-16 Maximum negative moment (base of cap) vs. total pile cap load for piles (a) 1-N, (b) 1-M, and (c) 1-S in cap 1 during test 1.

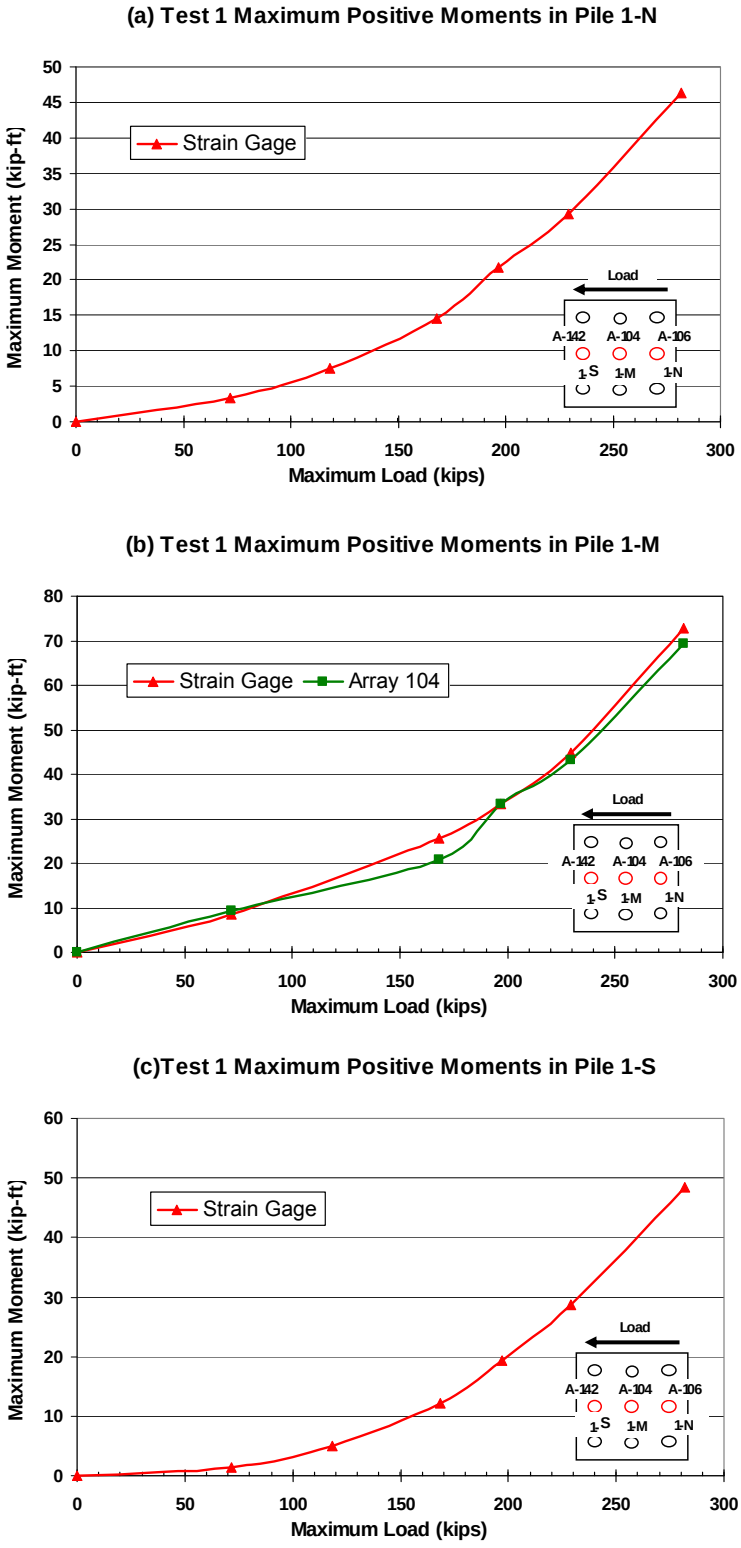

Figure 5-17 Maximum positive moment vs. total pile cap load for piles (a) 1-N, (b) 1-M, and (c) 1-S in cap 1 during test 1.

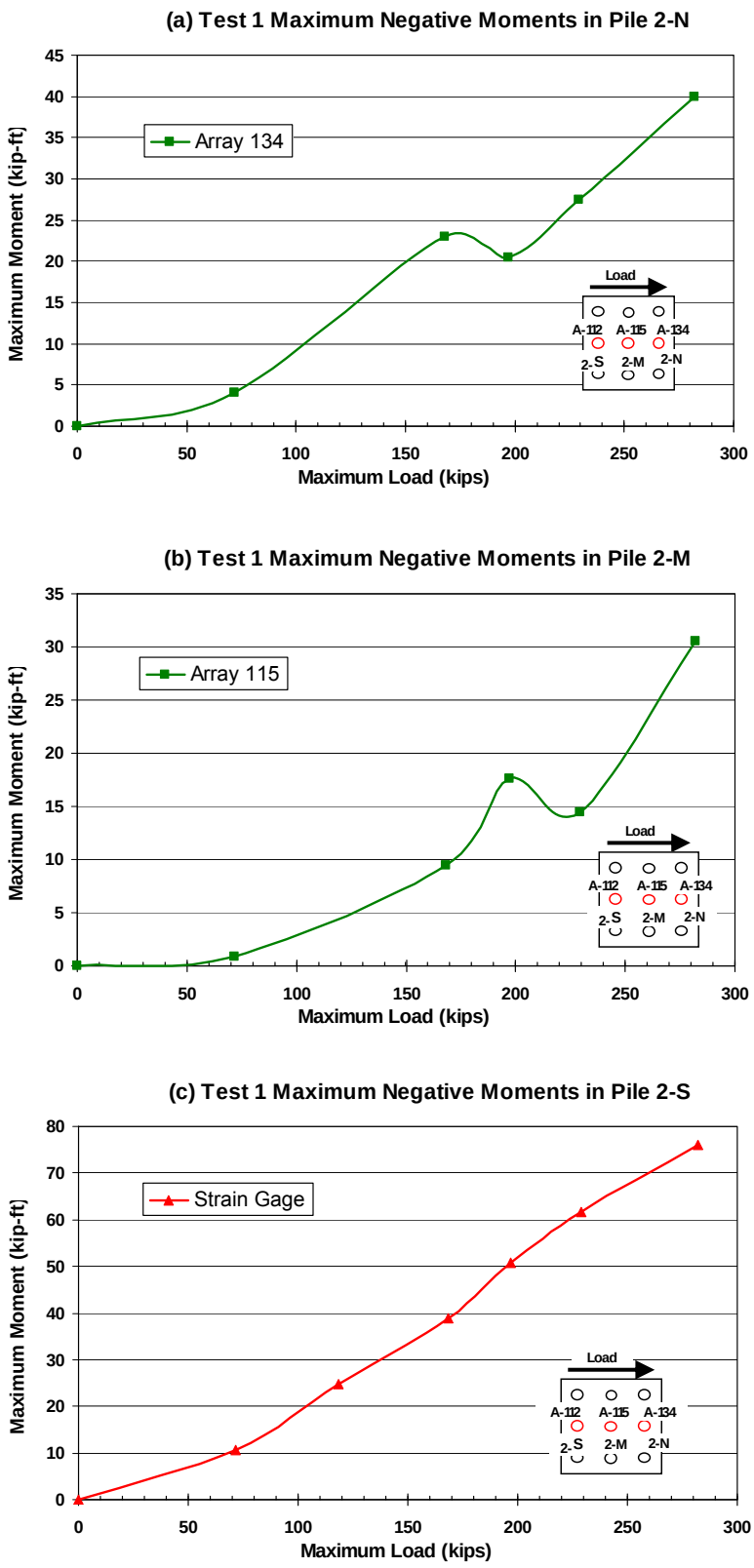

Figure 5-18 Maximum negative moment vs. total pile cap load for piles (a) 2-N, (b) 2-M, and (c) 2-S in cap 2 during test 1.

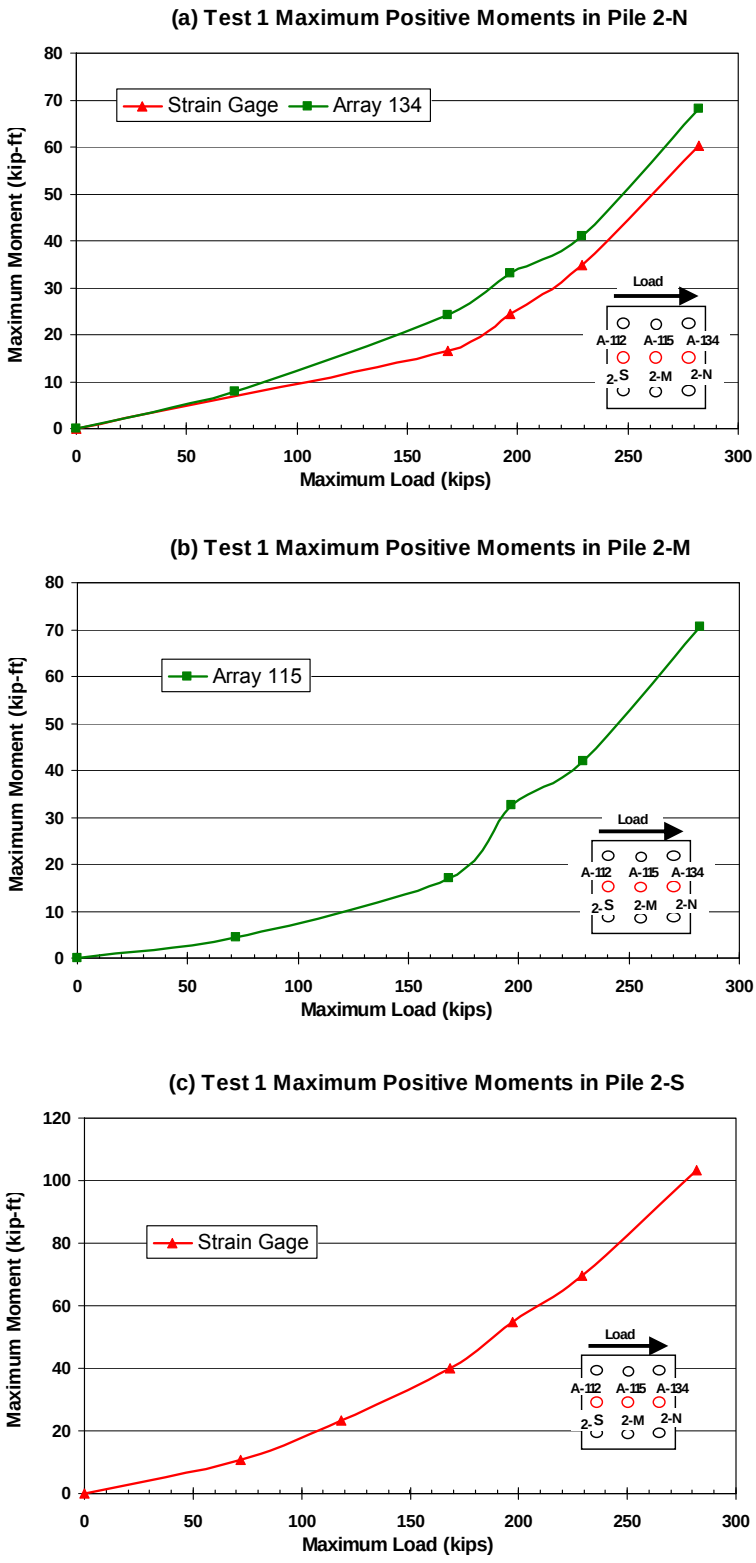

Figure 5-19 Maximum positive moment vs. total pile cap load for piles (a) 2-N, (b) 2-M, and (c) 2-S in cap 2 during test 1.

5.2 Virgin Clay Test without Soil Adjacent to the Pile Cap

After pile caps 1 and 2 were pulled together laterally into the virgin soil, another lateral load test was performed by pushing the two pile caps apart. However, prior to testing, the soil directly behind the pile cap was excavated to the base of the cap to evaluate the decrease in passive resistance. The purpose of this test was to determine how much of the lateral resistance measured in test 1, the virgin soil test, was due to the passive resistance provided by the soil behind the cap. To accomplish this, a one ft wide excavation of the virgin soil along the north face of cap 1 to the depth of the cap was made as shown in Figure 4-13.

The baseline values for the displacements in test 2 were the initial measurements taken prior to test 1. Since test 2 took place after the pile caps had been pulled together in the test 1, there was still some residual displacement once the load was released in the direction of the original displacement. Thus, test 2 started with a negative initial displacement of about 0.3 inches. The instrumentation was in place and was identical to that of test 1. The test followed the standard procedure with one exception: due to the residual gap and initial offset resulting from test 1, the 0.125 inch test increment for test 2 was omitted.

5.2.1 Load vs. Displacement Results

Figure 5-20 and Figure 5-21 provide the complete pile cap load vs. pile head displacement curves for caps 1 and 2, respectively during test 2. Load was obtained from the actuator pressure transducer and displacements from the string potentiometers attached to their corresponding cap. The actuator pushed the caps to target the prescribed

increments of 0.25, 0.5, 0.75, 1.0, 1.5 inches, being referenced to cap 1 rather than cap 2, which was stronger. The actual displacements for cap 1 with the residual offset of -0.27 inches were -0.01, 0.26, 0.48, 0.75, and 1.28, inches respectively. The displacements for cap 2 with the residual offset of -0.32 inches were -0.12, 0.06, 0.19, 0.34, and 0.63 inches, respectively, as measured by the corresponding string potentiometers. These displacements are consistent with expectations as cap 1 had no passive soil resistance directly behind it. Because of the reduction in lateral resistance due to the elimination of passive force on the pile cap, cap 1 displaced 1.28 inches while cap 2 only displaced 0.63 inches.

During reloading, the slope of the Load vs. Displacement curves flattened but exhibited about same shape as the curve for virgin loading. However, at larger displacements there is a change of slope in the re-loading curve indicative of gapping. During reloading, the load at the previous peak displacement typically decreased to between 4% and 10% of the previous peak value. The decrease in lateral resistance was similar for both caps and was also about the same as that observed for test 1. As displacements increase beyond the previous peak displacement, the Load vs. Displacement curve appears to rejoin the virgin curve. After the peak load for a given increment was reached, the actuator pulled the pile caps backward to reach the original actuator position. In most cases, this required some tensile force because of movement of the soft soil into the gap behind the piles created during loading. Because of differences in the lateral resistance in the two caps, there was some residual displacement at the end of each load cycle even though the actuator returned to its original position.

Figure 5-22 provides the maximum Load vs. Displacement curves for caps 1 and 2 during test 2. It is evident the softer behavior of cap 1 where the passive force behind cap 1 had been removed. Figure 5-23 provides the Load vs. Displacement curves for caps 1 and 2 during tests 1 and 2. The Load vs. Displacement curves for test 2 have been shifted right 0.15 inch to account for the apparent flow of the soft clay into the gap between the soil and pile cap that occurred when displacing the pile cap in the opposite direction. When this minor adjustment in displacement is made, the curve for cap 2 matches the curves for caps 1 and 2 during test 1 at larger displacements as would be expected. A comparison of Load vs. Displacement curves for cap 1 with and without passive soil force acting on the pile cap can then be made. Assuming zero passive force at zero displacement and then obtaining the difference between the Load vs. Displacement curves for cap 1 with and without passive force at displacements for 0.25, 0.5, 0.75, 1.0, and 1.5, inches Figure 5-24 was obtained. Thus, based on the curves in Figure 5-23, the passive force vs. displacement curve shown in Figure 5-24 has been developed which indicates that the full passive force of approximately 50 kips was essentially developed by a displacement of about 0.75 inches.

5.2.2 Rotation vs. Load Results

Pile head load vs. rotation curves obtained from string potentiometer and shape array measurements for the pile caps 1 and 2 during test 2 are provided in Figure 5-25 and Figure 5-26, respectively. Because of the initial negative offset, the pile caps had a slight negative rotation at the start of the test. As load increased, the rotation shifted to a positive value.

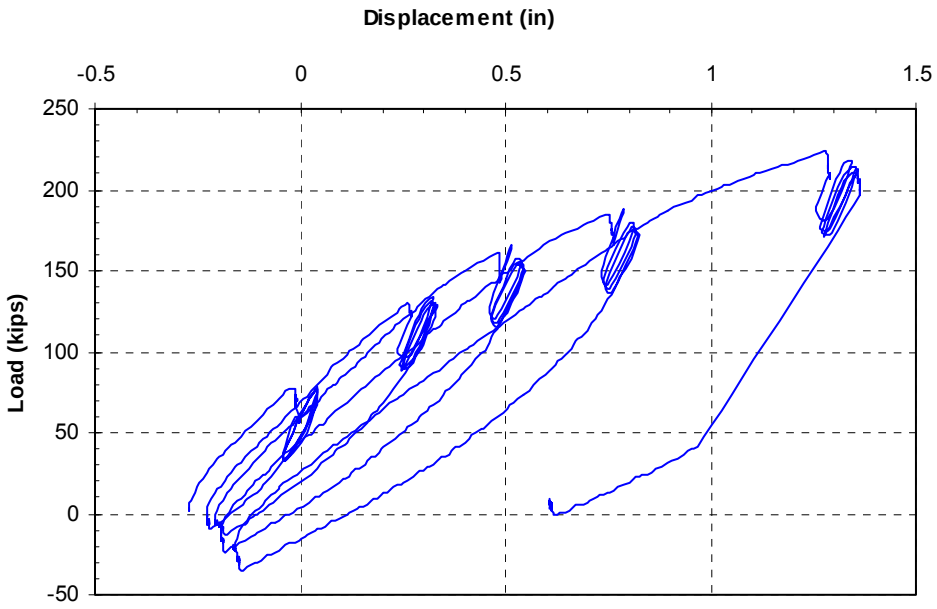

Figure 5-20 Complete pile cap load vs. pile head displacement curve for cap 1 during test 2.

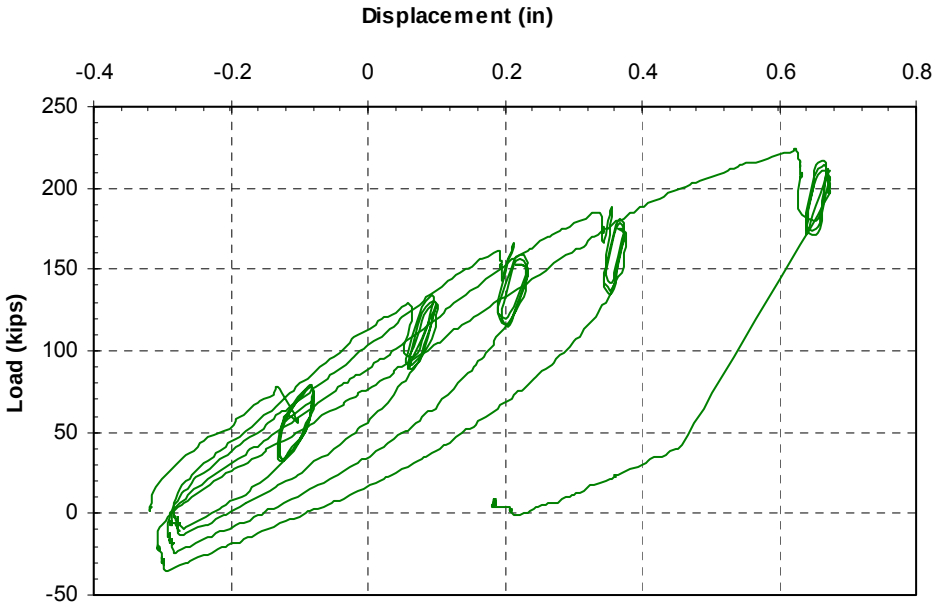

Figure 5-21 Complete pile cap load vs. pile head displacement curve for cap 2 during test 2.

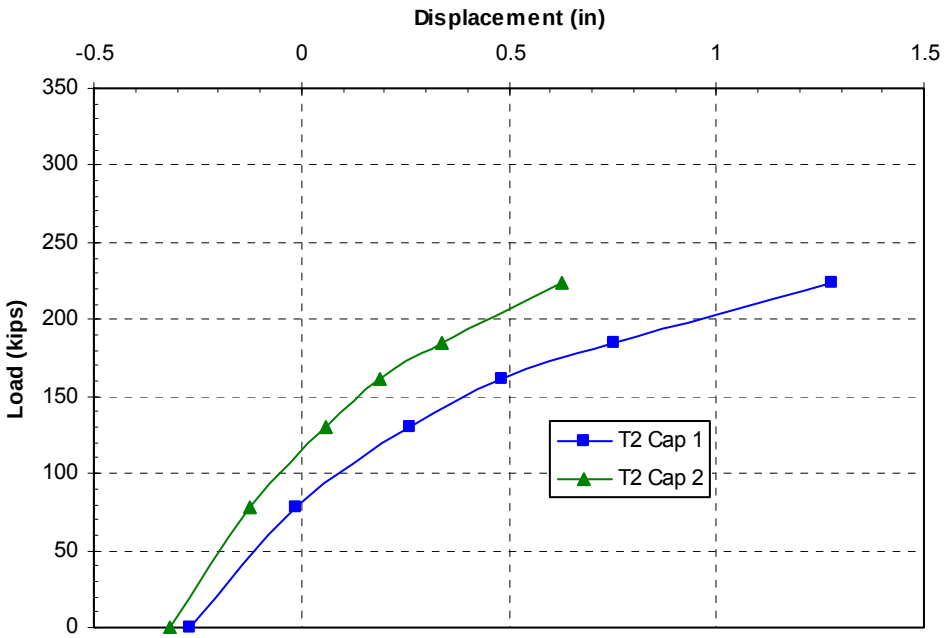

Figure 5-22 Peak pile cap load vs. pile head displacement curves for caps 1 and 2 during test 2.

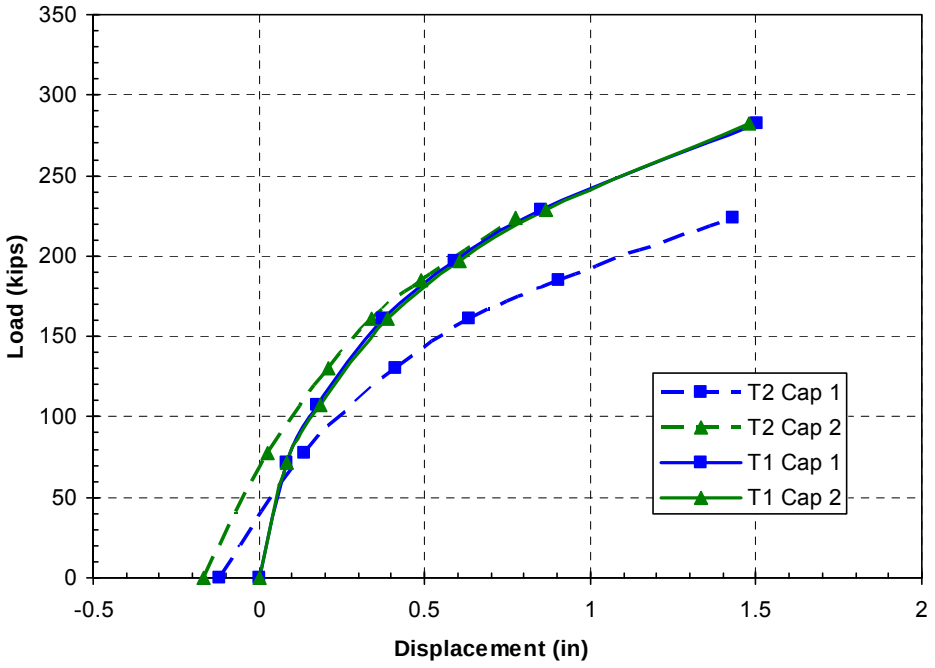

Figure 5-23 Comparison of peak pile cap load vs. pile head displacement curves for caps 1 and 2 during tests 1 and 2.

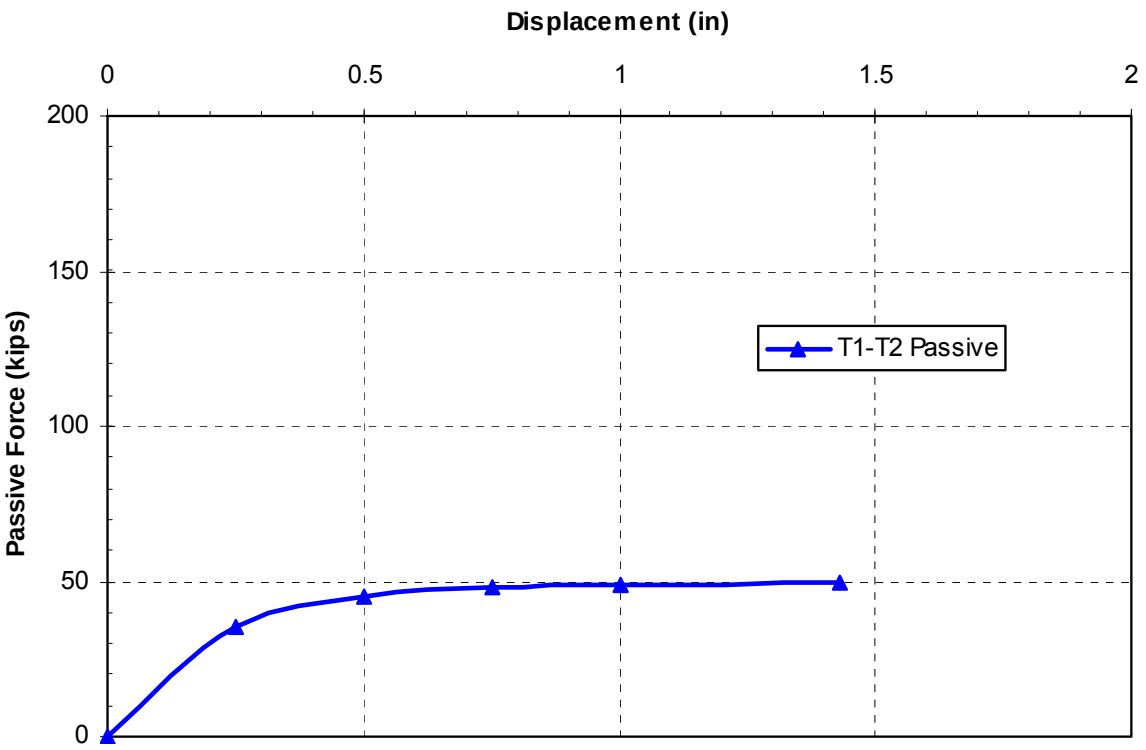

Figure 5-24 Development of passive force for virgin clay around cap 1.

Rotation of pile cap 1, where passive force was absent, exceeds that of pile cap 2 at higher load levels. The total rotation measured on pile cap 1 was about 0.3 degrees. This is significantly greater than the rotations observed on both caps during test 1, which measured about 0.17 degrees at the same load. This was expected as pile cap 1 of test 2 had the passive force directly behind the cap removed.

5.2.3 Depth vs. Displacement Results

Since cap 1 had the passive force on the pile cap removed, the remaining sections in this chapter will focus on the results from cap 1. It is sufficient to note that the Load vs. Displacement curves for cap 2 were consistent with that for test 1.

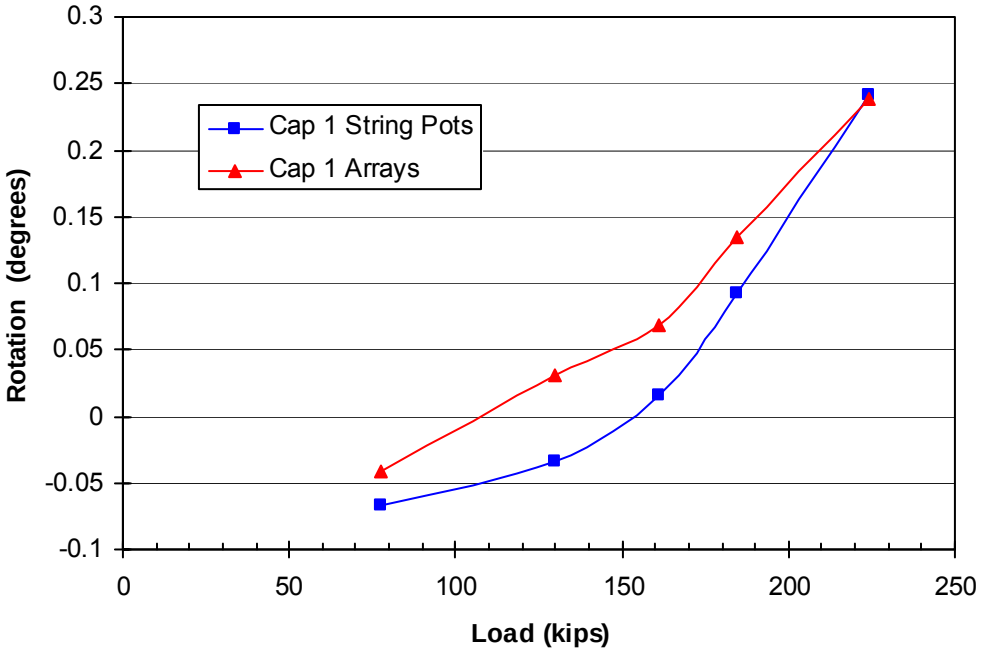

Figure 5-25 Peak pile cap load vs. pile head rotation for cap 1 during test 2 obtained from string potentiometer and shape array measurements.

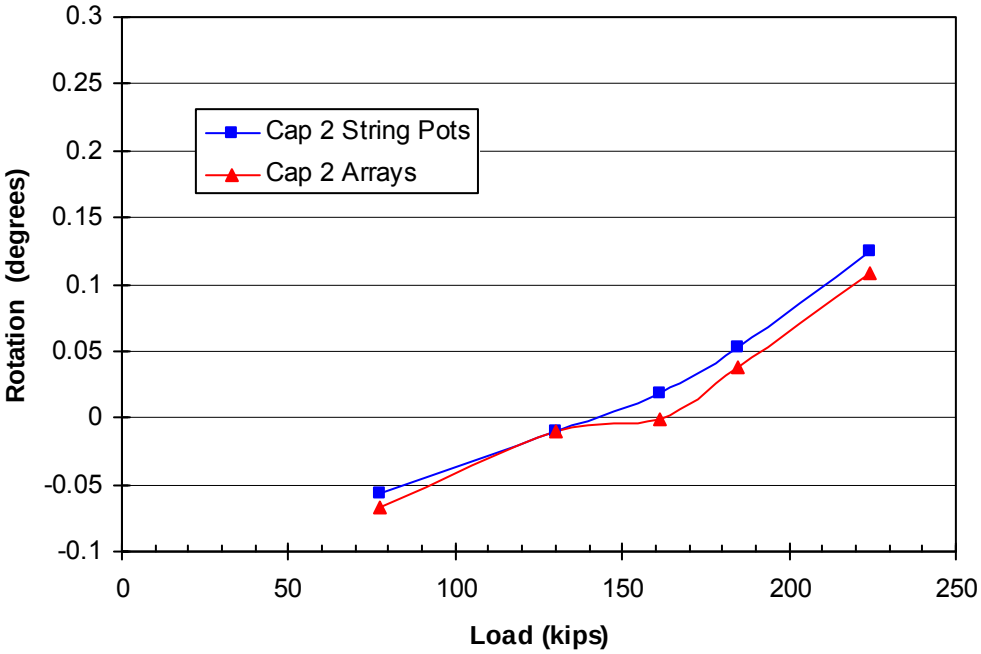

Figure 5-26 Peak pile cap load vs. pile head rotation for cap 2 during test 2 obtained from string potentiometer and shape array measurements.

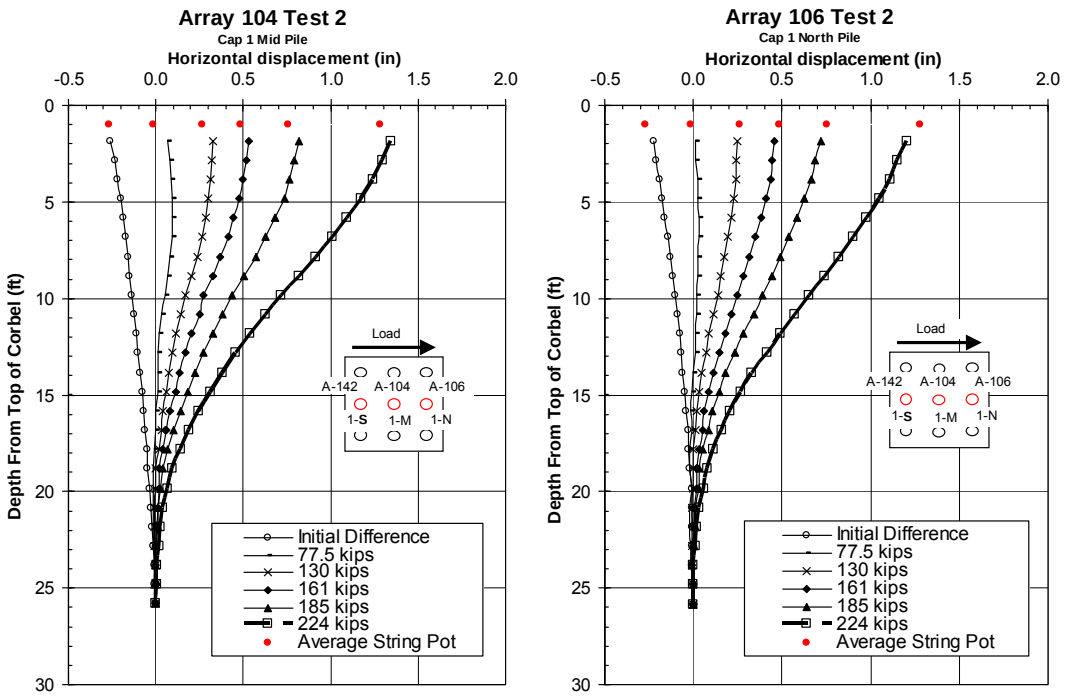

Figure 5-27 Displacement vs. depth curves obtained from shape arrays at several displacement increments for pile cap 1 during test 2. Pile head displacement from string potentiometers are shown for comparison.

Test 2 depth vs. displacement profiles for cap 1 are shown in Figure 5-27. As mentioned before, there is no array data from the south pile due to the defective array 142. Displacements at the elevation of the applied load at 1 ft below the top of the corbel are also shown to provide an indication of the relative accuracy of the measurements. Because of the initial offset, the displacement vs. depth curves start with a negative displacement and slope. As load increases, the displacement increases and the slope becomes positive. The agreement between the shape arrays and the string potentiometers is reasonable for cap 1. Using the trendline extrapolation method described in section 5.1.3, the pile cap displacement from the center pile array (A-104) varied 0.1 inch from the measurements made with the string potentiometers in the worst case, while the pile cap displacements from the north array (A-106) varied by 0.03 inches or less from string

potentiometer measurements. Typically, the pile cap displacements from the shape arrays were within about 1% to 3% of those obtained from the string potentiometer. This is essentially the same level of agreement noted in test 1 for cap 1.

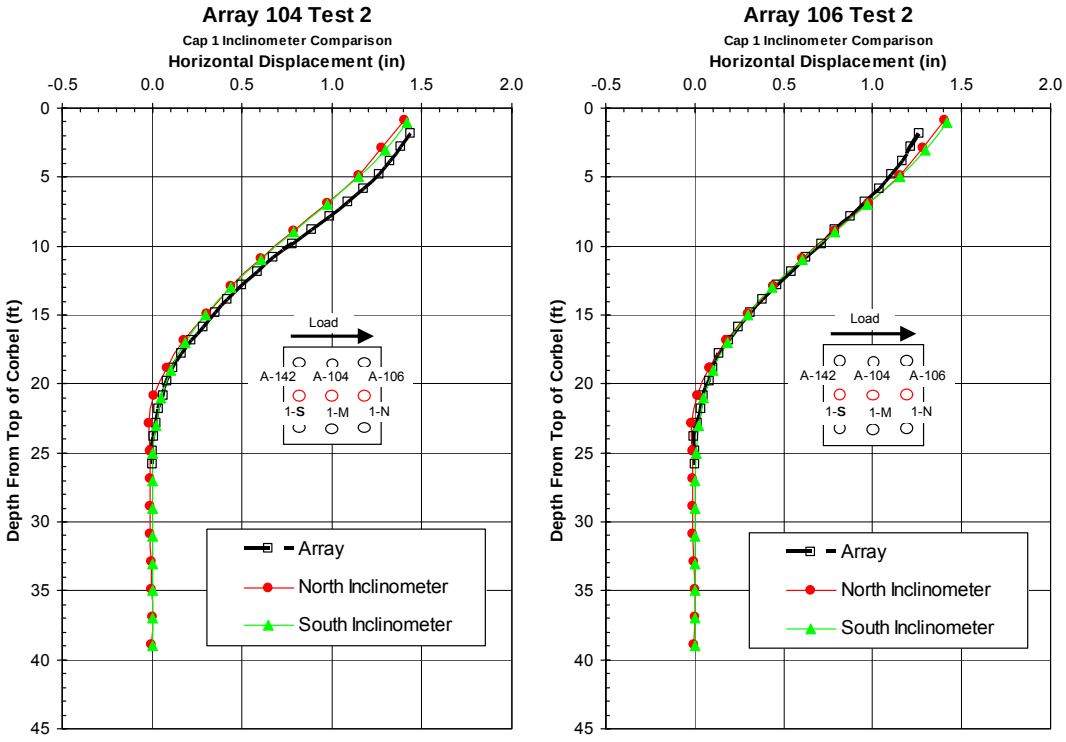

Figure 5-28 Displacement vs. depth profiles measured by shape arrays and inclinometers for the center and north piles in cap 1 during test 2 at maximum displacement.

Figure 5-28 shows the depth vs. displacement profiles of the arrays and inclinometer readings on cap 1 at the maximum displacement during test 2. There is good agreement in the north pile even though there is a slight discrepancy starting at about 6 ft below the top of the corbel. The instrumentation in the center pile experiences slight variance with the greatest discrepancy being about 0.1 inches or less. This discrepancy is also noted in the string potentiometer data shown in Figure 5-27. In spite of the minor discrepancies, the general trend and slope of the depth vs. displacement

profiles are consistent and provide an accurate representation of the displacements the piles are experiencing.

5.2.4 Bending Moment vs. Depth Results

Bending moments were calculated from the depth vs. displacement profiles from the center and north piles on cap 1 using the method described in Section 5.1.4. Figure 5-29 and Figure 5-30 provide bending moment vs. depth curves at the five target displacement levels during test 2. The curves were obtained from the shape arrays while the individual points represent moments computed from the strain gages. The datum for the depth on the figures has been moved to the bottom of the cap.

The maximum positive bending moments from the center pile array in Figure 5-29 occur from about 11.5 ft to 13.5 ft below the bottom of the cap. The positive moments measured from the strain gages are within 7 kip-ft (10% to 15%) or less of the moments calculated from the array data, with the only exception of the 185 kip load or 1 inch test increment. The positive moments from the north pile in Figure 5-30 seem to be a little more consistent as the depths of the maximum moments occur at about 13.5 ft below the bottom of the cap. The moments calculated from the strain gage data are within 7 kip-ft (10% to 15%) or less of array moments at all test increments. Also, with the exception of the 77.5 kip load or 0.25 inch test increment, the positive moments calculated from the arrays are within 2 kip-ft or less when comparing the two piles at the corresponding load. The trends for the negative moments calculated from the array data in the center pile are in close agreement with the moments calculated from the strain gage data. If the array trends were to continue to the base of the cap only the 0.25 inch (77.5

kips) and 0.75 inch (161 kips) test increments would vary by more than 5 kip-ft. On the other hand, the array trends for the negative moments from the north pile are more inconsistent when compared to the strain gages. Most test increments are off by 8 kip-ft (12% to 17%) if the array trends were to continue to the bottom of the cap.

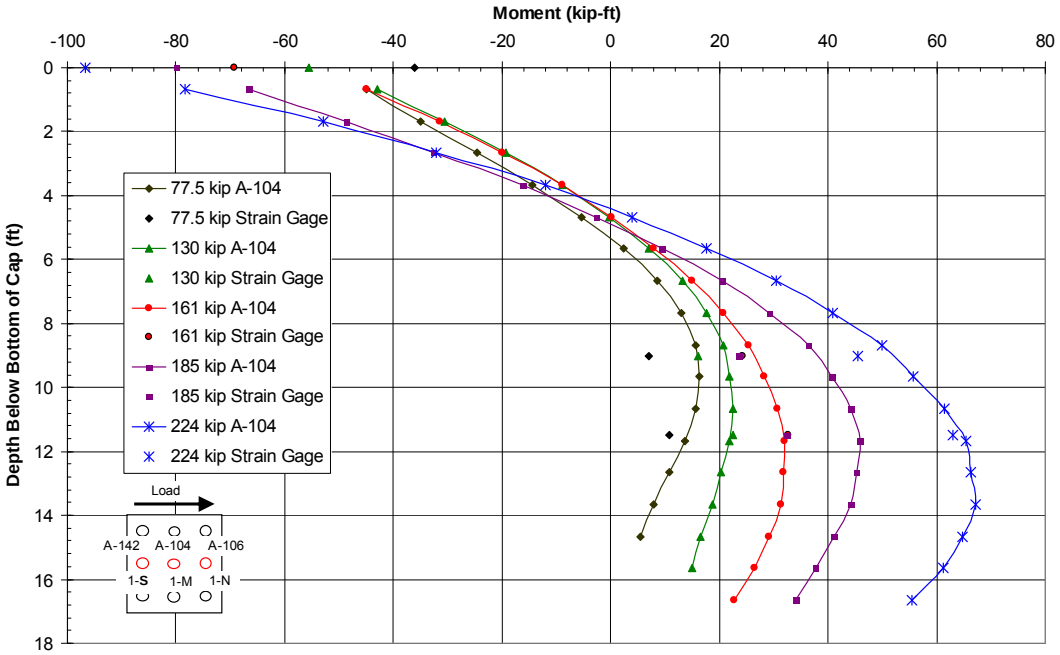

Figure 5-29 Test 2 bending moment vs. depth profiles from array data and strain gages on the center pile of cap 1.

The 1.5 inch or 224 kip load is the only one that appears to be in agreement. In addition, the magnitude of the maximum negative moment at each test increment is about 13 kip-ft higher on the center pile than on the north pile.

A comparison of the moments derived from the arrays and inclinometers at the maximum displacement is shown in Figure 5-31. There is good agreement with the inclinometers; however the trends from the arrays vary somewhat. The inclinometers and

the center array result in the maximum positive bending moment at about 11.5 ft, but the north array results are slightly lower at 12.5 ft.

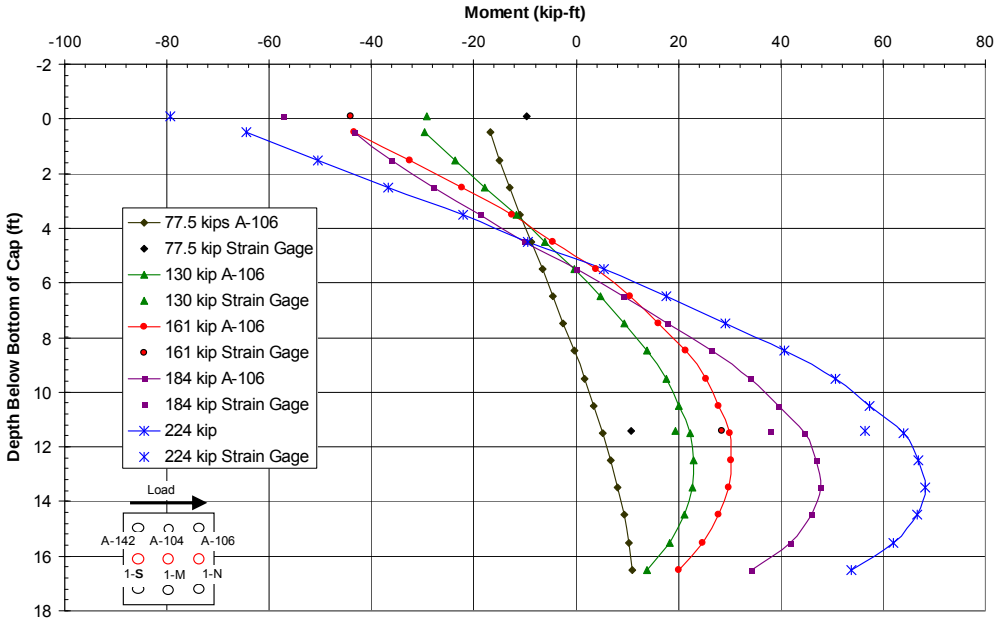

Figure 5-30 Test 2 bending moment vs. depth profiles from array data and strain gages on the north pile of cap 1.

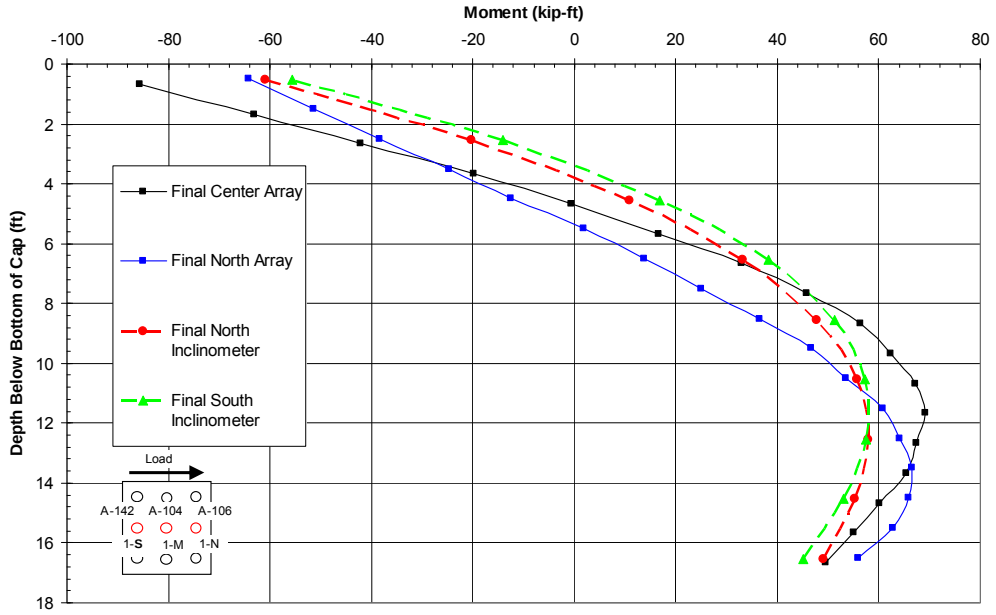

Figure 5-31 Test 2 moment vs. depth profiles from the arrays and inclinometers taken at the maximum displacement.

The magnitude of the maximum positive moment, calculated from the inclinometer data is about 58 kip-ft, while that calculated from the north array data is 66.5 kip-ft, and from the center array data 69 kip-ft. The north array and the inclinometers are in fair agreement at the maximum negative moment resulting in around -60 kip-ft, while the center array gives a higher value at about -95 kip-ft. The discrepancy in the negative moments for the center array is due to the fact that it recorded greater displacements at depths closer to the cap than the inclinometers as shown in Figure 5-28.

When comparing these results to that of test 1, the location of the maximum positive moment on the center pile was about one ft lower without the passive force behind the cap, but the magnitude stayed relatively similar at the same displacement increment. On the north pile, the location of the maximum positive moment stayed within one ft or closer, but decreased about 5 kip-ft on average without the passive force. The maximum negative moments on the center pile remained at the bottom of the cap, but increased 10 to 15 kip-ft on average from test 1. The maximum negative moments on the north pile also remained at the bottom of the cap, but decreased about 10 kip-ft on average without the passive force. The inconsistency in the magnitudes of the negative moments calculated from the strain gage data and array data makes it difficult to determine a difference in the trend between tests 1 and 2. However, it appears that the magnitudes of the negative moments for test 2 stayed within a range of plus or minus 10 kip-ft of the moments for test 1 at the same displacement increment, which would imply there was minimal change between test 1 and 2.

In summary, without the passive force behind the cap, the magnitudes of the positive bending moments decreased slightly, while the negative moments remained about the same, being consistently in a range of plus or minus 10 kip-ft. The depth to the maximum positive moment typically increased about one ft, while the location of the maximum negative moments remained at the bottom of the cap. It is difficult to conclude at this point if the one ft increase in depth to the location of the maximum positive moment was due to inaccuracies in the numerical method used to compute moment or indeed a reality.

5.2.5 Moment vs. Load Results

Figure 5-32 and Figure 5-33 show the maximum positive and negative bending moments vs. applied pile cap load respectively for cap 1 during test 2. Similarly, Figure 5-34 and Figure 5-35 show the maximum positive and negative bending moments vs. applied pile cap load, respectively for cap 2 during test 2. Bending moments were calculated from both shape array and strain gauge data when available. Initially, the curves are relatively linear; however, the bending moment tends to increase more rapidly with load at the higher load levels as the soil resistance is overcome. The curves from the strain gauges provide relatively consistent moment vs. load curves with little evidence of strong group interaction effects for the displacement levels involved. The agreement between the curves computed by the strain gauges and shape arrays is generally reasonable. The results appear to be somewhat more consistent for the positive moments than for the negative moments.

Figure 5-36 illustrates the combined trends of the maximum positive moment vs. load curves for test 1 and 2 on pile cap 1. Moments experiencing a wide range of values are not shown to allow for comparisons of the general trend. At a given load, moments from test 2 show are larger, which is expected since test 2 had no passive resistance behind the pile cap and thus experienced greater displacement or bending at the same load. Figure 5-37 shows similar plots for the maximum negative moment vs. load comparisons for test 1 and 2 on pile cap 1. Likewise, moments for test 2 are also larger at the same loading than test. This is what would be expected as piles in test 2 experienced greater displacements at the same load.

5.3 Load Test Involving Low Strength Flowable Fill Around Pile Group

The purpose of this test was to measure the difference in lateral resistance that was caused by placing flowable fill underneath the pile cap and around the piles (see Figure 4-14 for the testing diagram). It should be noted that at the 0.25 inch increment all of the shape array data were corrupted and will not be shown in any of the subsequent results.

5.3.1 Load vs. Displacement Results

Figure 5-38 shows the complete Load vs. Displacement curve for test 3 including the cyclic loading cycles at each load increment and the full load, unload, and reload curves. Data for Figure 5-38 was obtained from the actuator pressure transducer and the string potentiometer attached to the cap. As shown, the test started at zero load with zero initial displacement.

(a) Test 2 Maximum Negative Moments in Pile 1-N

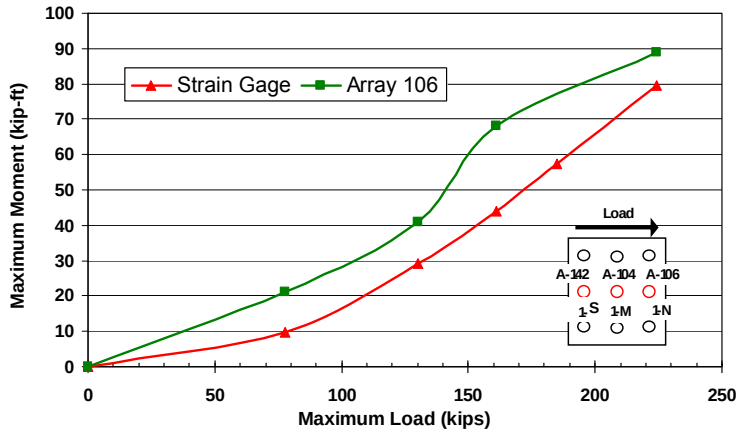

(b) Test 2 Maximum Negative Moments in Pile 1-M

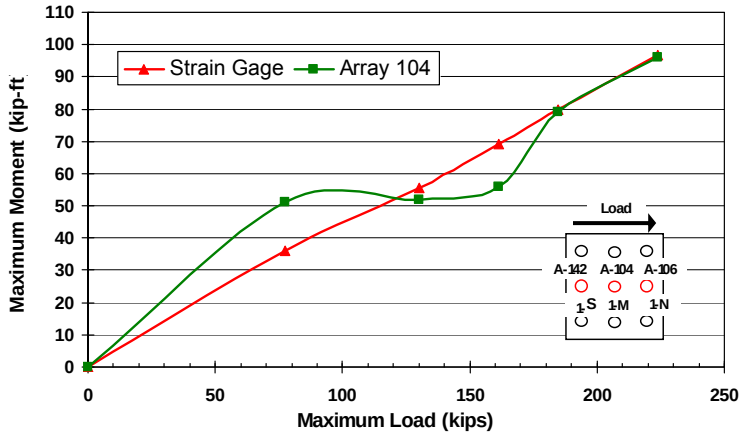

(c) Test 2 Maximum Negative Moments in Pile 1-S

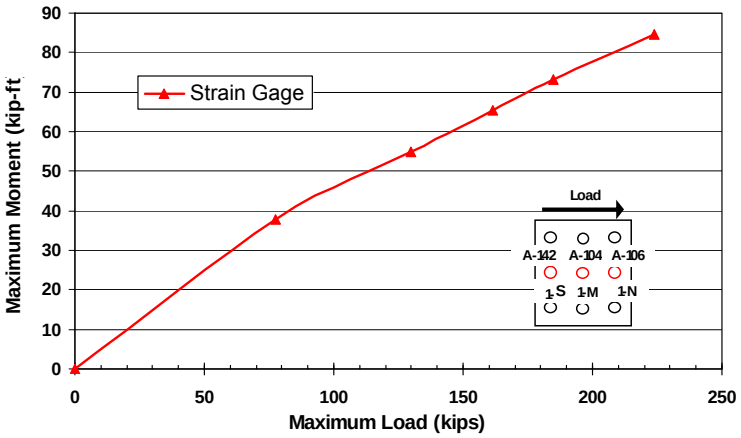

Figure 5-32 Maximum negative moment (base of cap) vs. total pile cap load for piles (a) 1-N, (b) 1-M, and (c) 1-S in cap 1 during test 2.

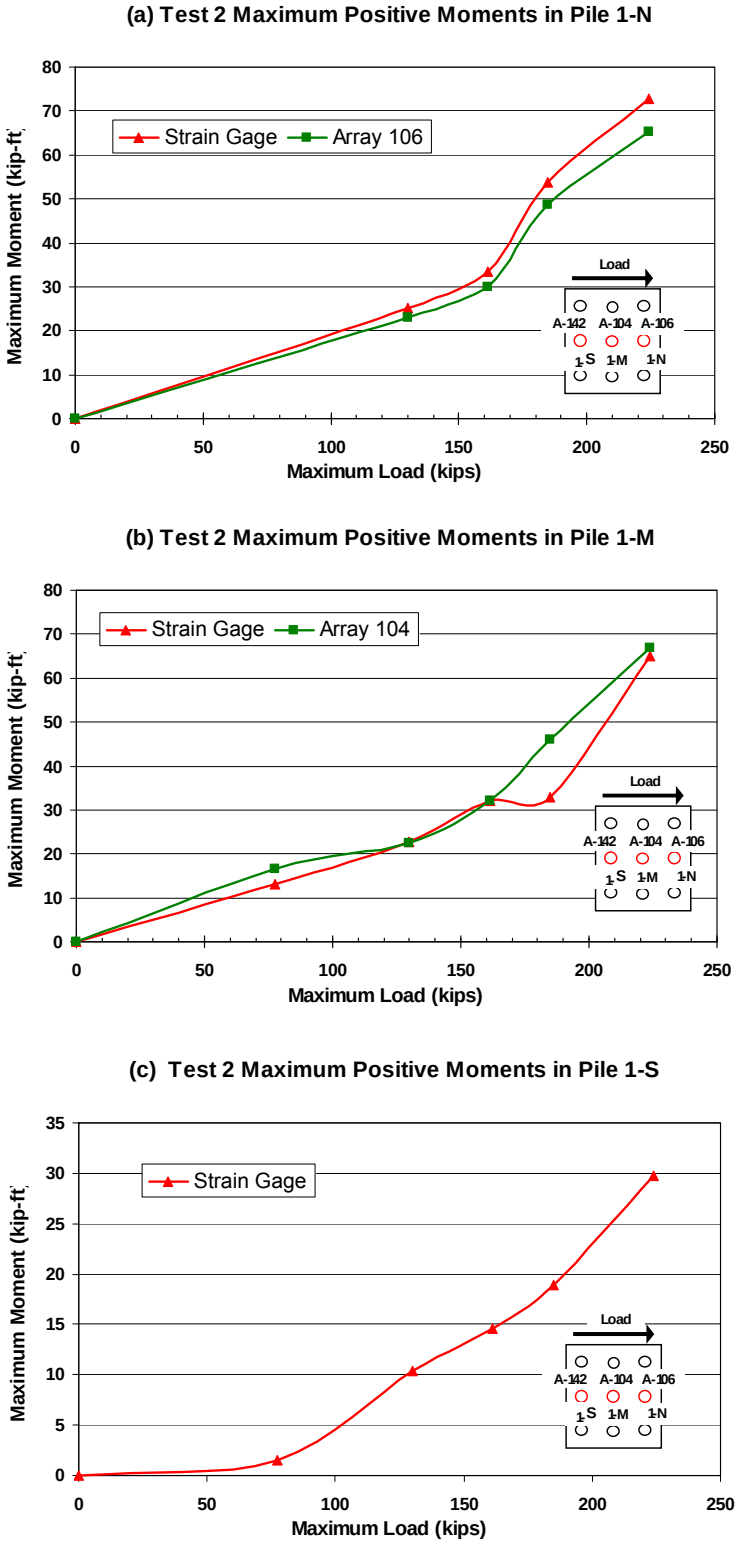

Figure 5-33 Maximum positive moment vs. total pile cap load for piles (a) 1-N, (b) 1-M, and (c) 1-S in cap 1 during test 2.

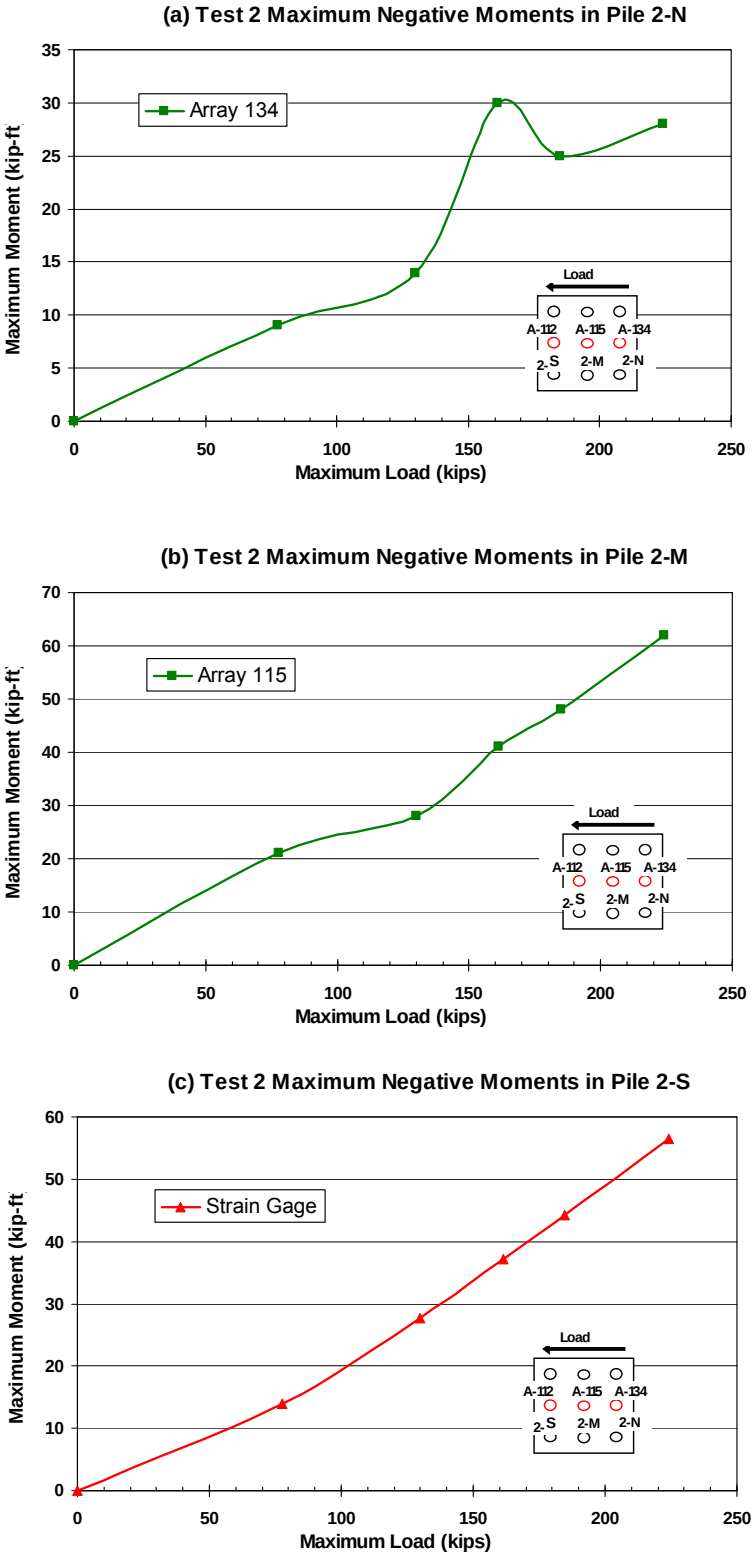

Figure 5-34 Maximum negative moment vs. total pile cap load for piles (a) 2-N, (b) 2-M, and (c) 2-S in cap 2 during test 2.

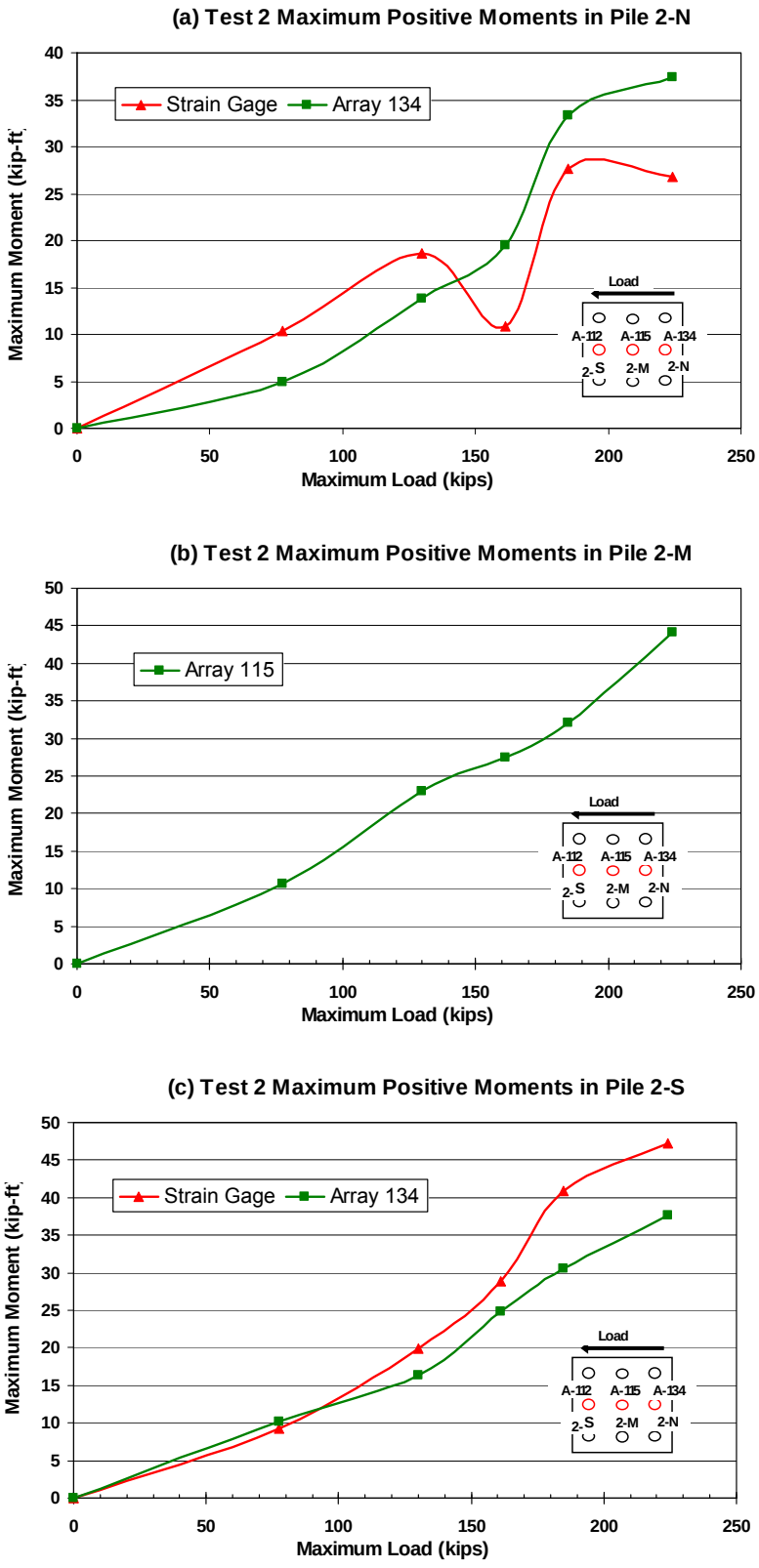

Figure 5-35 Maximum positive moment vs. total pile cap load for piles (a) 2-N, (b) 2-M, and (c) 2-S in cap 2 during test 2.

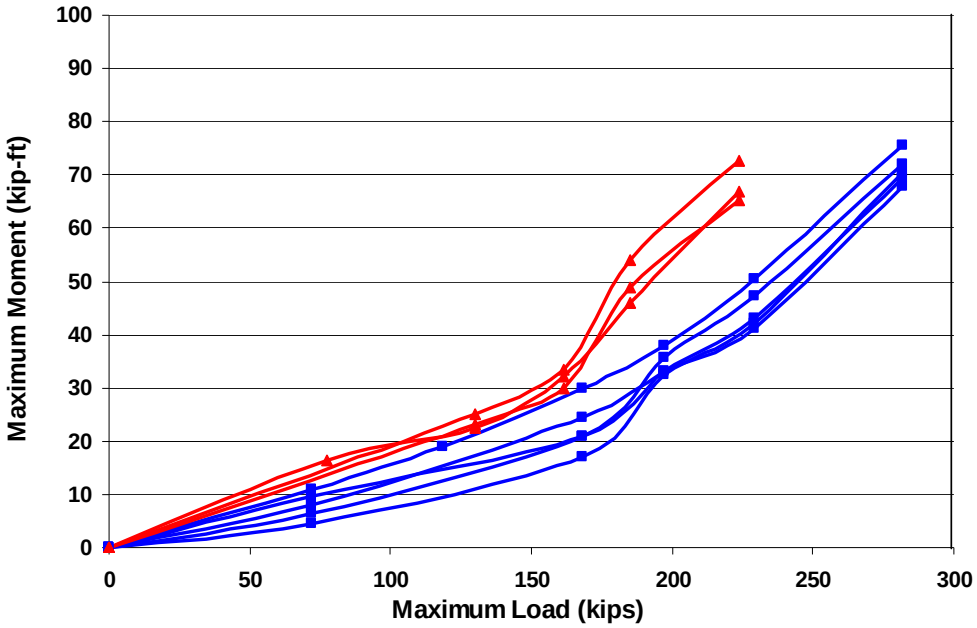

Figure 5-36 Maximum positive moment vs. load plots from test 1 and 2. (Test 1 plots are marked with a square while Test 2 plots are marked with a triangle.)

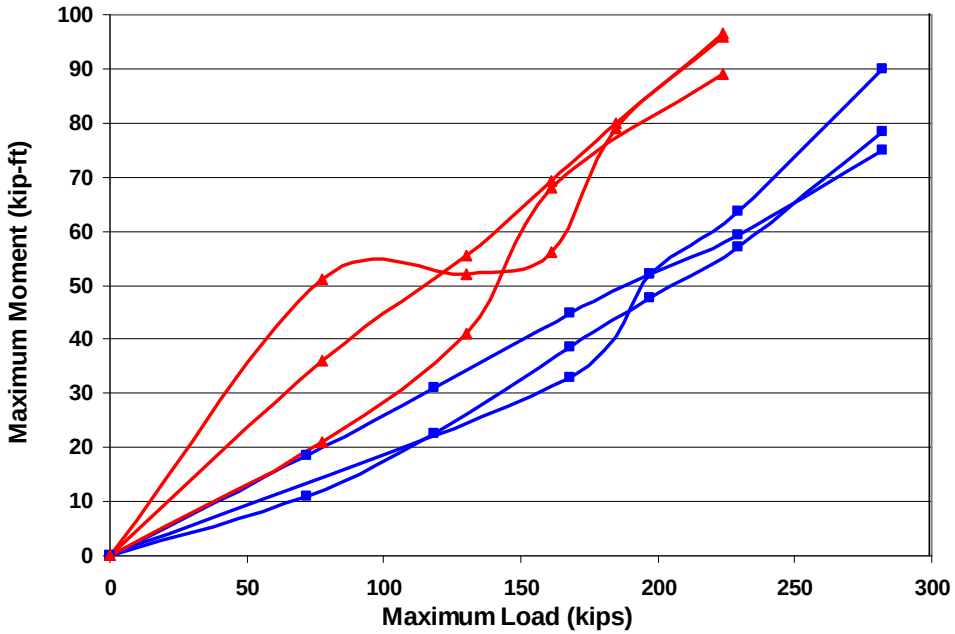

Figure 5-37 Maximum negative moment vs. load plots from test 1 and 2. (Test 1 plots are marked with a square while Test 2 plots are marked with a triangle.)

The actuator pushed the cap to target displacement increments of 0.125, 0.25, 0.5, 0.75, 1.0, and 1.5 inches; however, because of variations in the lateral resistance of cap 4 which served as the reaction foundation, the actual pile cap displacements were, 0.05, 0.13, 0.31, 0.50, 0.68, and 1.09 inches respectively. Because the flowable fill apparently moved into the gap behind the piles as the test was performed, a tensile force was required to pull the cap back to zero displacement for most displacement increments. Other reasons for the tensile force could include, side friction, and soil flowing in behind the entire flowable fill zone. These results suggests that the flowable fill was acting more like a granular material than a soilcrete mass.

Figure 5-39 shows the Load vs. Displacement curve obtained by connecting the points defining the maximum load applied at each of the displacement increments. The maximum applied load during the last push was 269.5 kips and resulted in a displacement of 1.09 inches.

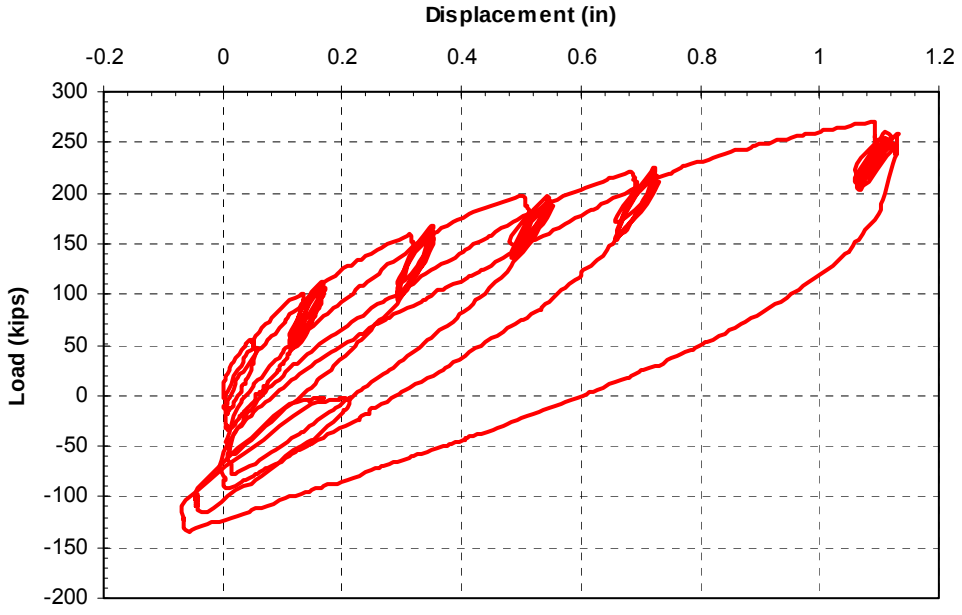

Figure 5-38 Test 3 load vs. displacement curves for complete test.

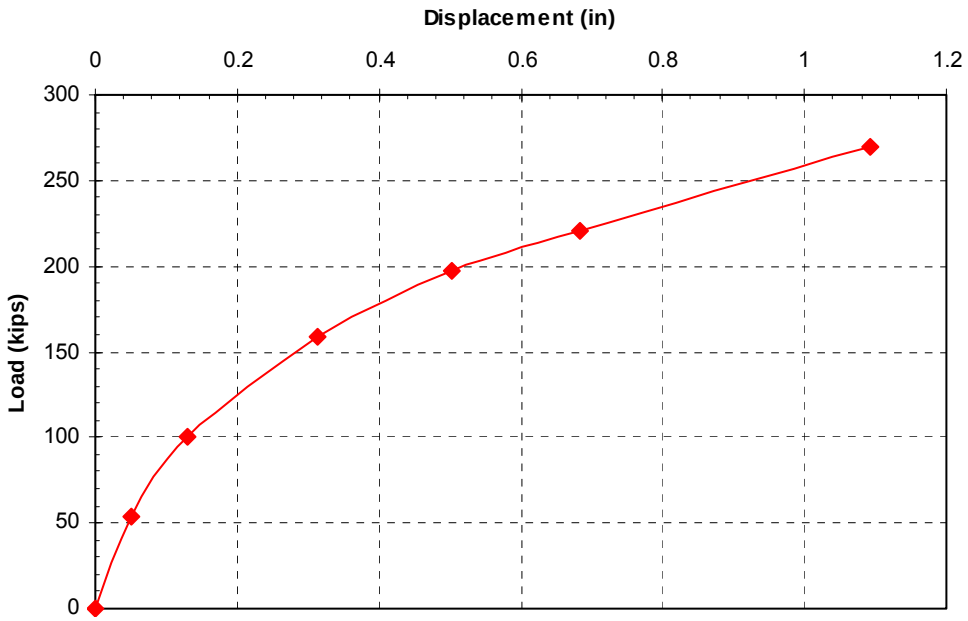

Figure 5-39 Test 3 maximum load vs. displacement of each displacement increment.

5.3.2 Rotation vs. Load Results

Load vs. pile head rotation curves obtained from string potentiometer and shape array measurements for pile cap 3 are provided in Figure 5-40. Rotation was measured from the string potentiometers located directly above the corbel of pile cap 3. The distance between the string potentiometers was approximately 109 inches. Rotation was also measured from the shape arrays. The difference in node displacements near the bottom of the pile cap and the top of the corbel was used to measure the rotation from shape array 112 and shape array 134. Generally, the agreement between the rotation obtained from the various methods is very good. For example, the maximum rotation measured by the string potentiometers, shape array 112 and shape array 134 were 0.285, 0.277, and 0.282 degrees, respectively. Shape array 134 does show a negative rotation until about 60 kips.

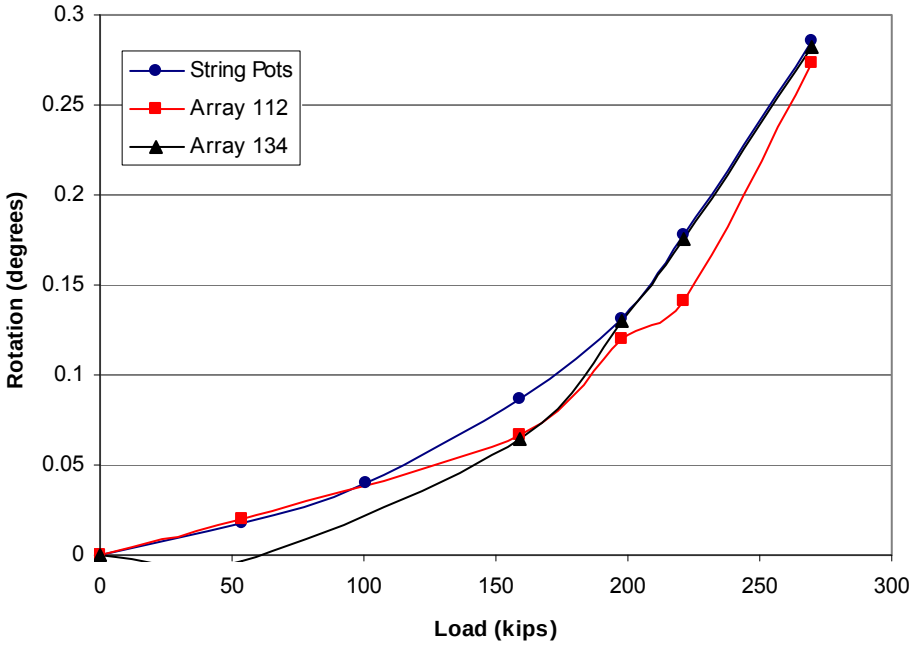

Figure 5-40 Peak pile cap load vs. pile head rotation for cap 3 during test 3.

5.3.3 Pile Displacement vs. Depth

The datum for depth was the top of the corbel, thus the load point was 11 inches down from the top of the corbel. Since this was the first test involving this cap all of the initial string potentiometers and inclinometers were zeroed at the start of this test. The initial inclinometer profiles are not present on the following graphs but they would be a vertical line along the y-axis showing zero displacement.

Figure 5-41(a) shows the displacements of the north inclinometer compared to the north shape array (112). Figure 5-41 (b) shows the displacement of shape array 112 and the string potentiometers. At the smaller displacements, measurements from the shape arrays and the string potentiometers vary by about 0.031 inches, and at the largest displacements measurements vary by only 0.019 inches. The 0.25 inch increment

displacement is shown for the string potentiometer, but the shape array profile is not shown because the data was corrupted.

Figure 5-42 (a) shows the displacements of the south inclinometer compared to the south shape array (134). The final inclinometer and final shape array differ by only 0.0126 inches at the top. As seen in the previous figure below 22 ft the displacement is zero. Figure 5-42 (b) shows the displacement of shape array 134 compared to the string potentiometers. Reasonable agreement is shown between the shape arrays and the string potentiometers, differing by as much as 0.069 inches and as little as 0.039 inches. The shape array data for the 0.25 inch increment displacement is not show because of corrupted data.

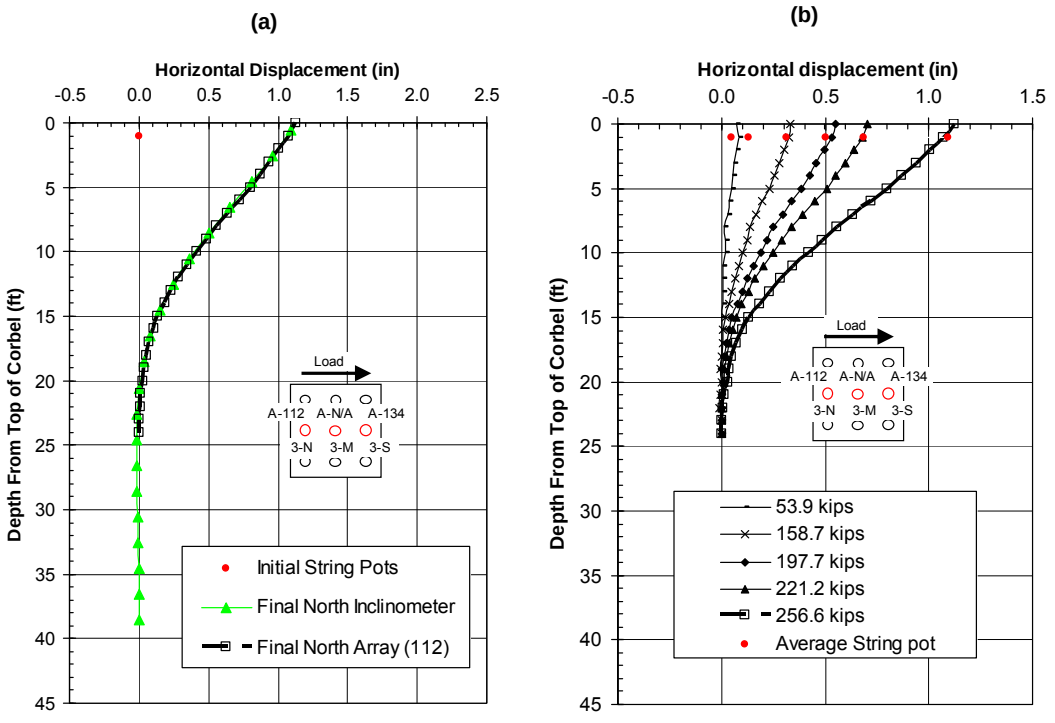

Figure 5-41 Test 3(a) displacement vs. depth profiles comparing the initial and final inclinometer measurements to that of the north array. (b) Displacement vs. depth curves obtained from shape array 112 and string potentiometers at several displacement increments for pile cap 3.

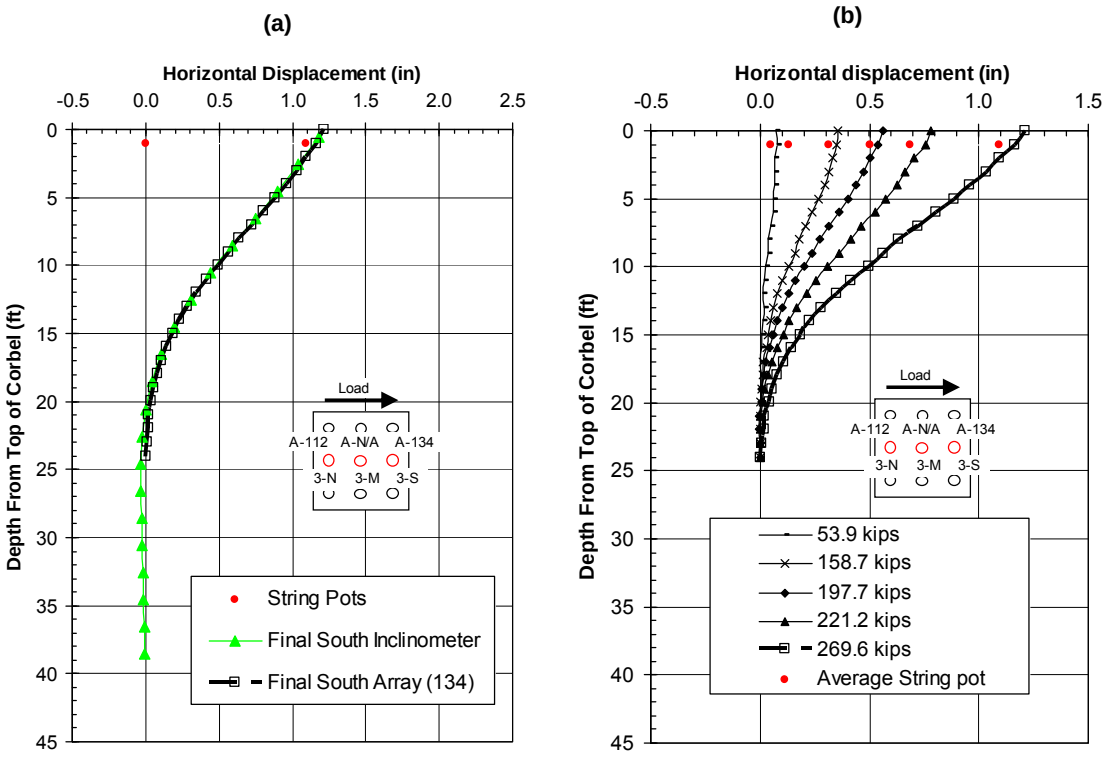

Figure 5-42 Test 3(a) displacement vs. depth profiles comparing the initial and final inclinometer measurements to that of the south array. (b) Displacement vs. depth curves obtained from shape array 134 and string potentiometer at several displacement increments for pile cap 3.

5.3.4 Bending Moment vs. Depth

Using the method described previously the bending moments vs. depth curves in Figure 5-43 were obtained from the array displacements and strain gage measurements on the north pile. The array measurements show that the location of the maximum positive bending moments increased slightly with load and displacement. The strain gages and the shape arrays measurements show that the maximum positive bending moment is between 11 to 12 ft. For positive bending moments, the strain gage measurements vary from the shape arrays by as much as 17%. The negative bending moments have greater variation: the moments calculated from strain gage data are as much as 63 % greater than those calculated from the shape arrays.

Figure 5-44 shows the comparison of moment vs. depth obtained from the north inclinometer and north shape array. Maximum negative moments vary considerably. For example, negative moments calculated from the inclinometer data is -12.7 kip-ft, which is half that calculated from the shape array, -24.9 kip-ft; the maximum negative moment calculated from strain gage data is -64 kip-ft. In contrast, the maximum positive moments calculated using the different measurements show reasonable agreement. The inclinometer data results in a maximum positive moment of 47 kip-ft at 10.5 ft below the pile cap. The maximum positive moment calculated from the shape array is 59.4 kip-ft and occurs at a depth of about 11.5 ft.

Figure 5-45 shows the bending moment vs. depth profile for the south pile. The shape array results are consistent with the results from the shape array in the north pile, varying only by 4 kip-ft, on the maximum end and 12.5 kip-ft on the minimum end. The strain gages results however, give a maximum positive moment of 46 kip-ft at a depth of about 9 ft.

Figure 5-46 shows the bending moment vs. depth profile for the south pile obtained from the shape arrays data and inclinometer data. The two sets show very good correlation; varying by 8 kip-ft at the most. The two data sets also agree in the location of the maximum positive at around 11 ft.

5.3.5 Moment vs. Load Results

Figure 5-47 provides plots of the maximum negative moment in the three instrumented piles in the group as a function of the applied load.

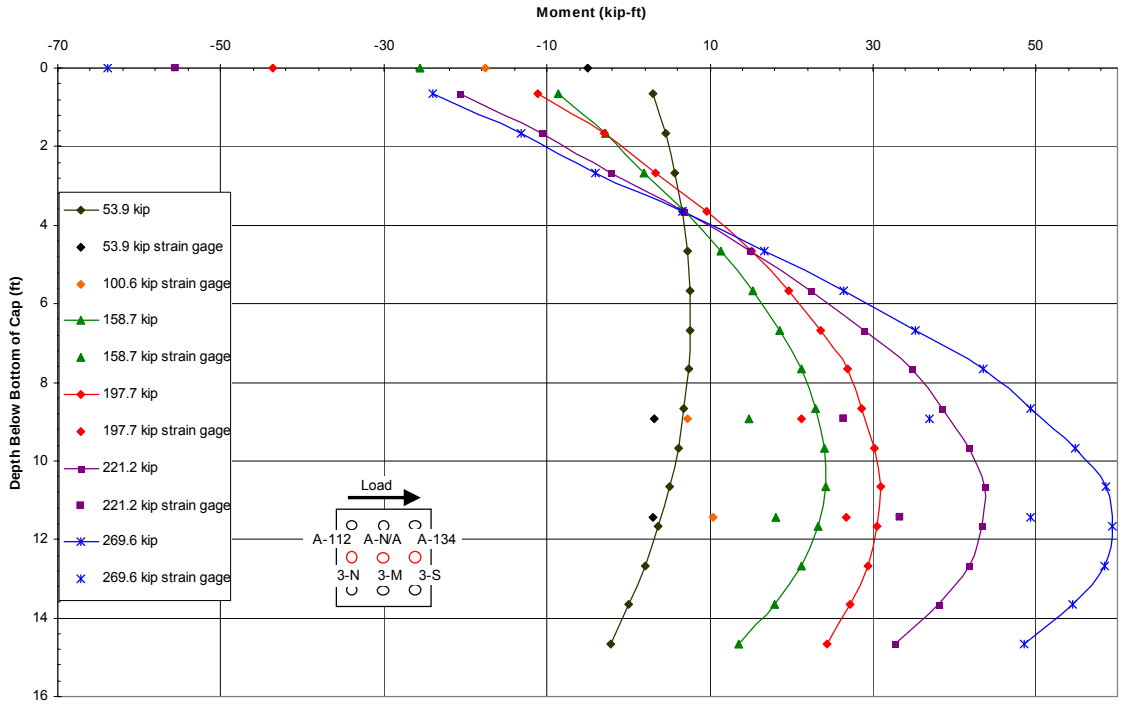

Figure 5-43 Test 3 bending moment vs. depth profiles obtained from array 112 and strain gage data as instrumented on the north pile.

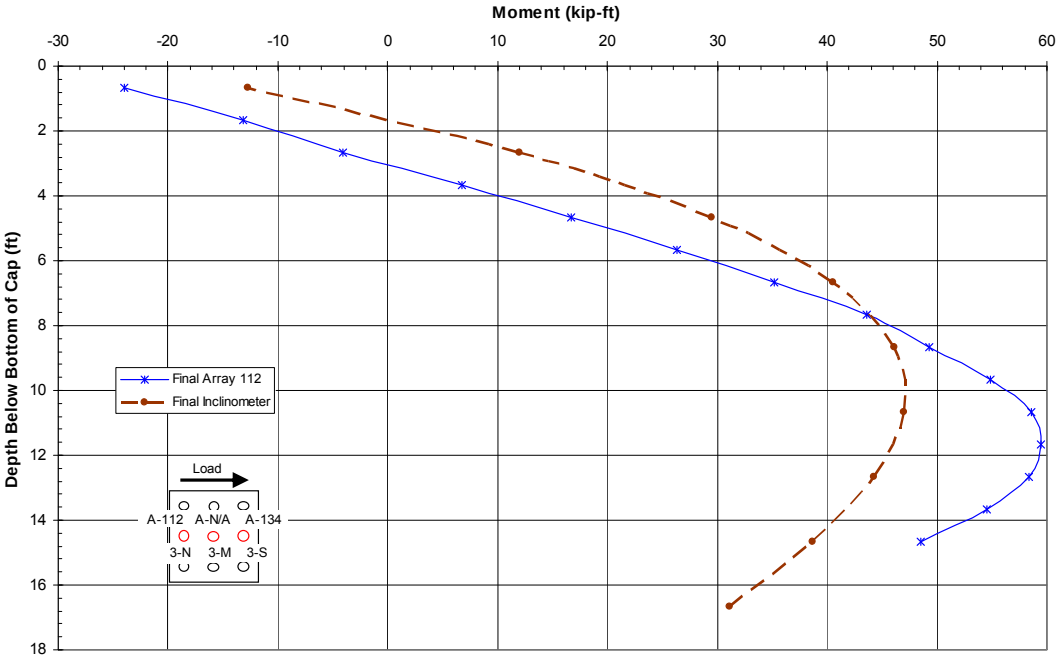

Figure 5-44 Test 3 bending moment vs. depth comparison of array 112 and the north inclinometer at maximum load.

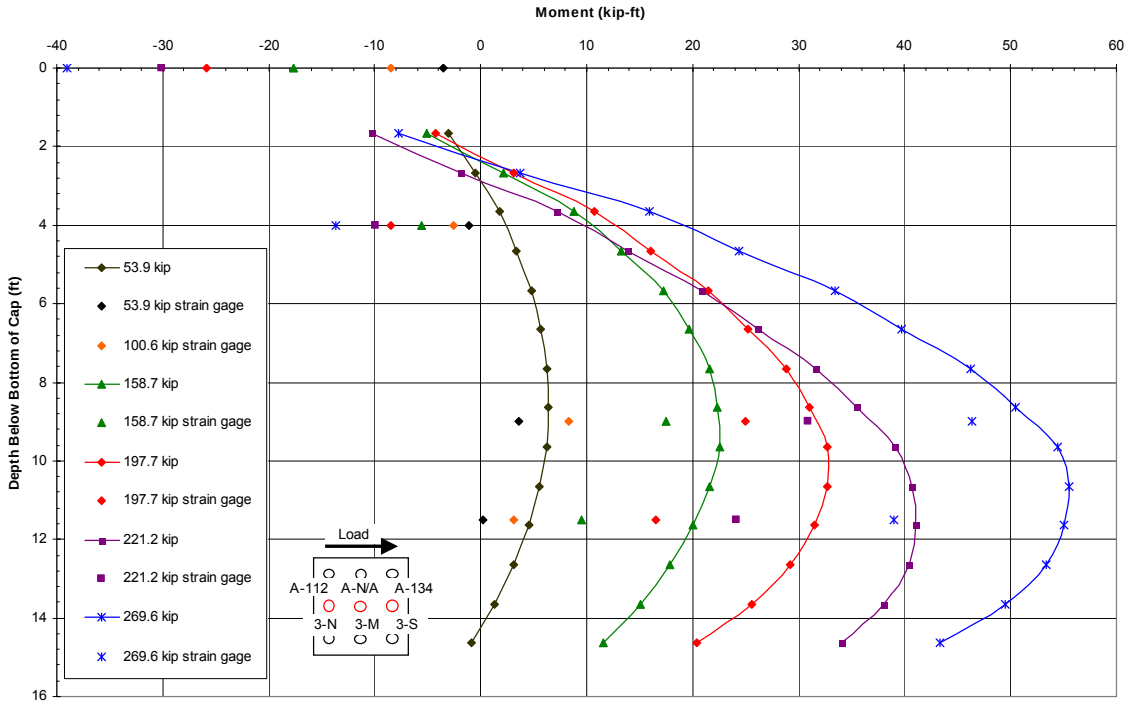

Figure 5-45 Test 3 bending moment vs. depth profiles obtained from array 134 and strain gage data as instrumented on the south pile.

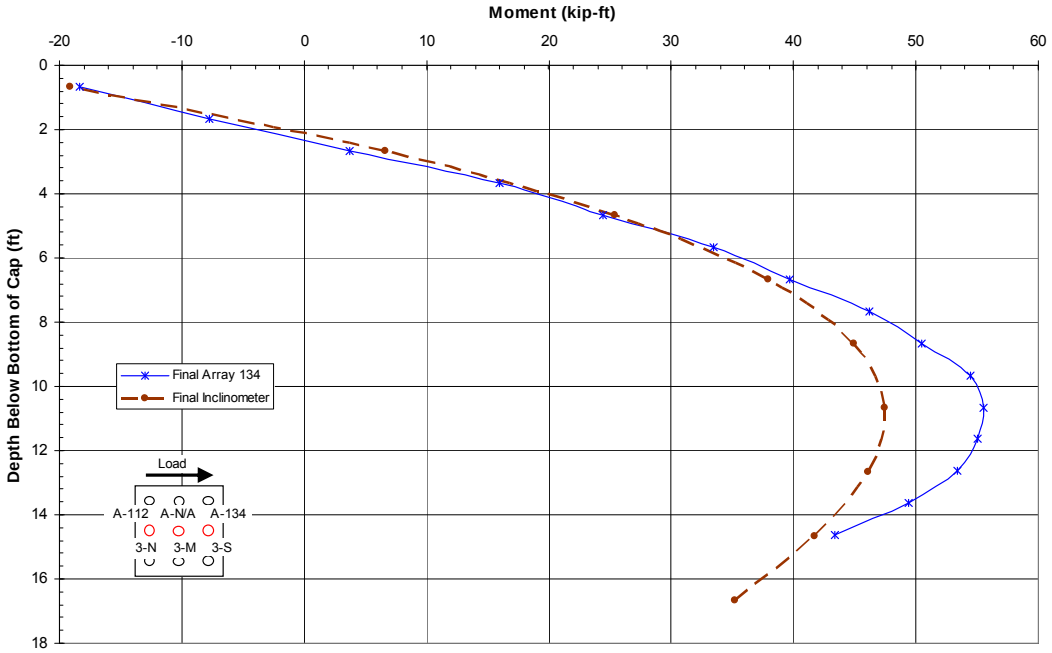

Figure 5-46 Test 3 bending moment vs. depth comparison of array 134 and the south inclinometer at maximum load.

Moment curves calculated from the two arrays and strain gages on the middle pile are relatively close; however, moments calculated from the strain gages on the north pile appear to be abnormally greater (about double) and are likely not reliable. The moments for the middle and back row piles are somewhat higher than that for the front row as one would expect from pile group interaction effects for example see Rollins et al, 2006. Interaction of the shear zones for trailing row piles typically leads to a softer soil reaction so that greater moment results for a given load. However, in this case, the differences are relatively small considering that the piles are closely spaced. Perhaps the strength of the granular soil within the perimeter of the pile group has been improved by the pile driving process which would tend to compact the surrounding soil.

Figure 5-48 provides plots of the maximum positive moment in the three instrumented piles in the group as a function of the applied load. The moment vs. load curves for the three piles are relatively consistent. It should be noted that the maximum positive moment calculated from the strain gages on the south pile is around 9 ft while the others are around 11 to 12 ft deep.

5.4 Load Test Involving Low Strength Flowable Fill Around Pile Group 3 without Passive Resistance behind the Pile Cap

The lateral load test involving the weaker flowable fill beneath cap 3 without any passive resistance was test 5. The results of this test will be compared to those from test 3 to determine the increase in lateral resistance that is directly attributable to the flowable fill. Although there was no material directly behind the pile cap to increase passive resistance, there was a section of flowable fill that extended 4.5 ft to the north of the pile cap. Figure 4-14 shows the geometry of soil improvement during this test.

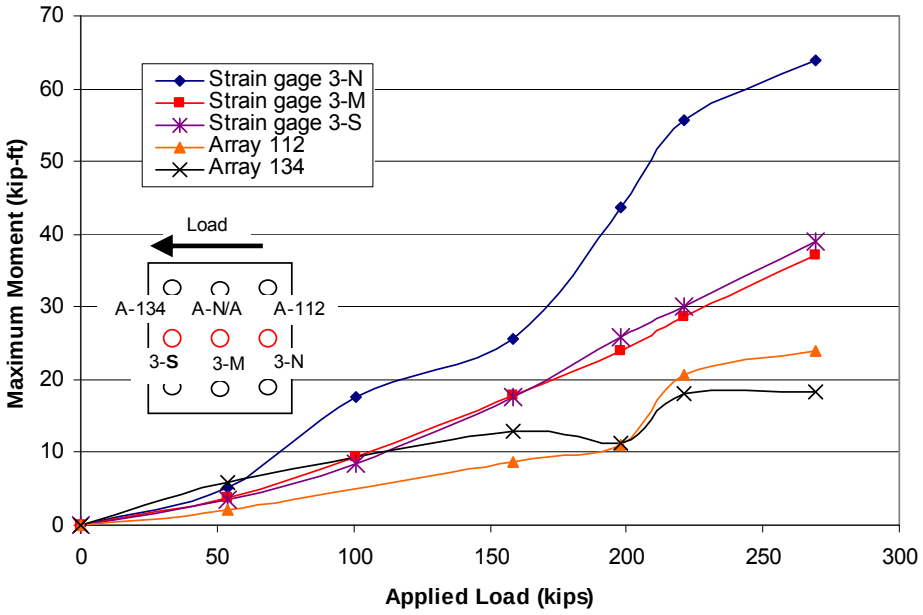

Figure 5-47 Test 3 maximum negative moments from the strain gage and shape array data.

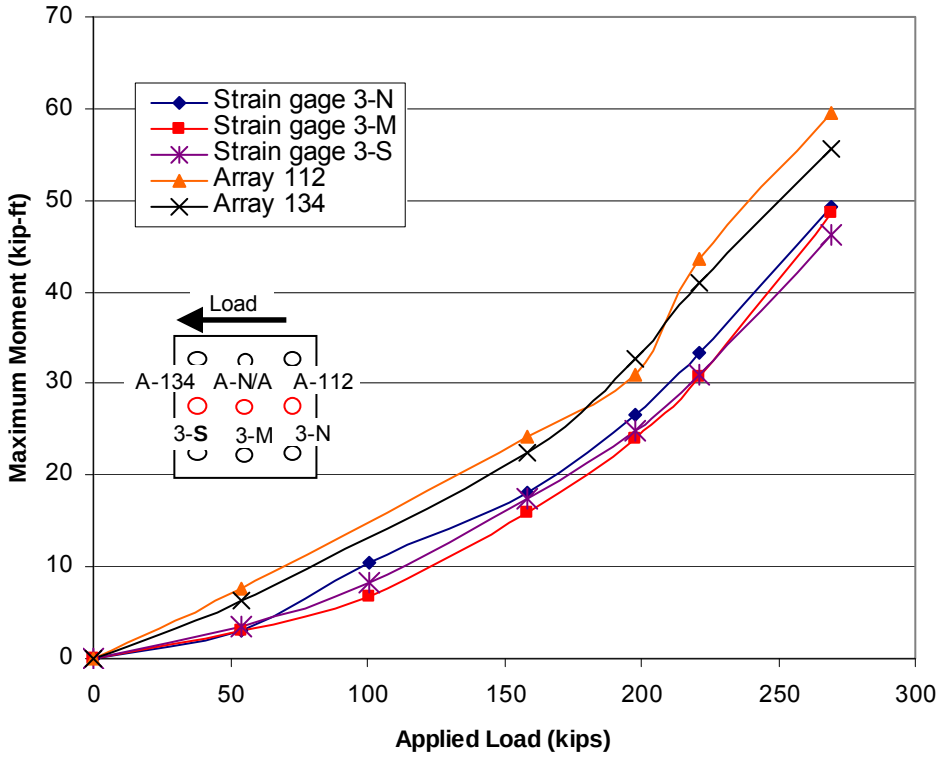

Figure 5-48 Test 3 maximum negative moments from the strain gage and shape array data.

5.4.1 Load vs. Displacement Results

Figure 5-49 provides a continuous plot of pile cap displacement vs. applied load for pile cap 3. Figure 5-49 shows the complete Load vs. Displacement curve for test 3 including the cyclic loading cycles at each load increment and the full load, unload, and reload curves. Data for Figure 5-49 was obtained from the actuator pressure transducer and the string potentiometer attached to the cap. The actuator pushed the cap to target the prescribed increments of 0.125, 0.25, 0.5, 0.75, 1.0, and 1.5 inches, however because of variations in the lateral resistance of cap 4 which served as the reaction foundation, the actual pile cap displacements were, -0.13, 0.049, 0.28, 0.61, 1.08, and 1.79 inches respectively. Pile cap 3 had an initial displacement of -0.26 inches, because during tests 3 and 4, pile caps 3 and 4, were pulled together. By zeroing the data pile cap 3 moved 0.13, 0.31, 0.55, 0.87, 1.33, 2.05 inches, respectively for the various displacement intervals relative to its initial position.

Figure 5-50 shows the Load vs. Displacement curve obtained by connecting the points defining the maximum load applied at each of the displacement increments. Looking at the Load vs. Displacement data, it suggests that the soft clay had flowed into the gap behind the formed during tests 3 and 4 so that at the end of test 4 93 kips of force was required to position the pile cap back to -0.26 inches of displacement. The maximum applied load on the last push during test 5 was 299 kips and resulted in a displacement of 1.79 inches.

5.4.2 Rotation vs. Load Results

Load vs. pile head rotation curves obtained from string potentiometer and shape array measurements for pile cap 3 are provided in Figure 5-51.

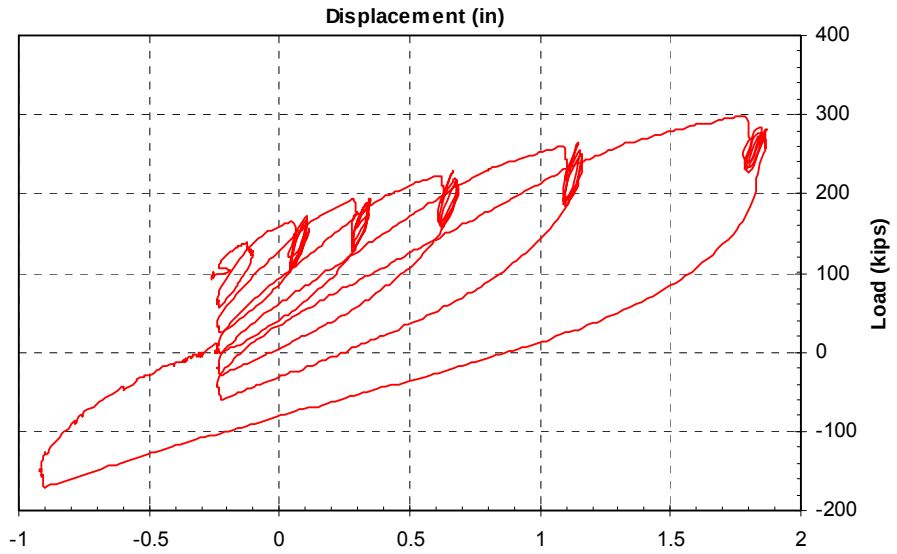

Figure 5-49 Plot of continuous pile cap displacement vs. applied load for pile cap 3 test 5.

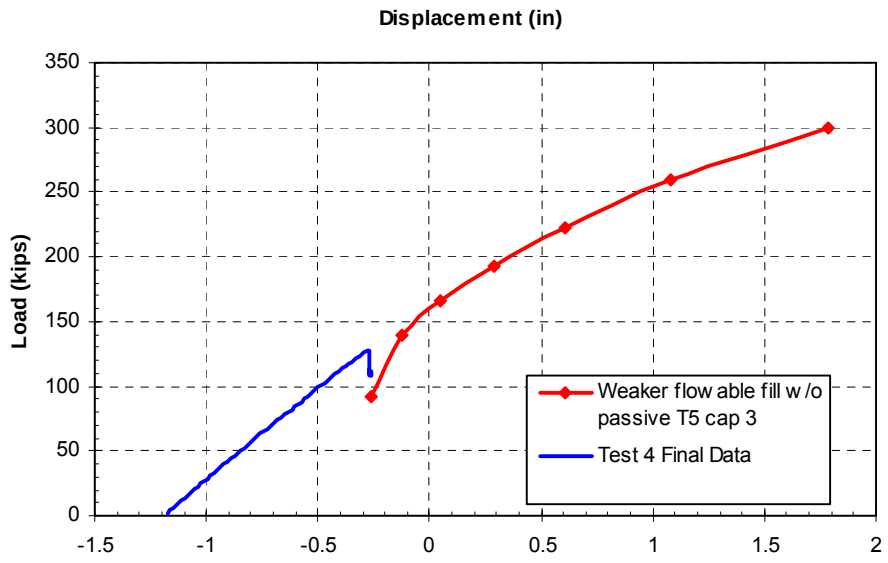

Figure 5-50 Plot of pile cap displacement vs. peak applied load for each increment of test 5 with the final displacement data from test 4.

Rotation was measured from the string potentiometers located directly above the corbel of pile cap 3. The distance between the string potentiometers was approximately 109 inches. Rotation was also measured from the shape arrays. The difference in node displacements near the bottom of the pile cap and the top of the corbel was used to calculate the rotation from shape array 112 and shape array 134. The total rotation measured by the string potentiometers, shape array 112 and shape array 134 was 0.543, 0.546, and 0.582 degrees, respectively which is quite consistent. The graph starts at 90 kips because it took 93 kips to push pile cap 3 back to an initial displacement of -0.26 inches at the start of the test.

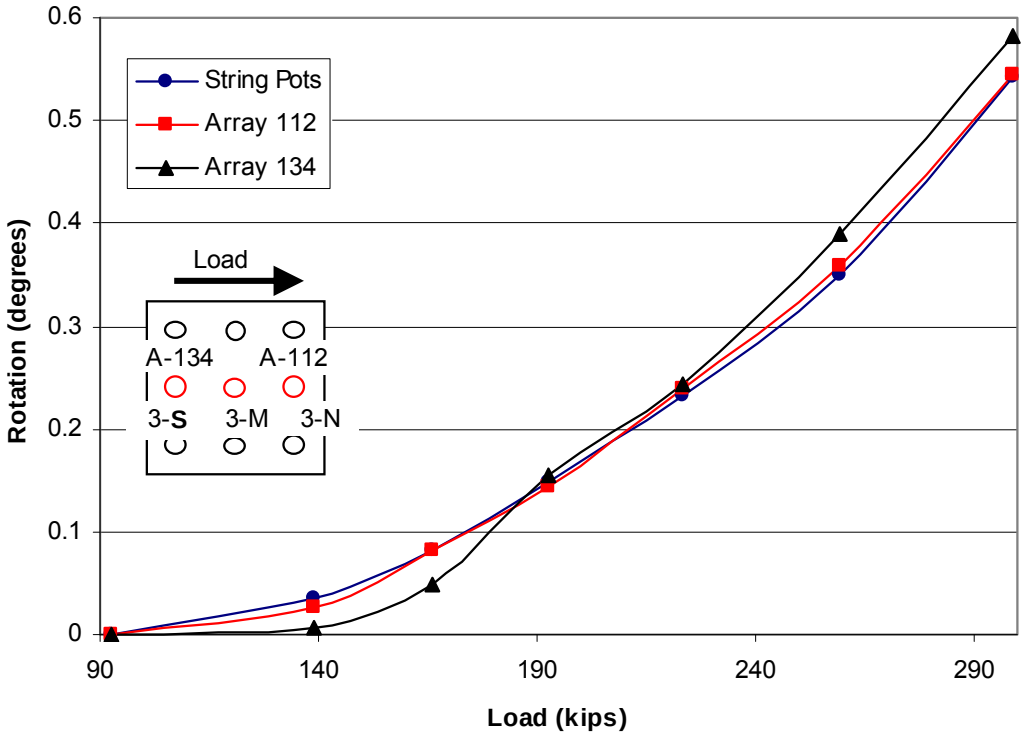

Figure 5-51 Peak pile cap load vs. pile head rotation for cap 3 during test 5.

5.4.3 Pile Displacement vs. Depth

Figure 5-52 shows the depth vs. displacement profiles for the final position of shape array 112, the north inclinometer, shape array 112, and the sting potentiometers at various load increments. The inclinometer and shape array have very good agreement. The inclinometer data indicate that the pile has some negative displacement from 24 to 36 ft. As mentioned previously pile cap 3 starts out with a negative displacement of -0.26 inches and at the 0.125 (139.2 kip) inch load increment the string potentiometer measured -0.126 inches. Aside from the 0.125 (139.2 kip) inch load increment, where the string potentiometer is 0.22 inches smaller than the shape array, the string potentiometers measurement was about 0.1 inches smaller than that of the shape array at the various load increments.

Figure 5-53 shows the displacement vs. depth profiles from the south inclinometer, the south array (134), and the string potentiometer data. The 0.125 inch load increment shape array data was erroneous and are not shown. The final inclinometer and the final array data have reasonable agreement, varying only slightly from 4 ft to 12 ft in depth. The displacement increments on the shape array show that the pile has a negative displacement from depths of 3 ft to 21 ft for the 0.25 (166.1 kip) inch load increment and 14 ft to 20 ft for the 0.5 (192.8 kip) inch increment. This could be the result of tests 3 and 4 where the pile cap was pulled in the opposite direction. The string potentiometer measurements vary by less than 6 % from that of the south shape array.

5.4.4 Bending Moment vs. Depth

Figure 5-54 shows the bending moment vs. depth for the north pile.

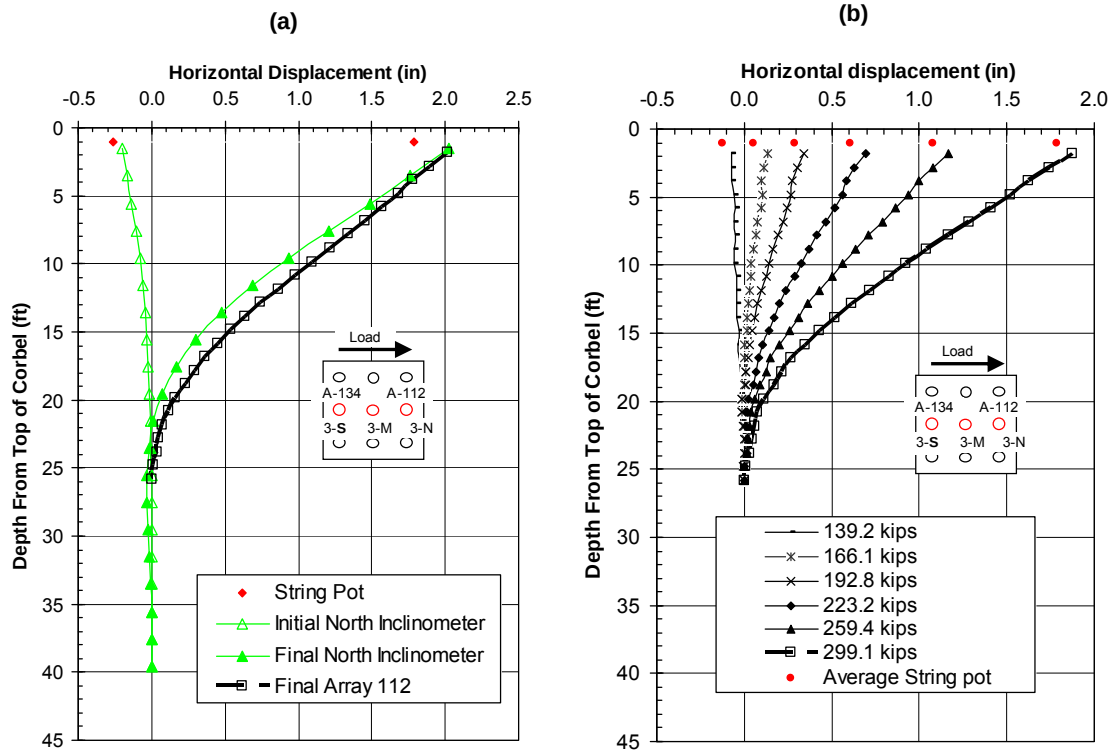

Figure 5-52 Test 5 (a) displacement vs. depth profiles comparing the final inclinometer to north array. (b) Displacement vs. depth curves comparing shape array to string potentiometer data

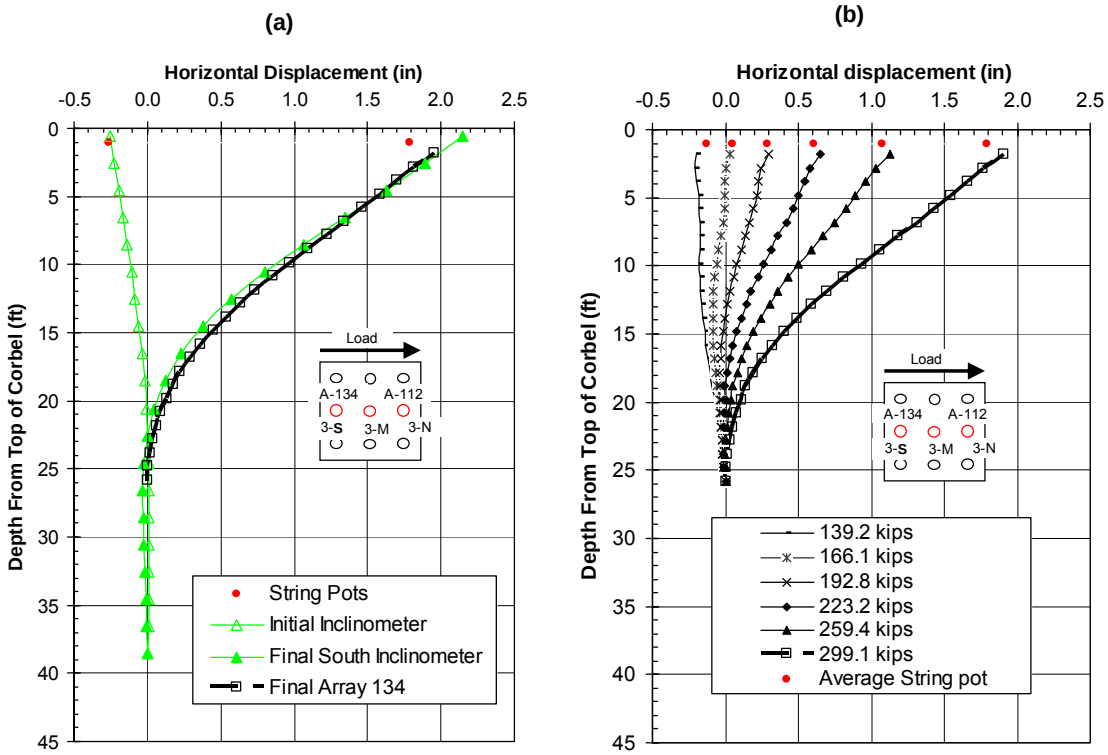

Figure 5-53 Test 5 (a) displacement vs. depth profiles comparing the final inclinometer to south array. (b) Displacement vs. depth curves comparing shape array to string potentiometer data

The values for the 0.125 (139.2 kip) inch load increment show that the pile had a reverse curvature; this is caused by the previous two tests that pulled the pile cap in the opposite direction. Also the shape array data from the 0.5 (192.8 kip), 0.75 (223.2 kip), 1.0 (259.4 kip) inch load increment bent the piles in the opposite direction, these are not shown. The shape array data shows that the location of the maximum positive bending moment is deeper with increasing load except for the 1.5 (299.1 kip) inch load increment where the depth is about 12.5 ft. The strain gage for the north and south piles was unreliable and is not presented; however the data from the middle strain gages was reliable except for the strain gages at 9 ft.

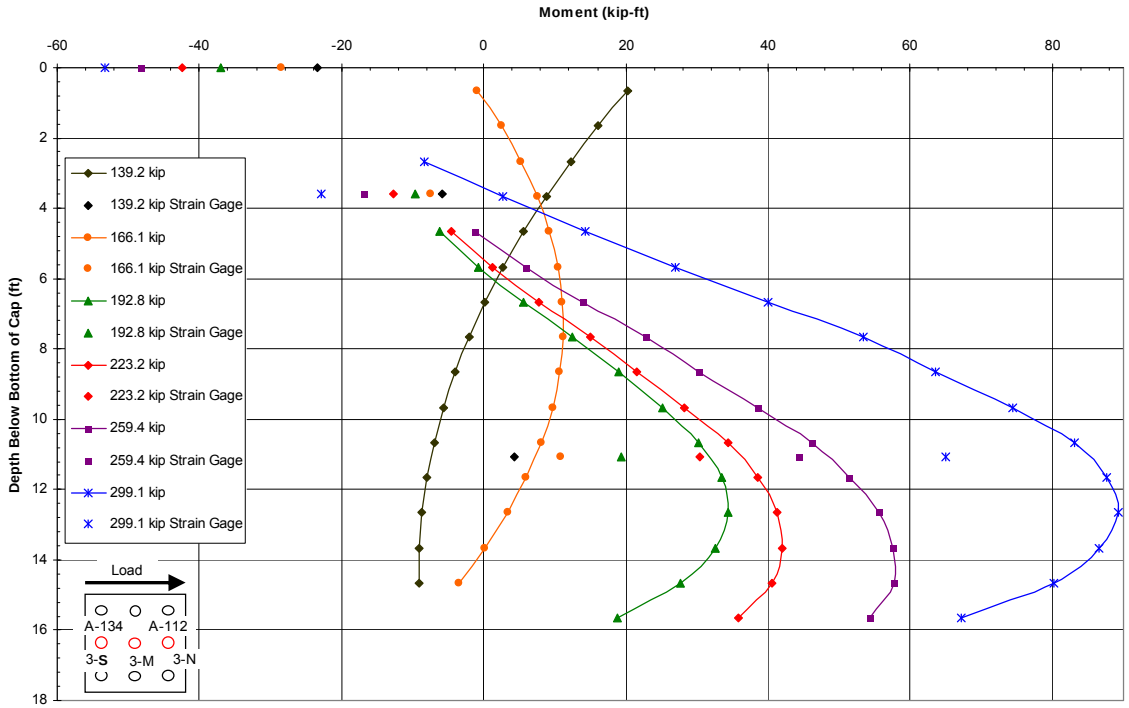

Figure 5-54 Test 5 bending moment vs. depth profiles obtained from array 112 and strain gage data as instrumented on the middle pile.

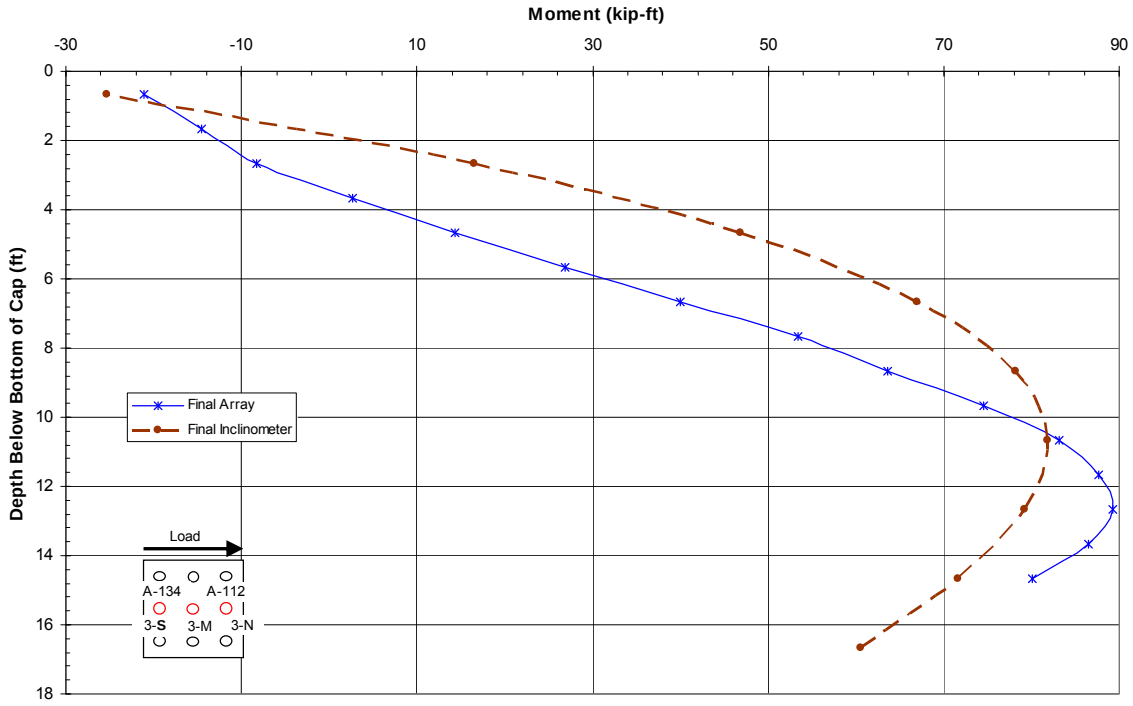

Figure 5-55 Test 5 bending moment vs. depth comparison of array 112 and the north inclinometer at maximum load.

Figure 5-55 shows the data from the south inclinometer and the north shape array. The data for the north inclinometer was not recorded. The maximum positive bending moment from the shape array data is 89 kip-ft and that from the inclinometer data is 78.5 kip-ft. Both sets show the maximum positive bending moment occuring at a depth of about 12.5 ft.

Figure 5-56 shows the bending moment vs. depth calculated using data from the shape array 134 in the south pile and strain gages located on the middle pile. As with Figure 5-54 the smaller displacement increments (0.125 (139.2 kip) and 0.25 (166.1 kip) inches) show a reverse curvature that is most likely caused by the two previous tests which pulled the pile cap in the opposite direction. Also the 0.5 (192.8 kip) inch increment shows that the depth of the maximum positive bending moment is around 6.5

ft, while the 0.75 (223.2 kip) and 1.0 (259.4 kip) inch increments show that the depth to be around 12 ft. The 1.5 inch increment shows that the depth of the maximum positive bending moment is closer to 11 ft.

Figure 5-57 show the comparison between the south inclinometer and the south array. The shape array has a maximum positive bending moment of 85 kip-ft at a depth of 11 ft while the inclinometer has a maximum positive bending moment of 78.5 kip-ft at a depth of about 12.5 ft.

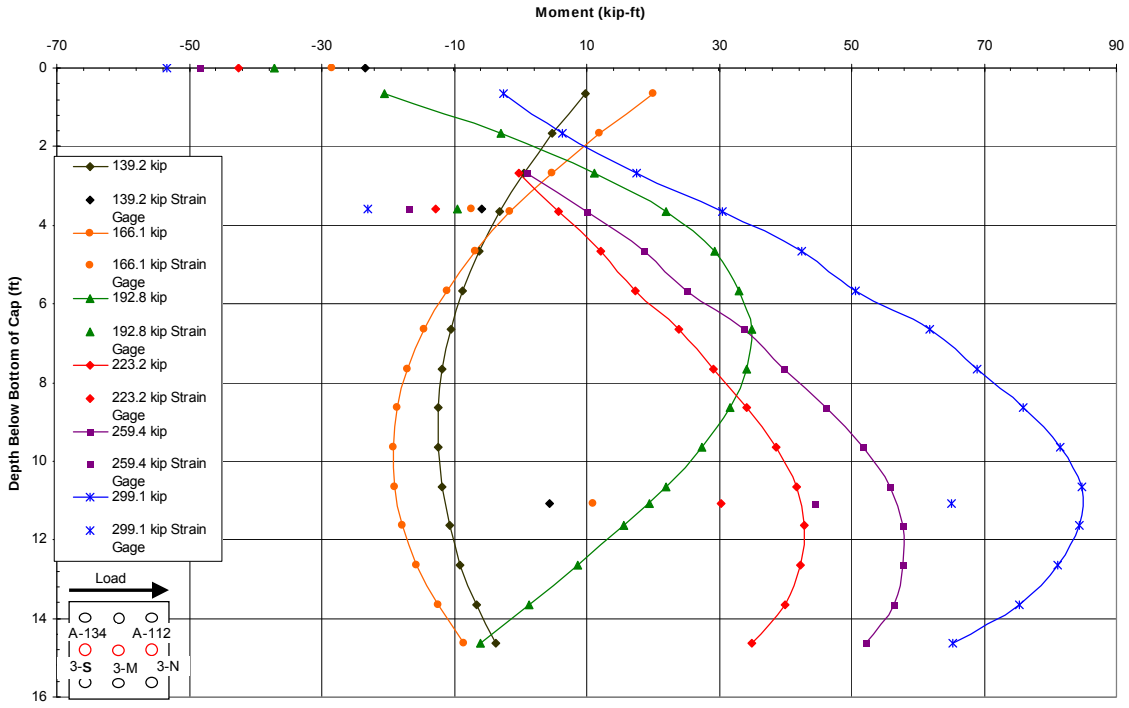

Figure 5-56 Test 5 bending moment vs. depth profiles obtained from array 134 and strain gage data as instrumented on the middle pile.

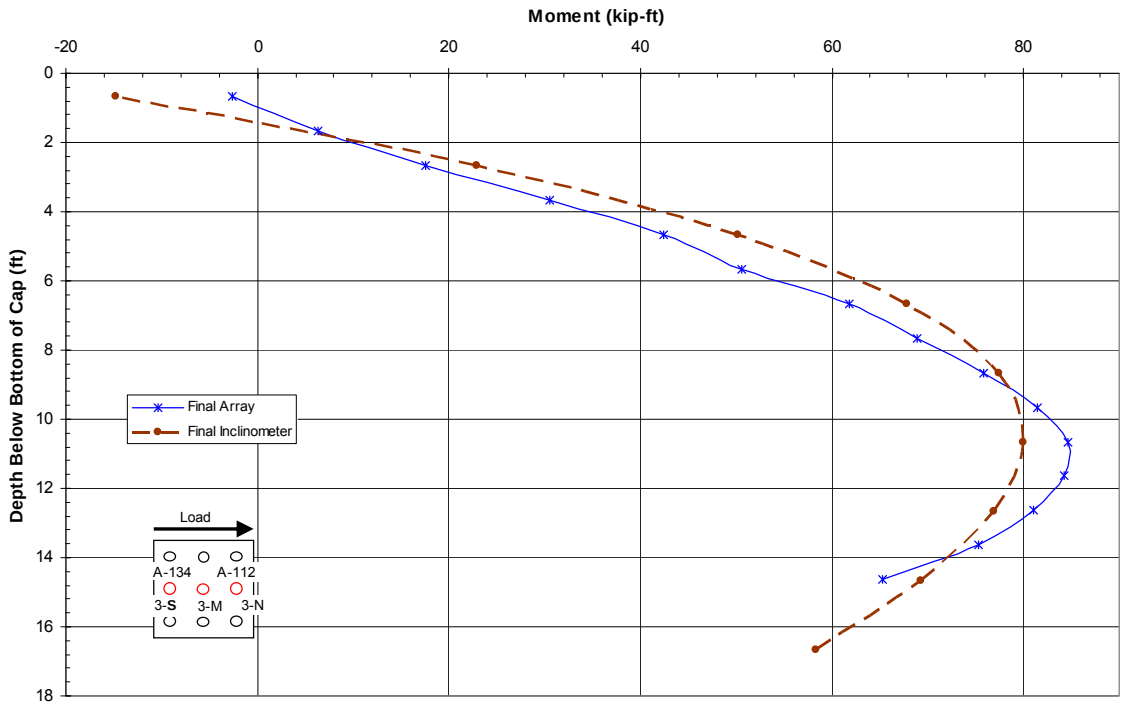

Figure 5-57 Test 5 bending moment vs. depth comparison of array 134 and the south inclinometer at maximum load.

5.4.5 Moment vs. Load Results

Figure 5-58 shows the maximum positive bending moment with respect to the applied load. Data was obtained from both shape arrays, but only the from strain gages on the middle pile. Figure 5-58 does not show the maximum negative bending moments, because of the initial opposite curvature of the piles which develop rather large negative moments near the top of the piles, which should not have been the case. The shape array data show good correlation varying by only 5 kip-ft at 299 kips of load.

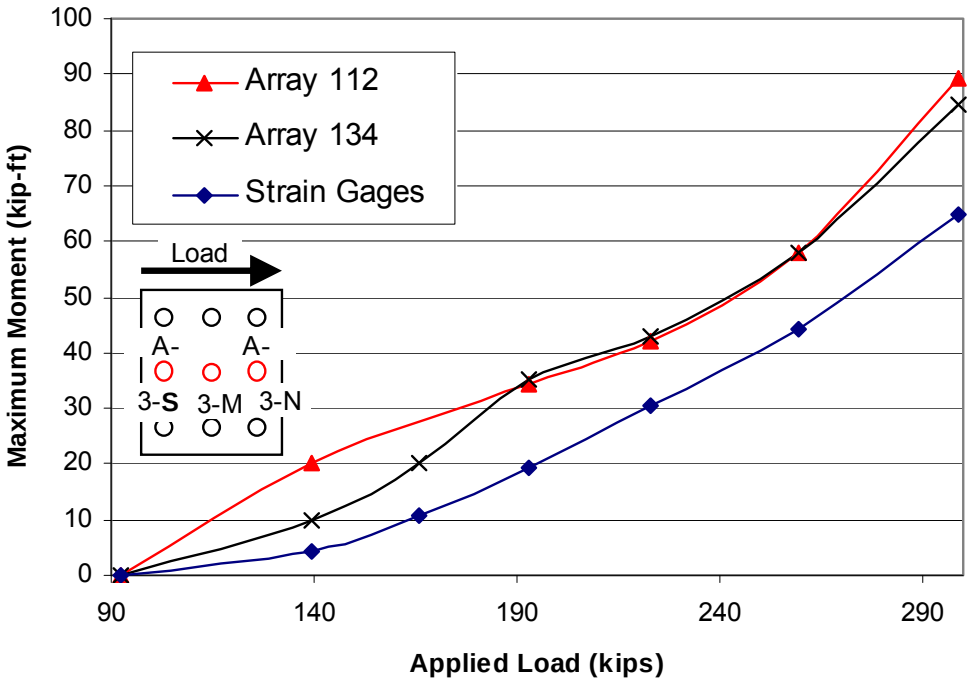

Figure 5-58 Test 5 maximum negative moments from the strain gage and shape array data.

5.5 Load Test with Higher Strength Flowable Fill behind Pile Cap 3

The lateral load test involving the higher strength flowable fill was test 10 of. Figure 4-16 shows the testing layout. The test was performed by pushing pile cap 3 and pile cap 2 apart. The test was performed on 24 August 2008 after a higher strength flowable fill was used to replace the native clay soil on the south side of pile cap 3. The section that was replaced with flowable fill was 12 ft wide (perpendicular to loading), 6 ft wide (in the direction of loading) and 6 ft deep. Pile cap 2 had previously been treated with eight jet-grout columns around the pile group prior to this test.

5.5.1 Load vs. Displacement Results

The actuator pushed to target displacements of 0.125, 0.25, 0.5, 0.75, 1.0, and 1.5 inches. The measured displacements on cap 3 were, however, 0.113, 0.27, 0.59, 0.77, 1.14, and 1.89, inches respectively. At each displacement increment 10 cycles of displacement were applied to evaluate reloading stiffness and damping. A continuous graph of the applied actuator load vs. displacement for pile cap 3 during this test is shown in Figure 5-59. This graph shows the load path taken during loading, unlading and reloading for each cycle. Reloading typically required a load that was 10 to 20% lower than the virgin load at that displacement. Subsequent cycles of reloading led to progressively greater reductions in lateral resistance within the range where load had previously been measured. These subsequent reductions in resistance are likely associated with the development of a gap in front of the pile.

The negative loads indicate the actuator force necessary to pull the actuator back to its initial position during un-loading. As shown in Figure 5-59, this typically brought the pile cap back to within 0.1 inch of its original position. Shortly after the 1.5 inch increment was reached, the data acquisition system was accidentally turned off so data is not available for the final unloading case. Although the pile did not yield during the loading, 50 to 60 kips were required to overcome base shear, side friction, and soil resistance from that that might have moved into the gap behind the pile during loading.

Figure 5-60 provides the peak pile cap load vs. displacement for each displacement increment which represents the “backbone” curve for the test. The curve shows a typical hyperbolic shape for a lateral load test on a pile in soil. Displacement is

increasing substantially with load relative to the initial part of the curve indicating that the soil near the ground surface is reaching its ultimate resistance.

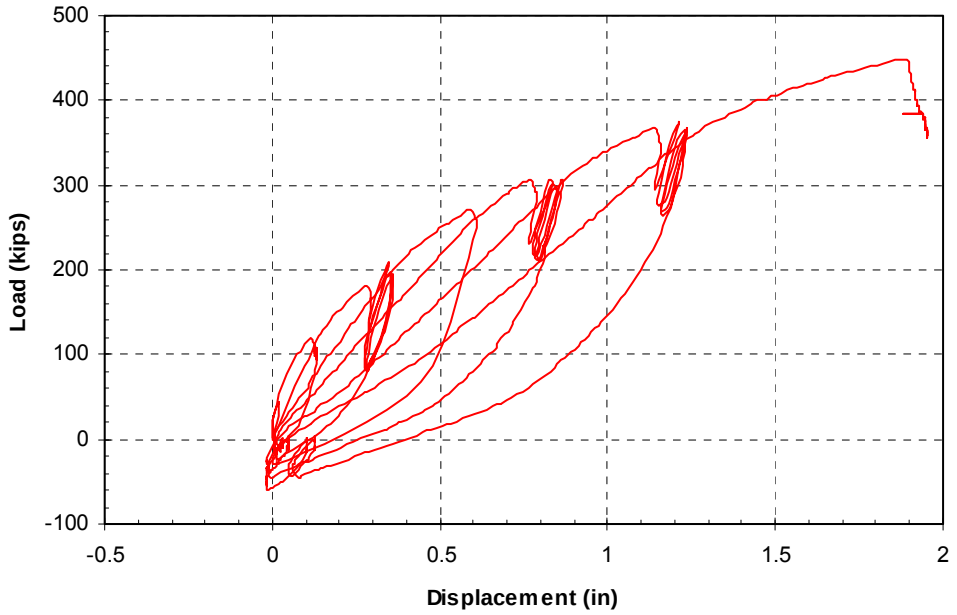

Figure 5-59 Plot of continuous pile cap displacement vs. applied load for pile cap 3 during test 10.

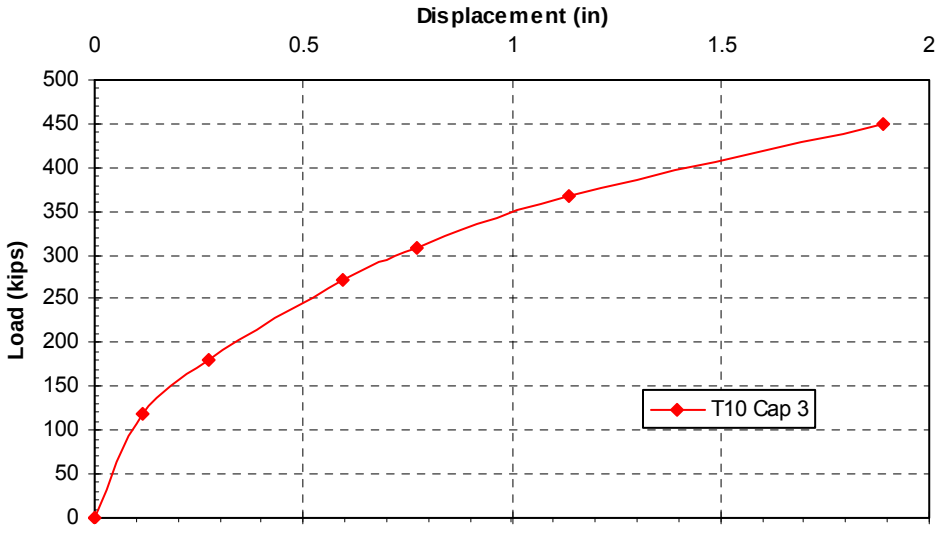

Figure 5-60 Plot of displacement vs. peak load curve for pile cap 3 during test 10.

5.5.2 Pile Cap Rotation vs. Load

Peak rotations vs. load curves for test 10 are shown inFigure 5-61. Rotation was calculated using both the shape arrays and string potentiometer that were located on top of the pile cap. All three curves showed good agreement with the peak rotation varying from 0.38 to 0.41 degrees at the peak load of 449 kips. The curves are linear until about 280 kips, then the rotation begins to increase more rapidly with increasing load. Comparing the pile cap rotations of test 1 to test 10, test 10 had a rotation of 0.35 degrees at a load of 420 kips while for the same rotation test 1 piles resisted only 282 kips. This shows that flowable fill increased the stiffness of the foundation substantially. In the linear portion of the graph the pile cap exhibits a "fixed end" condition, while at the higher loads and larger rotation the cap exhibits a partially fixed end condition.

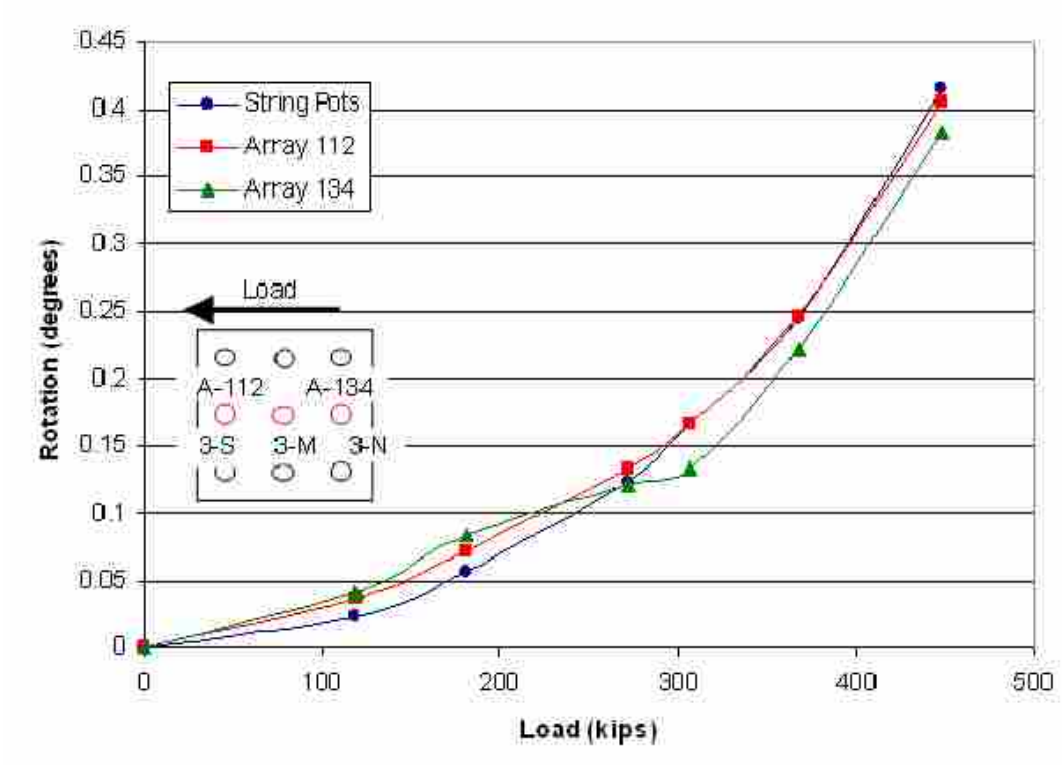

Figure 5-61 Peak pile cap load vs. pile head rotation for cap 3 during test 10.

5.5.3 Displacement vs. Depth Results

Displacement vs. depth curves obtained from the shape arrays and inclinometer data are shown in Figure 5-62 and Figure 5-63. Figure 5-62 provides curves from array 112 data (pile on south side of cap) while Figure 5-63 provides curves from array 134 data (pile on north side of cap). Comparisons between the shape array and inclinometer curves are shown in Figure 5-62 (a) and Figure 5-63 (a) and comparisons between the shape array and string pot readings are provides in Figure 5-62 (b) and Figure 5-63 (b). Generally, the shape array, inclinometer, and string potentiometer data have good agreement regarding the displacements profiles for the cap. The string potentiometer data tends to show a little less displacement than that of the arrays but at larger displacements they are closer. The displacements from the inclinometers are generally consistent with displacements from the arrays. Displacements from shape array 134 are a little different then the inclinometer but the difference is small with an average difference of 0.064 inches, and shape array 112 and the north inclinometer are reading almost the exact same displacements with an average difference of 0.036 inches. As discussed previously in the rotation section, the lower displacements show fixed end behavior while the higher displacements show a partial fixed end behavior. Also with the larger displacements the depth to zero displacement also increases, from 11 ft with the 0.125 (119 kip) in. displacement to 21 ft at the 1.5 (448 kip) in. displacement. Test 10 was taken as a base line test meaning that all of the instrumentation was zeroed prior to this test, for this reason the initial inclinometer data are not presented, it would be zero displacement for the length of the inclinometer.

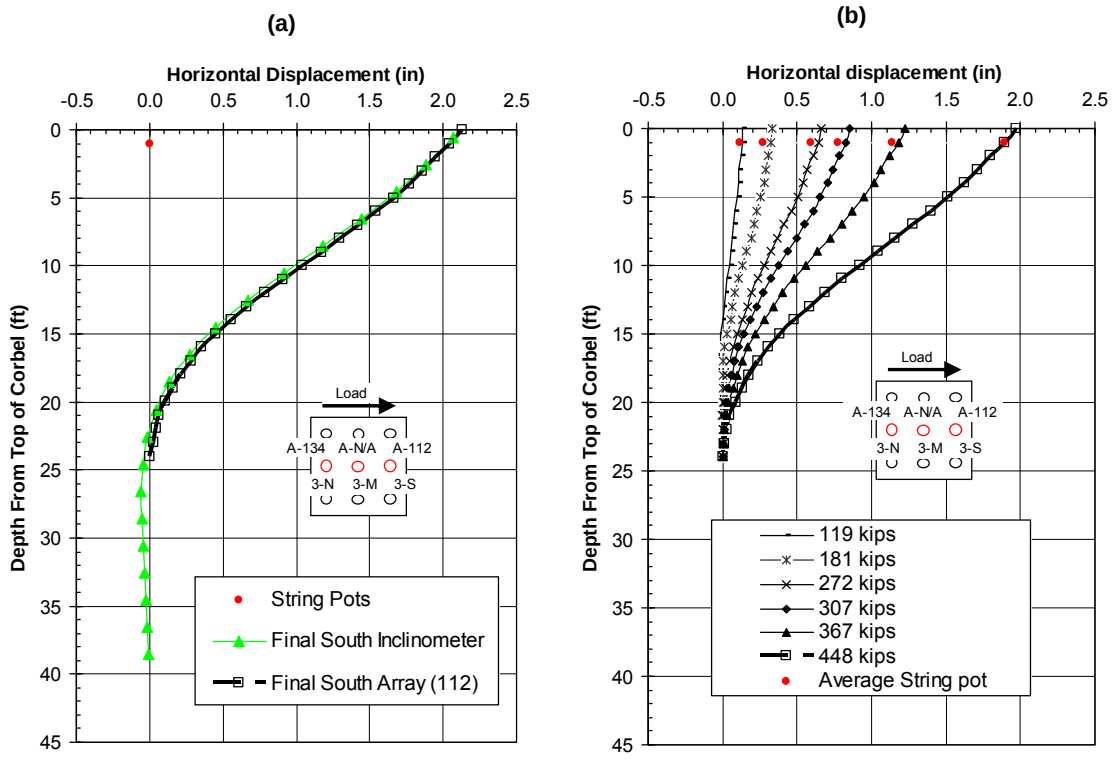

Figure 5-62 Test 10 (a) displacement vs. depth profiles comparing the final inclinometer to south shape array (112). (b) Displacement vs. depth curves comparing shape array to string potentiometer data.

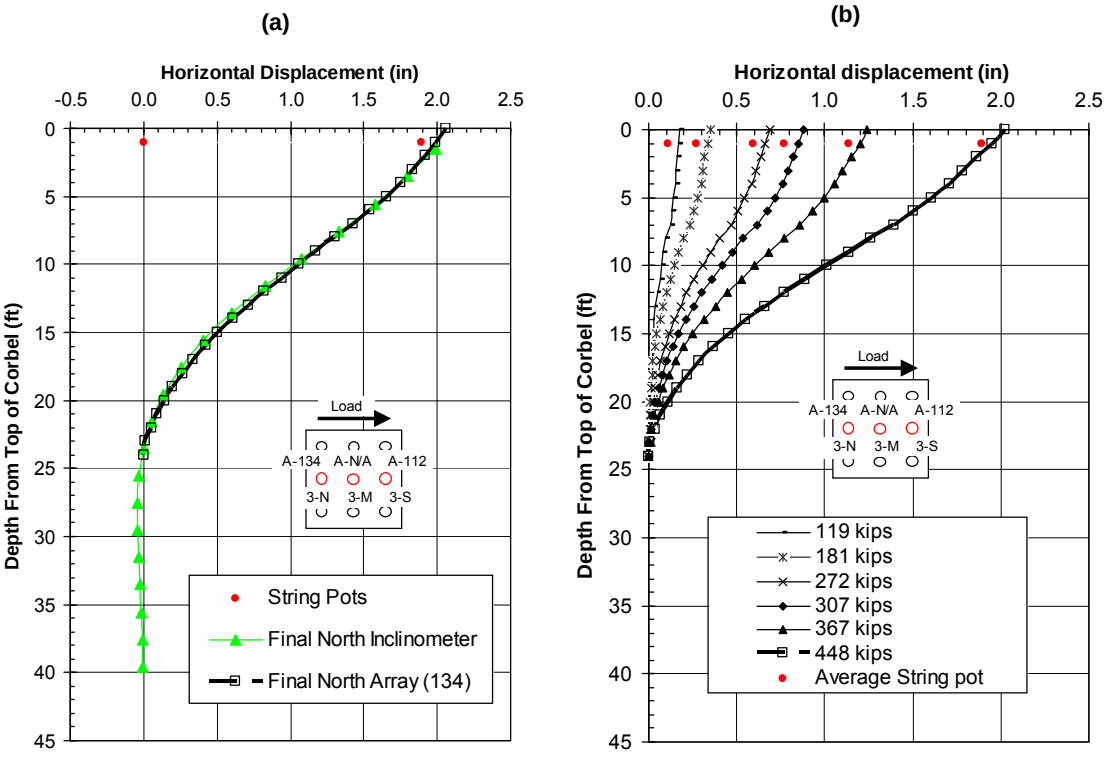

Figure 5-63 Test 10 (a) displacement vs. depth profiles comparing the final inclinometer to north shape array (134). (b) Displacement vs. depth curves comparing shape array to string potentiometer data.

5.5.4 Bending Moment vs. Depth

Figure 5-64 shows the bending moment vs. depth curves obtained from shape array 112 data and the strain gage data attached to the middle test pile. The data from the middle pile strain gages was used because all of the strain gages in the south pile were damaged or unreliable. The graph shows a maximum positive bending moment of 103.7 kip-ft at a depth of about 12.5 ft. The dashed lines show the linear extrapolation of the shape array data. The extrapolations are consistent with the bending moments calculated from the strain gages. Figure 5-65 shows the south inclinometer and the south shape array data (112) for the maximum load, maximums occur at around 12.5 ft in depth however the inclinometer shows that the maximum positive bending moment is about 78.5 kip-ft while that from the arrays is 103.5 kip-ft.

Figure 5-66 shows the bending moment vs. depth curves obtained from shape array 134 data and the strain gage data attached to the north test pile. The strain gage data show large negative bending moments near the pile pile-cap interface, which are questionable. Also the strain gage data for the 11.5 ft strain gage seem to be low. The shape array data shows that the maximum positive bending moment is 91.3 kip-ft at a depth of about 13.5 ft. Figure 5-67 shows the north inclinometer and north shape array computed bending moments for the maximum load. The maximum positive bending moment calculated from the inclinometer is about 73.4 kip-ft at a depth of about 12.5 ft. The north and south inclinometer data result in 15-25% lower for the maximum positive bending moments than that from the shape arrays.

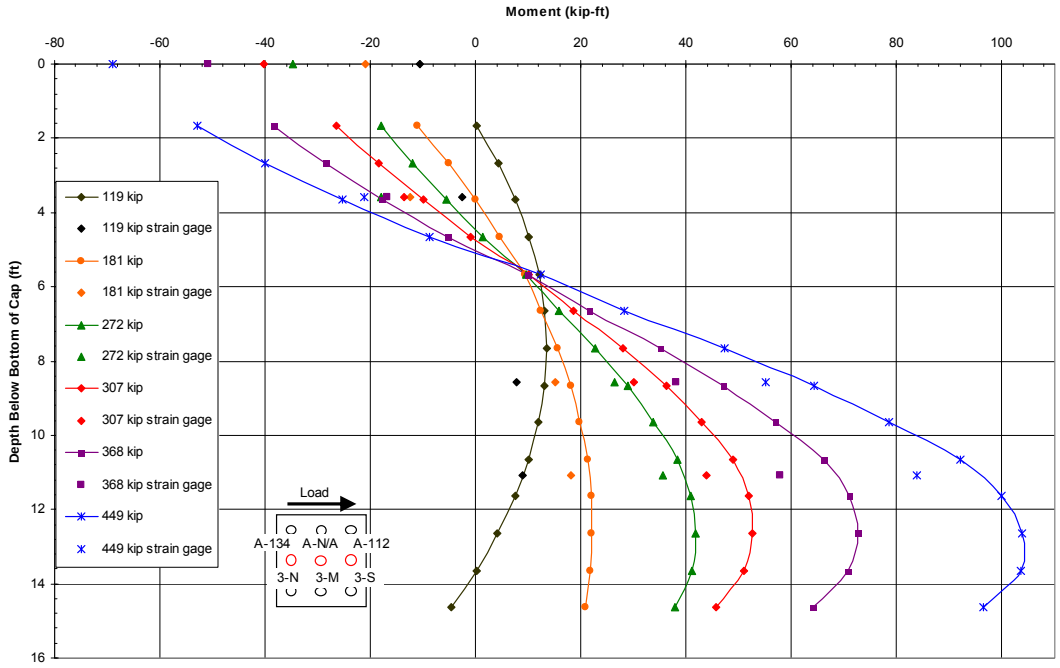

Figure 5-64 Test 10 bending moment vs. depth profiles obtained from array 112 and strain gage data as instrumented on the middle pile.

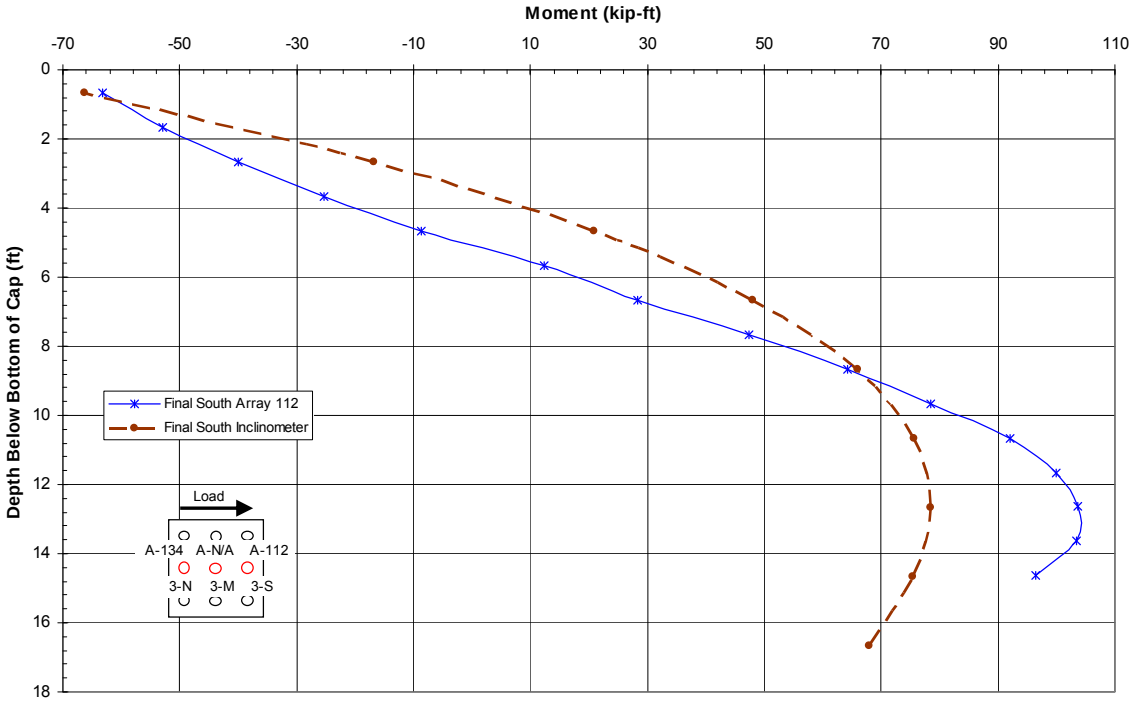

Figure 5-65 Test 10 bending moment vs. depth comparison of array 112 and the south inclinometer at maximum load.

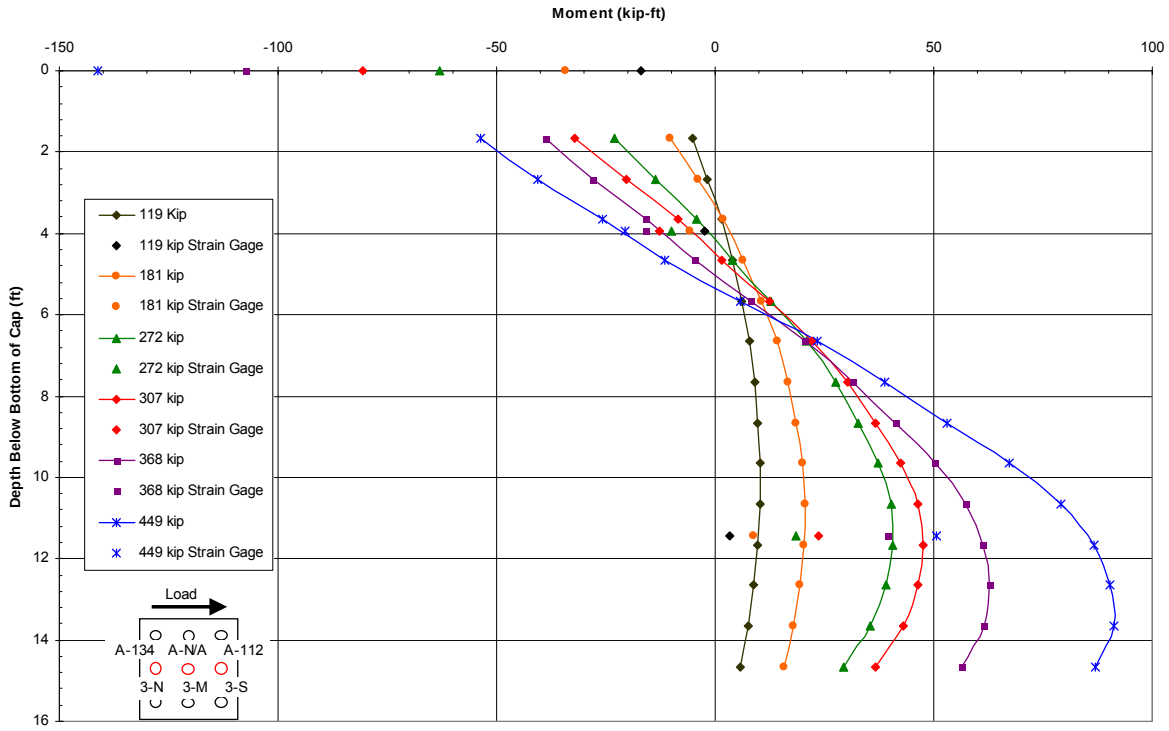

Figure 5-66 Test 10 bending moment vs. depth profiles obtained from array 134 and strain gage data as instrumented on the north pile.

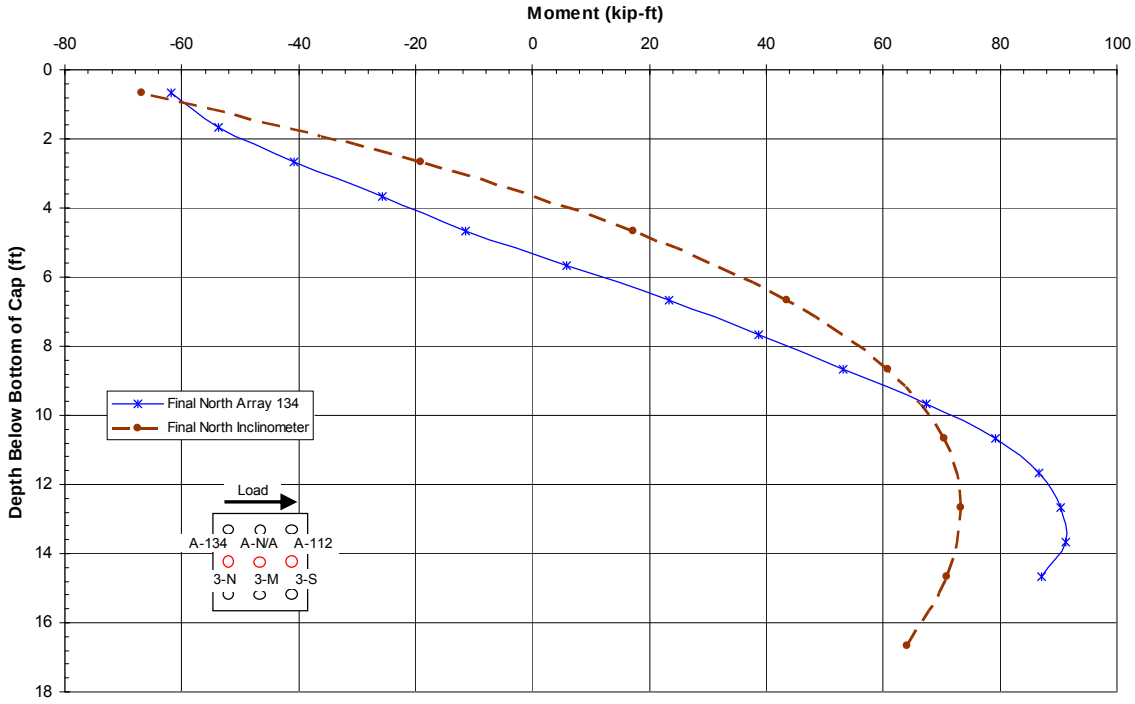

Figure 5-67 Test 10 bending moment vs. depth comparison of array 134 and the north inclinometer at maximum load.

5.5.5 Moment vs. Load Results

Figure 5-68 shows the maximum negative moment in the three instrumented piles in the group as a function of the applied load. Moment curves calculated from the two arrays and the strain gages on the middle pile are relatively similar, however, moments calculated from the strain gages on the north pile appear to be abnormally high (about double) and are likely unreliable. The moments for the middle and back row piles are somewhat higher than the that for the front row as one would expect from pile group interaction effects (Rollins et al, 2006). Interaction of the shear zones for trailing row piles typically leads to a softer soil reaction so that greater moment is produced for a given load. However, in this case, the differences are relatively small considering that the piles are closely spaced. Perhaps the strength of the granular soil within the perimeter of the pile group has been improved by the pile driving process which would tend to compact the surrounding soil.

Figure 5-69 shows the maximum positive moment in the three instrumented piles in the group as a function of the applied load. Once again the moment vs. load curve for the three piles are relatively similar, however, the maximum positive moment calculated for the north strain gage data is about half of that calculated from the other data and may be unreliable. In this case, the front row pile develops higher moments than that in the middle and back row piles, differences, however, are typically around 11%. Because of the limited number of strain gages on the piles the placement of the gage does not always correspond to the location of the maximum moment that is displayed by the arrays. If the strain gages were placed at the points of maximum moment there could have been better agreement.

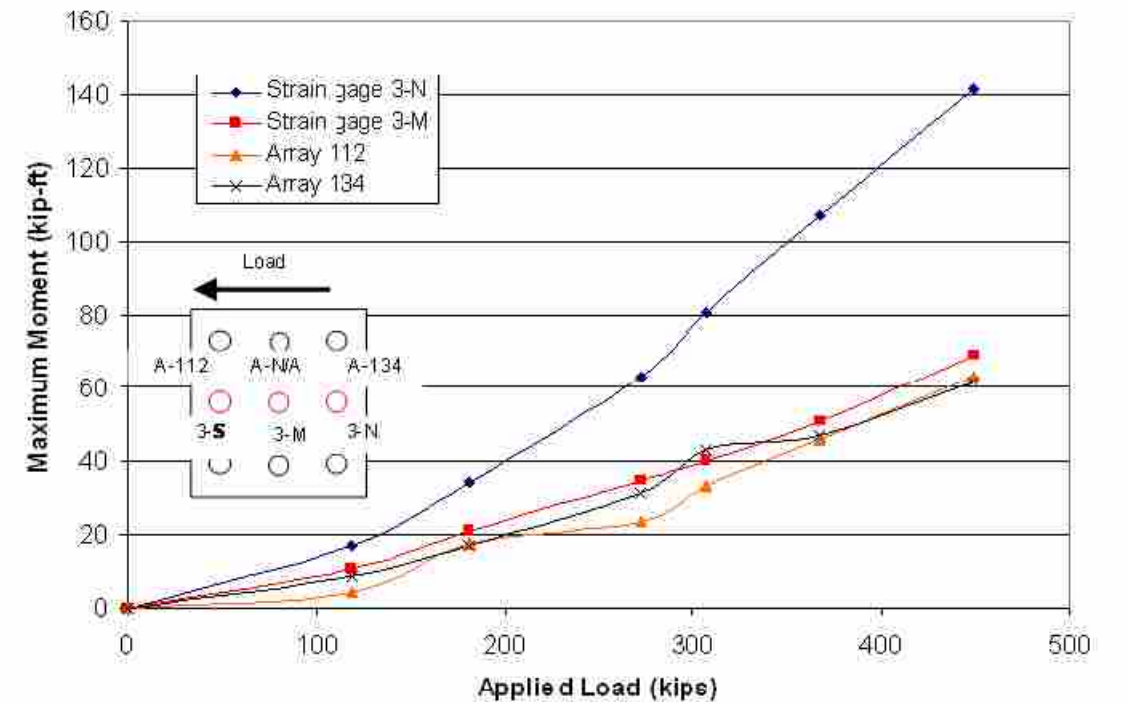

Figure 5-68 Maximum negative bending moments from test 10.

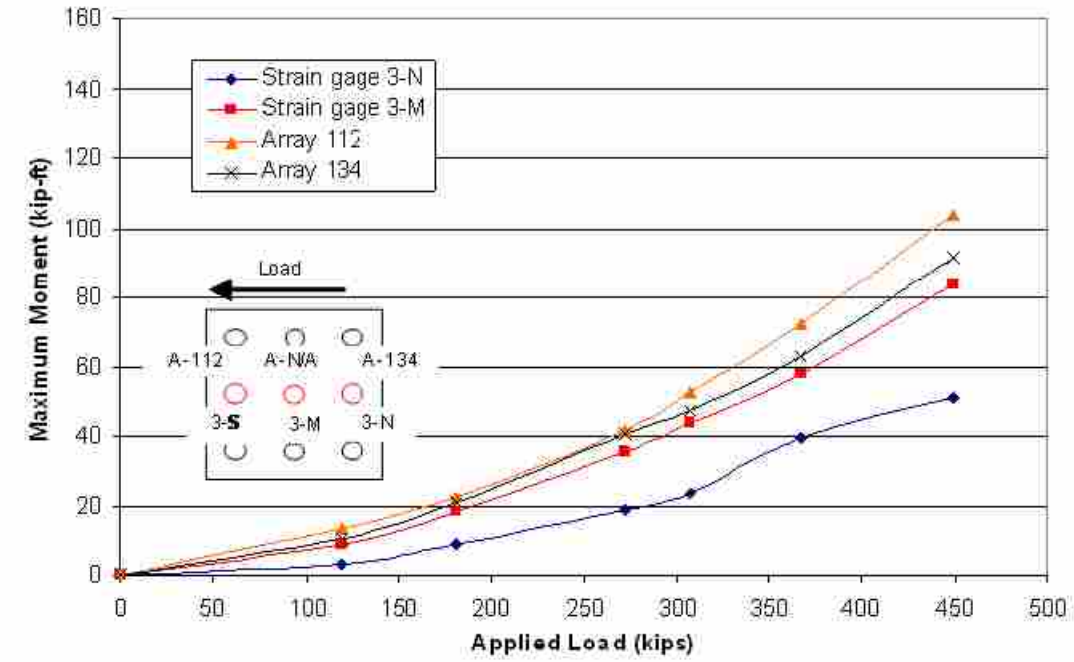

Figure 5-69 Maximum positive bending moments from test 10.

5.6 Higher Strength Flowable Fill behind Pile Cap 3 with a 1 Ft section Excavated behind the Pile Cap

5.6.1 Load Displacement Results

In a previous test, pile cap 3 was used as a reaction cap to test pile cap 2 which had been reinforced with jet-grout (Adsero, 2008). Pile cap 2 was much stronger than pile cap 3 which caused pile cap 3 to have excessive displacements. The displacements that mostly affect this test came from trying to push pile cap 2 back to its original position.

In this new test (test 12) pile cap 3 started with an initial average inclinometer displacement of about 0.86 inches. All of the data for test 12 was going to use test 10 as the initial measurements, however the string potentiometers show excessive displacements, 1.14 and 1.47 inches respectively. Given these initial displacements it was determined that by setting the zero point for the start of test 12 at 0.86 inches (the average initial inclinometer displacement), the data would best described what happened during the test.

Figure 5-70 shows the continuous load displacement results. The actuator pushed the pile cap to the displacements of 0.32, 0.67, 1.07, 1.424, 2.17, 2.78 inches, while the string potentiometers zeroed to the inclinometer data read, 0.86, 1.08, 1.33, 1.62, 1.88, 2.44, and 2.95 inches respectively. The loads corresponding to these displacements are 75.4, 119.8, 164.8, 201.4, 274.1, and 313.7 kips respectively.

Figure 5-71 shows the peak load vs. displacement obtained from the string potentiometers that have been zeroed to the initial inclinometer data.

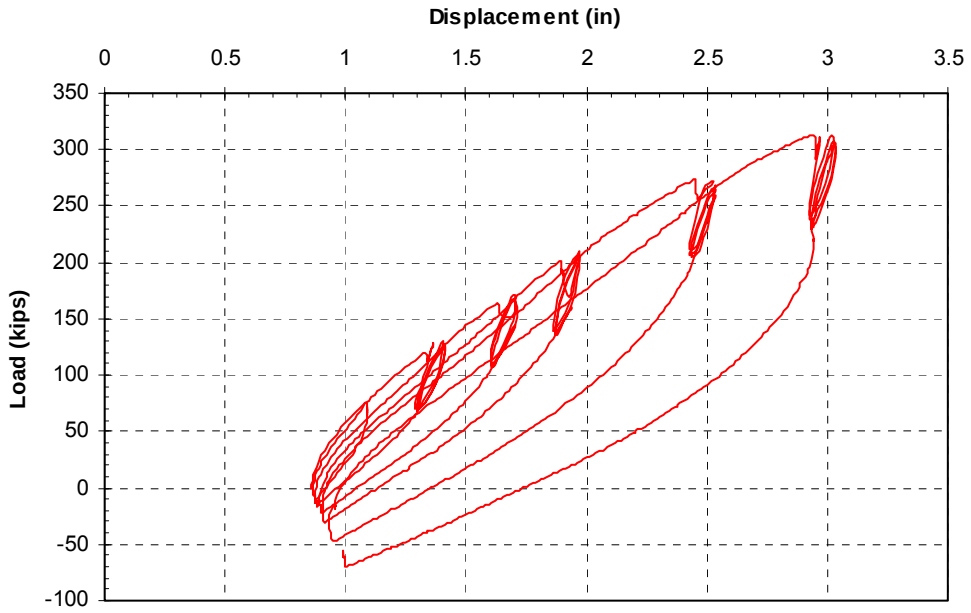

Figure 5-70 Plot of continuous pile cap displacement vs. applied load for pile cap 3 during test 12.

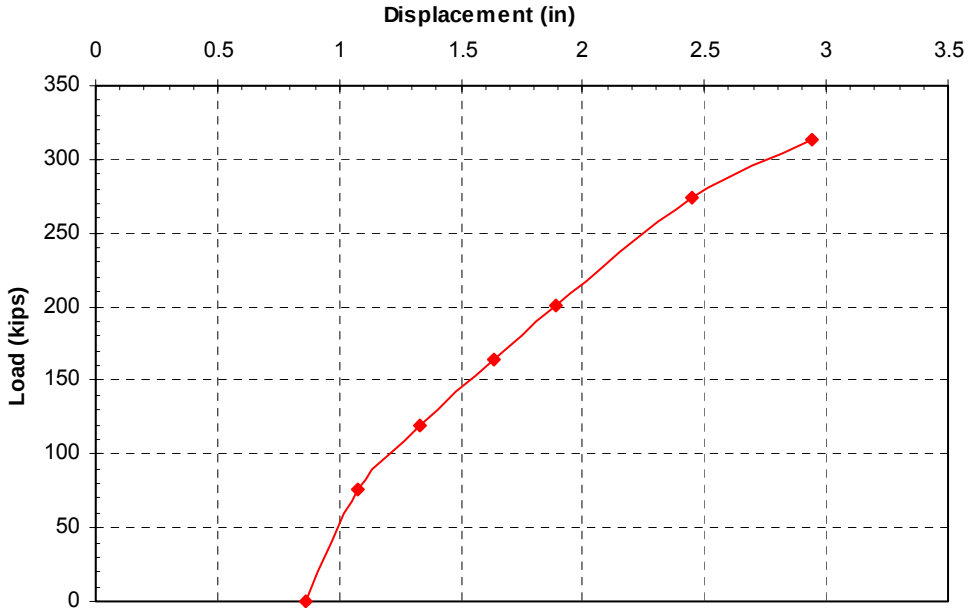

Figure 5-71 Plot of displacement vs. peak load curve for pile cap 3 during test 12.

5.6.2 Pile Cap Rotation vs. Load

Figure 5-72 shows the rotation vs. load for pile cap 3. The pile cap starts off with an initial rotation of about 0.25 degrees according to the string potentiometers, 0.18 and 0.17 degrees according to the shape arrays. This is consistent with the large initial displacement on the pile cap.

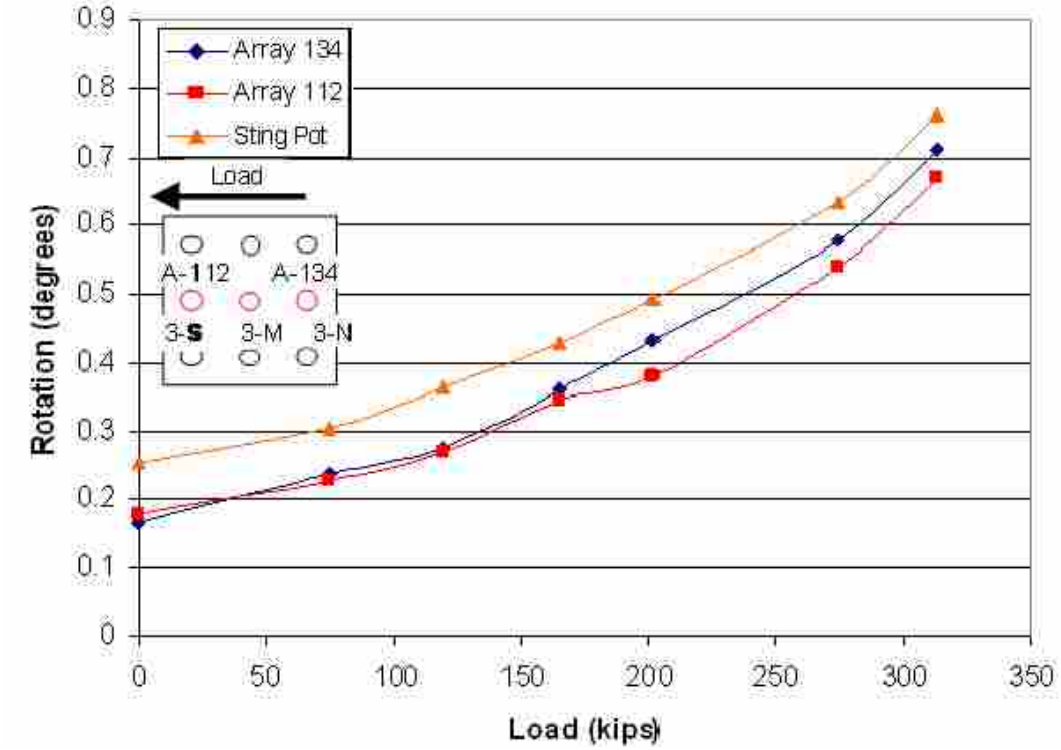

Figure 5-72 Peak pile cap load vs. pile head rotation for test 12.

5.6.3 Displacement vs. Depth Results

Figure 5-73 shows the depth vs. displacements for the north pile. The data show good agreement. The string potentiometers were adjusted to the initial inclinometer; the initial inclinometer data shown on the graph is with respect to test 10. The string

potentiometer data show very good agreement with the shape array data at all respective displacement increments.

Figure 5-74 shows the depth vs. displacement for the south pile. The data for this pile doesn't have as close of an agreement as that observed for the north pile. These small discrepancies could be from using the average value from the initial inclinometer measurements. The average was 0.86 inches, however the south inclinometer had an initial displacement of 0.91 inches when the later value is used the agreement is significantly better.

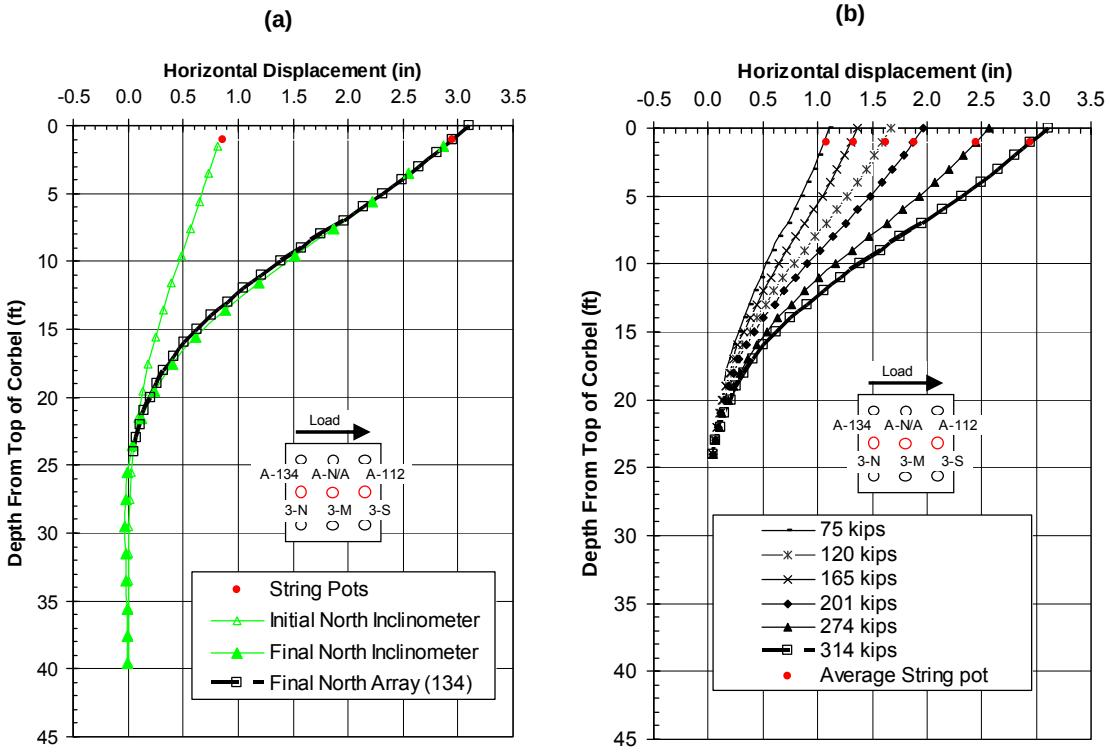

Figure 5-73 Test 12 (a) displacement vs. depth profiles comparing the final inclinometer to north shape array (134). (b) Displacement vs. depth curves comparing shape array to string potentiometer data.

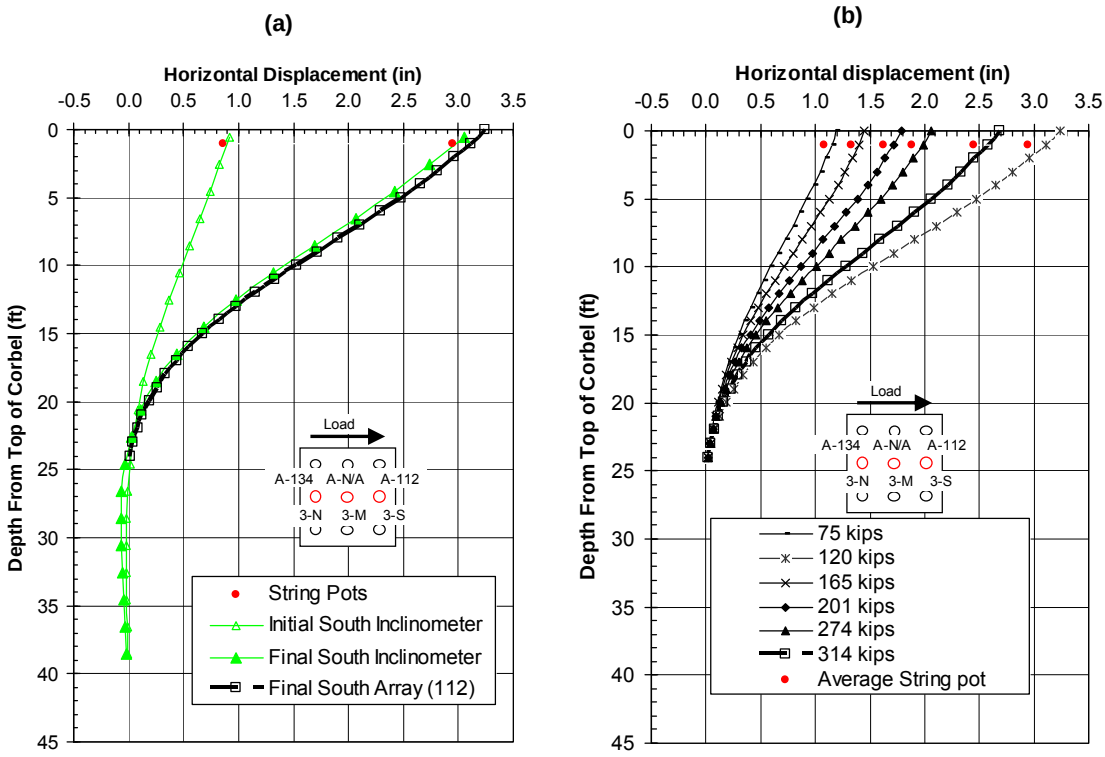

Figure 5-74 Test 12 (a) displacement vs. depth profiles comparing the final inclinometer to south shape array (112). (b) Displacement vs. depth curves comparing shape array to string potentiometer data.

5.6.4 Bending Moment vs. Depth

Figure 5-75 shows the bending moment vs. depth as computed from the shape arrays and the strain gage data on the north pile in pile cap 3. The strain gage data shows very large negative bending moments at the pile pile-cap interface with the largest moment being -98 kip-ft. At the depth the strain gages calculated moments 20-30 kip-ft lower than that calculated using the shape arrays data. The shape arrays show that the location of maximum positive bending moment is around 13.5 ft for the 314 kip (2 in) load increment and 12-13 ft for the 274 kip (1.5 in) and 201 kip (1 in) load increments.

The maximum positive bending moment for the 314 kip (2in) load increment was 104.7 kip-ft.

Figure 5-76 shows the bending moments calculated using the final inclinometer data and the corresponding shape array data for the north pile. The two curves show good agreement until a depth of 9 ft where the shape array data tends to have a higher positive bending moment value than that of the inclinometer. The maximum positive bending moment calculated from the inclinometer data is 95.8 kip-ft at a depth of 12.5 ft. The shape array calculated maximum positive bending moment is 104.6 kip-ft at a depth of 13.5 ft. This difference could be from seating of the shape array in the p.v.c pipe, or discrepancies in the numerical method used to calculate the bending moments.

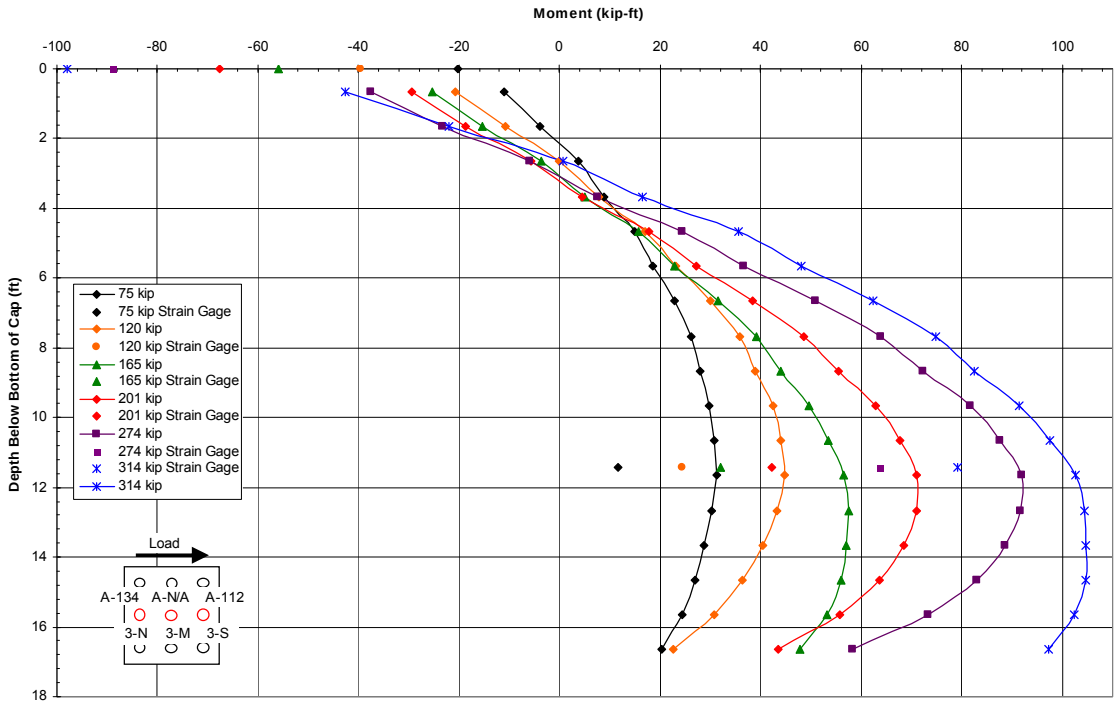

Figure 5-75 Test 12 bending moment vs. depth profiles obtained from array 134 and strain gage data as instrumented on the north pile.

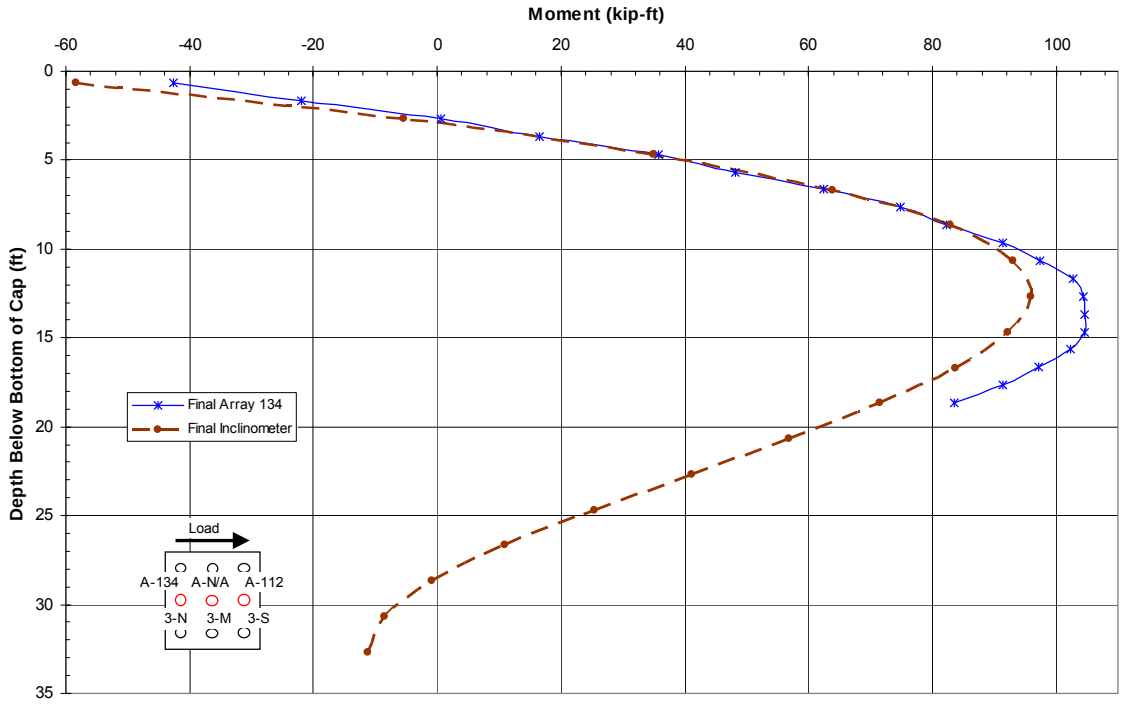

Figure 5-76 Test 12 bending moment vs. depth comparison of array 134 and the north inclinometer at maximum load.

Figure 5-77 shows the bending moment vs. depth profile calculated from south shape array (112) data and the moments calculated from the strain gages. The strain gage data are reading on average about 30 kip-ft lower at the 11.5 ft depth with the 274 kip (1.5 inch) load increment reading about 50 kip-ft lower than the shape array. The location of the maximum positive bending moment is at about 12.5 ft deep except for the 314 kip (2.0 inch) load increment where it is located at 14.5 ft deep; however the shape array jumps in value at the 14 ft mark so that data may not reliable. The trend shows that the maximum positive bending moment would be between 12.5 ft and 15 ft deep.

Figure 5-78 shows the bending moment vs. depth profile calculated using shape array measurements and final south inclinometer measurements. The north shape array (134) data is also shown on this graph. The south inclinometer data and the north array

data have very good agreement. The inclinometer data shows that the maximum positive bending moment is 103.4 kip-ft at a depth of 12.5 ft while the north shape array (134) data shows the maximum positive bending moment is 104.6 kip-ft at a depth of 13.5 ft. The south array (112) data shows good agreement with the inclinometer until a depth of about 10 ft and it increases at a faster rate then the inclinometer does. The south shape array (112) data shows that the maximum positive bending moment is 122.3 kip-ft at a depth of 14.5 ft.

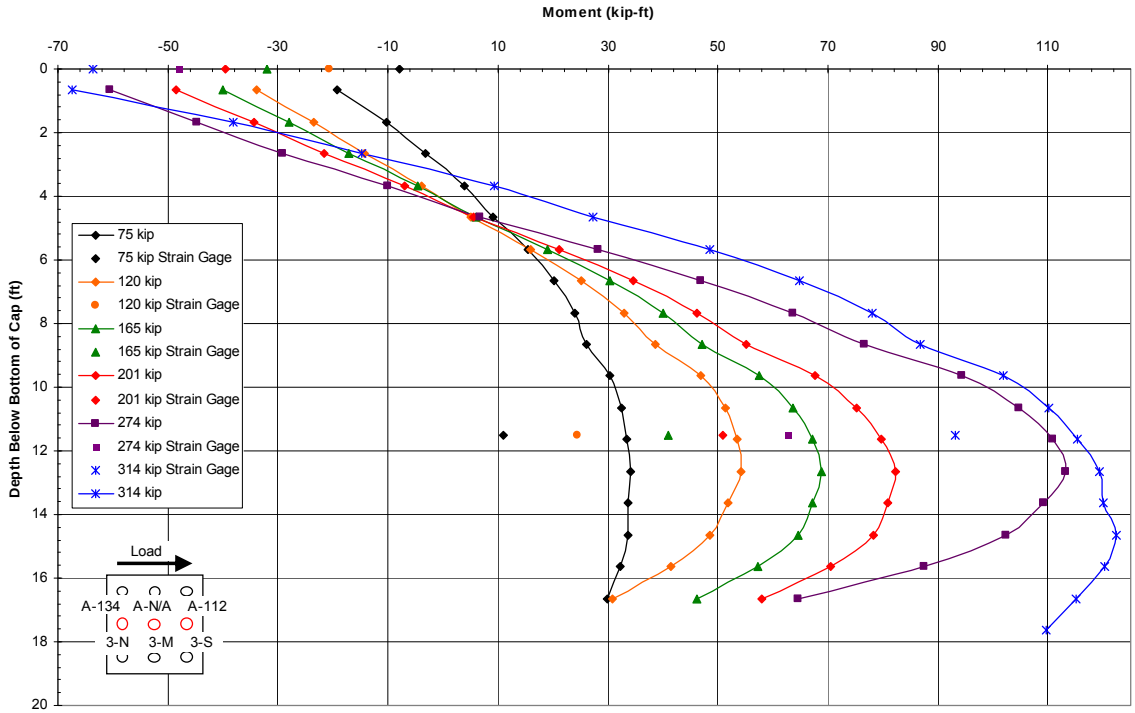

Figure 5-77 Test 12 bending moment vs. depth profiles obtained from the array (112) and strain gage data as instrumented on the south pile.

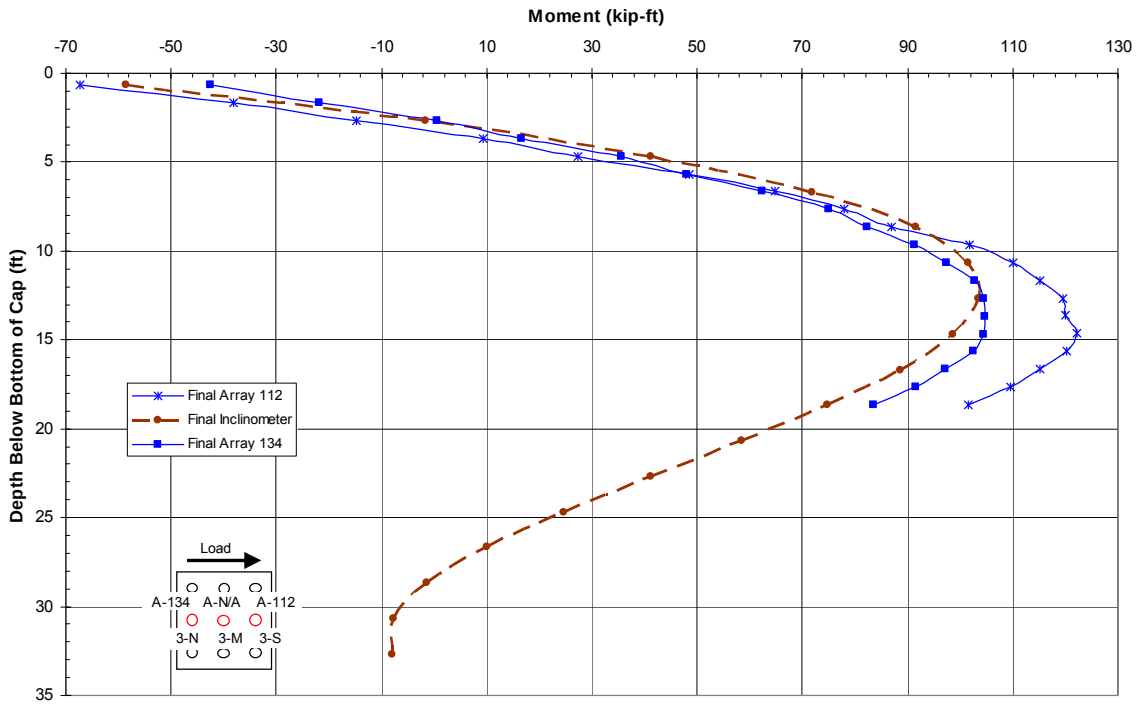

Figure 5-78 Test 12 bending moment vs. depth comparison of north array (134), the south array (112) and the south inclinometer at maximum load.

5.6.5 Moment vs. Load Results

Figure 5-79 shows the maximum negative bending moments in pile-cap 3. The data for this graph was obtained from the strain gages and the shape array measurements. The data does not show good agreement, which could be from the inconsistencies in calculating the bending moments at the pile pile-cap interface. The south shape array (112) data and the strain gage data on the middle pile are the only measurements that show good agreement. The south shape array (112) data is about 3 kip-ft greater than that from the strain gages. Figure 5-80 shows the maximum positive bending moments in pile-cap 3. This data does not agree well. Maximum values range from 79 kip-ft to 122.3 kip ft.

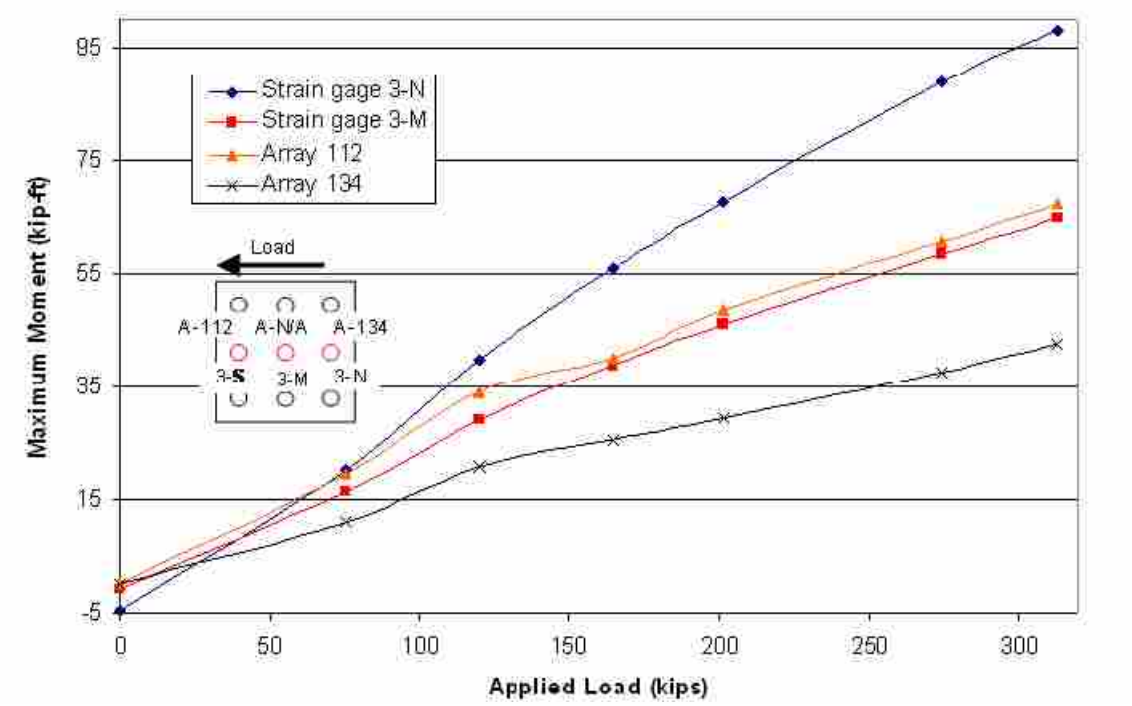

Figure 5-79 Maximum negative bending moments from test 12.

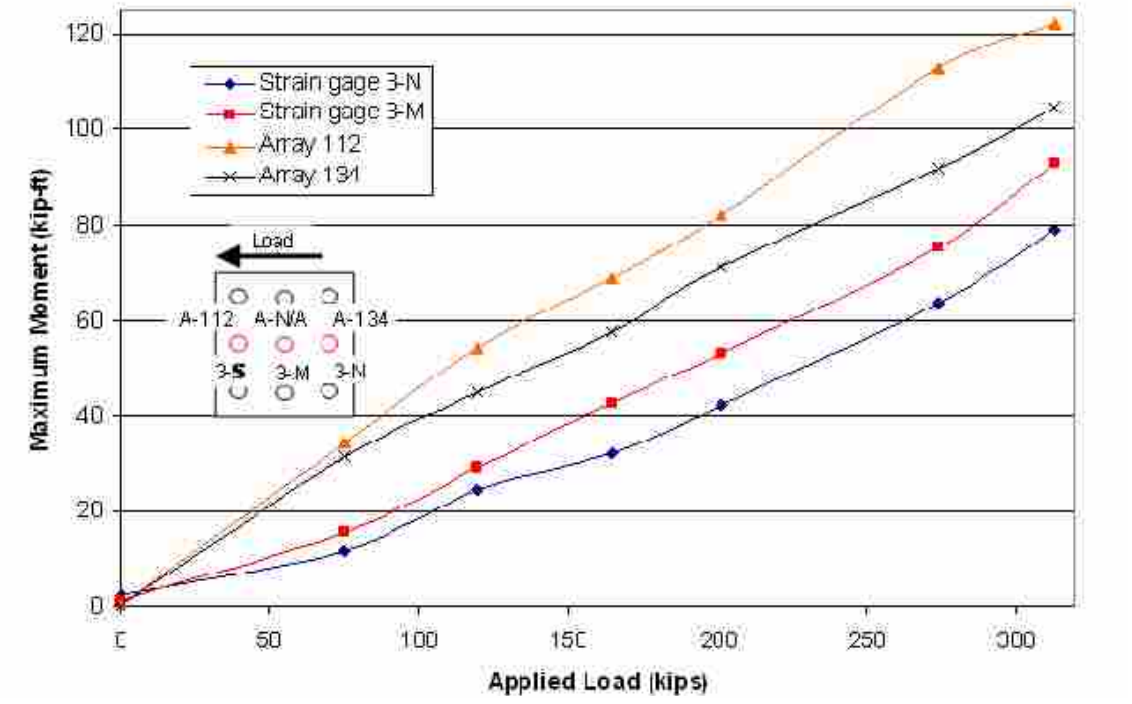

Figure 5-80 Maximum positive bending moments from test 12.

6 Discussion of Results

The results presented in chapter 5 are discussed in detail in this chapter.

6.1 Strength Increase from placing Low Strength (30 psi) Flowable Fill beneath the Cap surrounding the Piles

To evaluate the strength increase from the flowable fill, comparisons can be made between the results obtained from test 1 and test 2 in the native clay (see Sections 5.1 and 5.2) to test 3 and test 5 with the flowable fill (see Sections 5.3 and 5.4). The differences in these tests are that in test 3 the weaker flowable fill was placed surrounding the piles beneath the cap and had passive resistance from the native clay on the pile cap face and in test 5 had the weaker flowable fill beneath and in front of the cap without passive resistance.

6.1.1 Load vs. Displacement Discussion

Figure 6-1 shows the Load vs. Displacement curves for test 3 cap 3 compared to test 1 cap 2. The results follow the same general trend, howeverl with, test 3 showing that there is a strength increase of 10 to 20 kips. At the 0.5 inch displacement the strength increase was about 15 kips and at the 1.1 inch displacement the strength increase was about 20 kips. The initial stiffness of the cap with the flowable fill around the piles

increased to 1070 k/in compared to the 858 k/in of the native clay. This figure shows that the weaker flowable fill beneath the pile cap around the piles resulted in a minimal increase in lateral resistance. The last two points on the T3 cap 3 curve is an extension from test 4. The extension was necessary because the displacements in test 3 were not as large as the displacements during test 1.

Figure 6-2 compares test 5 cap 3 (test involving the weaker flowable fill beneath the pile cap without passive resistance on the pile cap) to test 2 cap 1 (test involving the untreated clay without passive resistance on the pile cap). In order to make a comparison possible test 5 was shifted by 0.35 inches, as was explained in section 5.2.1 due to the previous loading of the cap it is believed that soft clay filled in the gap behind the pile. Test 5 shows an increase in lateral resistance of about 30 kips compared to test 2. As seen from test 3 an increase of about 15-20 kips is from the flowable fill beneath the pile cap, while the other 10-15 kips could be from the flowable fill that was placed behind the cap. The stiffness of cap 3 remained essentially the same from test 3 to test 5 making the stiffness compared to test 2 much higher. The stiffness for test 5 was about 1070 kips/in while that for test 2 was about 300 kips/in. The increase in lateral resistance from the weaker flowable was minimal.

6.1.2 Moment vs. Load Comparison

Figure 6-3 shows the maximum positive moment vs. load curves for tests 3 and 5 for cap 3 as well as test 1 and 2 caps 2 and 1. The graph shows that the moments are fairly similar for all of the tests. Test 5 shows large moments in comparison to test 2

however that could be because larger loads were required to move the cap, also the shapes are consistent with one another.

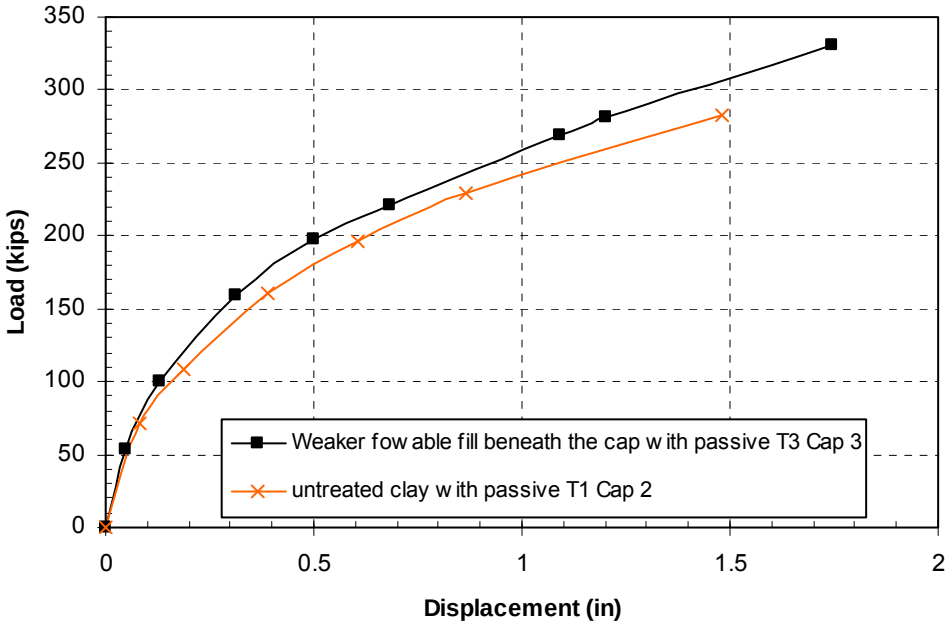

Figure 6-1 Load vs. displacement results comparing test 3 cap 3 to test 1 cap 2.

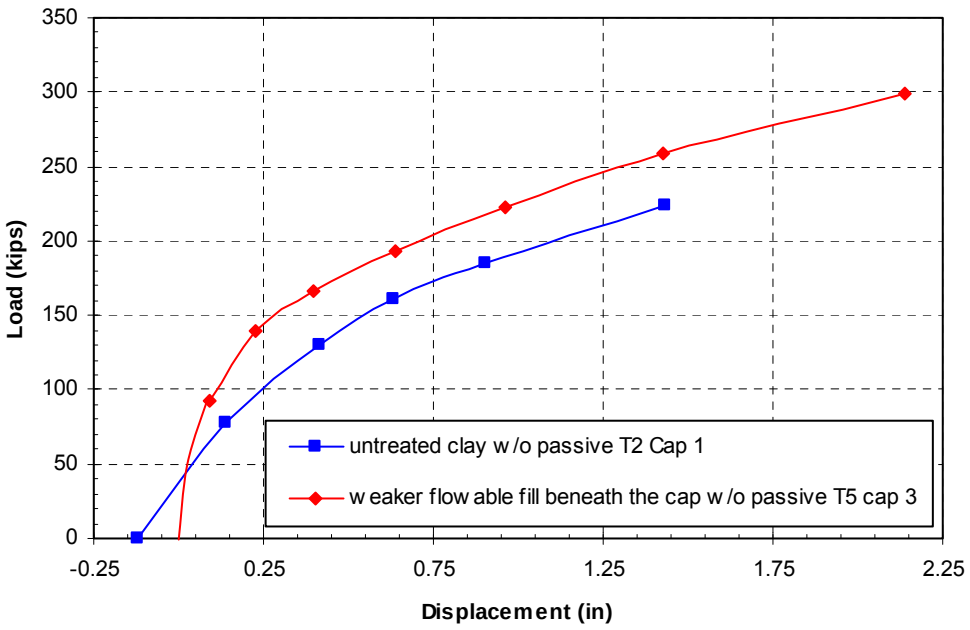

Figure 6-2 Load vs. displacement results comparing test 3 cap 1 to test 5 cap 3.

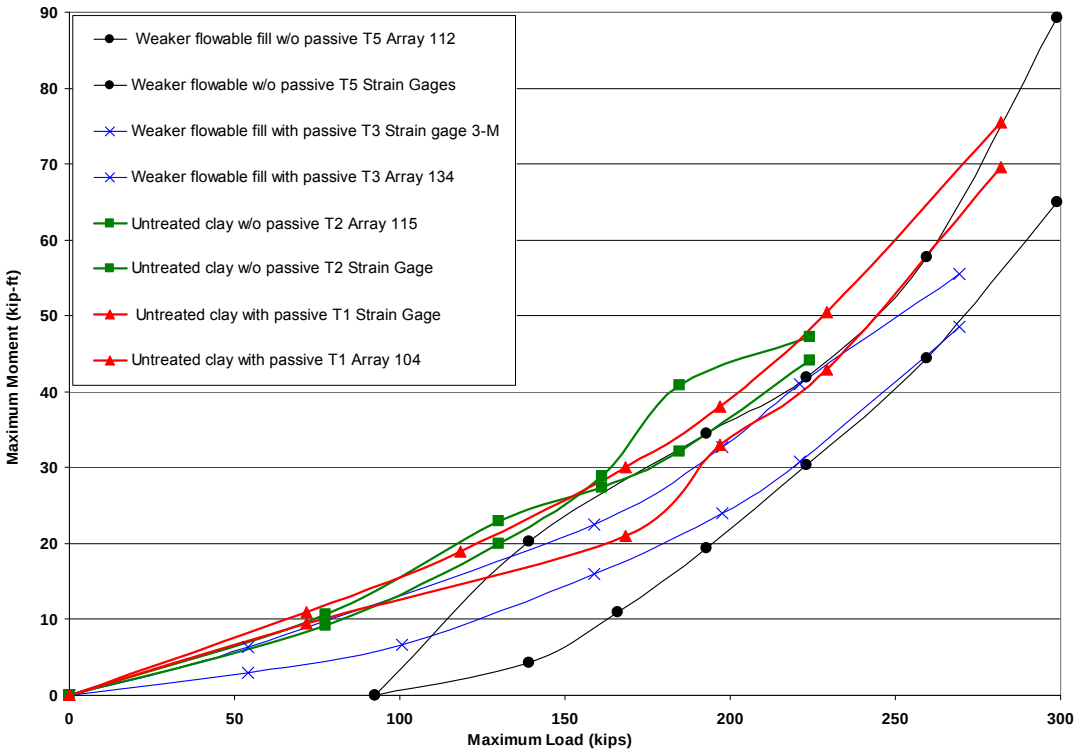

Figure 6-3 Comparing moment vs. load data from tests 1, 2, 3 and 5.

6.2 Strength Increase from placing 137 psi Flowable Fill behind Pile Cap 3

Although an increase of lateral resistance was seen as a result of the placement of the weak flowable the increase was quite minimal. Due to the low strength of the flowable fill material it was unable to cement the soil together to produce any appreciable increase. This section will evaluate the increase in lateral resistance produced by placing a stronger flowable fill material behind pile cap 3.

Due to the poor performance of the weaker flowable fill placed beneath the cap, it was decided to excavate the native clay material on the south side of the pile cap and replace it with a stiffer flowable fill material (the unconfined compressive strength of

which was about 137 psi). In this section tests 10 and 12 will be compared to the results of tests 1 and 2 to evaluate the increase in lateral resistance.

6.2.1 Load vs. Displacement Discussion

There are three comparisons that will be made from the tests involving the higher strength flowable fill placed behind pile cap 3. First comparisons will be made between test 10 (involving the higher strength flowable fill directly behind the pile cap) and test 1 (involving the native clay material with clay directly behind the pile cap). Next comparions will be made between test 12 (involving the higher strength flowable fill with a one ft excavation directly behind the pile cap) and test 2 (involving native clay with a one ft excavation directly behind the pile cap). Finally, comparisons will be made between test 10 (involving the higher strength flowable fill directly behind the pile cap) and test 12 (involving the higher strength flowable fill with a one ft excavation directly behind the pile cap).

Figure 6-4 shows the load displacement curves for tests 10 and 1. At a displacement of 1.5 inches test 10 shows an increase in lateral resistance of about 130 kips over test 1. This increase in strength is due to higher strength flowable fill block behind the pile cap. Prior to test 10 pile cap 3 had be loaded five times during other tests. Due to reloading effects, the increase in lateral resistance is believed to be higher that the difference between these two tests suggest. For a better comparison test 10 will be compared to test 12 in the subsequent paragraphs.

Figure 6-5 shows the load vs. displacement curves for tests 12 and 2. For comparison purposes, test 12 as shifted to zero. Due to large initial displacement of pile

cap 3 and the flow of clay into the gap behind the piles it is believed that the piles started pushing into clay at displacements less than the original zero point. Therefore, it was necessary to shift the curve without skewing the results. The two curves are similar in shape and magnitude. The Load vs. Displacement curve for test 12 shows a slight increase at larger displacements. This small difference (about 15 kips) is due to the weaker flowable fill beneath the cap.

Figure 6-6 shows the load vs. displacement curves for tests 10 and 12. This comparison is believed to be the most accurate in evaluating the increase in lateral passive resistance due to flowable fill behind the cap. The only difference in these two tests is a one ft wide excavation of the flowable fill was done just prior to test 12. Test 10 shows an increase in lateral resistance of about 150 kips over test 12. Because all the other testing conditions are the same it could be said that 90 % to 100% of the increased lateral resistance is likely attributed to the passive resistance on the flowable fill directly behind the cap along with side and bottom friction on the flowable fill wall.

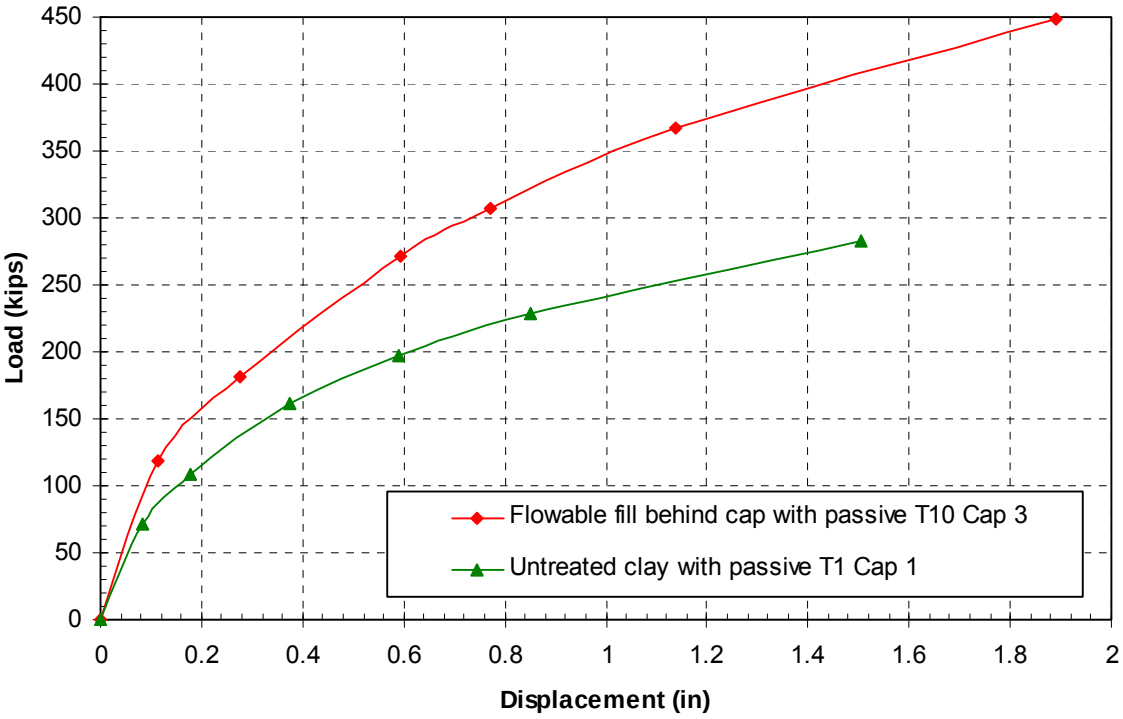

Figure 6-4 Load vs. displacement results comparing tests 10 and 1.

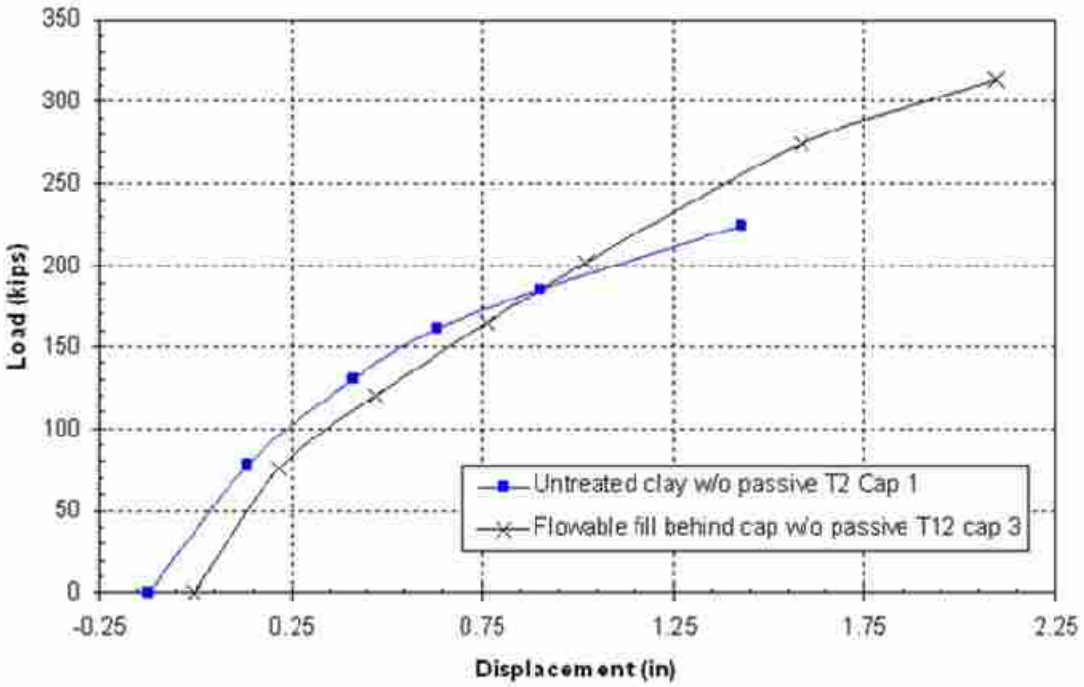

Figure 6-5 Load vs. displacement results comparing test 2 cap 1 to test 12 cap 3.

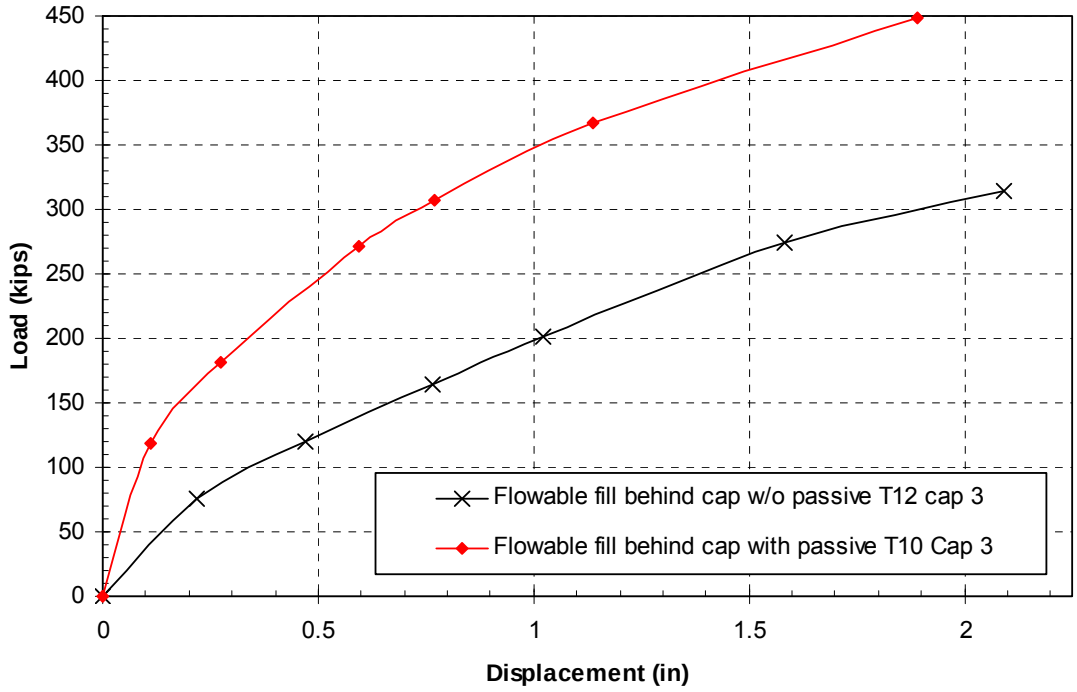

Figure 6-6 Load vs. displacement results comparing tests 12 and 10.

6.2.2 Moment vs. Load Comparison

Further evidence for the source of increased lateral resistance is also provided by a comparison of the maximum positive moment vs. load curves for tests 1, 2, 10, and 12 provided in Figure 6-7. Although moment data was obtained from many different instruments, the data used for this graph was chosen because it gave good representation all the other data. For more detailed information of the moment vs. load comparisons see the individual test result sections. As seen in the previous tests for a given load, the moment developed in the cap during test 2 is higher than that for test 1 because the passive resistance on the pile cap had been eliminated and the pile had to carry a greater load. The same effect can be seen when comparing test 12 to test 10. In addition, pile head restraint could have been reduced somewhat. The sources of the increased lateral

resistance are also consistent with the geometry involved. When the flowable fill wall was in contact with the pile cap, lateral movement of the pile cap would push the wall laterally so that passive force on the back of the wall and shear on the base on the base and side of the wall would develop increased lateral resistance. When the connection between the flowable fill wall and the pile cap was eliminated in test 12, this lateral resistance would not develop unless the piles impinged on the wall.

6.2.3 Potential Failure Mechanisms

Although the increase in lateral resistance appears to result from the movement of the flowable fill zone, it is not immediately apparent how this resistance was generated and what failure mechanisms were involved. To answer this question a few scenarios need to be considered.

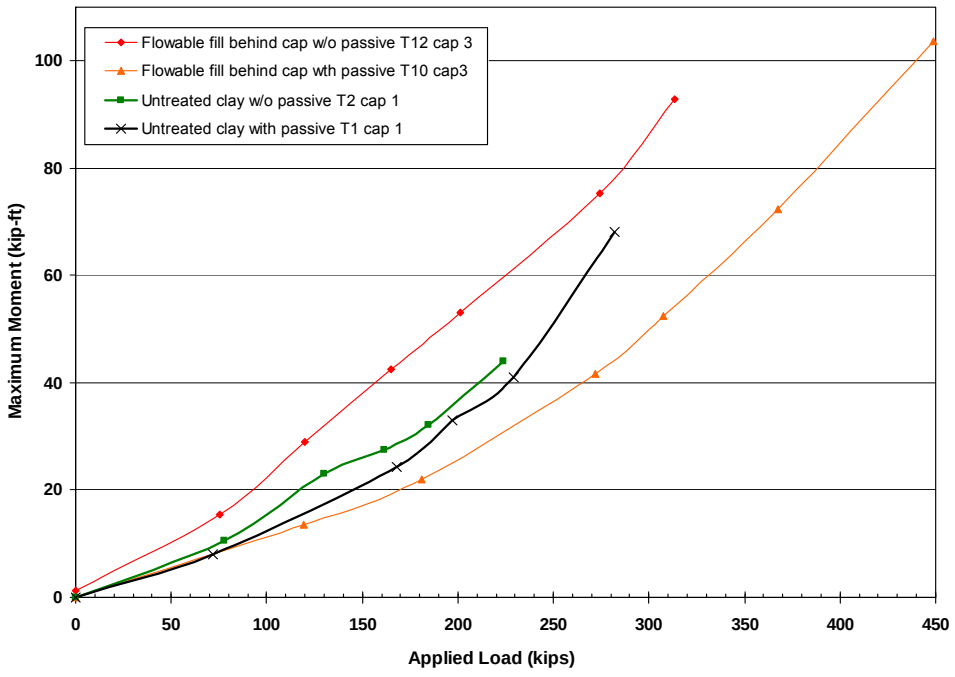

Figure 6-7 Comparing maximum positive moment vs. applied load of tests 1, 2, 10 and 12.

One scenario is that the flowable fill zone could have sheared and thus only a portion of it really contributed. Another scenario is that the whole flowable fill zone acted as a rigid block against the weak clay behind it.

To consider the first scenario that the flowable fill sheared, the shear strength of the flowable fill along a potential shear plane would need to be estimated. Assuming that the flowable fill did indeed have a consistent unconfined compressive strength of 137 psi, its shear strength would be one-half of the unconfined compressive strength or about 68.5 psi, which is equal to 9864 psf. By multiplying that shear strength by an assumed planar failure area of 12 ft by 6 ft, the shear capacity of the flowable fill would be about 710 kips. Considering that the maximum load applied on the pile cap was 449 kips it is unlikely that a shear failure could have occurred and the flowable fill zone likely acted as a rigid block.

6.2.4 Calculation of the Ultimate Lateral Force Provided by the Flowable Fill Zone

A better understanding of the forces acting on the flowable fill zone would be helpful in understanding the behavior of the zone and in analyzing potential failure mechanisms from shear and bending. This analysis would also be useful in determining if the increased lateral resistance produced by the flowable fill wall can be adequately accounted for using basic geotechnical design concepts.

Figure 6-8 (a) shows a free body diagram with all the forces acting on the flowable fill zone. (Hand calculations for the forces shown in the free body diagram are provided in Appendix B). The applied force on the flowable fill block was measured by subtracting the Load vs. Displacement results from test 12 from that of test 10 at 1.5

inches of displacement, which was about 150 kips. If the entire flowable fill zone did indeed contribute to the increase of the lateral resistance, this 150 kips should be equal to the passive resistance of the clay directly behind the flowable fill zone along with skin friction of the sides and bottom of the block. The ultimate passive force, P_u , was calculated using Rankine Theory. According to this theory the ultimate passive force is given by the equation (6-1)

$$P_u = \frac{1}{2}(\gamma)(H^2)(W)(K_p) + 2(c_u)(H)(W)(\sqrt{K_p}) \quad \textbf{(6-1)}$$

where γ is the unit weight of soil, H is the height of the wall or pile cap, B is the base width, c_u is the undrained cohesion or undrained shear strength of the soil, and K_p is the passive earth pressure coefficient. For undrained conditions, which are assumed for this situation, K_p is equal to 1.0. The passive resistance consisted of 67 kips from the ground surface to a depth of 2.5 ft and 37 kips between a depth of 2.5 ft and 6 ft. The passive force of 67 kips was calculated based on an average undrained shear strength of 1040 psf and a unit weight of 117 pcf for the clay from the ground surface to a depth of 2.5 ft acting over the 12 ft length of the flowable fill wall. This 1040 psf shear strength was back-calculated based on Rankine theory from the results of test 2 which showed that approximately 50 kips of passive force was provided by the virgin clay acting on the pile cap which was 9 ft wide and 2.5 ft deep. This strength value is reasonably consistent with the strength estimated by the CPT testing at the site , but somewhat higher than would be expected based on the torvane tests and unconfined compression test. The higher strength in this zone could be attributed to the partially saturated condition of the soil in this depth range during testing.

The average shear strength for the clay between 2.5 to 6 ft below the ground surface was taken to be 200 psf. This strength is consistent with the strength interpreted from the CPT data and the unconfined tests, and slightly lower than that from the torvane test. Therefore this strength value is reasonably consistent with the findings of the geotechnical site investigation. The lower portion of the passive resistance in Figure 6-8 (a) was also calculated using Rankine theory assuming this same shear strength of 200 psf and a unit weight of 112 pcf.

The shaded portion of Figure 6-8 represents the flowable fill zone and the arrows in that portion represent the side and bottom shear resistance due to skin friction or cohesion. Each of the components of the side resistance was based on the corresponding soil shear strength described previously and the bottom resistance was based on the sear strength of 200 psf as denoted in the geotechnical site investigation for 6 ft below the ground surface. In all calculations the width of the flowable fill wall was taken as 6 ft. The total resistance due to skin friction was calculated to be 54 kips and combined with the 104 kips of the passive resistance they produced the overall soil resistance of 158 kips. Since the additional lateral resistance of the pile cap produced by the installation of the flowable fill wall was between 150 and 160 kips, this analysis further bolsters the conclusion that nearly all of the increased lateral resistance was due to passive force and shear resistance on the flowable fill wall. The small difference between computed and measured resistance may be attributed to a slight increase in the soil-pile interaction or uncertainties in the soil strength parameters and geometry of the flowable fill zone.

After taking into account all the sources of resistance on the flowable fill zone, a more accurate estimate of the shear forces within the flowable fill zone can be obtained.

The shear diagram in Figure 6-8 shows that the maximum shear force which the flowable fill would experience was about 60 kips, which is significantly lower than the shear capacity of 710 kips, further supporting the contention that the flowable fill zone did not fail in shear but rather acted as a rigid block.

Another potential failure mechanism in addition to with shear failure is failure due to bending. Figure 6-8 (c) shows the bending moment diagram derived from the shear diagram. From the diagram, the maximum moment applied to the flowable fill zone would be about 75 kip-ft. Typical tensile strength values for concrete are on the order of about 8% to 15% the unconfined compressive strength (MacGregor 2005). If it is assumed that the flowable fill would crack at about 15% of its unconfined compressive strength of 137 psi, then the bending moment required to initiate cracking would be about 115 kip-ft. Since the maximum moment was about 75 kip-ft, this would imply that the flowable fill would most likely not have cracked, eliminating the possibility of a failure due to bending.

Figure 6-9 provides a photograph of the crack pattern around the flowable fill after test 10. This photo shows that there is not any cracking within the flowable fill zone. This is further evidence that the flowable fill zone acted as a rigid block. Based on the analyses and the observed performance of the flowable fill block it is believed that the flowable fill zone acted as a rigid block relative to the weaker clay behind it. This conclusion would suggest that 90% to 100% of the strength increase produced by placing the flowable fill was a result of the passive force behind the pile cap in conjunction with the skin friction on the bottom and sides.

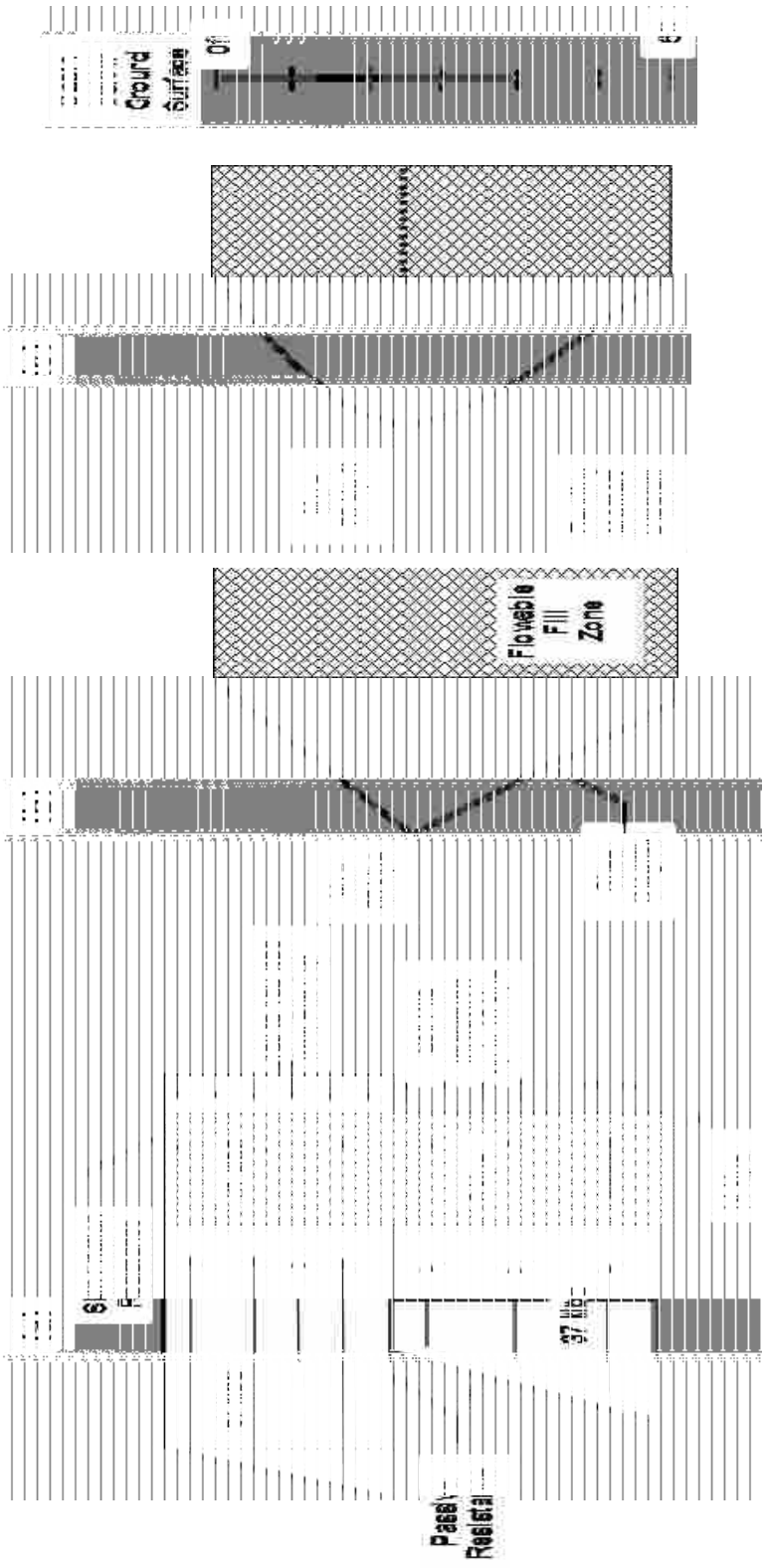

Figure 6-8 The free body, shear, and moment diagrams defining all the forces on the flowable fill zone as passive resistance, skin friction resistance, soil pile interaction, and the load transferred from the pile cap.

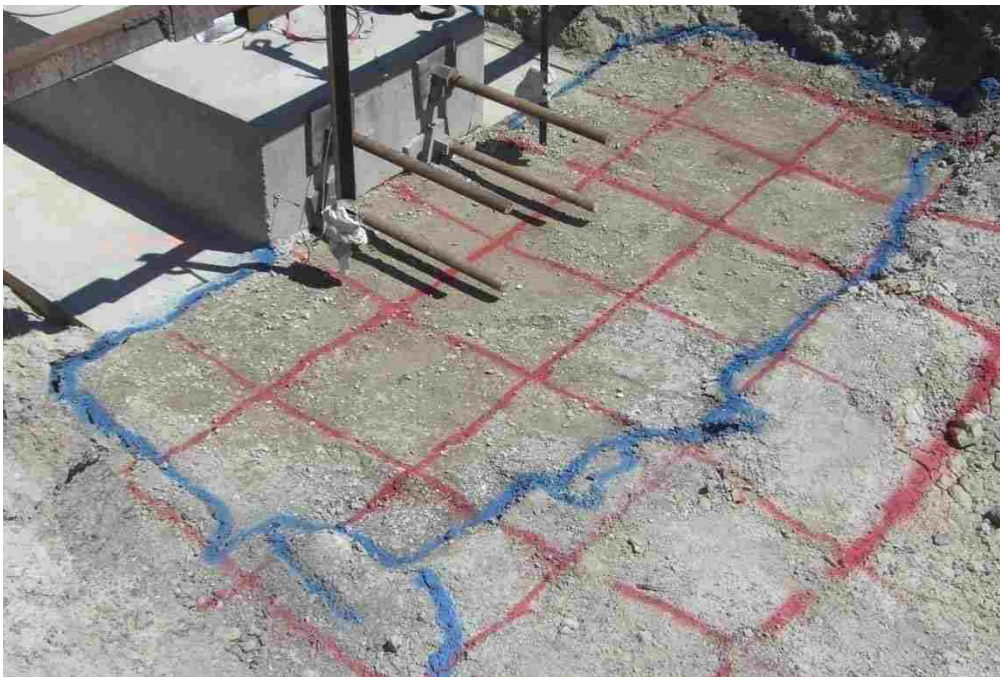

Figure 6-9 Photograph showing the flowable fill surface failure condition and that the zone acted as a rigid soil block.

6.2.5 Computed Lateral Force-Displacement Relationships

The total lateral force-displacement curve for the flowable wall is the resultant of the passive force-displacement curve and the shear force-displacement curve. Typically, the shear resistance on the side of a wall or a pile has been found to develop with relatively small movements while passive force develops after larger movements. Therefore, the lateral force-displacement curves for each component of force were developed separately and then combined to compute the total lateral force-displacement curve for the flowable fill wall.

The passive force-displacement behavior of the soft clay against the flowable fill wall was computed using the spreadsheet PYCAP developed by R.L. Mokwa and J.M. Duncan (2001). The spreadsheet computes the ultimate passive force and then uses a hyperbolic curve to compute the development of passive force with displacement. For

the undrained loading case, with ϕ=0, PYCAP computes the ultimate passive force using the Rankine theory and shear zones at the end of the wall are assumed to form parallel to the direction of loading so that 3-D effects need not be considered. PYCAP develops the hyperbolic force-displacement curve using the initial soil modulus to define the initial stiffness and the ultimate passive force as an asymptote as shown in Figure 6-10.

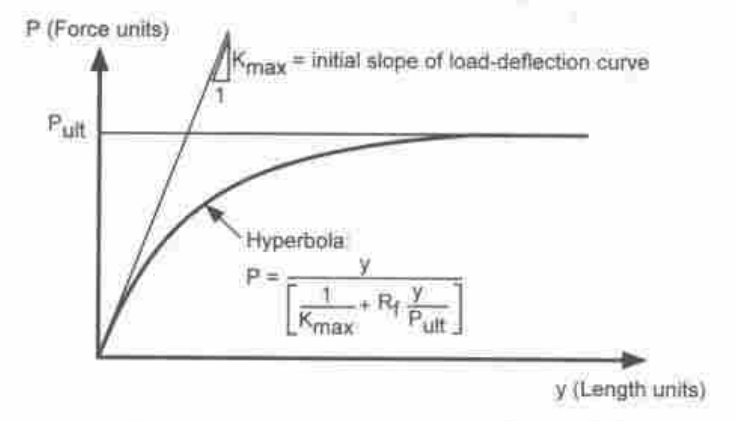

Figure 6-10 Graphic of the hyperbolic model (Duncan 2001).

Using PYCAP, a hyperbolic curve was computed to define the passive force-displacement curve based on the input values in Table 6-1. To do this the flowable fill was treated as a pile cap having a width of 12 ft and height of 6 ft. The initial soil modulus, E_i in kips/ft^2 was estimated using the equation

$$E_i \approx \frac{15 \cdot C_u}{PI(\%)} \qquad \textbf{(6-2)}$$

where cu is the undrained cohesion or shear strength of the soil in kips/ft2 and PI is the plasticity index in percent which was developed by (Termaat, 1985). For this analysis the

plasticity index was taken as 25% based on the geotechnical investigation. It was also assumed that the ultimate resistance would be developed for a wall movement equal to about 1.5% of the wall height based on findings by Brandenberg (2005) for naturally occurring cohesive soils. Table 6-1 shows an ultimate resultant passive force and the horizontal component of that force which is appropriate for comparisons with the measured force from these tests.

As indicated in the previous section, about 104 kips of force can be attributed to passive force on the flowable fill zone while an additional 54 kips would be due to shearing on the side and base of the flowable fill zone. Based on a Rankine analysis, an ultimate passive force of 104 kips would be predicted based on an average undrained shear strength or undrained cohesion of 550 psf in the upper 6 ft of the soil profile. This weighted average was based on an average strength of 1040 psf for the first 2.5 ft and 200 psf for the next 3.5 ft. This average was used to help simplify the PYCAP analysis. The computed passive force-displacement curve using this approach is presented in Figure 6-11 in comparison with the total measured increase force-displacement curve. Typically the passive force contributed about 66 % of the measured increase in lateral resistance.

To compute the development of the force due to side shear and base shear, it was necessary to estimate the movement required to develop full skin friction resistance. Evaluation of current literature suggests that maximum skin resistance based on load tests for both piles and drilled shafts is on the order of 0.12 to 0.4 inches (Bowles 1996). Another source suggests that skin friction is mobilized at about one-tenth of the displacement required to mobilize the end bearing resistance (Budha 2007). A value of 0.2 inches was used in this analysis for the development of side shear and base shear.

Using Budha's method a value of 0.11 inches would be required to develop side and base shear. Although 0.2 inches is a little high it still fits well within the 0.12 to 0.4 inch range suggested by Bowles. The combined side shear and base shear force-displacement curve is plotted in Figure 6-12 along with the total measured force-displacement curve. The base shear and side shear make up about 34 % of the total resistance.

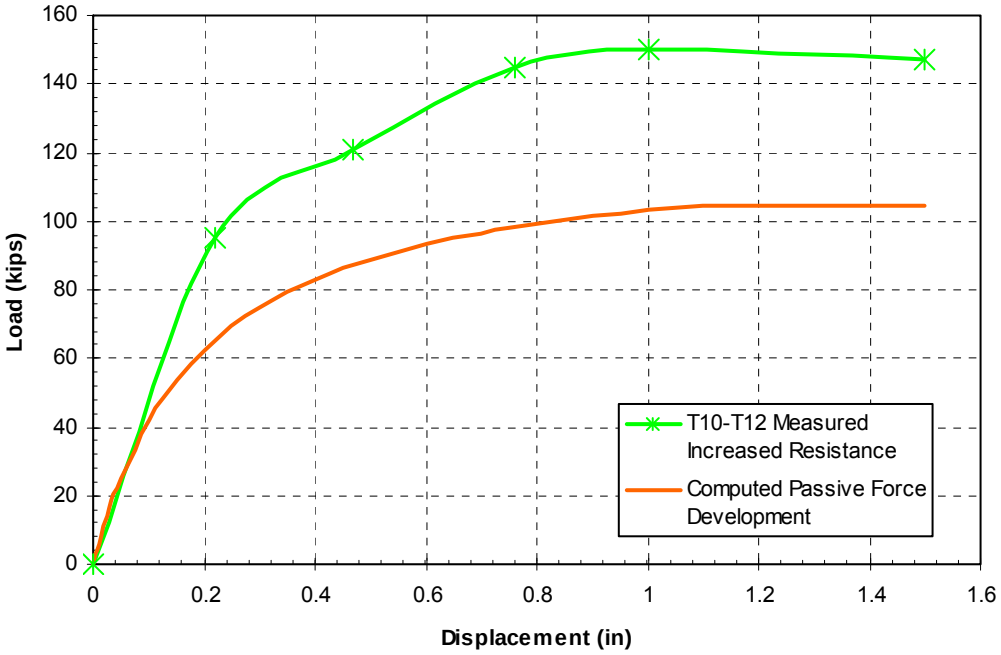

Figure 6-11 The measured increased total resistance in comparison with the computed passive force-displacement curve behind the flowable fill zone obtained from pycap.

Finally, the computed passive force-displacement curve and the computed side and base shear curves shown in Figure 6-11 and Figure 6-12 were combined by superposition to produce the computed lateral force-displacement curve shown in Figure 6-13. For comparison purposes the measured force-displacement curve representing the total increased resistance for the flowable fill wall is shown in these three figures. The

measured lateral force-displacement curve was obtained by subtracting the Load vs. Displacement curve for test 12, involving pile cap 3 with no soil adjacent to the pile cap, from the Load vs. Displacement curve for test 10, involving pile cap 3 with flowable fill directly behind the cap. The computed lateral force-displacement curve is a reasonably good fit to the measured lateral force-displacement from the flowable fill test. The curves vary by about 8 kips at 1 inch displacement which represents a margin of error of about 5%. This relatively close fit supports the contention that essentially all of the increased lateral resistance from the flowable fill was due to passive resistance or side and base shear against the flowable fill wall as the pile cap pushed the wall laterally.

Additionally, to verify the results of the PYCAP analysis, a hyperbolic curve was also fit to the measured passive force-displacement curve obtained from the tests on the pile caps in virgin clay. This was done by subtracting the Load vs. Displacement curve for pile cap 1 in test 2 from the Load vs. Displacement curve for the pile cap 1 in test 1 as shown in Figure 6-14. Then varying the inputs slightly so that the PYCAP model would equal the ultimate horizontal passive force of 50 kips as observed in the field tests. The input values remained fairly consistent with the soil profile from chapter 3 Geotechnical Site Characterization and are shown in Table 6-1. The cap dimensions were updated to that of the actual pile cap being 9 ft wide and 2.5 ft deep. The shear strength used in this comparison needed to be around 1040 psf which is high but in the range of the CPT data for the first 2.5 ft below ground surface.

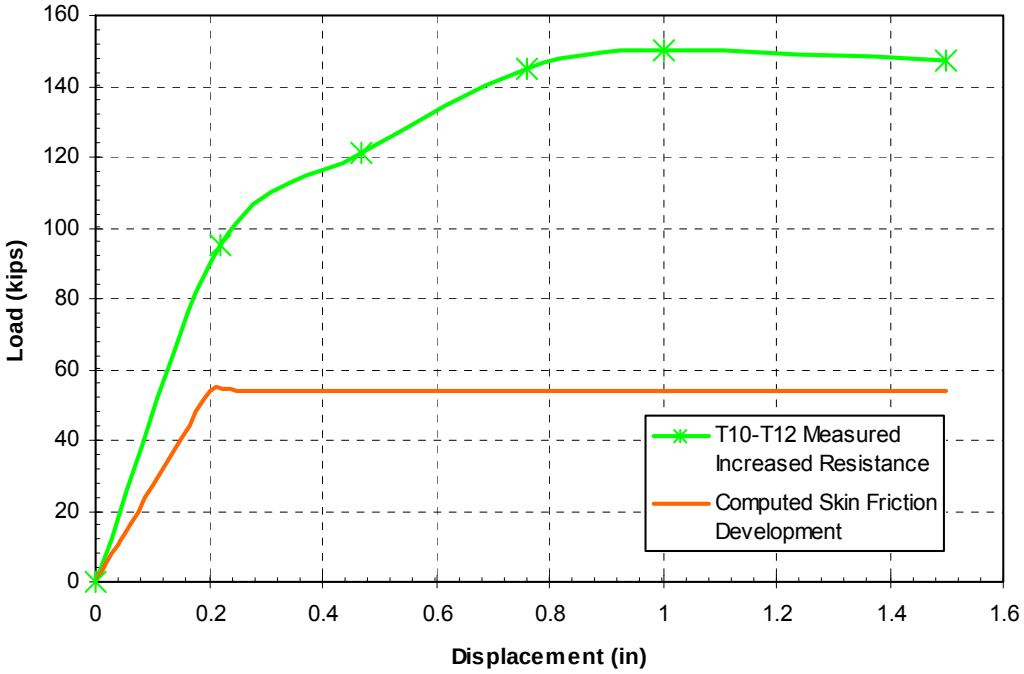

Figure 6-12 The portion of the measured increased total resistance due to side and bottom skin friction of the flowable fill zone as computed by pycap.

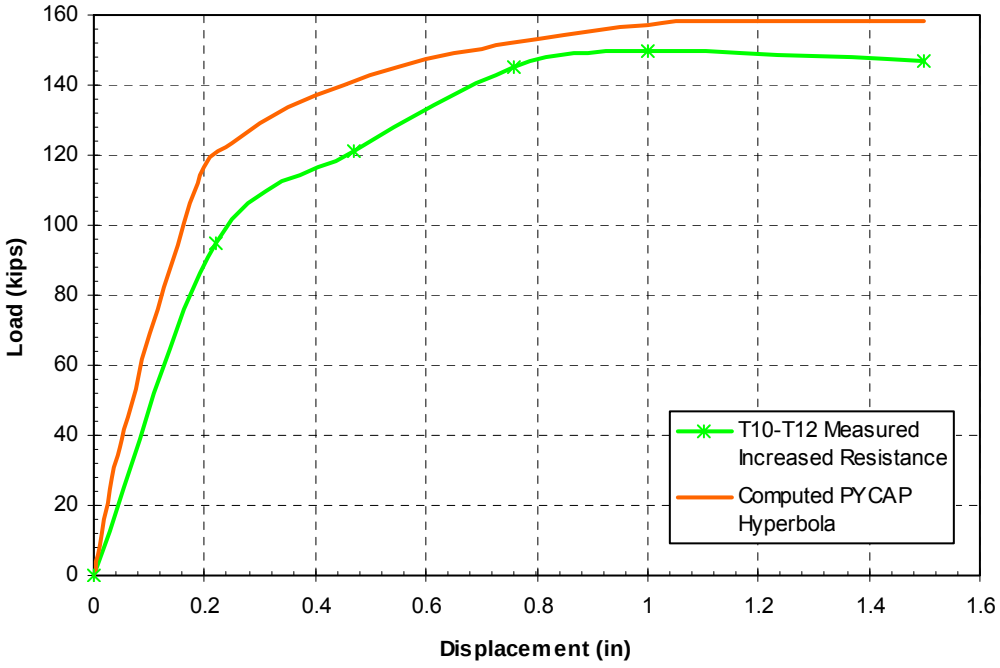

Figure 6-13 Comparison of the computed pycap hyperbolic method to the measured increased resistance obtained by subtracting the load vs. displacement curve of test 12 from test 10.

Table 6-1 Values from the pycap analysis treating the flowable fill as a rigid body.

Input Values		
cap width,	b (ft) =	**12.00**
cap height,	H (ft) =	**6.00**
embedment depth,	z (ft) =	**0.00**
surharge,	q_s (psf) =	**0.0**
cohesion,	c (psf) =	**550.0**
soil friction angle,	ϕ (deg.) =	**0.0**
wall friction,	δ (deg.) =	**0**
initial soil modulus,	E_i (kip/ft^2) =	**330**
poisson's ratio,	ν =	**0.50**
soil unit weight,	γ_m (pcf) =	**117.0**
adhesion factor,	α =	**0.00**
Δ_{max}/H, (0.04 suggested, see notes) =		**0.015**
Calculated Values		
K_a (Rankine) =		**1.00**
K_p (Rankine) =		**1.00**
K_p (Coulomb) =		**1.00**
$K_{p\phi}$ (Log Spiral, soil weight) =		**Rankine Kp**
K_{pq} (Log Spiral, surcharge) =		**Rankine Kp**
K_{pc} (Log Spiral, cohesion) =		**Rankine Kp**
E_p (kip/ft) =		**8.71**
Ovesen's 3-D factor, R =		**1.000**
k_{max}, elastic stiffness (kip/in) =		**639.9**
		phi = 0 Solution
$P_{ult\ (horz+vert)}$ (kips) =		**106.9**
Horizontal values using the Log Spiral theory		
P_{horz} (kips) =		**104.5**

In addition, the displacement necessary to mobilize full passive resistance, (Δmax) was increased to 2% of the wall height (H) as it provided a somewhat better fit than the 1.5% used previously. The computed passive force-displacement curve is plotted along with the measured curve in Figure 6-14. Overall, the hyperbolic method fit

the virgin soil passive curve reasonably well. However, there appears to be a discrepancy with the initial soil modulus. The slope of the initial soil modulus from the hyperbolic model appears to be too steep compared to the measured virgin clay passive curve. This discrepancy may in part be due to difficulties in accurately interpreting the field test results at these small displacement levels. Due to the initial offset and gap effects, the passive force-displacement curve between 0 and 0.25 inches is not highly reliable, which could account for the discrepancy in the "measured" and computed slope.

In summary, the computed force-displacement curves indicate that the increase in the lateral resistance recorded in the flowable fill improvement tests, did come as a result of the flowable fill acting as a rigid body 12 ft wide and 6 ft deep against the weaker clay behind it. This in turn increased the surface area that the clay could react against and also allowed for additional resistance to develop through skin friction along the sides and bottom, thus increasing the overall lateral resistance of the native clay by a factor 1.45. The results of these analyses also suggest that the increased resistance from the flowable fill can be predicted using established geotechnical design concepts associated with the development of passive force and side/base shear in clays. It should be noted that the results tend to be less conservative. It is believed that because the piles and pile cap had been load five times prior to tests 10 and 12, the actual results would be higher than what was measured in the field. Increasing the measured difference would make the Load vs. Displacement values closer and possibly greater than the values calculated using PYCAP, making the model more conservative. It should be noted that the conclusion of this analysis was based on the likelihood that a small amount of horizontal translation on the

order of 0.12 inches or greater (Bowles 1996) occurred at the base of the flowable fill zone.

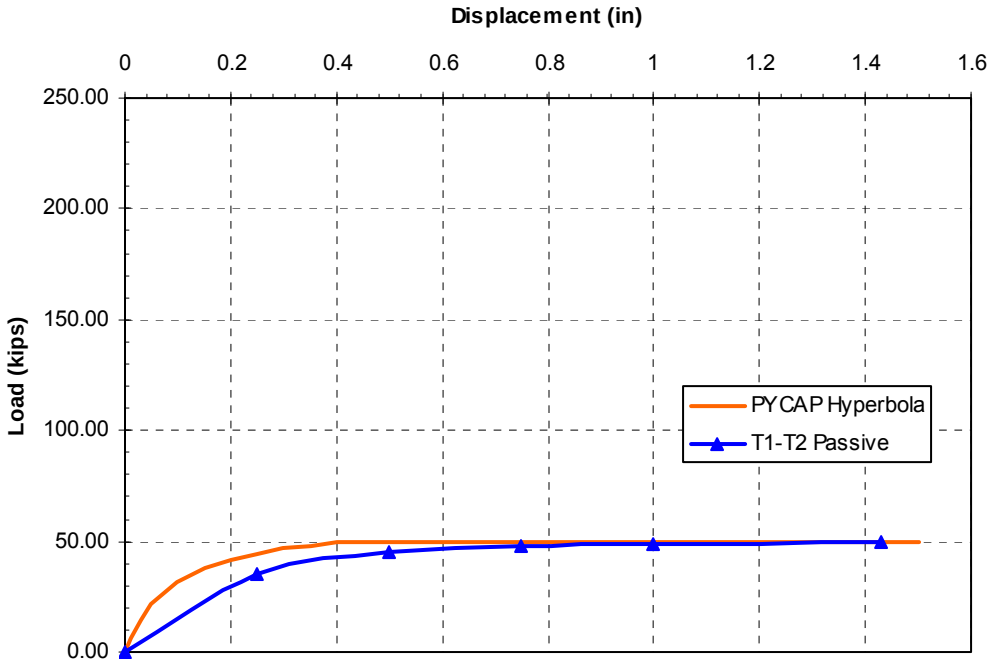

Figure 6-14 Comparison of the pycap hyperbola method to the passive force obtained by subtracting the load vs. displacement curve from test 2 from test 1.

Considering the maximum top surface displacement of 1.89 inches, the small rotation of 0.4 degrees measured on the pile cap at that displacement, and the relative shear or rigid strength of the flowable fill zone it does seem highly likely that the bottom surface would at least translate horizontally a minimum of 0.12 to 0.2 inches to develop a shear force along the bottom surface. However, it is still a possibility that the bottom surface of the flowable fill zone did not translate horizontally and instead the flowable fill rotated. If this were the case, very similar ultimate loads and Load vs. Displacement curves would be obtained if a higher average shear strength of the soil between 2.5 and 6 ft was used. The higher average shear strength would still be in reasonable agreement

with the measured strength profile. To completely validate either approach, further testing or numerical model analysis would need to be done to better establish the actual behavior at the interface between the bottom of the flowable fill and the underlying clay.

Table 6-2 Input data for the PYCAP analysis for the virgin soil directly behind the pile cap.

Input Values (red)		
cap width,	b (ft) =	**9.00**
cap height,	H (ft) =	**2.50**
embedment depth,	z (ft) =	**0.00**
surharge,	q_s (psf) =	**0.0**
cohesion,	c (psf) =	**1040.0**
soil friction angle,	ϕ (deg.) =	**0.0**
wall friction,	δ (deg.) =	**0**
initial soil modulus,	E_i (kip/ft^2) =	**624**
poisson's ratio,	ν =	**0.50**
soil unit weight,	γ_m (pcf) =	**117.0**
adhesion factor,	α =	**1.00**
Δ_{max}/H, (0.04 suggested, see notes) =		**0.020**
Calculated Values (blue)		
K_a (Rankine) =		**1.00**
K_p (Rankine) =		**1.00**
K_p (Coulomb) =		**1.00**
$K_{p\phi}$ (Log Spiral, soil weight) =		**Rankine Kp**
K_{pq} (Log Spiral, surcharge) =		**Rankine Kp**
K_{pc} (Log Spiral, cohesion) =		**Rankine Kp**
E_p (kip/ft) =		**5.57**
Ovesen's 3-D factor, R =		**1.000**
k_{max}, elastic stiffness (kip/in) =		**717.8**
		phi = 0 Solution
$P_{ult\ (horz+vert)}$ (kips) =		**74.3**
Horizontal values using the Log Spiral theory (Brinch Hansen)		
Phorz 2-D (kips) =		50.1

6.2.6 Displacement vs. Depth Discussion

The primary instrumentation used to measure the displacement and moments at various depths were the shape arrays. Despite some minor incongruities, the shape arrays proved to be fairly reliable when compared to the secondary instrumentation of string potentiometers, inclinometers, and strain gages.

The displacement vs. depth profiles for all tests showed that the majority of the displacement first occurred between 23 to 25 ft below the top of the corbel, with maximum curvature occurring between 10 to 15 ft. Then in most cases a fairly linear trend of displacement occurred from 10 ft to the load point around one ft below the top of the corbel. The displacement vs. depth profiles were then used to derive the bending moments for each test.

6.2.7 Bending Moment vs. Depth Discussion

When comparing the bending moments from the virgin clay test (test 1) to the flowable fill soil improvement test with the stiffer flowable fill (test 10), the locations of the maximum bending moments appear to increase in depth as the lateral load applied to the piles increased. The magnitudes of the positive bending moments were higher for flowable fill tests, which is mainly due to the larger displacements than the virgin clay test. Overall, the location of the maximum positive bending moment remained relatively consistent.

The magnitudes of the negative bending moment were difficult to measure and estimate as was evident to the inconsistencies between the arrays and strain gages. There is no reasonable explanation for this other than the general discrepancies brought about

by the disagreement in the instrumentation as the material properties, especially EI, change as the piles begin to enter the pile cap.

6.3 Long-Term Strength Development

Although the measured average unconfined compressive strength of the high strength flowable fill was 137 psi at the time of the field testing, there is some concern about long-term strength degradation of flowable fill below the water table. To evaluate potential strength degradation it was necessary to keep samples of the flowable fill and test them at a much later time. This section will discuss the results of these laboratory strength tests and available literature concerning long-term strength degradation in flowable fill with time.

Previous research has shown that mixing time and the curing environment after placement are the two most critical factors affecting the compressive strength of flowable fill (Pierce et-al 2002). Generally, increasing the mixing time decreases strength while curing in a saturated environment leads to reduced strength over time. The test data for the compressive strength of flowable fill has not been consistent. Recently the NCHRP has said "In general, there were substantial differences between the strength of CLSM cylinders stored outdoors and cylinders cured in the fog room. However, there was not a consistent trend for all the mixtures studied, illustrating that the effects of temperature and curing conditions are sensitive to material type and proportions." (Folliard et al, 2008)

Although we do not know the length that the flowable fill was mixed prior to placement, we do know that it was cured in a saturated environment with the lower four

ft beneath the water table. To simulate this environment, three test cylinders of the flowable fill were kept in a fog room for about 700 days after placement. The cylinders were 4 inches in diameter and 8 inches long. After 700 days, compressions tests were performed on the three cylinders and Table 6-3 shows the values obtained from the tests. The test results are very consistent and yield an average unconfined compressive strength of only about 57 psi in comparison with the 137 psi strength measured shortly after placement. This indicates a dramatic decrease in the compressive strength of nearly 56 %. Visual observations of the test cylinders did indicate that indeed some of the cementitious material had leached out. Leaching was observed as white streaks on the outside of the samples. The leaching occurred because water was able to flow into the flowable fill. If the flowable fill had higher cement content the leaching would have been reduced. Also if the water did not flow over the flowable fill the leaching would have been reduced or possibly eliminated. Another possible explanation for the different values in compressive from the seven and fourteen day tests is that it is unknown which concrete truck the 700 day samples were taken from. However the results for the seven and fourteen days tests had higher compressive strength and they were taken from both trucks.

Table 6-3 Unconfined compressive strength of the 137 psi flowable fill after 700 days.

Date Tested	Unconfined Compressive Strength (psi)
29 July 2009	54.9
29 July 2009	52.9
29 July 2009	53.3
Average	53.7

6.4 Basic Cost and Effectiveness Considerations

It was observed that the flowable fill improved the lateral resistance of the pile group by 150 kips. The cost of producing this increase due to the placement of flowable fill needs to be quantified to determine if it can be considered as a viable and cost effective solution. A rough estimate of the cost to produce the flowable fill wall will be compared to the alternative of adding more piles and a larger pile cap. The prices used indicate current market values of the materials and labor used. Costs were base in the summer of 2007 for Salt Lake City, Utah.

The expenses incurred from placing the flowable fill include, the flowable fill material from the mix plant, the excavator, and the operator. A supplier in Salt Lake City, Utah charged $71 per cubic yard for a 150 psi flowable fill mix. The volume used was 17 cubic yards and with the addition of the service charges cost $1237. The track hoe rented for excavation cost $1000/day with a $200/hr charge for the operator. The excavation and placement only took about 2 hours to complete bringing the total cost to around $2000.

One alternative to placing flowable fill would be to simply add more piles and increase the size of the pile cap. According to the test results for cap 1 during test 2, the maximum load taken by the piles was about 230 kips. If this load is distributed evenly, each pile would have carried about 26 kips. To obtain the same lateral resistance of 150 kips that the flowable fill achieved, about 7 piles would have to be added, thus making a new 4x4 pile configuration. Steel pipe pile costs during the project were on the order of $30/ft. Assuming typical pile lengths of 80 ft, 7 additional piles would cost $16,800. Mobilization and driving costs were about $15,000 plus $8/ft of driving. Therefore, the 7

additional piles would cost $20,120 to drive into place. Assuming the same pile spacing of 3 ft on center, the new pile cap would have dimensions 12'x12'x2.5' and would have a volume of 360 cubic ft. If the volume of the existing pile cap is subtracted from the 360 cubic ft the net additional volume of concrete needed for the additional pile cap would be 157.5 cubic ft or about 6 cubic yards. The average cost for concrete and reinforcement on the project was about $300 per cubic yard. That would amount to $1,800 for the additional pile cap. The volume of concrete needed to fill the additional 7 piles would be about 16 cubic yards and would amount to an additional $4800 of concrete and steel. The total estimated cost to obtain the same improvement in lateral resistance as the flowable fill by adding additional piles and increasing the pile cap would be about $44,000. In conjunction with the increased costs is also the increased time to add the 7 new piles and construct a new pile cap. The amount of time to construct the additional pile foundation would vary depending on number workers and experience. Considering the crane mobilization time and driving rate of the crew on the project, the seven new piles could be placed in about 1 day, with an additional 2 days to tie rebar and pour concrete, resulting in about an additional 3 days.

Installing piles and extending the cap would increase the lateral resistance in all directions. To have a similar increase in lateral resistance it would be necessary to place flowable fill on all four sides of the pile cap. This would increase the flowable fill cost by about four times, bringing the total cost to about $8000.The cost difference between $8000 for the flowable fill improvement and the $44,000 for additional plies appears to be significant. Therefore if the long term strength of the flowable fill can be correctly

calculated it would be a cost effective material to increase the lateral resistance of driven pile foundations.

7 Conclusions

In light of the findings in this thesis the following conclusions can be made in regards to using flowable fill as a soil improvement method to increase the lateral resistance of deep foundations in cohesive soils.

- Construction of a flowable fill wall (6 ft deep, 6 ft wide, and 12 ft long) adjacent to an existing pile cap (9 ft square and 2.5 ft deep) increased the lateral resistance from about 280 kips to 430 kips at a displacement of 1.5 inches. This increase of 150 kips represents a 53% increase in lateral resistance. However due to the weakening of the flowable fill material it is unknown how long a strength increase of that magnitude will hold up.
- Subsequent testing, after excavation of the flowable fill wall to the base of the pile cap, indicates that essentially all of the 150 kip increase was due to passive resistance and side/base shear against the soil mixed wall as the pile cap pushed the wall laterally.
- Only a small increase in lateral resistance could be attributed to soil-pile interaction. This is likely due to the fact that a very low strength flowable fill was placed beneath the cap while the higher strength flowable fill was about 1.5 ft away from the first row of piles.

- Analyses suggest that the shear strength of the flowable fill wall was sufficient to allow the wall to behave as a rigid block. Since the flowable fill zone extended 3.5 ft below the base of the cap, it essentially increased the surface area that the native soil could react against. Reasonable estimates of the lateral resistance for the wall can be obtained by considering passive force on the face of the wall and shear on the sides and base of the wall.
- Analyses of passive force vs. deflection response indicate that passive force in the soft clay was likely developed with lateral displacements between 1.5% and 2% of the wall height.
- Flowable fill provides the opportunity to significantly increase the lateral resistance of existing pile group foundations with relatively little investment of time, effort, and expense. However the site characteristics may lead to a decrease in the strength of the flowable fill. In locations where water can flow over/through the flowable fill, leaching of the cementitious may occur. In our tests we observed that specimens cured in a fog room for about 700 days had a 56% decrease in their unconfined compressive strength. For any long term use to increase lateral resistance of an existing pile group specific site testing would need to be done to ensure that the flowable fill material will not weaken beyond an acceptable limit.

References

Adaska, W. S.,(1997) "Controlled Low Strength Materials," Concrete International, Vol. 19, No. 4.

Adsero. M. (2008). "Effect of Jet Grouting on the Lateral Resistance of Soil Surrounding Driven-Pile Foundations." M.S. Thesis, Civil & Environ. Engrg. Dept., Brigham Young University, Provo, Utah.

American Concrete Institute, (1994), Committee 229, Controlled Low Strength Materials (CLSM), ACI 229R-94 Report.

Bowles, J. E. (1982). Foundation analysis and design. New York: New York : McGraw-Hill.

Brandenberg, S. J., Boulanger R.W., Kutter B. L., and Chang D.. (2005). Behavior of Pile Foundations in Laterally Spreading Ground during Centrifuge Tests. Journal of Geotechnical & Geoenvironmental Engineering 131, no. 11 (11) : 1378-1391.

Budhu, M. (2007). Soil Mechanics and Foundations. John Wiley and Sons Inc. 111 River St, Hobokan, NJ 07030-5774. pp. 407.

Duncan, J. M. and Mokwa, R.L. (2001). "Passive Earth Pressures: Theories and Test." Journal of Geotechnical and Geoenvironmental Engineering, 127(3), 248-257.

Folliard, K. J., Lianziang D., Trejo D., Halmen C., Sabol S., Leshchinsky D. (2008). Development of a Recommended Practice for Use of Controlled Low-Strength Material in Highway Construction. Transportation Research Board, NCHRP Repot 597, p 12, 40.

Herbst. M. (2008). Impact of Mass Mixing on the Lateral Resistance of Driven-pile Foundations. Brigham Young University Masters Thesis.

Hook W. (1998). Innovative uses of controlled low-strength material (CLSM) in Colorado. Fracture Mecanics, no. 1331: 137-150.

Kosmatka, S. H., Kerkhoff B., and Panarese W. C. (2003). Design and Control of Concrete Mixture. Illinois: Portland Cement Association.

Lemme, N. (In Press). Imapct of Compacted Fill and Rammed Aggreagate Piers on the Lateral Resistance of Diven-pile Foundations. Brigham Young University Masters Thesis.

MacGregor, J.G. and Wight, J.K. (2005). Reinforced Concrete Mechanics and Design. Prentice Hall, Upper Saddle River, New Jersey 07458. pp. 60.

Pierce C.E., Gassman S.L Richards T. M. (2002). Long-Term Strength Development of Controlled Low-Strength Material. ACI Materials Journal 99, no. 2: 157.

Rollins, K.M., Olsen, K.G., Jensen, D.H, Garrett, B.H., Olsen, R.J., and Egbert, J.J. (2006). "Pile Spacing Effects on Lateral Pile Group Behavior: Analysis." J. Geotechnical and Geoenvironmental Engineering., ASCE, Vol. 132, No. 10, p. 1272-1283.

Trejo, D., K. J. Folliard, and L. Du.(2004) "Sustainable Development Using Controlled Low-Strength Material (CLSM)". International Workshop on Sustainable Development and Concrete Technology, Tsinghua University, Beijing, China, May 20-21.

Appendix A. Design of Corbel

A.1 Corbel Specifications and Design Values

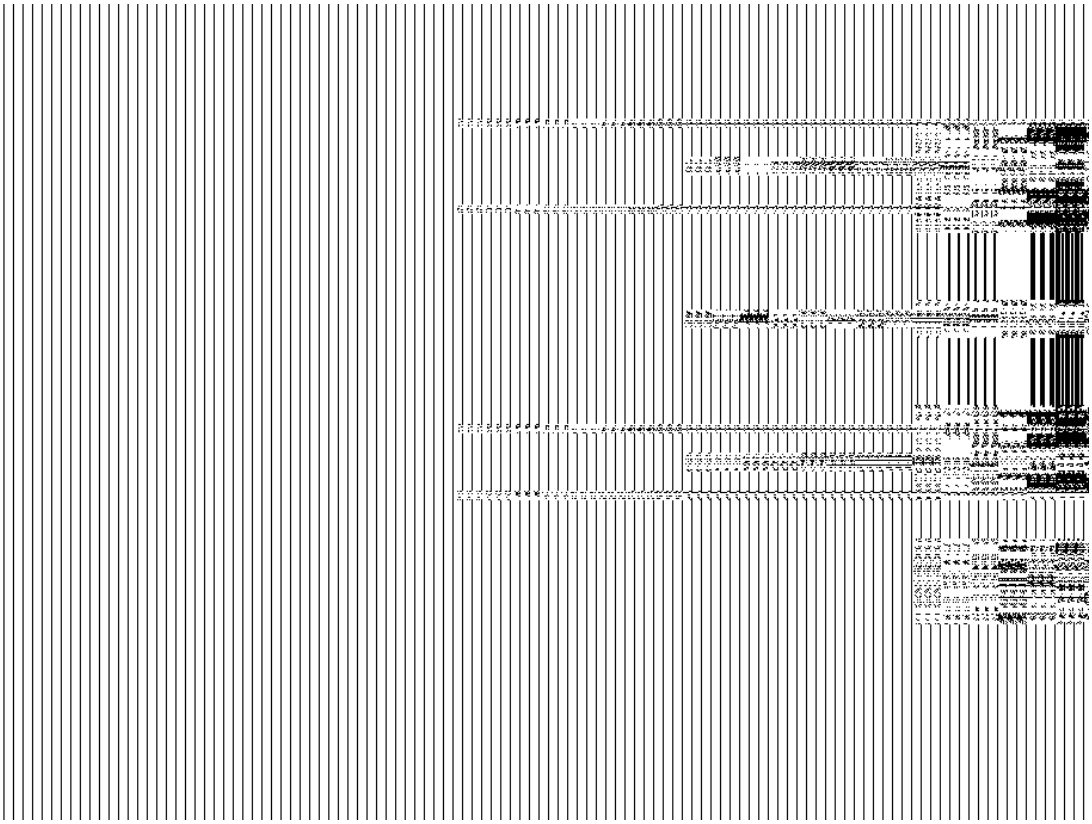

Figure A-1– Front view of the corbel steel where the actuator would connect to the corbel.

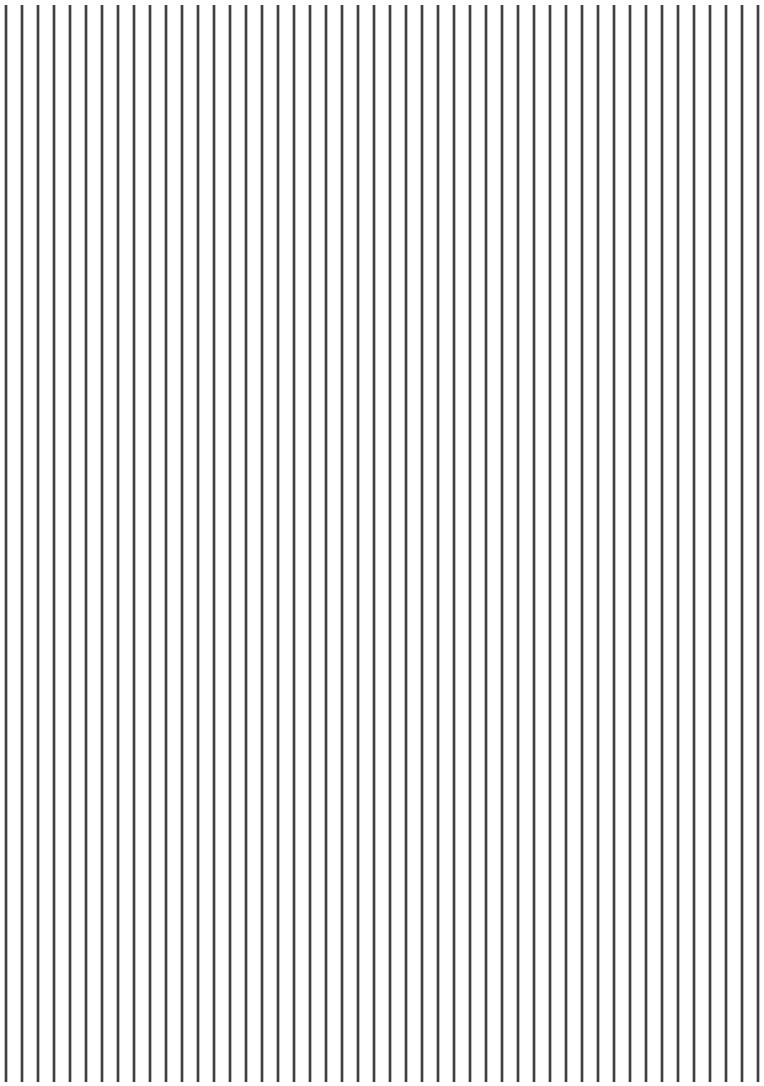

Figure A-2 – The #9 bar main reinforcement for the corbel.

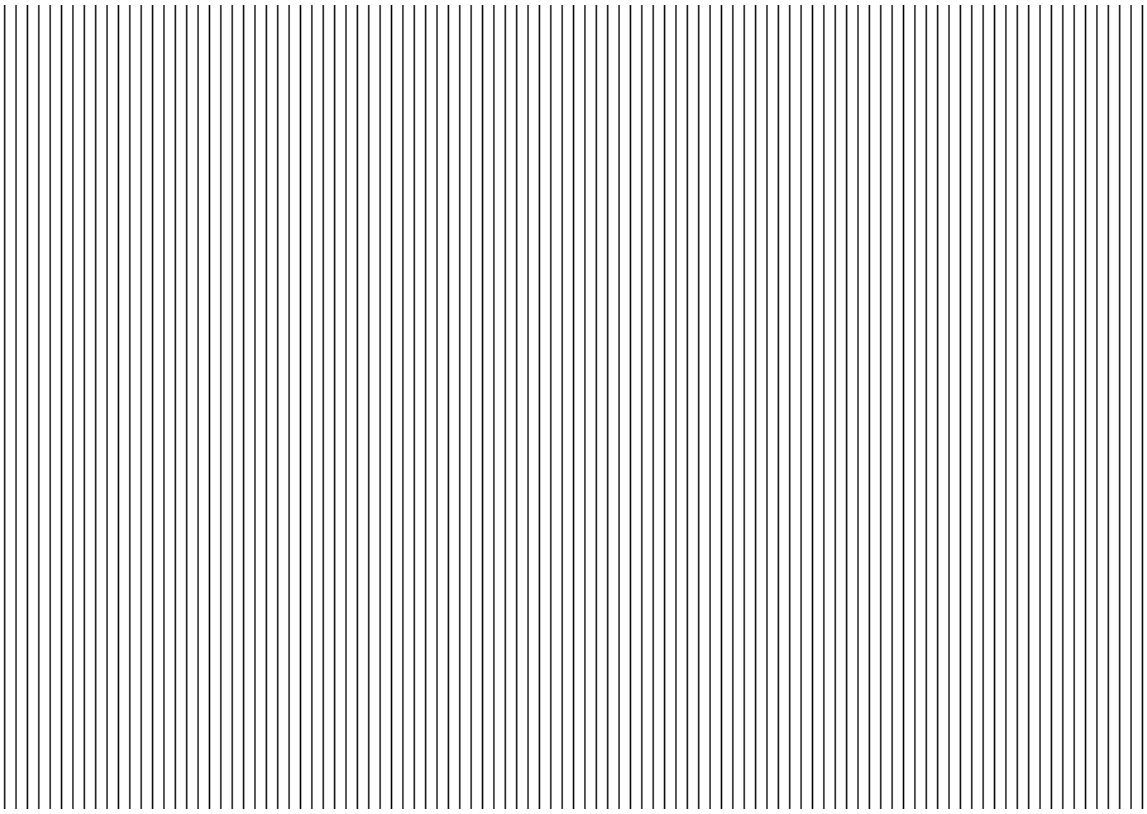

Figure A-3 – The transverse or hoop reinforcement for the corbel.

Mark Herbst
Corbel Design

Enter Value
Guess or Over Ride
Calculated Value

Parameters		
F'c	5000	psi
Vu (factored)	840	kips
Fy	60000	psi
Bw (guess)	50	inches

Bearing Plate Calcs			
b dim of plate	30		
Φ	0.65		
Bstress	2.7625	ksi	
Plate width	10.13574661	inches	try
L dim of plate	20	in min	30 x20x1.5 OK
L	22		

Depth of Corbel			
Vn(d)	50		
Vn(d)	40		
Used Vn(d)	40		Say
d min	28	inches	48 in
Φ	0.75		

Forces		
Nuc	168	kips
Av	10.5	in
h	50	in
d	48	
Mu	9156	kip-in
Φ	0.75	

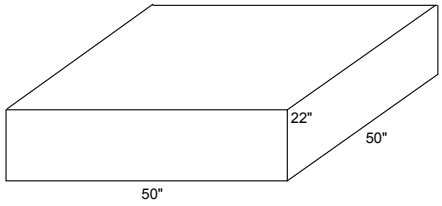

Shear Friction Steel		
λ	1	
Avf	13.33	in^2

Flexural Reinforcement		
Assume	d-a/2 = .9d	
Af	4.71	in^2
recompute a	1.33	
recompute Af	4.30	
An	3.733333333	in^2

Tension Tie Reinforcment	
Asc1	8.03
Asc2	12.62222222
Ascmin	8
	12.62

Bar Sizes	Area in^2	Diameter in	# Bars	Area	Total DofA w/#4 stirup	Spacing Cl	1 row clearance
3	0.11	0.378	115	12.6500	44.47	117	-111.47
4	0.2	0.5	64	12.8000	33	66	-49
5	0.31	0.625	41	12.7100	26.625	43	-19.625
6	0.44	0.75	29	12.7600	22.75	31	-3.75
7	0.6	0.875	22	13.2000	20.25	24	5.75
8	0.79	1	16	12.6400	17	18	15
9	1	1.128	13	13.0000	15.664	16.536	17.8
10	1.27	1.27	10	12.7000	13.7	14.43	21.87
11	1.56	1.41	9	14.0400	13.69	14.28	22.03
14	2.25	1.693	6	13.5000	11.158	11.465	27.377
18	4	2.257	4	16.0000	10.028	9.771	30.201

Size	#Bars	As	Enough Steel
9	13	13	YEP!

Area of Horizontal Stirrups		
Ah	4.44	in^2

Bar Sizes	Area in^2	Diameter in	# Bars	Area	Total DofA w/#4 stirup	Spacing Cl	1 row clearance
3	0.11	0.378	41	4.5100	16.498	43	-9.498
4	0.2	0.5	23	4.6000	12.5	25	12.5
5	0.31	0.625	15	4.6500	10.375	17	22.625

Size	#Bars	As	Enough Steel
5	8 Double leg	4.96	YEP!

Development Length			
Ldh	10.72	in	say 12
Db	1.128	in	
Reg Ld	62.21	in	5.1845069 ft
α	1.3		
β	1		
γ	1		
λ	1		
12*d	13.536		say 14

Figure A-4 – Corbel design calculated values using ACI section 11.9.

Appendix B. 150 PSI Flowable Fill Mix Design

CONCRETE MIX DESIGN

MIX ID : 1005 [20] 150 PSI 07/31/09

PROJECT : MASTER MIX FILE
SOURCE OF CONCRETE : GENEVA ROCK PRODUCTS
CONSTRUCTION TYPE : TYPE "B" STATE FLOWABLE FILL

WEIGHTS PER CUBIC YARD (SATURATED, SURFACE-DRY)		YIELD, CU FT
CEMENT, ASTM C-150, LB	47	0.24
FLY ASH, ASTM C-618, LB	158	1.10
POINT C-33 SAND, LB	1143	7.04
POINT PEA GRAVEL, LB	252	1.58
POINT #67 ROCK, LB	1429	8.98
WATER, LB (GAL-US)	334 (40.0)	5.35
TOTAL AIR, %	10.0	2.70
	TOTAL	27.00
WATER/CEMENT RATIO, LBS/LB	1.63	
SLUMP, IN	6.00	
CONCRETE UNIT WEIGHT, PCF	124.6	

SAND AGG. RATIO .60
POINT PEA GRAVEL SpG. 2.55
POINT SAND SpG. 2.60
POINT ROCK SpG. 2.55

PREPARED BY :

_____

JERRY G. HALL, TECHNICAL ENGINEER

Appendix C. Passive and Adhesive Resistance

Dustin Miner
Flowable Fill Thesis Calculations
Soil Passive Resistance and Side Friction

Basic Equation

$$\frac{1}{2}\cdot\gamma\cdot H^2\cdot B\cdot Kp + 2\cdot Cu\cdot H\cdot B\cdot\sqrt{Kp} + 2\cdot Cu\cdot H\cdot W$$

Soil Profile for depths 0 to 2.5 ft below ground surface

$H1 := 2.5\cdot ft$ $\quad B := 12ft$

$W := 6ft$ $\quad \gamma 1 := .1175\cdot\frac{kip}{ft^3}$

$Cu1 := 1.040\frac{kip}{ft^2}$ $\quad Kp := 1$

$$P1 := \frac{1}{2}\cdot\gamma 1\cdot H1^2\cdot B\cdot Kp + 2\cdot Cu1\cdot H1\cdot B\cdot\sqrt{Kp} + 2\cdot Cu1\cdot H1\cdot W$$

$P1 = 98.006\cdot kip$

Soil Profile for depths 2.5 to 6 ft below ground surface

$H2 := 3.5\cdot ft$ $\quad B := 12ft$

$W := 6ft$ $\quad \gamma 2 := .112\cdot\frac{kip}{ft^3}$

$Cu2 := .20\frac{kip}{ft^2}$ $\quad Kp := 1$

$$P2 := \frac{1}{2}\cdot\gamma 2\cdot H2^2\cdot B\cdot Kp + \left(2\cdot Cu2\cdot B\cdot\sqrt{Kp} + \gamma 1\cdot H1\cdot B\cdot Kp\right)\cdot H2 + 2\cdot Cu2\cdot H2\cdot W$$

$P2 = 45.769\cdot kip$ $\quad 2\cdot Cu2\cdot H2\cdot W = 8.4\cdot kip$

Bottom Friction

$Cu3 := .200 \cdot \frac{kip}{ft^2}$

$P3 := W \cdot B \cdot Cu3$

$P3 = 14.4 \cdot kip$

Total Resistance

$Ptotal := P1 + P2 + P3$

$Ptotal = 158.176 kip$

$FrictionF := 2 \cdot Cu1 \cdot H1 \cdot W + 2 \cdot Cu2 \cdot H2 \cdot W + P3$

$FrictionF = 54 \cdot kip$

Shear Forces $Force := 158.176 kip$

@ 0ft Depth

$V1 := 0$

@ 2.5ft Depth

$Vu := -Force + P1 \text{ float}, 4 \rightarrow -60.17 \cdot kip$

@ 6ft Depth

$V3 := -Force + P1 + P2 + P3 \text{ float}, 4 \rightarrow -0.0002501 kip$

Moment Forces $Increment := 2.5ft$

@ 0ft Depth

$M1 := 0$

@ 2.5ft Depth

$Mu := \frac{Increment \cdot Vu}{2} \text{ float}, 4 \rightarrow -75.21 \cdot ft \cdot kip$

@ 6ft Depth

$M3 := \frac{Increment \cdot V3}{2} \text{ float}, 4 \rightarrow -0.0003126 ft \cdot kip$